RECENT ADVANCES IN AGROMETEOROLOGICAL ANALYSIS TECHNIQUES FOR CROP MONITORING IN SUPPORT OF FOOD SECURITY EARLY WARNING

EDITED BY: Tamuka Magadzire, Andrew Hoell, Mphethe Tongwane and Catherine Lilian Nakalembe

PUBLISHED IN: Frontiers in Climate

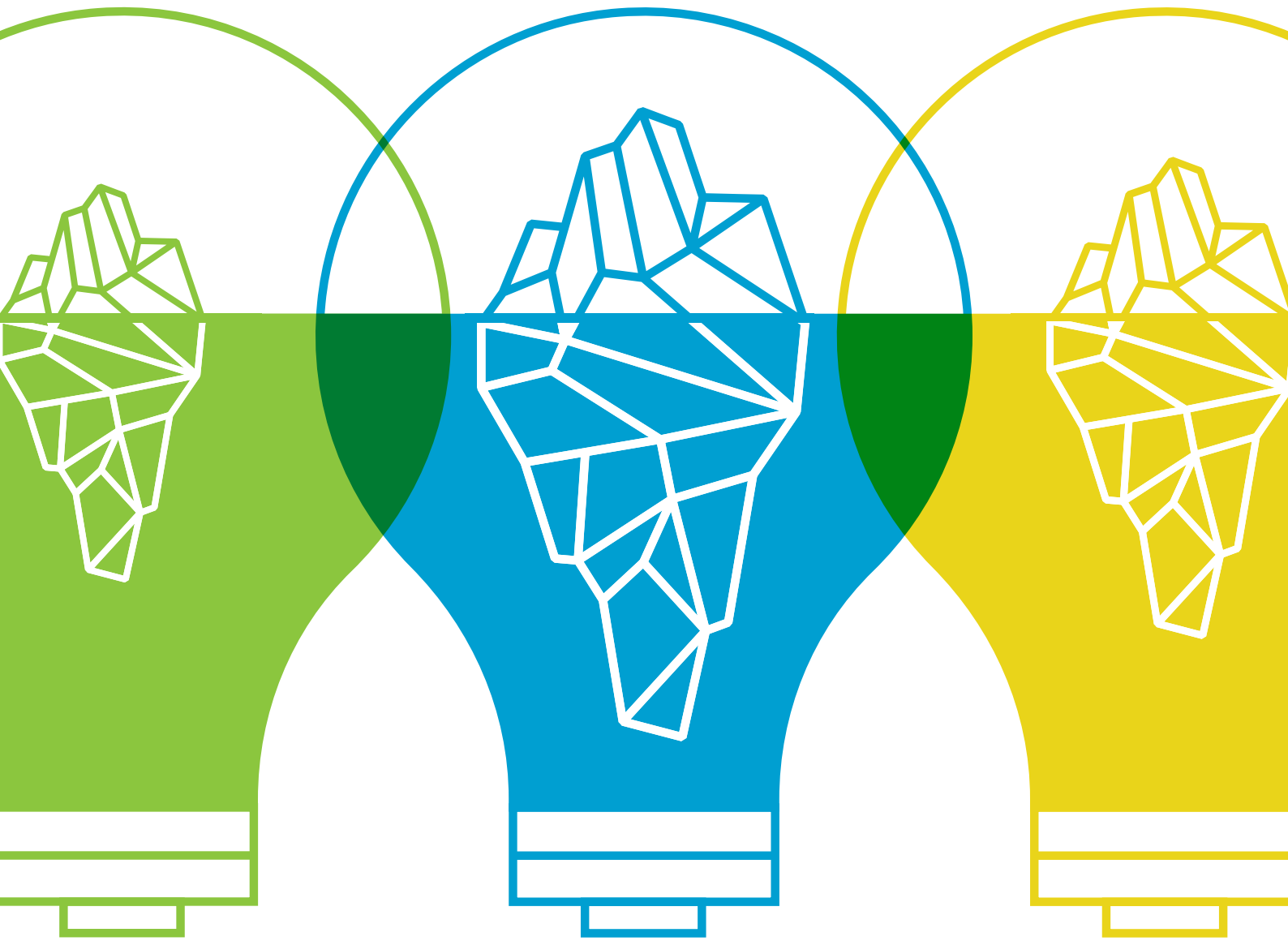

frontiers Research Topics

frontiers

ISSN 1664-8714
ISBN 978-2-83250-307-2
DOI 10.3389/978-2-83250-307-2

About Frontiers

Frontiers is more than just an open-access publisher of scholarly articles: it is a pioneering approach to the world of academia, radically improving the way scholarly research is managed. The grand vision of Frontiers is a world where all people have an equal opportunity to seek, share and generate knowledge. Frontiers provides immediate and permanent online open access to all its publications, but this alone is not enough to realize our grand goals.

Frontiers Journal Series

The Frontiers Journal Series is a multi-tier and interdisciplinary set of open-access, online journals, promising a paradigm shift from the current review, selection and dissemination processes in academic publishing. All Frontiers journals are driven by researchers for researchers; therefore, they constitute a service to the scholarly community. At the same time, the Frontiers Journal Series operates on a revolutionary invention, the tiered publishing system, initially addressing specific communities of scholars, and gradually climbing up to broader public understanding, thus serving the interests of the lay society, too.

Dedication to Quality

Each Frontiers article is a landmark of the highest quality, thanks to genuinely collaborative interactions between authors and review editors, who include some of the world's best academicians. Research must be certified by peers before entering a stream of knowledge that may eventually reach the public - and shape society; therefore, Frontiers only applies the most rigorous and unbiased reviews.
Frontiers revolutionizes research publishing by freely delivering the most outstanding research, evaluated with no bias from both the academic and social point of view. By applying the most advanced information technologies, Frontiers is catapulting scholarly publishing into a new generation.

What are Frontiers Research Topics?

Frontiers Research Topics are very popular trademarks of the Frontiers Journals Series: they are collections of at least ten articles, all centered on a particular subject. With their unique mix of varied contributions from Original Research to Review Articles, Frontiers Research Topics unify the most influential researchers, the latest key findings and historical advances in a hot research area! Find out more on how to host your own Frontiers Research Topic or contribute to one as an author by contacting the Frontiers Editorial Office: frontiersin.org/about/contact

RECENT ADVANCES IN AGROMETEOROLOGICAL ANALYSIS TECHNIQUES FOR CROP MONITORING IN SUPPORT OF FOOD SECURITY EARLY WARNING

Topic Editors:
Tamuka Magadzire, University of California, Santa Barbara, United States
Andrew Hoell, Earth System Research Laboratory (NOAA), United States
Mphethe Tongwane, University of the Free State Phuthaditjhaba, South Africa
Catherine Lilian Nakalembe, University of Maryland, College Park, United States

Citation: Magadzire, T., Hoell, A., Tongwane, M., Nakalembe, C. L., eds. (2022). Recent Advances in Agrometeorological Analysis Techniques for Crop Monitoring in Support of Food Security Early Warning. Lausanne: Frontiers Media SA.
doi: 10.3389/978-2-83250-307-2

Table of Contents

frontiers | Frontiers in Climate

TYPE Editorial
PUBLISHED 09 September 2022
DOI 10.3389/fclim.2022.950447

OPEN ACCESS

EDITED BY
Ana Maria Tarquis,
Polytechnic University of Madrid, Spain

REVIEWED BY
Mannava Sivakumar,
World Meteorological Organization, Switzerland

*CORRESPONDENCE
Tamuka Magadzire
tmagadzire@fews.net

SPECIALTY SECTION
This article was submitted to Climate Services, a section of the journal Frontiers in Climate

RECEIVED 22 May 2022
ACCEPTED 08 August 2022
PUBLISHED 09 September 2022

CITATION
Magadzire T, Hoell A, Nakalembe C and Tongwane M (2022) Editorial: Recent advances in agrometeorological analysis techniques for crop monitoring in support of food security early warning. *Front. Clim.* 4:950447. doi: 10.3389/fclim.2022.950447

Editorial: Recent advances in agrometeorological analysis techniques for crop monitoring in support of food security early warning

Tamuka Magadzire[1]*, Andrew Hoell[2], Catherine Nakalembe[3] and Mphethe Tongwane[4]

[1]Department of Geography, Climate Hazards Center, University of California, Santa Barbara, Santa Barbara, CA, United States, [2]National Oceanic and Atmospheric Administration (NOAA) Physical Q Sciences Laboratory, Boulder, CO, United States, [3]Department of Geographical Science, University of Maryland, College Park, MD, United States, [4]Department of Geography, University of the Free State, Phuthaditjhaba, South Africa

KEYWORDS

agrometeorology, crop area estimation, crop yield estimation, water stress, agrometeorological forecasting, crop pest damage assessment, agrometeorological advisory

Editorial on the Research Topic
Recent advances in agrometeorological analysis techniques for crop monitoring in support of food security early warning

Agrometeorological analysis is an essential component of effective crop monitoring systems, providing cost-effective complementarity to field surveys typically used to assess crop conditions and potential food security outcomes during each agricultural season. Using satellite-based agrometeorological techniques to strengthen crop monitoring can present significant cost saving to traditional field-based methods typically used for crop assessment. However, remote-sensing-based agrometeorological methods are not a replacement for field-based methods but complement, as the accuracy of the satellite-based methods often cannot be fully assessed or calibrated without compatible field-based measurements or equivalents.

In this collection, over thirty authors wrote articles that highlight critical aspects of agrometeorological analyses applied to crop monitoring for food security early warning. The themes covered a wide range of topics, including; (1) agrometeorological forecasting, (2) crop monitoring (including crop water balance and the assessment of pest damage), (3) estimation of crop production, (4) assessing water stress for croplands at a watershed scale, and (5) how to effectively deliver agrometeorological advisories to farmers. This set of themes can provide helpful guidance to assist practitioners develop and strengthen practical agrometeorological analysis and advisory systems.

The low-cost advantage of agrometeorology-based techniques is significant for poorly resourced institutions mandated with providing agrometeorological support for food security monitoring. Mashonganyika et al. used 10 m resolution satellite data from Sentinel-2 data to estimate wheat area in Zimbabwe, with an R-squared of 0.98 compared to farmer-reported planted area. Focusing on Malawi, Peterson and Husak used Sentinel-2 satellite data to map crop area with Google Earth Engine to an accuracy of 74% compared with official statistics. These examples illustrate the opportunity to use vast amounts of data at low cost, harnessing the power of cloud computing from a relatively low-end computer and on a small budget, which would be the typical scenario in a low-resourced institution. Mashonganyika et al. further highlighted the economic importance of such enhanced crop monitoring for developing country government initiatives. Many developing countries have agricultural input subsidy programmes to help farmers maximize agricultural productivity due to high input costs that would otherwise curtail farming activities. However, these subsidy programs, need to be monitored to ensure compliance and maximize outcomes. Large-scale, field-based crop monitoring is an expensive exercise that could quickly be sidelined due to the financial constraints typically facing developing country governments. The satellite-based crop monitoring methods demonstrated in this collection can thus play a critical role in effective crop monitoring.

Although the satellite analysis methods and services described in these articles are currently low-cost within a research framework, one risk in their application for operational use is the possibility of commercialization of these services in the future, which could put the benefits out of the reach of many under-funded institutions. Some tools and datasets are open access for research purposes, and operational or commercial uses require paid licenses.

While remote sensing agrometeorological applications have come a long way since the launch of the first earth observation satellites, not all remote sensing methodologies for agrometeorological monitoring have reached full maturity for operational use, highlighting the need for continual research and development. Adams et al. attempted to assess the impacts of the 2020 desert locust outbreak in East Africa using satellite data from various sensors. This proved largely unsuccessful—the localized nature of locust outbreaks could not be easily distinguished from senescence using satellite image analysis, underscoring the necessity of ground truth data.

Crop production is calculated as a function of yield and cropped area. Peterson and Husak and Mashonganyika et al. demonstrated how crop area could be estimated from remote sensing methods. However, to get a complete picture of crop performance, evaluating potential yield outcomes is equally important. Pervez et al. demonstrated an improved approach for seasonal vegetation monitoring that combines the use of two satellite-based analysis methods—normalized difference evapotranspiration (NDVI) and evapotranspiration (ET)—by identifying where each performs better, thus allowing optimal use of these methods for seasonal vegetation monitoring, an important step toward yield estimation.

Food and water security are inextricably linked, given agriculture's dependence on water. Khand et al. demonstrated how water stresses for rainfed and irrigated croplands could be estimated at a basin-scale and compared water stress levels for different basins and different years. This type of basin-scale analysis provides an opportunity for linking food security analysis into a more holistic basin-management approach.

Crop monitoring techniques compatible with short to medium-term forecasts facilitate planning food security, agricultural production, and disaster risk reduction. Funk, Turner et al. discussed a novel approach that simplifies the dekadal water requirements satisfaction index into a seasonal-scale parameter that can be used with medium-range to seasonal-scale forecasts. This will allow farmers and disaster risk reduction managers to make informed decisions regarding options for managing upcoming seasons and refine and update their plans as more observational data becomes available.

Ultimately, the agrometeorological techniques described above must be delivered to end-users through accessible systems. This is typically not a one-off process, as illustrated by Walker using three case studies of agrometeorological advisories for farmers, but rather involves extended interactions and feedback loops with users to refine the products and achieve high levels of acceptance and adoption by the user. Thus, agrometeorological analysis methodologies need to be developed in consultation with the intended users to ensure products with a high level of societal benefit and application for food security.

Concluding remarks

Despite the opportunities availing with the steady progress in technology, a fundamental limitation to the use and applications of agrometeorological innovations within critical institutions in developing countries remains the availability of skilled personnel to undertake the types of analyses described in this collection. Under-resourced agrometeorological institutions in developing countries need to highlight to beneficiaries the economic benefits of investing in their operations, both in terms of the technological and the human resource requirements, given the potential benefits that governments can realize from effectively utilizing agrometeorological analysis for crop monitoring in support of food security early warning.

Author contributions

TM, AH, CN, and MT contributed to the writing of this editorial and to the editing of the articles published under

the article collection that this editorial covers. All authors contributed to the article and approved the submitted version.

Funding

TM acknowledges support of the United States Agency for International Development (USAID) cooperative agreement #72DFFP19CA00001.

Acknowledgments

We wish to express our gratitude to all the authors who contributed to this Research Topic, and to the reviewers who took the time to go through the papers and ensure the high quality of each article that was published in this collection.

Conflict of interest

The authors declare that the research was conducted in the absence of any commercial or financial relationships that could be construed as a potential conflict of interest.

Publisher's note

frontiers in Climate

ORIGINAL RESEARCH
published: 26 January 2021
doi: 10.3389/fclim.2021.589981

Vegetation Monitoring Optimization With Normalized Difference Vegetation Index and Evapotranspiration Using Remote Sensing Measurements and Land Surface Models Over East Africa

Shahriar Pervez[1]*, *Amy McNally*[2,3,4], *Kristi Arsenault*[3,4], *Michael Budde*[5] and *James Rowland*[5]

[1] Arctic Slope Regional Corporation (ASRC) Federal Data Solutions, Contractor to U.S. Geological Survey, Earth Resources Observation and Science Center, Sioux Falls, SD, United States, [2] United States Agency for International Development, Washington, DC, United States, [3] Science Application International Corporation, McLean, VA, United States, [4] Hydrological Sciences Laboratory, National Aeronautics and Space Administration (NASA) Goddard Space Flight Center, Greenbelt, MD, United States, [5] U.S. Geological Survey, Earth Resources Observation and Science Center, Sioux Falls, SD, United States

OPEN ACCESS

Edited by:
Mphethe Tongwane, Zutari, South Africa

Reviewed by:
Mingguo Ma, Southwest University, China
Lilian Wangui Ndungu, Regional Centre for Mapping of Resources for Development, Kenya

***Correspondence:**
Shahriar Pervez
spervez@contractor.usgs.gov

Specialty section:
This article was submitted to Climate Services, a section of the journal Frontiers in Climate

Received: *31 July 2020*
Accepted: *05 January 2021*
Published: *26 January 2021*

Citation:
Pervez S, McNally A, Arsenault K, Budde M and Rowland J (2021) Vegetation Monitoring Optimization With Normalized Difference Vegetation Index and Evapotranspiration Using Remote Sensing Measurements and Land Surface Models Over East Africa. Front. Clim. 3:589981. doi: 10.3389/fclim.2021.589981

The majority of people in East Africa rely on the agro-pastoral system for their livelihood, which is highly vulnerable to droughts and flooding. Agro-pastoral droughts are endemic to the region and are considered the main natural hazard that contributes to food insecurity. Drought begins with rainfall deficit, gradually leading to soil moisture deficit, higher land surface temperature, and finally impacts to vegetation growth. Therefore, monitoring vegetation conditions is essential in understanding the progression of drought, potential effects on food security, and providing early warning information needed for drought mitigation decisions. Because vegetation processes couple the land and atmosphere, monitoring of vegetation conditions requires consideration of both water provision and demand. While there is consensus in using either the Normalized Difference Vegetation Index (NDVI) or evapotranspiration (ET) for vegetation monitoring, a comprehensive assessment optimizing the use of both has not yet been done. Moreover, the evaluation methods for understanding the relationships between NDVI and ET for vegetation monitoring are also limited. Taking these gaps into account we have developed a framework to optimize vegetation monitoring using both NDVI and ET by identifying where they perform the best by using triple collocation and cross-correlation methods. We estimated the random error structure in Moderate Resolution Imaging Spectroradiometer (MODIS) NDVI; ET from the Operational Simplified Surface Energy Balance (SSEBop) model; and ET from land surface models (LSMs). LSM ET and SSEBop ET have been found to be better indicators for vegetation monitoring during extreme drought events, while NDVI could provide better information on vegetation condition during wetter than normal conditions. The random error structures of these variables suggest that LSM ET is most likely to provide important information for vegetation monitoring over low and high ends of the vegetation fraction areas. Over moderate vegetative areas, any of these variables could provide important vegetation

information for drought characterization and food security assessments. While this study provides a framework for optimizing vegetation monitoring for drought and food security assessments over East Africa, the framework can be adopted to optimize vegetation monitoring over any other drought and food insecure region of the world.

Keywords: triple collocation, East Africa, vegetation monitoring, evapotranspiration, normalized difference vegetation index

INTRODUCTION

East Africa, with around 330 million inhabitants (Gebremeskel et al., 2019), is one of the chronically food insecure regions of the world. Most of the people, around 80%, live in rural areas and depend on subsistence agriculture and livestock for their livelihood (IGAD, 2020). The agro-pastoral system of the region heavily depends on the prevailing weather conditions, especially rainfall, and is highly vulnerable to extreme weather and climate events such as droughts (high climate variability). Agro-pastoral droughts are endemic to the region and are considered the main natural hazard that contributes to food insecurity (Gebremeskel et al., 2019; Qu et al., 2019). However, the onset of droughts is often slow, providing opportunities for interventions (Funk et al., 2019). Drought begins with rainfall deficit, which leads to soil moisture deficit, higher land surface temperature, and finally impacts to vegetation growth. Vegetation plays an important role in many Earth system processes. Its growth and productivity couple the land and atmosphere as they are active components of the water cycle, energy cycle, and other biogeochemical processes (Lanning et al., 2019). Furthermore, plants provide a wide range of important goods and services to humans, ranging from forest products and fodder to food production. Therefore, monitoring vegetation, among other variables, is essential to understanding drought's progression, potential effects on food security, and early warning and information needed for mitigation decisions. Remote sensing and land surface models are playing an increasingly important role in assisting large-scale land surface monitoring, by providing comprehensive information about the dynamics of Earth's physical, chemical, and biological processes (Biggs et al., 2015; Zhao and Li, 2015). The Normalized Difference Vegetation Index (NDVI), developed with the remote sensing measurements of Near-infrared and Red reflectance by sensors on board satellites, has been used extensively for vegetation monitoring and drought assessments. Earlier studies have utilized NDVI from spectral measurements from the Advanced Very High Resolution Radiometer (AVHRR) on board National Oceanic and Atmospheric Administration (NOAA) satellites in monitoring vegetation and food security assessments over Africa (Justice et al., 1986; Townshend and Justice, 1986; Sannier et al., 1998; Anyamba and Tucker, 2005). With the launch of the Moderate Resolution Imaging Spectroradiometer (MODIS) instrument on board National Aeronautics and Space Administration's (NASA) Terra and Aqua satellites, more recent studies have developed different methods utilizing MODIS-NDVI for monitoring vegetation dynamics, drought progression, and food security assessments (Brown, 2016; Klisch and Atzberger, 2016; Zewdie et al., 2017; Mbatha and Xulu, 2018). These studies take advantage of the higher spatial resolution and more accurate geolocation data provided by MODIS sensors over AVHRR (Townshend and Justice, 2002). Many other indices have also been developed based on relative changes in NDVI and land surface temperature such as Vegetation Condition Index (VCI), Vegetation Health Index (VHI), and Temperature Condition Index (TCI) for vegetation monitoring and drought assessment at large scales (Kogan, 1995; Du et al., 2013). It has been observed over East Africa that the start of growing period is advancing with an elongated growing season, while drought's impact on vegetation is enhancing with a concomitant decline in gross primary productivity (Workie and Debella, 2018; Robinson et al., 2019). Using MODIS-NDVI and its derivatives (VCI, TCI, VHI), Qu et al. (2019) observed significant long-term increases in temperature and decreases in crop health over the major growing period and associated them with the impacts of drought events over the greater horn of Africa. Using MODIS-NDVI, among other variables, Robinson et al. (2019) demonstrated the negative response of vegetation growth to the 2010–2011 drought in East Africa.

Land surface evapotranspiration (ET) is the sum of water surface evaporation, soil moisture evaporation, and plant transpiration from Earth's surface to the atmosphere (Biggs et al., 2015). ET has been used in monitoring vegetation and drought progression. Because of ET's dependence on land cover and soil moisture and its direct link with carbon dioxide assimilation in plants, ET becomes an important variable in monitoring and estimating crop yield and biomass for decision makers interested in food security assessments (Bastiaanssen et al., 2005). The changes in vegetation conditions have been successfully associated with changes in ET over the Nile basin by Alemu et al. (2014). Baruga et al. (2019) demonstrated a connection between agricultural droughts and high heatwaves in Uganda using ET. Vegetation water stress has been mapped using ET by Chirouze et al. (2013). Kimosop (2019) used ET to define onset, duration, severity, intensity, and frequency of agricultural drought in Kenya.

While ET can be measured directly using a variety of methods ranging from weighing lysimeter devices to eddy covariance and scintillometry, their applications are limited to field scale (Allen et al., 2007). But using remote sensing measurements, ET can be estimated both at field and regional scales. However, as ET is the sum of multiple processes that transfer liquid water from the surface to vapor phase into the atmosphere using heat energy, satellite sensors cannot measure ET directly. Rather, the spectral radiance measures they provide are used in models or

retrieval algorithms to estimate ET. Most of the methods that use remote sensing data to estimate ET can be categorized into two groups: (a) vegetation-based methods and (b) surface energy balance methods. In vegetation-based methods, remotely sensed vegetation indices such as NDVI or Leaf Area Index (LAI) are used with surface resistance determined from meteorological data in Penman-Monteith (Mu et al., 2007) or Priestly-Taylor (Fisher et al., 2008) equations to project ground-estimated ET to a larger scale. The energy balance methods are based on the fact that ET is a change of state of water that uses energy for vaporization. The vaporization reduces the surface temperature, suggesting a tight coupling between water availability and surface temperature under water stress conditions (Biggs et al., 2015). This allows estimating ET by using remotely sensed surface temperature data in solving the energy balance by partitioning net radiation between sensible, latent, and soil heat flux. The methods of estimating ET from remote sensing inputs are well-documented in the literature (Glenn et al., 2007; Biggs et al., 2015); more specifically, Kalma et al. (2008) reviewed energy balance methods that utilize surface temperature to estimate ET. ET can also be estimated with land surface models (LSM) that are parameterized with remote sensing inputs. LSMs yield global estimates of the land surface states and fluxes by incorporating global-scale, ground-based, and/or remote sensing–derived soil moisture, vegetation, and atmospheric forcing data (Xu et al., 2019). The advantage of LSM ET over ET from remote sensing measurements is that it overcomes some of the shortcomings of remote sensing measurements of land surface temperature because of the low signal-to-noise ratio and signal saturation in an optical sensor (Senay et al., 2013).

Vegetation monitoring using NDVI emphasizes the vegetation conditions from a water provision perspective as it is a measurement of vegetation vigor driven primarily by land surface water availability, whereas the use of ET emphasizes the vegetation conditions from a water demand perspective as it incorporates surface and soil evaporation and plant transpiration driven primarily by atmospheric conditions (Meza, 2005; Van Beek et al., 2011). As the vegetation growth and productivity processes couple the land and atmosphere, monitoring of vegetation condition will require consideration of both water provision and demand over any region. While there is a consensus in using either NDVI or ET for vegetation monitoring, drought characterization, or food security assessments, a comprehensive assessment optimizing the use of NDVI and ET by location has not yet been done. Moreover, the three-way evaluation methods for understanding the relationships between NDVI, ET from remote sensing measurements, and ET from land surface models for vegetation monitoring are also limited. Taking these gaps into account, this research focused on developing a method for optimizing vegetation monitoring by using NDVI and ET from remote sensing and land surface models as well as exploring the relationships between them in a three-way format (between the three variables). The specific objectives are to (1) develop a process to estimate random errors in NDVI, ET from remote sensing, and ET from land surface models, (2) evaluate the spatial-temporal correlations between these variables, and (3) assess the performance of each of these variables in optimizing vegetation monitoring in East Africa. To achieve these objectives, we employed Triple Collocation (TC) analysis. We incorporated ET from two sources and NDVI into the TC analysis. We opted for TC analysis because in TC, random error structure of the variables can be determined independently without treating any as perfectly observed truth in a three-way format assuming errors in the variables are random and uncorrelated between each other (Gruber et al., 2016). We also used a traditional statistical measure of cross-correlation to evaluate agreements between these variables.

MATERIALS AND METHODS

Study Area

Geographically, East Africa encompasses areas from both northern and southern hemispheres, including Sudan, South Sudan, Eritrea, Ethiopia, Djibouti, Somalia, Kenya, Uganda, Rwanda, Burundi, and Tanzania, and is located between the latitudes of 11°S and 23°N and longitudes of 21°E and 51°E. The climate and topography vary from wet highlands covering Ethiopian Highlands and parts of Kenya and Tanzania to arid lowlands of eastern Ethiopia, Djibouti, and Somalia (Dinku et al., 2011). Agriculture is the primary source of livelihood complemented by crop production and livestock rearing. The agro-pastoral system primarily responds to rainfall. The rainfall regime varies from north to south. The annual mean rainfall ranges from 800 to 1,200 mm, with higher rainfall over the Ethiopian Highlands and lower rainfall over northeastern Kenya and Somalia (Fenta et al., 2017). **Figure 1** shows the map of the study area along with the monthly Climate Hazards Infrared Precipitation with Stations (CHIRPS) mean rainfall computed over the period 2000–2018 over three different administrative boundaries in the region. A map of CHIRPS mean annual rainfall over the East Africa region can also be found in Figure 2A of Fenta et al. (2017). CHIRPS is an infrared-based rainfall product, bias corrected with climatology and gauge station observed rainfall records. Details on the CHIRPS rainfall are provided in Funk et al. (2015). The rainfall distribution near the equator is typically bimodal over Kenya with the main rainy season (long rains) between March and June followed by the second season (short rains) in October to December. The rainy season over 5° north and south of the equator is typically unimodal, and most of the rain occurs between May and October in the north (over Sudan and South Sudan) and between November and April of the following year in the south (Tanzania). In this study, while compiling rainfall, NDVI, and ET time series over the wetter half of the year, we considered two regimes: May to October for Sudan, South Sudan, Ethiopia, Eritrea, Djibouti, and Somalia, Kenya, and Uganda; and November to April for Kenya, Uganda, Rwanda, Burundi, and Tanzania.

NDVI and ET From Remote Sensing Measurements

Since 2003, NDVI and actual ET data have been produced by the U.S. Geological Survey (USGS) Famine Early Warning Systems Network (FEWS NET) using the operational simplified surface energy balance (SSEBop) model (Senay et al., 2013).

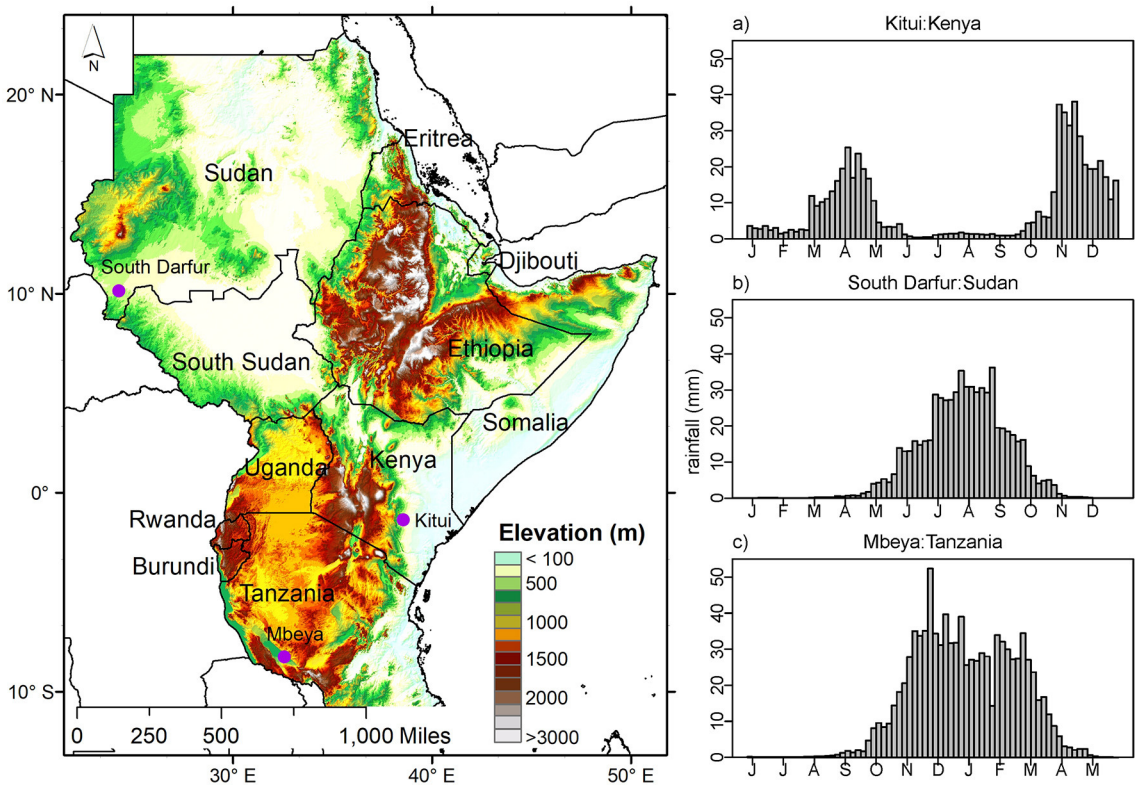

FIGURE 1 | Geographical location of East Africa and average (2000–2018) rainfall over three level 1 administrative districts, **(A)** Kitui in Kenya, **(B)** South Darfur in Sudan, and **(C)** Mbeya in Tanzania. Rainfall source: Climate Hazards Infrared Precipitation with Stations.

SSEBop is one of many energy balance–based approaches for estimating ET using remote sensing measurements. The SSEBop setup is based on the Simplified Surface Energy Balance (SSEB) approach (Senay et al., 2013) with a unique parameterization for operational applications. It combines ET fractions generated from remotely sensed MODIS thermal imagery, acquired every 10 days at 1 × 1 km spatial resolution, with reference ET using a thermal index approach. The unique feature of the SSEBop parameterization is that it uses pre-defined, seasonally dynamic, boundary conditions that are unique to each pixel for the "hot/dry" and "cold/wet" reference points (FEWSNET, 2019). The original formulation of SSEB is based on the hot and cold pixel principles of SEBAL (Bastiaanssen et al., 1998) and METRIC (Allen et al., 2007) models. While there are many NDVI and ET products from remote sensing measurements available, the use of MODIS NDVI (Jenkerson et al., 2010) and SSEBop ET in this research is primarily determined by the consistency in their method and production and their long history of readily available data. Furthermore, SSEBop ET estimates were found to be in good agreement with observed FLUXNET ET (Velpuri et al., 2013).

ET From Land Surface Models

Utilizing NASA's state-of-the-art Land Information System (LIS) (Kumar et al., 2008) framework, FEWS NET Land Data Assimilation System (FLDAS) incorporates multiple LSM and produces multi-forcing estimates of land surface states and fluxes such as ET and soil moisture. The output variables are driven by the CHIRPS rainfall product that performs well over data sparse regions. CHIRPS is available over a long historical record, and complements other remote sensing products used by FEWS NET for vegetation, drought, and food security monitoring (McNally et al., 2017). We included ET from three LSMs to better understand their usefulness in monitoring vegetation and drought over East Africa. The ET from the LSMs used in this study include Noah, Variable Infiltration Capacity (VIC), and Catchment Land Surface Model (CLSM). The meteorological forcing data for the LSMs come from NASA's Modern Era Reanalysis for Research and Applications, version 2 (MERRA 2) (Bosilovich et al., 2015). Other parameters include GTOPO 30 elevation, MODIS International Global Biosphere Project (IGBP) land cover for Noah, University of Maryland (UMD) land cover for VIC (Hansen et al., 2000; Friedl et al., 2010), National Centers for Environmental Prediction (NCEP) monthly greenness fraction, albedo (Gutman and Ignatov, 1998; Csiszar and Gutman, 1999), and STATSGO/FAO soil texture. These LSMs use monthly climatology of greenness fraction or leaf area index (LAI) derived from composites of NDVI dataset (Myneni et al., 1997; Gutman and Ignatov, 1998; Dirmeyer et al., 2006) to parameterize vegetation presence. They do not require time series of vegetation information (e.g., NDVI, LAI).

TABLE 1 | International Geosphere Biosphere Program (IGBP) land cover classes.

Land cover index	Description	Land cover index	Description
1	Evergreen needleleaf	8	Savannas
2	Evergreen broadleaf	9	Grassland
3	Deciduous broadleaf	10	Permanent wetland
4	Mixed forest	11	Cropland
5	Closed forest	12	Urban built-up
6	Open shrubland	13	Crop/natural vegetation
7	Woody savannas	14	Barren/sparsely vegetated

TABLE 2 | Average correlation coefficient by country for between Noah, VIC, and CLSM ET.

Country	Noah/VIC ET	Noah/CLSM ET	VIC/CLSM ET
Sudan	0.94	0.97	0.93
South Sudan	0.97	0.97	0.95
Eritrea	0.90	0.95	0.88
Djibouti	0.89	0.96	0.91
Ethiopia	0.94	0.93	0.92
Somalia	0.94	0.95	0.92
Kenya	0.92	0.89	0.88
Uganda	0.91	0.89	0.92
Rwanda	0.92	0.91	0.92
Burundi	0.89	0.96	0.89
Tanzania	0.95	0.95	0.93

Noah

The Noah LSM (Chen et al., 1996) employs a single column soil-vegetation-atmosphere transfer scheme, discretized using finite difference methods and split-hybrid (water and energy balance) temporal integration. We adopted model version 3.3, which runs at a 15-min timestep and produces ET at 0.1° spatial and daily temporal resolutions. ET in Noah 3.3 includes three components: wet canopy evaporation, transpiration, and evaporation from bare soil. The transpiration is defined using Penman-Monteith formulation with stomatal resistance and constrains using water storage terms that are dependent upon precipitation instead of vapor pressure. The bare soil evaporation is parametrized with soil moisture and the wet canopy evaporation and transpiration are functions of the intercepted canopy water content, which is a residual of water balance. ET is the sum of these three components.

VIC

The VIC model is a semi-distributed macroscale hydrologic model (Liang et al., 1994) in which ET includes similar components as in Noah. The computation of wet canopy evaporation and transpiration is similar to Noah, but unlike Noah the maximum intercepted canopy water content is a function of LAI climatology in VIC. The soil component of VIC employs an area integration to define the soil moisture constraint on transpiration defined using Penman-Monteith with zero stomatal resistance. VIC runs at a 1-h timestep in energy and water balance mode and produces ET at 0.25° spatial resolution.

CLSM

CLSM (Koster et al., 2000) was developed by the NASA Global Modeling and Assimilation Office and is the land-surface component of the Goddard Earth Observing System model version 5 general circulation model. It simulates water and energy balances on irregular topographically derived catchments. ET is calculated from three water balance prognostic variables, surface excess, root zone excess, and catchment deficit, for the dynamically changing saturated, non-saturated, and below wilting areas within the catchment. The primary soil moisture prognostic variable is the catchment deficit, defined as the average amount of water that would have to be added to bring the catchment to saturation. The root zone excess and surface excess describe average amounts of water that are out of equilibrium within the root zone and surface across the catchment. CLSM runs at a 15-min timestep and produces ET at 0.1° spatial and daily temporal resolutions.

Data Processing

Prior to performing the analyses, all the data were collocated in both space and time. The spatial resolution of LSM ET is 0.1°, SSEBop is 1 km, and NDVI is 250 m. Therefore, all the datasets were resampled to 5 km spatial resolution. The three datasets are also available at different temporal scales; LSM ET is daily, NDVI is a 10-days composite, and SSEBop ET is dekadal (10-days equivalent), thus all the respective datasets were temporally aggregated to a monthly timescale. Additionally, the NDVI time series was smoothed using the weighted least-squares approach to remove artifacts caused by unexpected distortions (e.g., clouds, missing data). Prior to the computation, we masked out the areas that receive <200 mm of rainfall annually as desert regions of East Africa (Nicholson, 1996). Studies show anomalies rather than actual values are better indicators for vegetation conditions (Tadesse et al., 2015), therefore, we used anomalies in the analyses. ET anomalies for any given 10-days period were calculated by subtracting the 10-days period value from its historical median (2003–2016). Similarly, NDVI anomalies were calculated by subtracting the 10-days value from its historical median (2003–2016). After computing the mean μ and standard deviation σ, the LSM ET and NDVI anomalies were linearly scaled to the data space of SSEBop ET using **Equations (1, 2)**. We also standardized anomalies for ET and NDVI to bring them under the same scale. These composites allow qualitative comparison of how similarly each of the datasets represents vegetation conditions for different hydrologic regimes over the study area. However, they do not provide direct information with

respect to interannual comparisons between the datasets.

$$E'_{LSM} = \mu_{SSEBop} + (E_{LSM} - \mu_{LSM}) \frac{\sigma_{SSEBop}}{\sigma_{LSM}} \quad (1)$$

$$E'_{NDVI} = \mu_{SSEBop} + (E_{NDVI} - \mu_{NDVI}) \frac{\sigma_{SSEBop}}{\sigma_{NDVI}} \quad (2)$$

where E and E' are the actual and scaled anomalies.

The annual maximum vegetation fraction derived from 12 years of Collection 5 MODIS NDVI data (MOD13A2) (Broxton et al., 2014) and IGBP land cover map were processed to use them in the relationship and error analyses between ET and NDVI by vegetation fractions and land cover types. The descriptions of the IGBP land cover classes are provided in **Table 1**.

Triple Collocation Analysis

Triple Collocation (TC) (Stoffelen, 1998) is a statistical method for characterizing consensus and discrepancies across multiple independent datasets. TC analysis has been used to estimate the random errors in NDVI and ET variables. TC analysis is particularly valuable in regions that lack *in situ* observations for evaluations, as consensus anomaly estimates derived from multiple independent datasets can be interpreted as a measure of confidence in the absence of adequate *in situ* evaluation data (van der Schalie et al., 2018). TC uses a set of three or more linearly related and collocated variables with independent error structures. It produces root mean square error (RMSE) of the random error component of the individual variable, in the absence of a variable that can be used as the absolute truth (van der Schalie et al., 2018). We employed TC analysis to quantify random errors in LSM ET, SSEBop ET, and NDVI where two of the variables were measuring hydrologic flux and the third one was measuring vegetation vigor. The variables depict reasonable cross-correlations across most of the study area, indicating linear relationships between them at monthly scale. Therefore, they are suitable for TC analysis framework. As stated before, the objective is not to validate any one variable against a different one, but rather to evaluate the skill of these products relative to one another and how the variables can be used together in optimizing vegetation monitoring in East Africa. The TC analysis is performed with the assumption that errors in the datasets are uncorrelated between each other and are independent (Gruber et al., 2016). The LSMs are forced with CHIRPS and MERRA2 inputs, whereas the primary forcing for SSEBop is MODIS radiometric temperature data, and NDVI is derived from MODIS surface reflectance data. In addition, there are substantial differences in underlying modeling approaches between LSM ET and SSEBop ET. Therefore, it is fair to assume that errors in these datasets are independent and uncorrelated.

In this study, we have taken an ensemble mean of the Noah, VIC, and CLSM ET anomaly time series because of the similarities between them and designated the ensemble mean as "LSM ET" in successive analyses. **Table 2** shows the

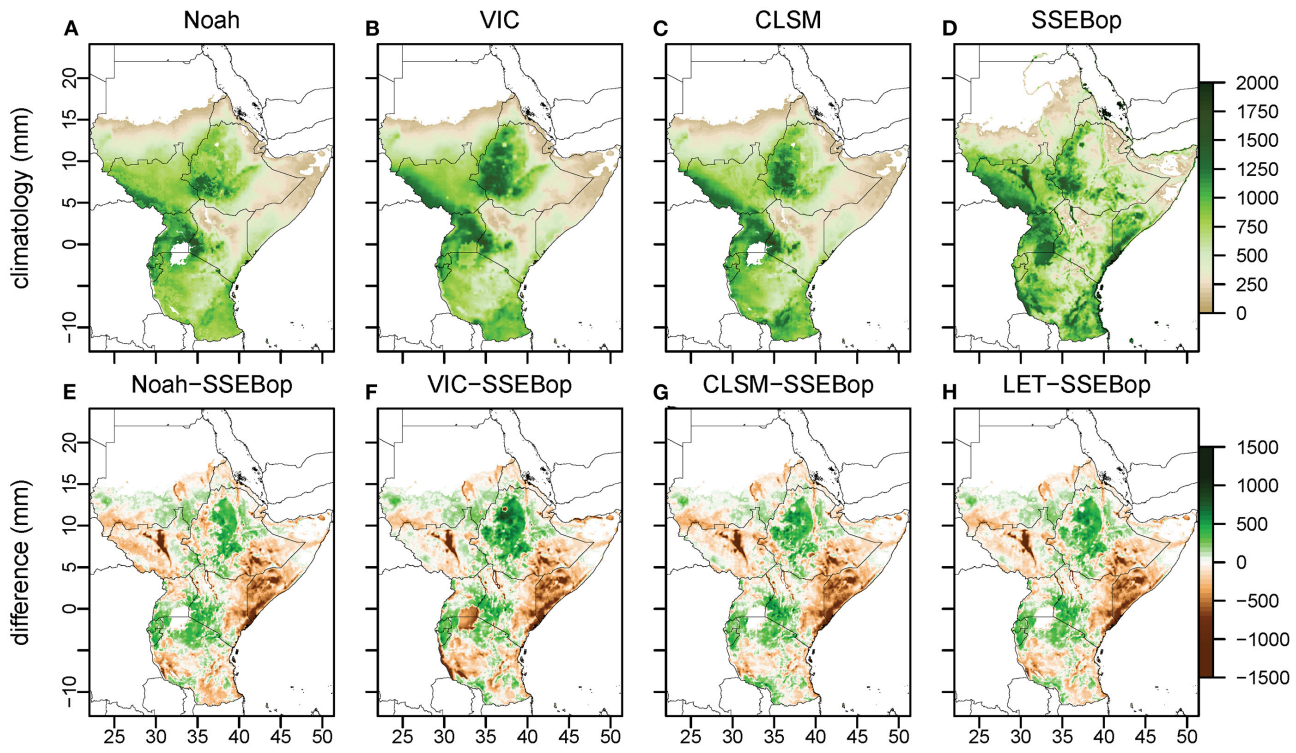

FIGURE 2 | Annual total evapotranspiration (ET; in mm) for the period 2003–2016 from **(A)** Noah, **(B)** VIC, **(C)** CLSM, **(D)** SSEBop. The bottom row shows the difference in ET climatology between **(E)** Noah minus SSEBop, **(F)** VIC minus SSEBop, **(G)** CLSM minus SSEBop, and **(H)** ensemble mean of Noah, VIC, and CLSM minus SSEBop.

correlations between Noah, VIC, and CLSM ET by country. As required, we designated SSEBop ET as the reference variable, which by no means assumes that the SSEBop is perfect, but rather we assume errors in the SSEBop ET are effectively independent from those impacting errors in LSM ET and NDVI. Finally, the TC errors were computed for the May–October and November–April composites for each of the datasets, using the following equations:

$$\varepsilon_{LSM} = \left\langle \left(E'_{LSM} - E_{SSEBop}\right) \quad \left(E'_{LSM} - E'_{NDVI}\right) \right\rangle \tag{3}$$

$$\varepsilon_{NDVI} = \left\langle \left(E'_{NDVI} - E_{SSEBop}\right) \quad \left(E'_{NDVI} - E'_{LSM}\right) \right\rangle \tag{4}$$

$$\varepsilon_{SSEBop} = \left\langle \left(E_{SSEBop} - E'_{LSM}\right) \quad \left(E_{SSEBop} - E'_{NDVI}\right) \right\rangle \tag{5}$$

where ε is the TC error for each dataset, E and E' are the actual data scaled data, respectively, and $\langle - \rangle$ is the corresponding average over the period. TC produces the random error metric, where numbers closer to zero indicate better performance and vice versa.

Statistical Measure

Spatially distributed statistical measures, including long-term annual mean, standardized monthly anomalies (spatial, temporal), and Pearson's correlation coefficient r, are used to compare these variables during the wetter half of the year.

$$r = \frac{\sum_i^n \left(E_i - \overline{E}\right)\left(S_i - \overline{S}\right)}{\sqrt{\sum_i^n \left(E_i - \overline{E}\right)^2 \sum_i^n \left(S_i - \overline{S}\right)^2}}, \; -1 \le r \le 1 \tag{6}$$

where E_i represents the LSM ET or NDVI monthly anomaly, S_i represents monthly SSEBop ET anomaly, $\overline{E}$ and $\overline{S}$ are the respective mean, n is the total number of data records in the time series, and the subscript i denotes the *ith* number of samples. As suggested in Hain et al. (2011), we used anomalies instead of actual values for correlation to minimize impacts of differences in mean and standard deviation values between SSEBop ET, LSM ET, and NDVI variables due to differences in input data and modeling approaches.

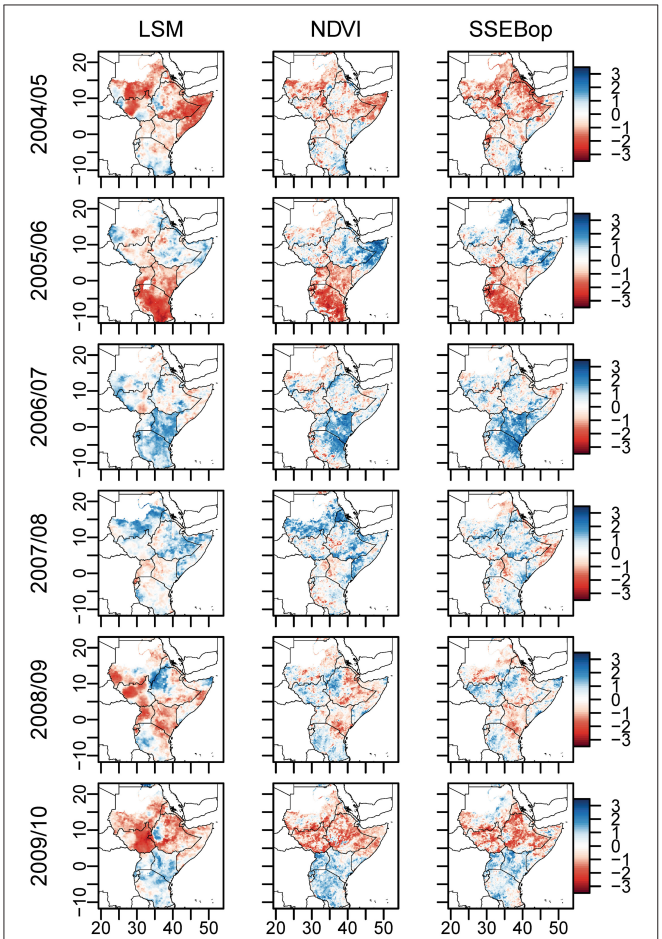

FIGURE 3 | Standardized anomaly composites of LSM ET, NDVI, and SSEBop ET over the wetter half of the year for the period 2004–2010. May–October for Sudan, South Sudan, Ethiopia, Eritrea, Djibouti, Uganda, and Somalia, and November–April for Kenya, Uganda, Rwanda, Burundi, and Tanzania.

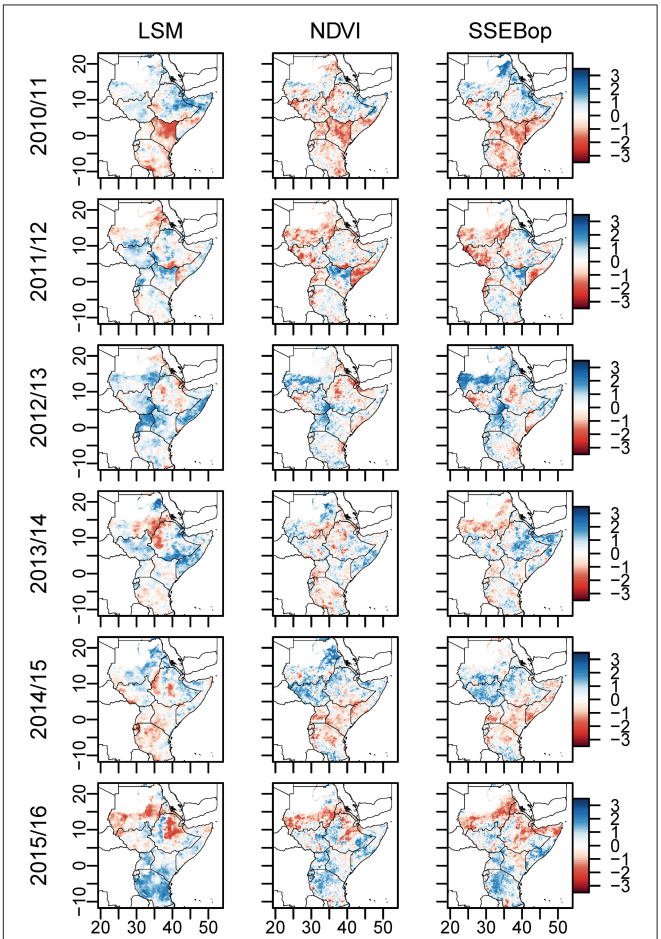

FIGURE 4 | Standardized anomaly composites of LSM ET, NDVI, and SSEBop ET over the wetter half of the year for the period 2011–2016. May–October for Sudan, South Sudan, Ethiopia, Eritrea, Djibouti, and Somalia, and November–April for Kenya, Uganda, Rwanda, Burundi, and Tanzania.

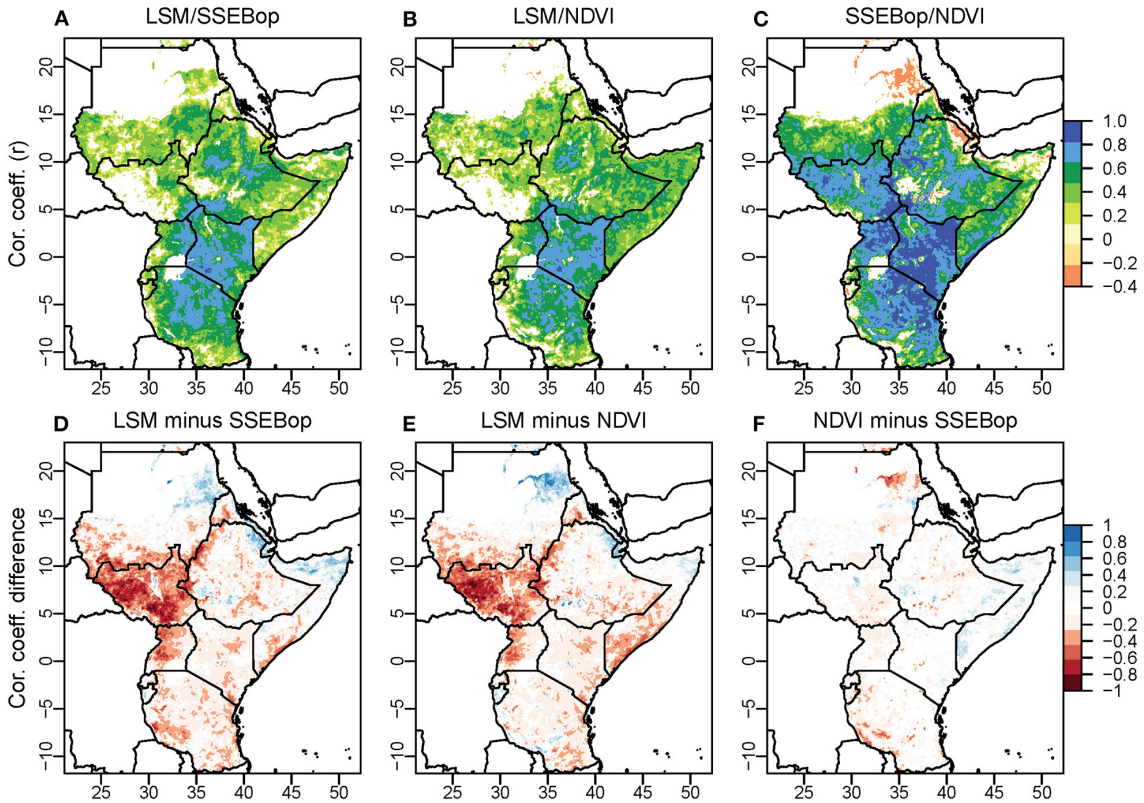

FIGURE 5 | Time series anomaly cross-correlation coefficient calculated over the wetter half of the year for 2003–2016 for **(A)** LSM ET/SSEBop ET, **(B)** LSM ET/NDVI, and **(C)** SSEBop ET/NDVI. **(D)** The difference in anomaly cross-correlation where blue (red) shading indicates LSM ET/NDVI correlation is greater (less) than NDVI/SSEBop ET correlation. **(E)** The difference in anomaly cross-correlation where blue (red) shading indicates LSM ET/SSEBop ET correlation is greater (less) than NDVI/SSEBop ET correlation. Only pixels that exhibit a statistically significant correlation at 90% confidence interval are shown ($p < 0.1$). **(F)** The difference in anomaly cross-correlation where blue (red) shading indicates LSM ET/SSEBop ET correlation is greater (less) than LSM ET/NDVI correlation.

RESULTS

Annual ET

The annual total ET (in mm) that reflects the period 2003–2016 is shown in **Figure 2** for the LSMs and for SSEBop ET. The annual total ET values over the land surface (top row in **Figure 2**) are generally highest across the Inter-Tropical Convergence Zone (ITCZ) and over the Ethiopian Highlands. In contrast, low ET can be seen over Somalia. The spatial distribution of annual ET resembles the annual rainfall gradient in the region, which is mostly determined by surface heating and confluence of the tropical easterlies (Novella and Thiaw, 2013). A CHIRPS-based rainfall gradient map over East Africa is available in Figure 2A of Fenta et al. (2017).

Over the region, high annual ET values of over 1,400 mm are found in the southern part of the Ethiopian Highlands. High ET of around 1,000 mm per year is also found in southwestern South Sudan and adjacent areas of Lake Victoria in Uganda and Kenya. Besides the desert areas, parts of southern Sudan, the leeward side of the Ethiopian Highlands, eastern Somalia, and Kenya produce ET below 200 mm per year. The spatial distributions of annual total ET for the three models are similar. The correlation coefficient between Noah, VIC, and CLSM ET are greater than 0.8 with $P < 0.1$ across the study area. At country level, the average correlation coefficient is even greater (**Table 2**) between these LSM ET. The similar spatial resemblance of Noah, VIC, and CLSM ET further justifies use of their ensemble mean. A difference map between the LSM ensemble mean ET and SSEBop ET is shown in **Figure 2H** along with differences between SSEBop ET and individual LSM (Noah, VIC, CLSM) ET in **Figures 2E–G**.

Spatial Anomaly Comparison

Bearing in mind the predominantly arid conditions of the study region, we evaluated the performances of these variables in identifying vegetation conditions during different hydrologic regimes. To do so, we mapped the standardized seasonal anomaly composites of ET and NDVI over the wetter half of the year for the last 12 years from the time series (2004/05 to 2015/16). We used standardized anomalies because of the differences in units for ET and NDVI. The seasonal anomaly maps are presented in **Figure 3** for the 2004/2005 to 2009/2010 seasons and in **Figure 4** for the 2010/2011 to 2015/2016 seasons. The seasonal anomalies were computed over May to October over Sudan, South Sudan, Ethiopia, Eritrea, Djibouti, and Somalia; and over November to April over Kenya, Uganda, Rwanda, Burundi, and Tanzania.

The droughts of 2004/2005 and 2009/2010 due to failed rainfall (McNally et al., 2016) have been well-captured in LSM ET,

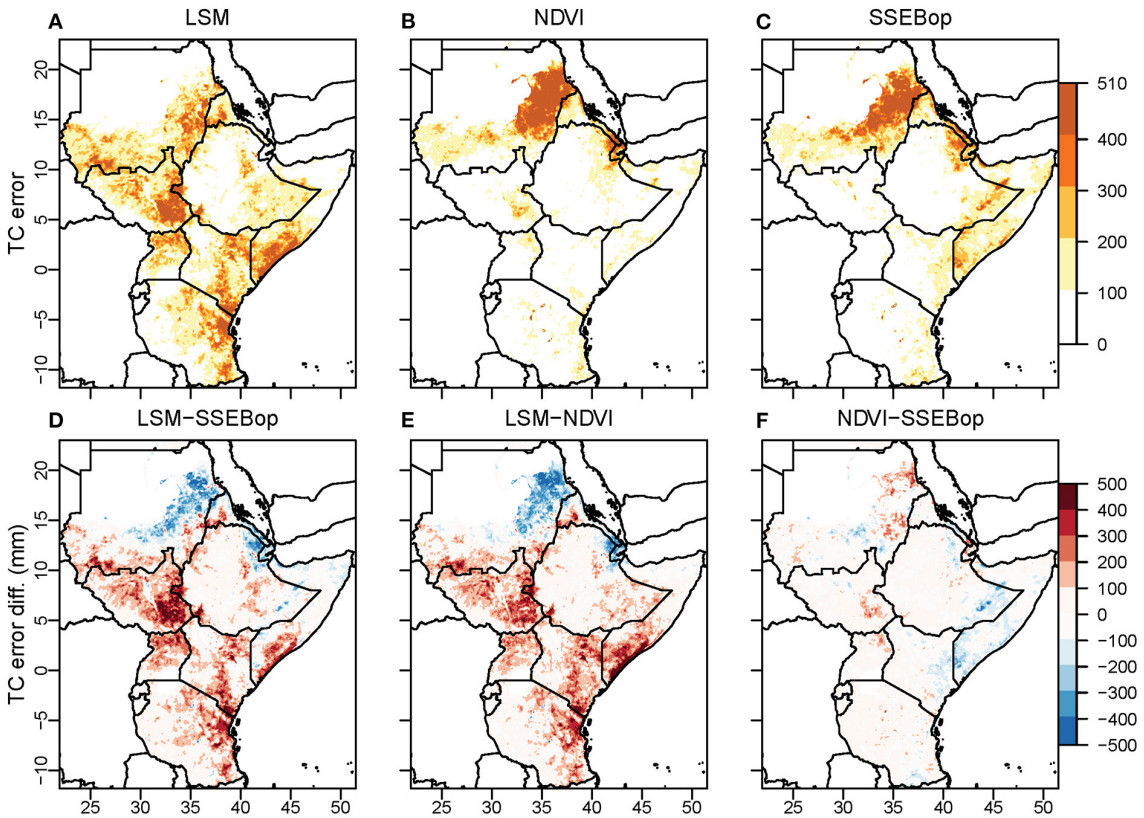

FIGURE 6 | Triple Collocation (TC) error estimates (in mm) over the 2003–2016 for **(A)** LSM ET, **(B)** NDVI, and **(C)** SSEBop ET. LSM ET and NDVI have been rescaled to SSEBop ET. The difference in TC error between **(D)** LSM ET and SSEBop ET, **(E)** LSM ET and NDVI, **(F)** SSEBop ET and NDVI.

SSEBop ET, and NDVI. The extreme severity of the 2004 drought over eastern Ethiopia, Somalia and the 2009/2010 drought over South Sudan have been particularly well-depicted by LSM ET (Gebremeskel et al., 2019), while the 2010/2011 drought over Somalia and Kenya (Robinson et al., 2019) has been well-portrayed by all three variables. Conversely, healthy to average vegetation condition of 2006/2007 due to the wettest rainfall season since 1982 across the region has been better reflected in all three variables.

More recently, the 2015/2016 El Niño caused a dramatic decrease in rainfall, especially over Ethiopia and Sudan, resulting in severe drought (Qu et al., 2019), which has been well-identified in LSM ET. While a coherent condition is portrayed by LSM ET, NDVI, and SSEBop ET during the anomalously dry or wet years, they tend to differ slightly during some hydrologically average years. For example, during 2008/2009 LSM ET differs from NDVI and SSEBop ET over South Sudan by showing below average conditions, and in 2011/2012 LSM ET shows above average conditions over the same area while NDVI and SSEBop ET show below average conditions.

Temporal Anomaly Correlation

Figure 5 shows the temporal cross-correlation between the anomalies of the variables (between LSM ET and SSEBop ET in **Figure 5A**, between LSM ET and NDVI in **Figure 5B**, and between SSEBop and NDVI in **Figure 5C**) using monthly composites during the wetter half of the year for the period 2003–2016. This provides information about the temporal correlation between two datasets and yields a measure of skill for either LSM ET, SSEBop, or NDVI relative to each other. Only the pixels that have a statistically significant correlation coefficient at 90% confidence interval ($P < 0.1$) are shown on the maps in **Figure 5**. In general, LSM shows good temporal agreement with SSEBop or NDVI over Ethiopian Highlands, Kenya, Uganda, and central Tanzania, but poor performance over South Sudan and southern Somalia. In contrast, SSEBop ET is strongly correlated with NDVI across much of the area. LSM exhibits statistically significant r values over 67% of the pixels, while NDVI shows statistically significant correlation over 77% of the pixels with SSEBop. LSM also exhibits statistically significant correlation with NDVI over 72% of the pixels. Although SSEBop shows better correlation with NDVI than LSM ET, portions of the study area are associated with statistically significant negative correlation between SSEBop and NDVI. These results relate with findings of Joiner et al. (2018) based on weekly climatology composites of fraction of potential ET and NDVI over East Africa. The same study also suggests up to 2 weeks of time lag in NDVI response. However, we have observed, when NDVI is summarized to monthly scale, the lag becomes less evident for the relationships between NDVI and ET over East Africa.

Figures 5D–F shows differences in temporal cross-correlation between the variables, comparing correlation computed between

them. **Figure 5D** shows the difference in correlation between LSM/NDVI and SSEBop/NDVI. Blue shading denotes pixels where LSM is more strongly correlated and red shading denotes pixels where SSEBop is more strongly correlated with NDVI, highlighting regions where each variable shows relative advantages and disadvantages. Similarly, in **Figure 5E**, blue shading shows pixels where LSM ET is more strongly correlated with SSEBop ET and red shading indicates pixels where NDVI is more strongly correlated with SSEBop ET. It can be inferred that LSM ET is not a good indicator of vegetation conditions over South Sudan.

TC Analysis

The spatial distributions of relative error estimates computed using **Equations (3–5)** for LSM ET, NDVI, and SSEBop ET are shown in **Figure 6**. The TC error values are relative to SSEBop ET and are shown in millimeters as the LSM ET and NDVI have been linearly scaled to SSEBop ET as required by the TC computation. The domain-averaged relative TC errors are observed to be 130 mm for the LSM ET and 93 mm for SSEBop ET.

Although the domain-averaged TC errors are relatively low, there are substantial differences in spatial distribution of the errors within the study area. LSM ET shows high TC error over South Sudan, southern Somalia, and eastern Tanzania; NDVI shows high TC error over eastern Sudan; and SSEBop shows high TC error over eastern Sudan and the border region between Kenya and Somalia. **Figures 6D–F** shows the difference in TC errors between LSM, NDVI, and SSEBop to highlight areas of high and low TC errors by each variable. The red shaded pixels in **Figures 6D,E** denote where LSM has higher TC error and the blue shaded pixels where LSM has lower TC errors compared to TC errors in SSEBop and NDVI. It also becomes clear that the areas of positive LSM TC errors are similar to the areas where LSM did not correlate well with SSEBop or NDVI and vice versa (**Figures 5D,E**). These similarities indicate that both TC error and cross-correlation techniques are providing qualitatively similar information. Similar findings are also reported by Hain et al. (2011) while comparing three different soil moisture datasets in the U.S.

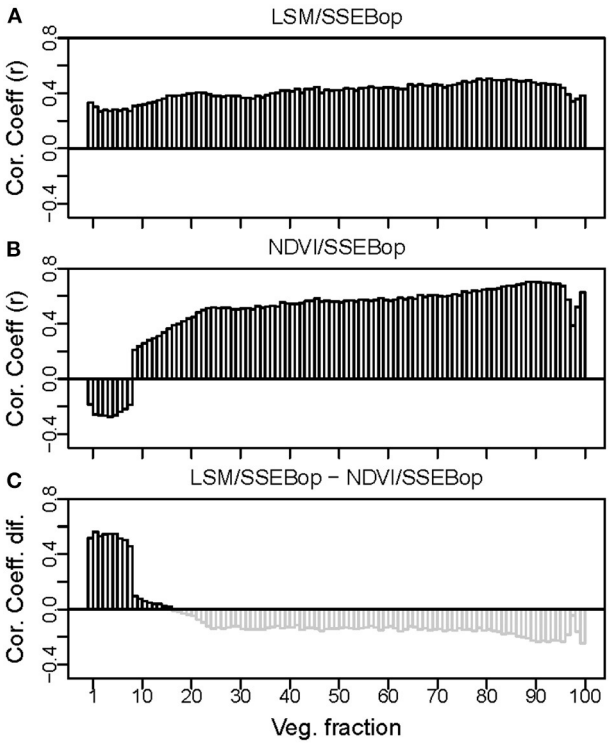

FIGURE 7 | The cross-correlation coefficient for the 2003–2016 as a function of vegetation fraction for **(A)** LSM ET/SSEBop ET, **(B)** NDVI/SSEBop ET, and **(C)** the difference in correlation between LSM ET/SSEBop ET and NDVI/SSEBop ET.

DISCUSSION

Both LSM ET and SSEBop ET show similar spatial patterns in annual total ET distribution but are not identical in magnitude. The high LSM or SSEBop ET along the ITCZ and Ethiopian Highlands can be attributed to the intense surface heating and high precipitation amounts over the Ethiopian Highlands. All the models agree well with very low ET over the arid regions of eastern Ethiopia and Somalia. Precipitation is very low over these regions because of the cool air ventilated from the western Indian Ocean where sea surface temperatures are low along with cool ocean currents adjacent to the East Africa land area (Yang et al., 2015), rendering as poor vegetative growth. ET from VIC tends to show higher estimates than SSEBop and the other two models, especially over the Ethiopian Highlands. Over southern Somalia, encompassing the catchments of the Juba and Shabelle Rivers and central South Sudan, all the LSMs tend to underestimate ET. SSEBop ET obtains its measurement based on radiometric temperature differences between theoretical hot and cold pixels. The radiometric temperatures vary depending on the amount of vegetation present. Typically, the higher the vegetation presence, the lower the surface temperature over well-watered locations because of the cooling effect of ET. Therefore, the performance in ET computation is expected to increase with increasing vegetation cover as the processes integrate both the effects of surface evaporation and plant transpiration. Thus, SSEBop ET could be more responsive to changes in the presence of vegetation cover than the LSM ET. The spatial resolution difference between LSM ET and SSEBop ET could also have played a role in resolving energy balance while estimating ET.

It can be inferred from **Figures 3**, **4** that ET from both LSM and remote sensing measurements could be better indicators of vegetation conditions during extreme drought events (e.g., in the years 2004/2005, 2009/2010, and the El Niño year of 2015/2016). Because they are mostly driven by surface energy balance, they are more sensitive to higher atmospheric demand due to higher temperatures and lower soil moisture, which relates to lack of rainfall during extreme drought events. Conversely, NDVI could be a better indicator of vegetation conditions during wetter than normal conditions because it is more sensitive to availability of water due to higher than normal rainfall conditions (e.g., the year of 2006/2007).

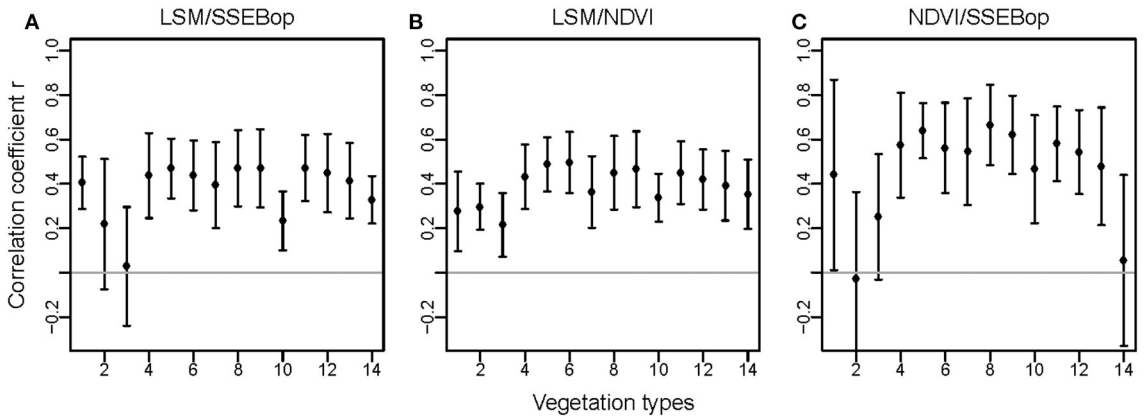

FIGURE 8 | The average correlation for the 2003–2016 by IGBP land cover types for **(A)** LSM ET/SSEBop ET, **(B)** LSM ET/NDVI, and **(C)** NDVI/SSEBop ET.

While LSM ET correlates positively with SSEBop ET and NDVI over a majority of the study area, some areas had negative correlation between SSEBop and NDVI. These areas of negative correlation collocate with both dense and sparsely vegetated areas (**Figure 5C**). This can be attributed to the issues in NDVI due to signal saturation over densely vegetated areas and high noise-to-signal ratio over areas where the presence of vegetation is very low (Huete, 1988). To investigate these further, we plotted the average correlation as a function of vegetation fraction and type in **Figures 7**, **8**, respectively. The cross-correlation does not vary between LSM ET and SSEBop ET with the increase of vegetation presence, but it increases between SSEBop ET and NDVI. This means that SSEBop ET and NDVI are more influenced by vegetation cover than it is for LSM ET (**Figure 7B**). On the other hand, the correlation between LSM ET and SSEBop ET is better over vegetation fraction <18% (**Figure 7C**). NDVI suffers from high noise-to-signal ratio over areas with high albedo (low vegetation cover) and SSEBop ET utilizes a correction factor to adjust surface temperature while computing ET fraction over high albedo areas (Senay et al., 2013). The correction process might have helped correlate SSEBop ET better with LSM ET than with NDVI over sparsely vegetated areas. The average correlation by land cover types also confirms that neither SSEBop ET nor NDVI performs well over evergreen and deciduous broadleaf as well as barren/sparsely vegetated land cover types (**Figure 8C**). This implies that LSM ET could be a better indicator for vegetation condition over sparsely vegetated areas. Over moderately vegetative areas (vegetation fraction of $>$ 20%), a consistent correlation ($r > 0.5$) can be observed between ET and NDVI at the monthly time scale, which implies that any of these variables could be a good indicator of vegetation condition over moderately vegetated areas. A similar pattern of correlation between ET and NDVI is also reported by Mbatha and Xulu (2018) during 2002–2016 over southern Africa.

As with the cross-correlations between the variables, the spatial variability of the random error values during the rainy season for each variable has been evaluated as a function of the vegetation fraction (**Figure 9**). The plots show that the random errors in LSM ET are lower than the random errors in SSEBop ET over low-density vegetated areas (vegetation fraction of 40% or less). When the vegetation fraction increases, the error in LSM gradually increases, but again decreases for the very high end of the vegetation fraction (95% or more) (**Figure 9A**). As a remotely sensed surface temperature–based estimation of SSEBop ET, it is expected that the accuracy of the estimate would decrease over areas of dense vegetation mostly due to inaccuracies in remotely sensed surface temperature data over high densely vegetated areas. Compared to NDVI errors, LSM ET errors are lower over the low (20% or lower) end of the vegetation fraction and the errors start to decrease for LSM ET as the vegetation fraction increases toward full coverage (95% or higher). **Figure 9C** shows that NDVI might have the most error over the low and high ends of the vegetation fraction areas and therefore may not be a good variable for vegetation monitoring over these areas. Over these areas, LSM ET is most likely to provide better information for vegetation monitoring. These results are also consistent with correlation analysis (**Figure 7**), which indicates that LSM ET shows better correlations compared to other two data sources over the low-density vegetated areas.

To further investigate the random errors by vegetation type, we plotted average TC error for each variable as a function of vegetation type in **Figure 10**. Only a few pixels belong to evergreen needleleaf forest (type 1), permanent wetland (type 10), and urban built-up (type 12) areas in the study area; therefore, they may not be a true representation of the TC errors. Among other land cover types, LSM ET has lower TC error over cropland and barren/sparsely vegetated areas compared to TC error in SSEBop ET and NDVI. For the remaining land cover types, TC errors in LSM ET are higher than those in SSEBop ET or NDVI. More specifically, LSM ET TC errors are higher over the savanna and woody savanna land cover types collocated in South Sudan. This could be due to vegetation parameterization differences in LSM ET.

Finally, we compiled the TC errors for each pixel to identify the variable with the lowest random error. The map in **Figure 11**

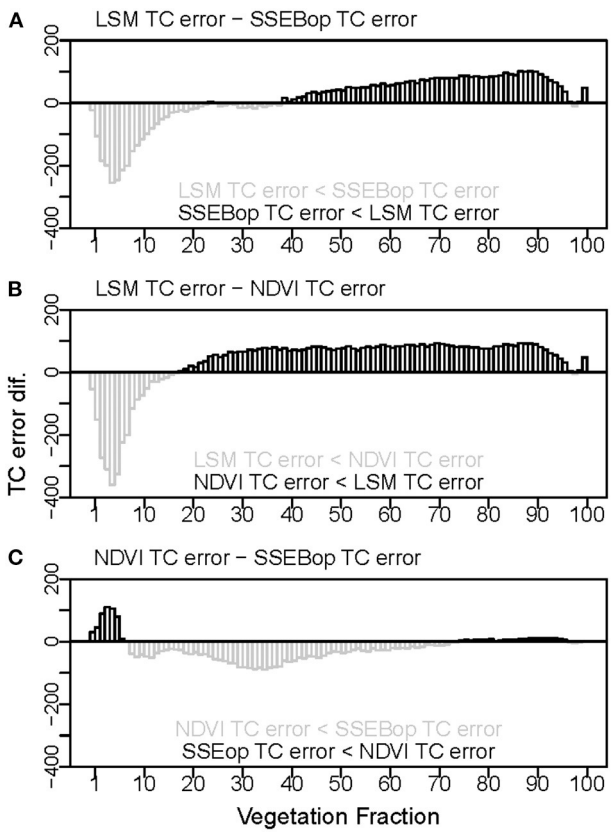

FIGURE 9 | Average TC error difference as a function of vegetation fraction for **(A)** LSM ET TC error minus SSEBop ET TC error, **(B)** LSM ET TC error minus NDVI TC error, and **(C)** NDVI TC error minus SSEBop ET TC error.

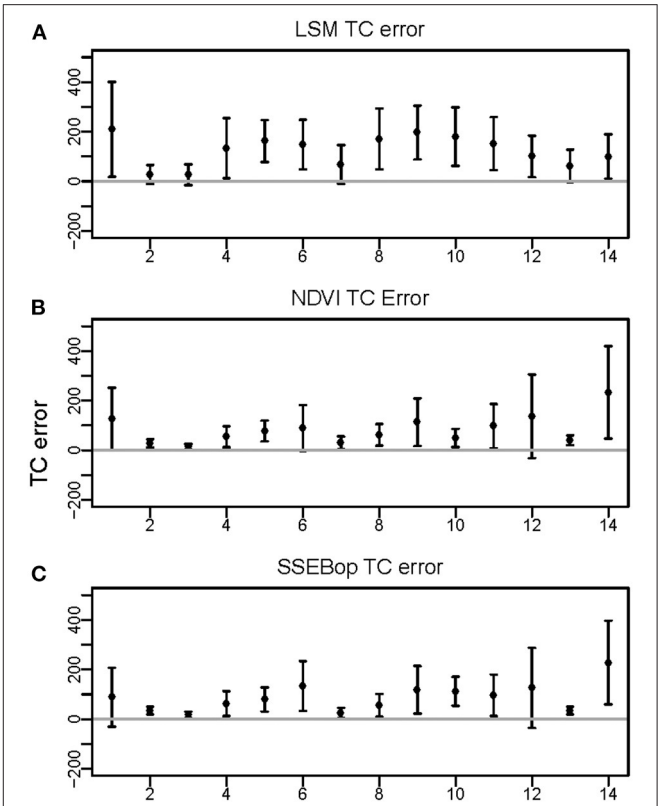

FIGURE 10 | Average TC error by land cover type for **(A)** LSM ET TC error, **(B)** NDVI TC error, and **(C)** SSEBop ET TC error. The corresponding vegetation type for the numbers along the x-axis are shown in **Table 1**.

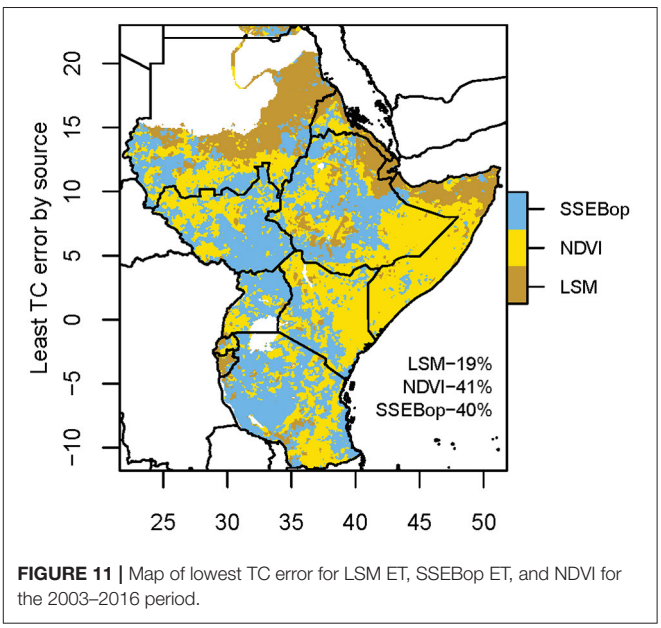

FIGURE 11 | Map of lowest TC error for LSM ET, SSEBop ET, and NDVI for the 2003–2016 period.

shows the lowest TC error by variable for each pixel. Based on this map, NDVI would provide better information for vegetation monitoring over 41% of the study area, mostly covering parts of Ethiopia, Somalia, and eastern Kenya. SSEBop would provide better information over 40% of the study area, covering the Ethiopian Highlands, South Sudan, western Kenya, Uganda, and Tanzania, and LSM ET would provide better information for monitoring vegetation condition over 19% of the study area, mostly covering areas in Sudan, parts of Somalia, Eritrea, and Ethiopia. This map can be used as a guide along with other ancillary socio-economic information by analysts to optimize vegetation monitoring using both ET and NDVI for drought and food security assessments.

CONCLUSIONS

We performed cross-correlation and triple collocation analyses to characterize relationships between ET from remotely sensed measurements (SSEBop) and from LSMs (Noah, VIC, and CLSM) and a biophysical variable directly computed from surface reflectance measured by satellite sensors, NDVI. In general, SSEBop ET and LSM ET show good spatial agreement in annual total ET distribution following the annual precipitation gradient in East Africa. However, there are differences in magnitude between them. LSM ET and SSEBop ET were found to be better indicators for vegetation monitoring during the extreme

drought events, while NDVI could provide better information for vegetation conditions during wetter than normal conditions. Spatially, LSM ET correlates reasonably well with NDVI and SSEBop ET over most of the study area except over South Sudan and southern Somalia, whereas SSEBop ET and NDVI show relatively better agreement over southern Somalia. Correlations between the variables suggest that LSM ET could be a better indicator for vegetation condition over sparsely vegetated areas, while any of these variables could be a good indicator of vegetation condition over moderately vegetated areas. The TC error estimation technique estimated relative random error in LSM ET, SSEBop ET, and NDVI. The errors of these variables suggest that NDVI might have the most error over the low and high ends of the vegetation fraction areas and therefore may not be a good variable for vegetation monitoring over these areas. Over these areas, LSM ET is most likely to provide important information for vegetation monitoring. Finally, a map was produced by compiling the lowest random error by variable that can be used in optimizing vegetation monitoring by using LSM ET, SSEBop ET, and NDVI over the areas where they perform the best. The map would be useful especially over the extremely dry landscapes of Djibouti and parts of arid and semi-arid lands of Somalia, Ethiopia, and northern and eastern Kenya where very high reflectance of sandy soils poses critical challenges in comprehensive monitoring of vegetation conditions. As NDVI emphasizes vegetation conditions from water supply perspective and ET emphasizes vegetation conditions from water demand, perhaps a ratio of NDVI and ET could also be explored for comprehensive vegetation monitoring. While this study provides a framework for optimizing vegetation monitoring for drought and food security assessments over East Africa, the framework can be adopted to optimize vegetation monitoring over any other drought and food insecure regions of the world.

DATA AVAILABILITY STATEMENT

Publicly available datasets were analyzed in this study. This data can be found at: https://earlywarning.usgs.gov; http://disc.sci.gsfc.nasa.gov/uui/datasets?keywords=FLDAS; https://earthdata.nasa.gov/search?q=igbp+land+cover.

AUTHOR CONTRIBUTIONS

SP and AM conceptualized the research. SP defined the methods, analyzed the findings, composed the figures, and drafted the manuscript. KA drafted and provided CLSM data. AM, KA, and MB provided additional analysis. All authors revised and improved the manuscript.

FUNDING

This research was supported by the U.S. Agency for International Development (USAID) Famine Early Warning Systems Network Interagency agreement with the U.S. Geological Survey, USAID Interagency Agreement with NASA Goddard and NASA Harvest.

ACKNOWLEDGMENTS

Work performed under USGS contract 140G0119C0001.We sincerely thank Dr. Gabriel Senay and Stefanie Kagone for providing SSEBop ET data and suggestions made throughout the research. We greatly appreciate the astute comments made by the reviewers and technical comments and edits provided by USGS reviewers that helped us to improve the manuscript. Any use of trade, firm, or product names is for descriptive purposes only and does not imply endorsement by the U.S. Government. All the data sources used in this study are publicly available with links in the cited references respectively.

REFERENCES

Alemu, H., Senay, G. B., Kaptue, A. T., and Kovalskyy, V. (2014). Evapotranspiration variability and its association with vegetation dynamics in the Nile Basin, 2002–2011. *Remote Sensing* 6, 5885–5908. doi: 10.3390/rs6075885

Allen, R. G., Tasumi, M., and Trezza, R. (2007). Satellite-based energy balance for mapping evapotranspiration with internalized calibration (METRIC)—model. *J. Irrigat. Drainage Eng.* 133, 380–394. doi: 10.1061/(ASCE)0733-9437(2007)133:4(380)

Anyamba, A., and Tucker, C. J. (2005). Analysis of Sahelian vegetation dynamics using NOAA-AVHRR NDVI data from 1981–2003. *J. Arid Environ.* 63, 596–614. doi: 10.1016/j.jaridenv.2005.03.007

Baruga, C. K., Kim, D., and Choi, M. (2019). A national-scale drought assessment in Uganda based on evapotranspiration deficits from the Bouchet hypothesis. *J. Hydrol.* 580:124348. doi: 10.1016/j.jhydrol.2019.124348

Bastiaanssen, W., Noordman, E., Pelgrum, H., Davids, G., Thoreson, B., and Allen, R. (2005). SEBAL model with remotely sensed data to improve water-resources management under actual field conditions. *J. Irrigat. Drainage Eng.* 131, 85–93. doi: 10.1061/(ASCE)0733-9437(2005)131:1(85)

Bastiaanssen, W. G., Menenti, M., Feddes, R., and Holtslag, A. (1998). A remote sensing surface energy balance algorithm for land (SEBAL). 1. Formulation. *J. Hydrol.* 212, 198–212. doi: 10.1016/S0022-1694(98)00253-4

Biggs, T., Petropoulos, G., Velpuri, N., Marshall, M. H., Glenn, E., Nagler, P., et al. (2015). "Remote sensing of actual evapotranspiration from croplands," in *Remote Sensing of Water Resources, Disasters, and Urban Studies*, ed P. S. Thenkabail (Boca Raton, FL: Taylor & Francis), 59–100.

Bosilovich, M. G., Akella, S., Coy, L., Cullather, R., Draper, C., Gelaro, R., et al. (2015). *MERRA-2: Initial Evaluation of the Climate.* Vol. 43. NASA Technical Report. Series on Global Modeling and Data Assimilation, NASA/TM–2015-104606. Available online at: https://gmao.gsfc.nasa.gov/pubs/docs/Bosilovich803.pdf (accessed November 10, 2019).

Brown, M. E. (2016). Remote sensing technology and land use analysis in food security assessment. *J. Land Use Sci.* 11, 623–641. doi: 10.1080/1747423X.2016.1195455

Broxton, P. D., Zeng, X., Scheftic, W., and Troch, P. A. (2014). A MODIS-based global 1-km maximum green vegetation fraction data set. *J. Appl. Meteorol. Climatol.* 53, 1996–2004. doi: 10.1175/JAMC-D-13-0356.1

Chen, F., Mitchell, K., Schaake, J., Xue, Y., Pan, H. L., Koren, V., et al. (1996). Modeling of land surface evaporation by four schemes and comparison with FIFE observations. *J. Geophys. Res. Atmos.* 101, 7251–7268. doi: 10.1029/95JD02165

Chirouze, J., Boulet, G., Jarlan, L., Fieuzal, R., Rodriguez, J., Ezzahar, J., et al. (2013). Inter-comparison of four remote sensing based surface energy balance methods to retrieve surface evapotranspiration and water stress of irrigated

fields in semi-arid climate. *Hydrol. Earth Syst. Sci. Disc.* 18, 1165–1188. doi: 10.5194/hessd-10-895-2013

Csiszar, I., and Gutman, G. (1999). Mapping global land surface albedo from NOAA AVHRR. *J. Geophys. Res. Atmos.* 104, 6215–6228. doi: 10.1029/1998JD200090

Dinku, T., Ceccato, P., and Connor, S. J. (2011). Challenges of satellite rainfall estimation over mountainous and arid parts of east Africa. *Int. J. Remote Sensing* 32, 5965–5979. doi: 10.1080/01431161.2010.499381

Dirmeyer, P. A., Gao, X., Zhao, M., Guo, Z., Oki, T., and Hanasaki, N. (2006). GSWP-2: Multimodel analysis and implications for our perception of the land surface. *Bullet. Am. Meteorol. Soc.* 87, 1381–1398. doi: 10.1175/BAMS-87-10-1381

Du, L., Tian, Q., Yu, T., Meng, Q., Jancso, T., Udvardy, P., et al. (2013). A comprehensive drought monitoring method integrating MODIS and TRMM data. *Int. J. Appl. Earth Observ. Geoinform.* 23, 245–253. doi: 10.1016/j.jag.2012.09.010

Fenta, A. A., Yasuda, H., Shimizu, K., Haregeweyn, N., Kawai, T., Sultan, D., et al. (2017). Spatial distribution and temporal trends of rainfall and erosivity in the Eastern Africa region. *Hydrol. Process.* 31, 4555–4567. doi: 10.1002/hyp.11378

FEWSNET (2019). *Famine Early Warning Systems Network*. FEWS NET. Available online at: https://earlywarning.usgs.gov/fews/product/134 (accessed June 6, 2019).

Fisher, J. B., Tu, K. P., and Baldocchi, D. D. (2008). Global estimates of the land–atmosphere water flux based on monthly AVHRR and ISLSCP-II data, validated at 16 FLUXNET sites. *Remote Sensing Environ.* 112, 901–919. doi: 10.1016/j.rse.2007.06.025

Friedl, M. A., Sulla-Menashe, D., Tan, B., Schneider, A., Ramankutty, N., Sibley, A., et al. (2010). MODIS Collection 5 global land cover: algorithm refinements and characterization of new data sets. *Remote Sensing Environ.* 114, 168–182. doi: 10.1016/j.rse.2009.08.016

Funk, C., Peterson, P., Landsfeld, M., Pedreros, D., Verdin, J., Shukla, S., et al. (2015). The climate hazards infrared precipitation with stations—a new environmental record for monitoring extremes. *Sci. Data* 2:150066. doi: 10.1038/sdata.2015.66

Funk, C., Shukla, S., Thiaw, W. M., Rowland, J., Hoell, A., McNally, A., et al. (2019). Recognizing the Famine Early Warning Systems Network (FEWS NET): over 30 years of drought early warning science advances and partnerships promoting global food security. *Bullet. Am. Meteorol. Soc.* 100, 1011–1027. doi: 10.1175/BAMS-D-17-0233.1

Gebremeskel, G., Tang, Q., Sun, S., Huang, Z., Zhang, X., and Liu, X. (2019). Droughts in East Africa: causes, impacts and resilience. *Earth Sci. Rev.* 193, 146–161. doi: 10.1016/j.earscirev.2019.04.015

Glenn, E. P., Huete, A. R., Nagler, P. L., Hirschboeck, K. K., and Brown, P. (2007). Integrating remote sensing and ground methods to estimate evapotranspiration. *Crit. Rev. Plant Sci.* 26, 139–168. doi: 10.1080/07352680701402503

Gruber, A., Su, C.-H., Zwieback, S., Crow, W., Dorigo, W., and Wagner, W. (2016). Recent advances in (soil moisture) triple collocation analysis. *Int. J. Appl. Earth Observ. Geoinform.* 45, 200–211. doi: 10.1016/j.jag.2015.09.002

Gutman, G., and Ignatov, A. (1998). The derivation of the green vegetation fraction from NOAA/AVHRR data for use in numerical weather prediction models. *Int. J. Remote Sensing* 19, 1533–1543. doi: 10.1080/014311698215333

Hain, C. R., Crow, W. T., Mecikalski, J. R., Anderson, M. C., and Holmes, T. (2011). An intercomparison of available soil moisture estimates from thermal infrared and passive microwave remote sensing and land surface modeling. *J. Geophys. Res. Atmos.* 116:JD015633. doi: 10.1029/2011JD015633

Hansen, M., DeFries, R., Townshend, J. R., and Sohlberg, R. (2000). Global land cover classification at 1 km spatial resolution using a classification tree approach. *Int. J. Remote Sensing* 21, 1331–1364. doi: 10.1080/014311600210209

Huete, A. R. (1988). A soil-adjusted vegetation index (SAVI). *Remote Sensing Environ.* 25, 295–309. doi: 10.1016/0034-4257(88)90106-X

IGAD (2020). *About the Agriculture and Environment Devision*. Intergovermental Authority for Development. Available online at: https://igad.int/about-igad/49-about-us/95-about-the-agriculture-and-environment-devision (accessed June 15, 2020).

Jenkerson, C. B., Maiersperger, T., and Schmidt, G. (2010). *eMODIS: A user-friendly data source: U.S. Geological Survey Open-File Report 2010–1055*. 10 p. doi: 10.3133/ofr20101055

Joiner, J., Yoshida, Y., Anderson, M., Holmes, T., Hain, C., Reichle, R., et al. (2018). Global relationships among traditional reflectance vegetation indices (NDVI and NDII), evapotranspiration (ET), and soil moisture variability on weekly timescales. *Remote Sensing Environ.* 219, 339–352. doi: 10.1016/j.rse.2018.10.020

Justice, C., Holben, B., and Gwynne, M. (1986). Monitoring East African vegetation using AVHRR data. *Int. J. Remote Sensing* 7, 1453–1474. doi: 10.1080/01431168608948948

Kalma, J. D., McVicar, T. R., and McCabe, M. F. (2008). Estimating land surface evaporation: a review of methods using remotely sensed surface temperature data. *Surveys Geophys.* 29, 421–469. doi: 10.1007/s10712-008-9037-z

Kimosop, P. (2019). Characterization of drought in the Kerio Valley Basin, Kenya using the Standardized Precipitation Evapotranspiration Index: 1960– 2016. *Singapore J. Trop. Geogr.* 40, 239–256. doi: 10.1111/sjtg.12270

Klisch, A., and Atzberger, C. (2016). Operational drought monitoring in Kenya using MODIS NDVI time series. *Remote Sensing* 8:267. doi: 10.3390/rs8040267

Kogan, F. N. (1995). Application of vegetation index and brightness temperature for drought detection. *Adv. Space Res.* 15, 91–100. doi: 10.1016/0273-1177(95)00079-T

Koster, R. D., Suarez, M. J., Ducharne, A., Stieglitz, M., and Kumar, P. (2000). A catchment-based approach to modeling land surface processes in a general circulation model: 1. Model structure. *J. Geophys. Res. Atmos.* 105, 24809–24822. doi: 10.1029/2000JD900327

Kumar, S. V., Reichle, R. H., Peters-Lidard, C. D., Koster, R. D., Zhan, X., Crow, W. T., et al. (2008). A land surface data assimilation framework using the land information system: description and applications. *Adv. Water Resourc.* 31, 1419–1432. doi: 10.1016/j.advwatres.2008.01.013

Lanning, M., Wang, L., Scanlon, T. M., Vadeboncoeur, M. A., Adams, M. B., Epstein, H. E., et al. (2019). Intensified vegetation water use under acid deposition. *Sci. Adv.* 5:eaav5168. doi: 10.1126/sciadv.aav5168

Liang, X., Lettenmaier, D. P., Wood, E. F., and Burges, S. J. (1994). A simple hydrologically based model of land surface water and energy fluxes for general circulation models. *J. Geophys. Res. Atmos.* 99, 14415–14428. doi: 10.1029/94JD00483

Mbatha, N., and Xulu, S. (2018). Time series analysis of MODIS-derived NDVI for the Hluhluwe-Imfolozi Park, South Africa: impact of recent intense drought. *Climate* 6:95. doi: 10.3390/cli6040095

McNally, A., Arsenault, K., Kumar, S., Shukla, S., Peterson, P., Wang, S., et al. (2017). A land data assimilation system for sub-Saharan Africa food and water security applications. *Sci. Data* 4:170012. doi: 10.1038/sdata.2017.12

McNally, A., Shukla, S., Arsenault, K. R., Wang, S., Peters-Lidard, C. D., and Verdin, J. P. (2016). Evaluating ESA CCI soil moisture in East Africa. *Int. J. Appl. Earth Observ. Geoinform.* 48, 96–109. doi: 10.1016/j.jag.2016.01.001

Meza, F. J. (2005). Variability of reference evapotranspiration and water demands. Association to ENSO in the Maipo river basin, Chile. *Glob. Planetary Change* 47, 212–220. doi: 10.1016/j.gloplacha.2004.10.013

Mu, Q., Heinsch, F. A., Zhao, M., and Running, S. W. (2007). Development of a global evapotranspiration algorithm based on MODIS and global meteorology data. *Remote Sensing Environ.* 111, 519–536. doi: 10.1016/j.rse.2007.04.015

Myneni, R. B., Ramakrishna, R., Nemani, R., and Running, S. W. (1997). Estimation of global leaf area index and absorbed PAR using radiative transfer models. *IEEE Trans. Geosci. Remote Sensing* 35, 1380–1393. doi: 10.1109/36.649788

Nicholson, S. E. (1996). A review of climate dynamics and climate variability in Eastern Africa. *Limnol. Climatol. Paleoclimatol. East African Lakes* 2, 25–56. doi: 10.1201/9780203748978-2

Novella, N. S., and Thiaw, W. M. (2013). African rainfall climatology version 2 for famine early warning systems. *J. Appl. Meteorol. Climatol.* 52, 588–606. doi: 10.1175/JAMC-D-11-0238.1

Qu, C., Hao, X., and Qu, J. J. (2019). Monitoring extreme agricultural drought over the Horn of Africa (HOA) using remote sensing measurements. *Remote Sensing* 11:902. doi: 10.3390/rs11080902

Robinson, E. S., Yang, X., and Lee, J.-E. (2019). Ecosystem productivity and water stress in tropical East Africa: a case study of the 2010–2011 drought. *Land* 8:52. doi: 10.3390/land8030052

Sannier, C. A. D., Taylor, J. C., Du Plessis, W., and Campbell, K. (1998). Real-time vegetation monitoring with NOAA-AVHRR in Southern Africa for wildlife

management and food security assessment. *Int. J. Remote Sensing* 19, 621–639. doi: 10.1080/014311698215892

Senay, G. B., Bohms, S., Singh, R. K., Gowda, P. H., Velpuri, N. M., Alemu, H., et al. (2013). Operational evapotranspiration mapping using remote sensing and weather data sets: a new parameterization for the SSEB approach. *JAWRA* 49, 577–591. doi: 10.1111/jawr.12057

Stoffelen, A. (1998). Toward the true near-surface wind speed: error modeling and calibration using triple collocation. *J. Geophys. Res. Oceans* 103, 7755–7766. doi: 10.1029/97JC03180

Tadesse, T., Senay, G. B., Berhan, G., Regassa, T., and Beyene, S. (2015). Evaluating a satellite-based seasonal evapotranspiration product and identifying its relationship with other satellite-derived products and crop yield: a case study for Ethiopia. *Int. J. Appl. Earth Observ. Geoinform.* 40, 39–54. doi: 10.1016/j.jag.2015.03.006

Townshend, J. R., and Justice, C. O. (2002). Towards operational monitoring of terrestrial systems by moderate-resolution remote sensing. *Remote Sensing Environ.* 83, 351–359. doi: 10.1016/S0034-4257(02)00082-2

Townshend, J. R. G., and Justice, C. O. (1986). Analysis of the dynamics of African vegetation using the normalized difference vegetation index. *Int. J. Remote Sensing* 7, 1435–1445. doi: 10.1080/01431168608948946

Van Beek, L., Wada, Y., and Bierkens, M. F. (2011). Global monthly water stress: 1. Water balance and water availability. *Water Resourc. Res.* 47:WR009791. doi: 10.1029/2010WR009791

van der Schalie, R., De Jeu, R., Parinussa, R., Rodríguez-Fernández, N., Kerr, Y., Al-Yaari, A., et al. (2018). The effect of three different data fusion approaches on the quality of soil moisture retrievals from multiple passive microwave sensors. *Remote Sensing* 10:107. doi: 10.3390/rs10010107

Velpuri, N. M., Senay, G. B., Singh, R. K., Bohms, S., and Verdin, J. P. (2013). A comprehensive evaluation of two MODIS evapotranspiration products over the conterminous United States: using point and gridded FLUXNET and water balance ET. *Remote Sensing Environ.* 139, 35–49. doi: 10.1016/j.rse.2013.07.013

Workie, T. G., and Debella, H. J. (2018). Climate change and its effects on vegetation phenology across ecoregions of Ethiopia. *Glob. Ecol. Conserv.* 13:e00366. doi: 10.1016/j.gecco.2017.e00366

Xu, T., Guo, Z., Xia, Y., Ferreira, V. G., Liu, S., Wang, K., et al. (2019). Evaluation of twelve evapotranspiration products from machine learning, remote sensing and land surface models over conterminous United States. *J. Hydrol.* 578:124105. doi: 10.1016/j.jhydrol.2019.124105

Yang, W., Seager, R., Cane, M. A., and Lyon, B. (2015). The annual cycle of East African precipitation. *J. Climate* 28, 2385–2404. doi: 10.1175/JCLI-D-14-00484.1

Zewdie, W., Csaplovics, E., and Inostroza, L. (2017). Monitoring ecosystem dynamics in northwestern Ethiopia using NDVI and climate variables to assess long term trends in dryland vegetation variability. *Appl. Geogr.* 79, 167–178. doi: 10.1016/j.apgeog.2016.12.019

Zhao, W., and Li, A. (2015). A review on land surface processes modelling over complex terrain. *Adv. Meteorol.* 2015:607181. doi: 10.1155/2015/607181

Conflict of Interest: AM and KA were employed by the company, Science Application International Corporation.

The remaining authors declare that the research was conducted in the absence of any commercial or financial relationships that could be construed as a potential conflict of interest.

frontiers in Climate

ORIGINAL RESEARCH
published: 06 July 2021
doi: 10.3389/fclim.2021.693653

Crop Area Mapping in Southern and Central Malawi With Google Earth Engine

Seth Peterson and Greg Husak*

Climate Hazards Center, Department of Geography, University of California, Santa Barbara, Santa Barbara, CA, United States

Agriculture in sub-Saharan Africa consists primarily of smallholder farms of rainfed crops. Historically, satellite data were too coarse to account for the heterogeneity in these landscapes. Sentinel-2 data have improved spectral resolution and much higher spatial resolution (10 m) than previously available satellites with global coverage, such as Landsat or MODIS, making mapping smallholder farms possible. Spectral mixture analysis was used to convert the Sentinel-2 signal into fractions of green vegetation, non-photosynthetic vegetation, soil, and shade endmembers. Very high spatial resolution imagery in Google Earth Pro was used to identify locations of crop and natural vegetation classes, with over 20,000 reference points interpreted. The high temporal resolution of Sentinel-2 (5 days repeat) allows for classification of landcover based on the phenological signal, with natural areas having smoothly varying amounts of photosynthetic vegetation annually, while cropped areas show more abrupt changes, and also the presence of bare soil due to agricultural activity at some point during the year. We summarized the endmember values using monthly medians, extracted values for the reference data points, randomly split them into training and test data sets, and input the training data into the random forests algorithm in Google Earth Engine to map crop area. We divided southern and central Malawi into tiles, and found crop/no crop classification accuracies on the test data for each tile to be between 87 and 93%. The 10 m map of crop area was aggregated to the district level and showed an R^2 of 0.74 with ground-based statistics from the Malawi government and 0.79 with a remotely sensed product developed by the USGS.

Keywords: crop area, Africa, random forests, Google Earth Engine, phenology

OPEN ACCESS

Edited by:
Mphethe Tongwane, Zutari, South Africa

Reviewed by:
Yuan Xue, George Mason University, United States
Yagmur Derin, University of Oklahoma, United States

****Correspondence:***
Seth Peterson
seth@geog.ucsb.edu

Specialty section:
This article was submitted to Climate Services, a section of the journal Frontiers in Climate

Received: *11 April 2021*
Accepted: *11 June 2021*
Published: *06 July 2021*

Citation:
Peterson S and Husak G (2021) Crop Area Mapping in Southern and Central Malawi With Google Earth Engine. Front. Clim. 3:693653. doi: 10.3389/fclim.2021.693653

INTRODUCTION

Climate variability—combined with a lack of resources, social and political instability, pest outbreaks, and other contributing factors—have led to food-insecurity events throughout sub-Saharan Africa, compromising the lives and livelihoods of the most vulnerable populations (Devereux, 2009; Samasse et al., 2018; Funk, 2021). Homegrown food production is a function of crop area and crop yield, but these components are difficult to assess because agricultural statistics in sub-Saharan Africa are known to be inaccurate due to poor organization and data analysis (Devereux, 2009; Carletto et al., 2015). They are also quite coarse, being reported at the administrative unit level for ground-based statistics, and generally, 300–1,000 m pixels for satellite-based maps (Carletto et al., 2015; Samasse et al., 2018). The recent availability of 10 m Sentinel-2 data

in Google Earth Engine (GEE) allows for efficient processing of high spatial resolution data, making high spatial resolution crop area maps over large areas feasible (Chivasa et al., 2017; Samasse et al., 2018; Jin et al., 2019; Amani et al., 2020; Karlson et al., 2020; Kerner et al., 2020; Masiza et al., 2020; Tseng et al., 2020; Verde et al., 2020).

The high temporal (5-days repeat) resolution of Sentinel-2 data allows for the improved observation—and differentiation—of crop and natural vegetation phenology, as well as a higher likelihood of minimizing cloud impacts on the time series (Misra et al., 2020). The high spatial resolution allows for fewer mixed pixels in these landscapes characterized by smallholder farms, which result in mosaics of fields, forests, and pastures, often heterogeneously mixed at even the 30 m Landsat scale, and certainly at the 500 m MODIS scale (Ozdogan and Woodcock, 2006; Samasse et al., 2018; Jin et al., 2019; Misra et al., 2020). The major drawback of small pixel sizes is huge data set size, complicating both data storage/transfer and computational requirements. The use of GEE reduces these requirements because: (1) the data sets are already loaded into GEE; they do not have to be ordered, downloaded, and stored locally, and (2) processing can be done on Google's server cloud, effectively bringing supercomputing to the average user, for free (Gorelick et al., 2017).

Remotely sensed data have been used in agricultural applications since satellites were launched in the early 1970s (Hammond, 1975; MacDonald and Hall, 1980). Opening the Landsat archive to free access in 2008, quasi-daily MODIS data, and high temporal resolution Sentinel-2 data have allowed for techniques that leverage phenology to map crops and produce yield estimates (Lobell, 2013; Wang et al., 2020). The phenology of crops may differ from that of natural areas in many ways, due to growth form, irrigation, harvest, field management, and other factors. As the season progresses, crop areas will show bare soil due to plowing or clearing to prepare the area, followed by a steady increase in green vegetation as crops grow, then some vegetation die-back as crops mature, particularly in seasonal rainfed agriculture areas. Finally, there is a rapid decrease in vegetation amount due to harvest, leading to bare fields with a mix of soil and crop residue. In contrast, natural areas may show different trends. For instance, forested areas may stay green year-round; shrublands may green up earlier than crops or grasslands and stay green longer due to established root systems; grasslands may show similar timing in green up to crops in rainfed agricultural areas, but dry down would be more drawn out due to a lack of harvest, and bare soil likely would not be exposed.

Most of the studies using crop phenology to map crop area use either raw bands, vegetation indices (VIs) such as the Normalized Difference Vegetation Index (NDVI, Rouse et al., 1973), or a combination of the two (Samasse et al., 2018; Jin et al., 2019; Amani et al., 2020; Karlson et al., 2020; Kerner et al., 2020; Masiza et al., 2020; Tseng et al., 2020; Verde et al., 2020). In this study we took a different approach. Spectral mixture analysis (SMA, Roberts et al., 2002) decomposes the signal of a pixel into percentages/fractions of the scene components making up the pixel. These scene components are termed endmembers (EMs), and generally consist of the spectrally distinct constituents: green vegetation (GV), non-photosynthetic vegetation (NPV), soil, and shade. SMA works well on data sets that include broad spectral coverage, such as Landsat or MODIS. The addition of bands on the red edge for Sentinel-2 in comparison to earlier sensors further increases the confidence that SMA produces physically meaningful EM fractions. GV is generally highly correlated with NDVI and other VIs focusing on vegetation greenness [e.g., enhanced vegetation index (EVI, Huete et al., 1997)]. The other three EM fractions provide unique information. This is important, for instance, because a drop in NDVI in a pixel can result from either browning of vegetation (leading to a mixture of GV and NPV) or a partial crop harvest (leading to a mixture of GV and newly exposed soil), and while NDVI cannot distinguish between the two events, SMA can.

Malawi normally receives enough precipitation to produce most of the maize and other crops required to feed its people; there has not been a famine since 2001–2002 (Devereux 2009). However, what makes Malawi an excellent case study are two existing national reference data sets of crop area: (1) district-wide statistics from the Malawi Department of Agriculture, and (2) from a map based on manual interpretation of landcover on a 1 km grid by Gray Tappan of the U.S. Geological Survey (USGS). We also compare our results to two global data sets, from IIASA-IFPRI (Fritz et al., 2015) and a protype map from the European Space Agency (ESA, ESA-CCI, 2021).

MATERIALS AND METHODS

In this study, we used 2018 Sentinel-2 data to map crop area in central and southern Malawi (6752347 ha) at a 10 m pixel resolution. The basic approach was to manually identify reference data points using very high spatial resolution imagery (<1 m), randomly divide that data set into training and testing, extract phenologically-based predictor variables from Sentinel-2 for the training data set, input those predictor variables into random forests (RF) to map crop area, and evaluate classification accuracy, both with the test data set, and in relation to crop area from the two Malawi reference data sets and the two global data sets.

Study Area

Malawi has a population of 19.1 million people, with 9.4 million ha of land area, 3.7 million ha of which are in agriculture according to government statistics obtained through the Famine Early Warning System Network (FEWSNET) data warehouse. We focused on the southern and central regions of the country, as that captures 86% of the crop area of Malawi. Common cash crops include tea, tobacco, and cotton. Common food crops include maize, millet, cassava, sweet potatoes, and legumes. Farmers in Malawi have practically no access to irrigation, and as a result, agriculture is rain fed. Annual precipitation from CHIRPS, a satellite- and station-based product available at 5 km resolution (Funk et al., 2015) varies between 0.9 and 1.2 m across Malawi, with a pronounced seasonal signal (**Figure 1**). Crops are planted in November/December and harvested in April/May. Malawi contains a number of different landforms,

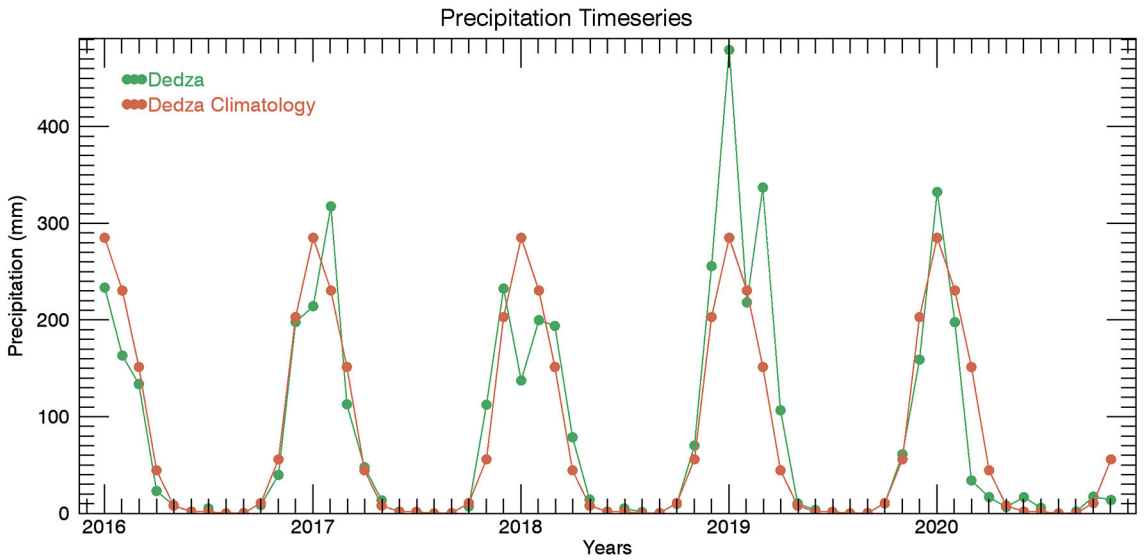

FIGURE 1 | Precipitation (green) and average (2000–2020) monthly precipitation (orange) from CHIRPS for a 5 km pixel in an agricultural part of Dedza District, Malawi, 14.34° S, 34.13° E.

including plateaus, mountains, lakes, and a large river valley, which influence the vegetation type and phenology (**Figure 2**).

Training Data

We divided Malawi into $1^0 \times 1^0$ tiles. This was primarily done for logistical reasons—memory restrictions in GEE. Six tiles covered the bulk of central and southern Malawi, with smaller areas added to cover the remaining portions (**Figure 2**). We classified the landscape into five classes: crop, open water, and three types of natural areas—sparse, shrub, forest—differentiated based on observed canopy cover. Air photo interpretation techniques were applied to very high spatial resolution (1 m pixels or less), true color imagery in Google Earth Pro (GE) to identify thousands of reference points for the crop, sparse, shrub, and forest classes, with fewer points needed for open water (**Table 1**). Points were identified in areas that were homogeneous over at least 20 m. The "show historical data" feature was used to examine all available imagery in GE for evidence of agricultural activity, with most imagery acquired between 2013 and 2020. Examples of different stages of agricultural activity visible in the imagery include fields plowed into regular rows, fields having regular geometric shapes, fields showing different vegetation greenness with linear distinctions—as if harvesting was in progress during image acquisition, and crop residue arranged in linear or circular patterns (**Figure 3**). For natural areas we sought to use imagery from 2017 or 2018 to minimize any possible landcover change effects. In contrast to agricultural areas, natural areas generally showed irregular vegetation canopies, both in terms of canopy shape and spacing between plants. They also do not show linear (man-made) features. Some manually interpreted points were able to be reused for adjacent tiles where landforms (and hence, climate/vegetation) were similar (e.g., Orig and 1N along the shore of Lake Malawi). Training data were added for each tile in an iterative process until the resulting RF classification for the tile did not contain spatially correlated errors. Points from adjacent tiles were always used to make an initial classification for a new tile to speed up the point selection process. For instance, if the initial classification map for a tile showed that forested areas were well-identified using existing training data from other tiles, no new training points were added for that class within the new tile. The reference point files were saved as KMLs and converted to shapefiles for use in GEE. Much of the effort in this research focused on the selection, interpretation, and refining of points used to drive the classification.

Independent Validation Data

The independent validation data used in this study came from four independent sources, the official statistics from the Government of Malawi for 2017, a map derived from interpreted satellite imagery from the USGS from 2017, the global IIASA-IFPRI crop area map from 2005 and the ESA-CCI Sentinel-2-based map from 2016. The Malawi government data consists of the area planted for each of 10–12 crop types at the district level, covering nine districts in central Malawi, and 13 in southern Malawi. The crop areas were summed and divided by the overall area of each district to get percent crop area. It should be noted that the government statistics for crop area may double count a field if it is intercropped with two different crops, hence fractions can be >1.0. The Tappan USGS map relies on expert interpretation of points on a regular 1 km grid, primarily using Landsat and Sentinel-2 data to make a determination of landcover at each point using the Rapid LandCover Mapping tool (Cotillon and Mathis, 2017). A total of 28 landcover classes were used, six of which represented agricultural areas (rainfed herbaceous crops,

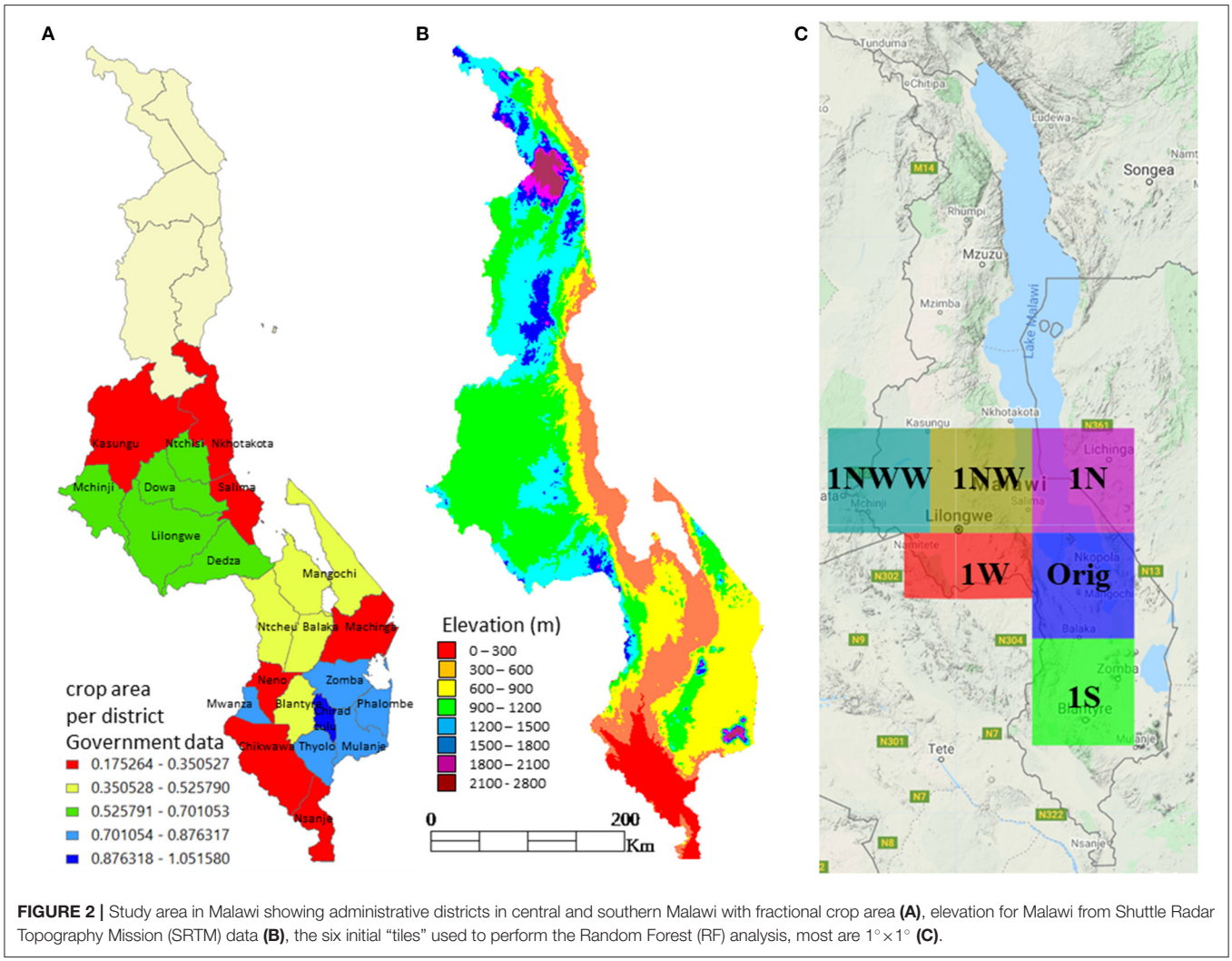

FIGURE 2 | Study area in Malawi showing administrative districts in central and southern Malawi with fractional crop area **(A)**, elevation for Malawi from Shuttle Radar Topography Mission (SRTM) data **(B)**, the six initial "tiles" used to perform the Random Forest (RF) analysis, most are 1°×1° **(C)**.

TABLE 1 | Training points generated in Google Earth Pro.

	Tile							
	Orig	**1S**	**1N**	**1W**	**1NW**	**1NWW**	**1SW, 1SE**	**1SS**
Crop	2,248	2,876	741	1,376	1,323	444	361	20
Sparse	657		207	171	515	272	94	264
Shrub	1,568	3,013	1,016	275	1,327	116		146
Forest	802				737	87		
Water	192							

*The geographical location of the primary six tiles is shown in **Figure 2**. 1SW, 1SE, and 1SS are west, east, and south of tile 1S, respectively.*

cultivated dambo, rice, sugar cane, tea, and tree plantation). The map was converted to binary (presence/absence) of agriculture at the 1 km pixel scale to calculate percent crop area for each district. The IIASA-IFPRI crop area map integrates existing maps from various sources, ranking and weighting them before combining them into the final global 1 km pixel crop area product (Fritz et al., 2015). The ESA-CCI map is derived from Sentinel-2 data and is available at 20 m resolution, it is unpublished and labeled as a prototype but is beginning to be evaluated in the literature (Samasse et al., 2018; Alkhalil et al., 2020).

Predictor Variables

SMA was applied to the 10 m Sentinel-2 time series for central and southern Malawi. We used the Level 1C, top of atmosphere (TOA) reflectance product rather than the Level 2A surface

reflectance product, as all of the Sentinel-2 data are available in this form, allowing us an extra 2 full calendar years in analyses, because the Level 2A data are only available from mid-2017 to present while the Level 1C data begins in October 2015 in Malawi. To identify and filter out clouds, the cloudscore algorithm was used for cloud and cloud shadow masking (Chastain et al., 2019). Due to the use of top of atmosphere reflectance data, we used image EMs, derived from pure Sentinel-2 pixels of maize, senesced vegetation, and bare soil in an agricultural area in central Kenya, where we had an informant who could identify landcover, rather than reference EMs convolved to Sentinel-2 band wavelengths from hyperspectral data. Thus, atmospheric effects are included in the image EM spectra. SMA was performed on each individual Sentinel-2 image in southern and central Malawi in 2018 with the same set of EMs, breaking each pixel of each image down into its components of GV, NPV, soil, and shade. **Table 2** lists the reflectance values used for each EM. For each pixel, the time series of EM fractions were summarized in two different ways: (1) the minimum, maximum, median, and range in values within each bi-monthly time step were calculated for each EM fraction (similar to the Jin et al., 2019 approach), and (2) the monthly median was calculated for each EM fraction (Kerner et al., 2020). Additionally, for each approach we calculated the annual minimum, maximum, median, and range for each EM fraction from the bimonthly/monthly medians. A threshold value of 0.4 for annual GV maximum was used to remove fields that showed evidence of agricultural activity at some point in GE imagery, but were fallow in 2018, from the crop training and test data sets. Even though these distilled datasets contain far less information than the five day repeat Sentinel-2 data, the resulting arrays of EM summary statistics were still very large, on the order of 20 GB per tile.

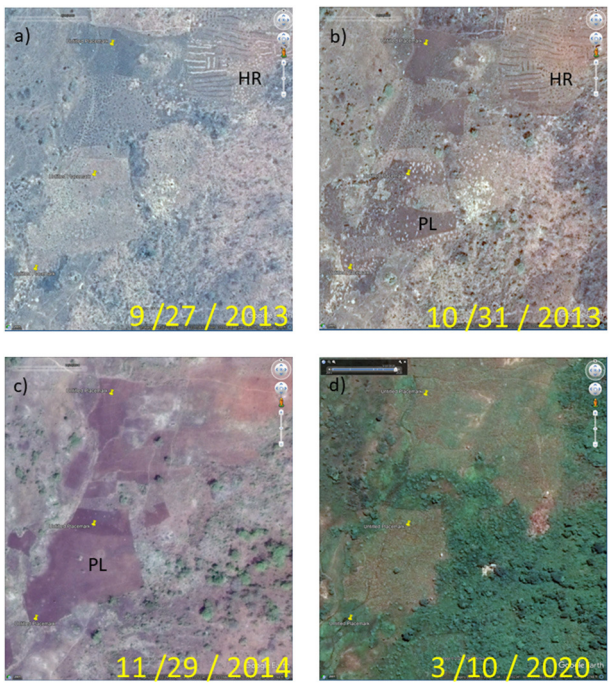

FIGURE 3 | Four different looks in Google Earth Pro at a smallholder agriculture area in east central Malawi near 13.72°S, 35.1°E on 9/27/2013 **(a)**, 10/31/2013 **(b)**, 11/29/2014 **(c)**, and 3/10/2020 **(d)**. Harvest residue (HR) in the north east corner of the 9/27 and 10/31 images identifies this area as cropped. Plowing (PL), exposing dark, smooth soil in 11/29, and to a lesser extent 10/31 identifies this area as cropped. The fine spatial resolution allows for the identification of plant canopies in the southeast portion of the image, the temporal information suggests some of them are evergreen trees, some deciduous shrubs.

Image Classification

In order to work within the computational limitations of GEE, analysis was performed for each tile individually. The first step was to separate the reference data points for each landcover class into training and test data sets. The reference points were split roughly 50/50 into training/test for crop and shrubs, and 80/20 for the remaining, less-populous classes. It is important that the amount of training data per class is roughly equal in order to obtain an accurate map (He and Garcia, 2009). The training points were used to extract training data from the predictor variable array. We used RF to perform the classification analysis. Decision trees use a series of predictor variable splits to divide the dependent variable into more and more homogeneous groups. RF consist of an ensemble of decision trees, where trees are made to differ by changing the subsets of data used to train each tree, and allowing only a subset of the predictor variables to be evaluated at each node. The results from 500 decision trees were aggregated to produce the RF output (classified maps and contingency tables); a large number of trees is suggested to minimize error, with 500 being recommended in the literature (Probst et al., 2019). RF have been shown to perform well for this crop area classification application (Jin et al., 2019). RF were

TABLE 2 | Sentinel-2 top of atmosphere reflectance values for the four endmembers used in this study, green vegetation (GV), non-photosynthetic vegetation (NPV), soil, and shade.

	Sentinel-2 central wavelength (nm)									
Endmember	**490**	**560**	**665**	**705**	**740**	**783**	**842**	**865**	**1,610**	**2,190**
GV	0.0917	0.101	0.056	0.114	0.394	0.507	0.501	0.555	0.214	0.0917
NPV	0.124	0.126	0.158	0.182	0.214	0.24	0.22	0.273	0.376	0.287
Soil	0.136	0.163	0.244	0.256	0.277	0.302	0.296	0.313	0.366	0.317
Shade	0	0	0	0	0	0	0	0	0	0

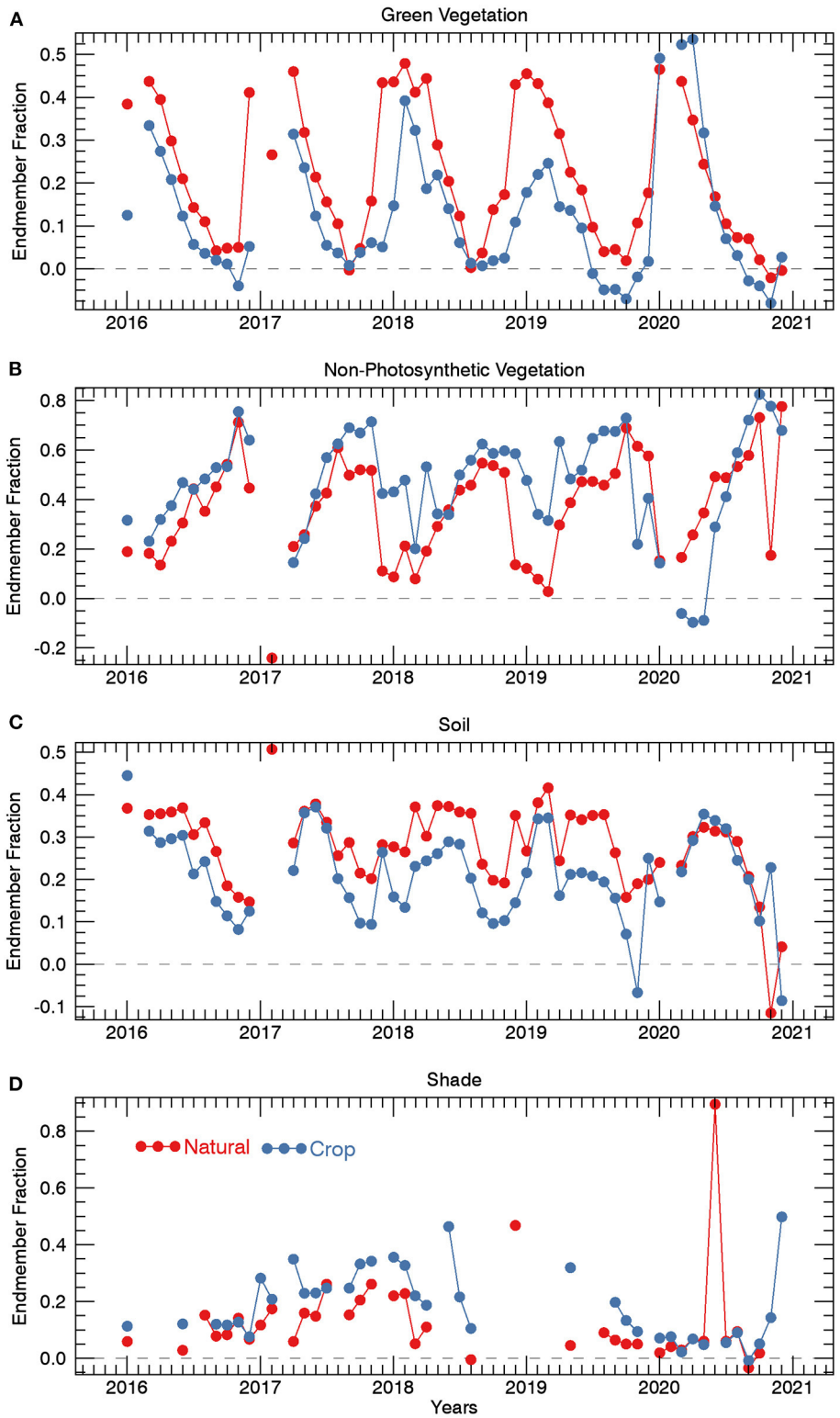

FIGURE 4 | Sample green vegetation (GV) **(A)**, non-photosynthetic vegetation (NPV) **(B)**, soil **(C)**, and shade **(D)** endmember (EM) trajectories for a crop area and a natural area, showing monthly median values.

TABLE 3 | Confusion matrices for the primary six tiles, the geographical location of the tiles is shown in **Figure 2**.

	Crop	Sparse	Shrub	Forest	Water	User's
Orig						
Crop	644	11	103	2	0	0.847368
Sparse	29	109	57	1	0	0.556122
Shrub	86	12	627	13	0	0.849593
Forest	9	2	26	150	0	0.802139
Water	0	0	0	0	47	1
Producer's	0.838542	0.813433	0.771218	0.903614	1	0.817946
1S						
Crop	1,254	19	99	7	0	0.909355
Sparse	30	179	20	0	0	0.781659
Shrub	213	14	1,364	10	0	0.851968
Forest	17	2	19	149	0	0.796791
Water	0	0	0	0	47	1
Producer's	0.828269	0.836449	0.908123	0.89759	1	0.8693
1W						
Crop	849	11	67	2	0	0.913886
Sparse	34	130	83	0	0	0.526316
Shrub	75	12	779	11	0	0.888255
Forest	9	0	31	129	0	0.763314
Water	0	0	0	0	47	1
Producer's	0.877973	0.849673	0.811458	0.908451	1	0.852358
1N						
Crop	925	11	78	0	0	0.912229
Sparse	26	136	68	0	0	0.591304
Shrub	155	17	1,095	14	0	0.854801
Forest	11	1	22	128	0	0.790123
Water	0	0	0	0	47	1
Producer's	0.828111	0.824242	0.866983	0.901408	1	0.852597
1NW						
Crop	406	18	18	1	0	0.916479
Sparse	10	69	9	2	0	0.766667
Shrub	27	16	396	29	0	0.846154
Forest	2	4	23	130	0	0.81761
Water	0	0	0	0	47	1
Producer's	0.91236	0.64486	0.887892	0.802469	1	0.868268
1NWW						
Crop	757	26	30	5	0	0.925428
Sparse	27	172	63	5	0	0.644195
Shrub	52	20	475	38	0	0.811966
Forest	13	9	25	201	0	0.810484
Water	0	0	0	0	47	1
Producer's	0.891637	0.757709	0.801012	0.807229	1	0.840712

run on the training data, developing a model which was then (1) evaluated with the test data and (2) applied to the entire tile to make a map. All of the individual tile maps were then mosaicked, and crop area values for the 22 districts in central and southern Malawi were compared between our analysis, that of the Malawi Department of Agriculture, the Tappan USGS map of crop area in Malawi, the IIASA-IFPRI map, and the ESA-CCI map.

RESULTS

The EM fraction trajectories reflect changes due to plant phenology. To highlight the separability of the different cover types, **Figure 4** shows sample EM trajectories for a crop field and a natural shrubland area, located within 100 m of each other. The GV EM trajectory for the natural area follows precipitation well; green up begins in October, peak greenness occurs between

January and March except for 2017, when the rainfall peak was a month late (**Figure 1**) and the GV peak was in April, and then there is a steady decline as the landscape dries down during the 6 months long dry season (**Figure 4**). Crop greenup is delayed a few months compared to shrub greenup, the timing of peak greenness is later in the season, and the peak is more pronounced than that of the natural area. Finally, there is an extended period of near zero GV values between harvest and planting the following growing season. Negative EM values, while not physically meaningful, occur because SMA is a matrix algebra transform with the constraint that fractions sum to 1.0, and can be interpreted as the absence of that EM for that time step. For this particular example the natural area demonstrated a higher GV fraction than the crop fields throughout 2018, but that is not always the case. NPV for the natural area has an inverse trend to GV, the new green leaves are dominant at the beginning of the season so NPV is low, then the leaves senesce, and woody shrub material and senesced ground cover become more exposed to the satellite, leading to an increase in NPV. A similar pattern is present during the growing season for the crop field, although it appears that harvest residue was left on the field in 2017 and 2018 as NPV remains high during the initial increase in GV for those years. The soil fractions stayed relatively consistent for the two areas in **Figure 4**, showing no evidence of plowing in this particular area, which is consistent with the observation, based on NPV, that harvest residue was left on the soil. Soil fraction was higher for crop areas, likely due to the presence of some exposed soil between crop rows. NPV and soil show more noise than GV, likely due to residual cloud contamination. Shade shows a similar pattern to GV as the landscape absorbs more light (high shade) when it is highly vegetated, and reflects more (low shade) when the ground is bare. Some locations experienced persistent cloud cover during parts of the rainy season, resulting in missing data in the satellite analysis and corresponding gaps in the plots shown in **Figure 4**.

We only present output for the monthly predictor variables (the second method of data distillation), as accuracies were slightly better, and the predictor variable data set was half the size of the bimonthly data set, thus it was more convenient. The overall accuracies when compared with independent test data for the six tiles with the most training data (**Table 1**) were on the order of 85% (**Table 3**). We also show data for classes re-coded to crop/no crop (**Table 4**), which is the more common way that crop area classifications are presented. Accuracies increased 5% for five of the six tiles, with three tiles exhibiting accuracy over 90%. Further analysis of the results in **Tables 3**, **4** show that the user's accuracy for crop tends to be a bit higher than the producer's accuracy, indicating a slight under-identification of agriculture in the model results, and an expected underestimate of the overall cropped area by a small amount. The biggest source of confusion was between crops and shrubs, though more crops were classified as shrub than vice versa (**Table 3**). It may be that the diversity in crop types and or farming intensity is more variable than shrub types, so the crop class is more heterogeneous and thus members of the class are more likely to appear to behave like shrubs.

Table 5 presents the variable importance values for each of the predictor variables for each of the six tiles in **Table 1**, with the top ten variables for each tile in bold. There are a number of interesting features. GV variables were generally most important. The median GV at the beginning of the growing season ranked high, while the median GV for the peak of the growing season (February) showed much lower importance. Natural areas green up earlier than crop areas, with separability being reduced at peak greenness (**Figure 4**). This also points to the advantage of monthly vs. bi-monthly variables as January and February values would have been grouped together, reducing the signal. Natural areas also remain green longer due to enhanced water availability due to established root systems, and this is reflected in high importance scores for GV variables as the season progresses. NPV showed lower importance than GV, though January was in the top ten for three tiles. January soil was also highly important. Also, soil in May, June, and July, while only in top ten importance for the NWW tile, tended to have relatively high importance. Hence, soil was important early in the growing season and during the harvest season when soil may be exposed in crop areas while natural vegetation is largely comprised of GV and NPV (**Figure 4**). Shade variables were second to GV in importance, with July and August being the most important months for four of the tiles. At this time of the year natural vegetation would show canopy shading due to uneven vegetation heights both within individual plants and between neighboring plants while

TABLE 4 | Confusion matrices for the primary six tiles, with the classes aggregated to crop/no crop.

	Crop	No crop	User's
Orig			
Crop	644	116	0.847368
No crop	124	997	0.889384
Producer's	0.838542	0.895777	0.872408
1S			
Crop	1,254	125	0.909355
No crop	260	1,757	0.871096
Producer's	0.828269	0.933581	0.886631
1W			
Crop	849	80	0.913886
No crop	118	1,175	0.908739
Producer's	0.877973	0.936255	0.910891
1N			
Crop	925	89	0.912229
No crop	192	1,481	0.885236
Producer's	0.828111	0.943312	0.895422
1NW			
Crop	406	37	0.916479
No crop	39	678	0.945607
Producer's	0.91236	0.948252	0.934483
1NWW			
Crop	757	61	0.925428
No crop	92	1,008	0.916364
Producer's	0.891637	0.942937	0.920229

*The geographical location of the tiles is shown in **Figure 2**.*

TABLE 5 | Random Forest variable importance measures for the six primary tiles, the geographical location of the tiles is shown in **Figure 2**.

	Variable importance					
Predictor variable	**Orig**	**1S**	**1N**	**1W**	**1NW**	**1NWW**
GV January median	**493**	**933**	**735**	**628**	**653**	**644**
GV February median	373	703	585	471	469	519
GV March median	**492**	**812**	**723**	**633**	**554**	551
GV April median	**494**	**894**	**736**	**637**	**594**	490
GV May median	**464**	811	**730**	**611**	465	551
GV June median	459	**877**	661	556	424	589
GV July median	**512**	**875**	**737**	**627**	508	573
GV August median	438	806	672	555	**538**	**628**
GV September median	424	**828**	646	604	**544**	**620**
GV October median	445	**816**	639	**623**	528	**609**
GV November median	414	777	612	540	532	**626**
GV December median	442	738	630	551	**546**	**642**
NPV January median	**511**	**845**	**712**	609	484	514
NPV February median	356	672	573	478	457	484
NPV March median	399	676	569	556	486	504
NPV April median	388	729	601	519	481	477
NPV May median	384	801	627	522	458	524
NPV June median	412	771	599	537	412	514
NPV July median	**482**	746	671	580	436	496
NPV August median	402	718	660	543	460	473
NPV September median	399	705	623	507	434	509
NPV October median	406	694	591	531	418	502
NPV November median	367	644	582	530	470	511
NPV December median	401	670	600	506	463	490
Soil January median	**472**	791	**780**	**613**	521	521
Soil February median	456	740	679	581	468	512
Soil March median	381	647	551	520	482	545
Soil April median	377	679	574	485	465	544
Soil May median	409	651	629	550	493	**598**
Soil June median	403	682	617	520	457	**623**
Soil July median	405	685	608	517	492	501
Soil August median	376	641	585	499	445	521
Soil September median	368	684	565	441	347	520
Soil October median	338	657	552	432	339	543
Soil November median	353	603	532	429	319	**616**
Soil December median	380	614	578	461	341	510
Shade January median	412	763	634	544	520	592
Shade February median	380	686	595	481	**538**	**595**
Shade March median	396	685	654	555	**535**	503
Shade April median	411	739	581	528	449	503
Shade May median	451	728	687	563	452	577
Shade June median	420	794	628	524	475	563
Shade July median	**522**	**903**	**833**	**693**	501	570
Shade August median	**563**	**846**	**813**	**698**	498	562
Shade September median	453	804	**732**	**613**	504	590
Shade October median	444	763	651	573	500	553
Shade November median	408	681	641	571	490	572
Shade December median	422	704	667	529	496	485
GV annual maximum	455	720	648	596	464	575

(Continued)

TABLE 5 | Continued

	Variable importance					
Predictor variable	**Orig**	**1S**	**1N**	**1W**	**1NW**	**1NWW**
GV annual minimum	405	699	590	599	487	425
GV annual range	407	714	649	564	**607**	518
NPV annual maximum	383	699	604	508	455	505
NPV annual minimum	422	747	663	580	480	377
NPV annual range	422	743	618	554	499	481
Soil annual maximum	447	753	709	604	490	504
Soil annual minimum	424	801	651	566	**543**	371
Soil annual range	441	732	668	589	479	509
Shade annual maximum	425	720	632	577	469	549
Shade annual minimum	418	685	634	588	450	401
Shade annual range	429	747	609	560	503	523

GV refers to green vegetation and NPV is non-photosynthetic vegetation. Values in bold are the top ten most important values for each tile.

harvested crop area would be relatively flat with higher albedo. For the remaining two tiles January was important, for similar reasons—young crops would be too small to cast much in the way of shadows compared to larger natural vegetation. The annual summary variables were generally not of high importance.

We mosaicked the maps from the individual tiles to generate a crop area map for all of southern and central Malawi. Seam lines were not noticeable, likely because the classification models were accurate, so there were not differences across tile boundaries. **Table 6** presents crop area estimates for the different data sources. Agreement in percent crop area at the district level (comparing sets of 22 values) is high for RF, Malawi government, and Tappan USGS data sets. R^2 for fractional crop area at the district level between RF and Malawi government is 0.74, between RF and USGS it is 0.79, and between Malawi government and USGS it is 0.53 (**Table 6**). It is interesting that the relationships between RF and Malawi government and RF and USGS are similar, but the relationship between Malawi government and USGS is lower. The primary differences between the RF map and Malawi government are possible double-counted fields and human error in gathering data, both data sources cover the entire region. Both RF and USGS rely on manual image interpretation to label landcover, but RF uses all of the imagery whereas USGS examined imagery on a 1 km grid. The Malawi government data and USGS map have less in common. The ESA-CCI map shows good agreement with the RF Sentinel-2 map (R^2 of 0.63), however **Figure 5** suggests that the ESA map systematically overpredicts crop area in southern Malawi.

DISCUSSION

Our accuracies compare favorably with the three published studies examining crop area in sub-Saharan African countries at 10 m resolution that we are aware of Kerner et al. (2020), Tseng et al. (2020), and Jin et al. (2019). Kerner et al. (2020) obtained 83% accuracy when classifying crop/no crop in the country of Togo. Jin et al. (2019) obtained 85% accuracy for crop/no crop in Kenya and Tanzania. Tseng et al. obtained 86% accuracy in Kenya. However, our accuracy values are based on many more samples, making them more robust.

Aside from the increase in accuracy, the main benefit of utilizing SMA for crop area mapping is that you use the entire electromagnetic spectrum as measured by Sentinel-2, reprojected into a more intuitive/interpretable GV, NPV, soil, shade data space. Jin et al. (2019) also used a suite of greenness measures for prediction, as well as raw bands, but used additional information on vegetation structure from radar data from Sentinel-1. NPV and particularly shade can give information on vegetation structure (Roberts et al., 2002). We explored the use of Sentinel-1 data but ultimately decided against it due to some irregularities in image registration between data from the two sensors, and because of the presence of shadows/data gaps in the radar data behind taller features, due to radar being side-looking.

We chose to use TOA data rather than surface reflectance because it allows us to do temporal analyses of crop area over 5 years (2016–2020) rather than three (2018–2020). For instance, 2016 and 2017 were low rainfall years in Kenya and we could study the effect of the drought on crop area. TOA data contain atmospheric scattering that primarily affects the visible bands. For instance, for surface reflectance data, the blue band (490 nm) reflectance is usually similar to red reflectance (665 nm) for GV, whereas for TOA data there is additional blue light (**Table 2**). Spatio-temporal variability in atmospheric scattering should incur noise when using TOA vs. surface reflectance data, however as atmospheric scattering primarily only affects three of the ten bands it may not have had a strong effect on EM fractions, and our classification accuracies remained high. Other sources of noise include residual cloud contamination and occasional geolocation errors (particularly considering the heterogeneity of small-scale farming areas). For instance, Tremas et al. (2015) found geolocation errors for Sentinel-2 data of 12.5 m, or over 1 pixel, which could cause an agricultural area pixel to have the EM values of a neighboring forest pixel

TABLE 6 | Fractional crop area for each district in central (Dedza-Salima) and southern (Balaka-Mangochi) Malawi for the four reference data sets and the Sentinel-2 based analysis.

		Fractional crop area per district				
District	**Area (ha)**	**Government Statistics**	**Tappan USGS**	**IIASA-IFPRI**	**ESA-CCI**	**RF Sentinel-2**
Dedza	371,787	0.65	0.6	0.39	0.45	0.53
Dowa	309,354	0.67	0.85	0.48	0.65	0.67
Kasungu	803,785	0.27	0.54	0.35	0.52	0.4
Lilongwe	619,355	0.6	0.76	0.39	0.63	0.64
Mchinji	314,342	0.68	0.76	0.38	0.59	0.55
Nkhotakota	436,043	0.18	0.32	0.21	0.26	0.11
Ntcheu	324,817	0.41	0.62	0.39	0.6	0.53
Ntchisi	170,980	0.64	0.73	0.50	0.58	0.53
Salima	215,985	0.29	0.64	0.21	0.36	0.42
Balaka	213,193	0.42	0.67	0.30	0.85	0.51
Blantyre	202,424	0.45	0.51	0.36	0.66	0.44
Chikwawa	488,222	0.28	0.42	0.27	0.44	0.26
Chiradzulu	76,311	1.1	0.84	0.34	0.95	0.76
Machinga	378,449	0.32	0.5	0.28	0.54	0.43
Mulanje	200,776	0.87	0.73	0.34	0.72	0.61
Mwanza	75,842	0.76	0.41	0.36	0.42	0.48
Neno	155,580	0.32	0.35	0.26	0.47	0.34
Nsanje	194,855	0.22	0.35	0.33	0.57	0.33
Phalombe	137,898	0.86	0.71	0.42	0.77	0.68
Thyolo	164,175	0.77	0.88	0.39	0.88	0.65
Zomba	253,570	0.76	0.71	0.37	0.8	0.65
Mangochi	644,604	0.42	0.47	0.23	0.45	0.29
R^2 vs. G.S.			0.53	0.34	0.45	0.74
R^2 vs. T.U.				0.39	0.52	0.79
R^2 vs. I.I.					0.23	0.50
R^2 vs. E.C.						0.63

R^2 is based on comparing the two sets of 22 values. G.S. referes to Government statistics, T.U. to Tappan USGS, I.I. to IIASA-IFPRI, and E.C. to ESA-CCI.

at certain timesteps, affecting monthly median and annual summary values.

Fritz et al. (2015) state that the global overall accuracy of the IIASA-IFPRI map is 82.4%, but it appears to be less accurate in Malawi, as the range in values is less than the other maps, and agreement at the district scale was low. Our finding that the IIASA-IFPRI map differed from the three other reference data sets and our classification map is in line with the findings of Samasse et al. (2018). They compared eight landcover maps in West African countries, and found that the coarser resolution maps, including IIASA-IFPRI, performed much worse than 30 m maps using Landsat data. Interestingly, the ESA-CCI 20 m map, using Sentinel-2 data, also performed worse than the Landsat-based maps with accuracies 10–40% points lower. Samasse et al. (2018) suggested the techniques and West Africa training data used in the ESA-CCI product needed to be re-examined. Alkhalil et al. (2020) also evaluated the ESA-CCI map in West Africa. They found extremely low producer's accuracies (over-prediction of crops) for three polygons in the Sahel (0.07, 0.34, 0.03) and less, but still some over-prediction for three polygons closer to the coast (producer's accuracies of 0.61, 0.72, 0.56), leading them to declare the ESA-CCI product was not an acceptable crop mask. Our research also showed overprediction of crop area by ESA-CCI when compared with the RF Sentinel-2 map, particularly in southern Malawi (**Table 6**, **Figure 5**).

RF are known as a greedy classifier, hence, a large number of manually interpreted points were identified—a total of 20,848. For comparison to other studies, central and southern Malawi comprise 6,752,347 ha. Kerner et al. (2020) mapped percent crop area in Togo (5,678,500 ha) using a different algorithm and hence, a fraction of the reference data-−1,319 crop or no crop points from within the country, and a global data set of 35,866 crop/no crop points. Tseng et al. (2020) used a similar algorithm and the same global 35,866 points, as well as 14,080 crop/no crop points for the much larger country of Kenya (58,036,700 ha). Jin et al. (2019) used RF to map crop/no crop in both Kenya and Tanzania (94,730,300 ha), 4,509 points were identified in Kenya, and 4,140 in Tanzania. The country areas are much larger than that of Malawi; however, the agricultural portion of the countries is much smaller than these numbers, making the comparison

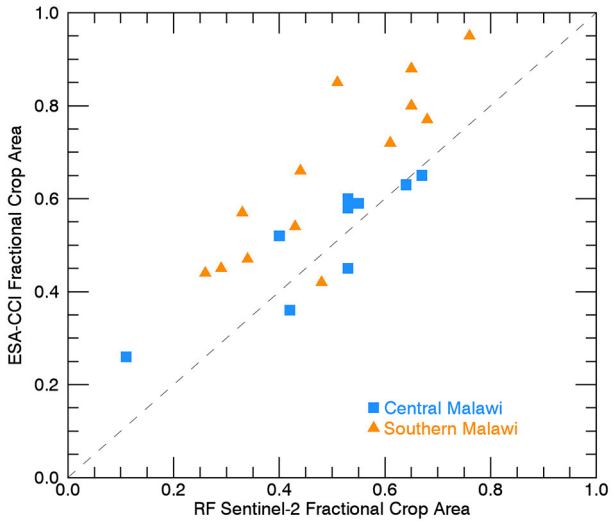

FIGURE 5 | Fractional crop area compared for the RF Sentinel-2 map and the ESA-CCI map. The ESA-CCI map overpredicts crop area by 10–20% for many of the districts in southern Malawi.

less straightforward, because large parts of each country could be excluded as potentially arable. In fact, latitude and longitude were included as predictor variables in Jin et al. (2019). Furthermore, it is not known exactly how many fewer points would have been needed if our analysis had been crop/no crop instead of crop, sparse, shrub, tree, and water. Another factor is we used roughly 50% of the data for training, 50% for testing while Jin et al. (2019) and Kerner et al. (2020) trained on 80% of the data and Tseng et al. (2020) trained on 90% of the data. Hence, they leveraged their points differently, and had fewer points for robust accuracy assessment. While our method may be less efficient and/or an excessive amount of reference points may have been identified, our accuracies are based on far more data points, which increases confidence.

This study generated a crop area map for southern and central Malawi with very high crop/no crop classification accuracies between 87 and 93%. The approach combined some of the oldest (air photo interpretation) and newest (cloud computing) remote sensing techniques. Overall, we find the results presented here to be a promising result for the potential to use GEE and RF algorithms to produce high-quality cropped area estimates for smallholder farms in rainfed agriculture regimes. EM phenology predictor variables and variable importance measures combine to produce interpretable, non-"black box" results. Accuracies for the two most populous classes, crop and shrub, are based on 50% of the reference data points so are extremely robust. A more accurate assessment of the cropped area in a region can help better understand the dynamics impacting food production and food security in vulnerable regions of sub-Saharan Africa. The method can be repeated using the same training data to perform the classification over multiple years which would be useful for the identification of changing landscape dynamics and for seasons when weather, agricultural inputs (seeds or fertilizer), or labor impacted the amount of cropped area for a particular season, over a region, relatively simply. The results presented here can also be utilized to develop an agricultural mask that can be used to better focus agroclimatic analysis over wide areas. All these different benefits could have a positive impact on the ability to anticipate, assess, and mitigate the impacts of cropped area on food security over sub-Saharan Africa.

DATA AVAILABILITY STATEMENT

Publicly available datasets were analyzed in this study. This data can be found here: Publicly available Sentinel-2 data were analyzed in this study, this data can be found in Google Earth Engine.

AUTHOR CONTRIBUTIONS

SP and GH conceptualized the research, revised, and improved the manuscript. SP defined the methods, analyzed the findings, composed the figures, and drafted the manuscript. Both authors contributed to the article and approved the submitted version.

FUNDING

We acknowledge support of the United States Agency for International Development (USAID) cooperative agreement #72DFFP19CA00001.

ACKNOWLEDGMENTS

We sincerely thank Juliet Way-Henthorne and Austin Sonnier for comments on the manuscript. Natasha Krell helped locate maize fields for determining endmember spectra. Sarah Shivers provided hyperspectral spectra of corn fields.

REFERENCES

Alkhalil, A., Kadaoure, I., and Kouadio, M. (2020). An evaluation of 20-m ESA-CCI S2 prototype LC product. *Front. Sustain. Food Syst.* 4:504334. doi: 10.3389/fsufs.2020.504334

Amani, M., Kakooei, M., Moghimi, A., Ghorbanian, A., Ranjar, B., Mahdavi, S., et al. (2020). Application of Google Earth Engine cloud computing platform, sentinel imagery, and neural networks for crop mapping in Canada. *Remote Sens.* 12:3561. doi: 10.3390/rs12213561

Carletto, C., Jolliffe, D., and Banerjee, R. (2015). From tragedy to renaissance: improving agricultural data for better policies. *J. Dev. Stud.* 51, 133–148. doi: 10.1080/00220388.2014.968140

Chastain, R., Housman, I., Goldstein, J., Finco, M., and Tenneson, K. (2019). Empirical cross sensor comparison of Sentinel-2A and 2B MSI, Landsat-8 OLI, and Landsat-7 ETM+ top of atmosphere spectral characteristics over the conterminous United States. *Remote Sens. Environ.* 221, 274–285. doi: 10.1016/j.rse.2018.11.012

Chivasa, W., Mutanga, O., and Biradar, C. (2017). Application of remote sensing in estimating maize grain yield in heterogeneous African agricultural landscapes: a review. *Int. J. Remote Sens.* 38, 6816–6845. doi: 10.1080/01431161.2017.1365390

Cotillon, S. E., and Mathis, M. L. (2017). *Mapping Land Cover Through Time With the Rapid Land Cover Mapper—Documentation and User Manual: U.S. Geological Survey Open File Report 2017-1012.* Sioux Falls, SD. doi: 10.3133/ofr20171012

Devereux, S. (2009). Why does famine persist in Africa? *Food Sec.* 1, 25–35. doi: 10.1007/s,12571-008-0005-8

ESA-CCI (2021). *CCI Land Cover—S2 Prototype Land Cover 20 m Map of Africa 2016*. Available online at: http://2016africalandcover20m.esrin.esa.int/ (accessed April 09, 2021).

Fritz, S., See, L., McCallum, I., You, L., Bun, A., Moltchanova, E., et al. (2015). Mapping global cropland and field size. *Glob. Change Biol.* 21, 1980–1992. doi: 10.1111/gcb.12838

Funk, C. (2021). *Drought, Flood, Fire: How Climate Change Contributes to Catastrophes*. London: Cambridge Press. doi: 10.1017/9781108885348

Funk, C., Peterson, P., Landsfeld, M., Pedreros, D., Verdin, J., Shukla, S. (2015). The climate hazards infrared precipitation with stations – a new environmental record for monitoring extremes. *Sci. Data* 2:150066. doi: 10.1038/sdata.2015.66

Gorelick, N., Hancher, M., Dixon, M., Ilyushchenko, S., Thau, D., and Moore, R. (2017). Google Earth Engine: planetary-scale geospatial analysis for everyone. *Remote Sens. Environ.* 202, 18–27. doi: 10.1016/j.rse.2017.06.031

Hammond, A. L. (1975). Crop forecasting from space: toward a global food watch. *Science* 188, 434–436. doi: 10.1126/science.188.4187.434

He, H., and Garcia, E. A. (2009). Learning from imbalanced data. *IEEE Trans. Knowl. Data Eng.* 21, 1263–1284. doi: 10.1109/TKDE.2008.239

Huete, A. R., Liu, H. Q., Batchily, K., and van Leeuwen, W. (1997). A comparison of vegetation indices over a global set of TM images for EOS-MODIS. *Remote Sens. Environ.* 59, 440–451. doi: 10.1016/S0034-4257(96)00112-5

Jin, Z., Azzari, G., You, C., Di Tommaso, S., Aston, S., Burke, M., et al. (2019). Smallholder maize area and yield mapping at national scales with Google Earth Engine. *Remote Sens. Environ.* 228, 115–128. doi: 10.1016/j.rse.2019.04.016

Karlson, M., Ostwald, M., Bayala, J., Bazie, H. R., Ouedraogo, A. S., Soro, B., et al. (2020). The potential of Sentinel-2 for crop production estimation in a smallholder agroforestry landscape, Burkina Faso. *Front. Environ. Sci.* 8:85. doi: 10.3389/fenvs.2020.00085

Kerner, H., Tseng, G., Becker-Reshef, I., Nakalembe, C., Barker, B., Munshell, B., et al. (2020). "Rapid response crop maps in data sparse regions," in *KDD 2020 Humanitarian Mapping Workshop, August 24, 2020* (San Diego, CA). arXiv:2006.16866v1

Lobell, D. B. (2013). The use of satellite data for crop yield gap analysis. *Field Crop. Res.* 143, 56–64. doi: 10.1016/j.fcr.2012.08.008

MacDonald, R. B., and Hall, F. G. (1980). Global crop forecasting. *Science* 208, 670–679. doi: 10.1126/science.208.4445.670

Masiza, W., Chirima, J. G., Hamandawana, H., and Pillay, R. (2020). Enhanced mapping of smallholder crop farming landscape through image fusion and model stacking. *Int. J. Remote Sens.* 41, 8739–8756. doi: 10.1080/01431161.2020.1783017

Misra, G., Cawkwell, F., and Wingler, A. (2020). Status of phenological research using Sentinel-2 data: a review. *Remote Sens.* 12:2760. doi: 10.3390/rs12172760

Ozdogan, M., and Woodcock, C. E. (2006). Resolution dependent errors in remote sensing of cultivated areas. *Remote Sens. Environ.* 103, 203–217. doi: 10.1016/j.rse.2006.04.004

Probst, P., Wright, M. N., and Boulesteix, A. (2019). Hyperparameters and tuning strategies for random forest. *WIREs Data Mining Knowl. Discov.* 9, e1301. doi: 10.1002/widm.1301

Roberts, D. A., Numata, I., Holmes, K., Batista, G., Krug, T., Monteiro, A., et al. (2002). Large area mapping of land-cover change in Rondonia using multitemporal spectral mixture analysis and decision tree classifiers. *J. Geophys. Res.* 107:8073. doi: 10.1029/2001JD000374

Rouse, J. W., Haas, R. H., Schell, J. A., and Deering, D. W. (1973). "Monitoring vegetation systems in the Great Plains with ERTS," in *Third ERTS Symposium* (pp. 309–317). NASA Special Publication SP-351(1).

Samasse, K., Hanan, N. P., Tappan, G., and Diallo, Y. (2018). Assessing cropland area in West Africa for agricultural yield analysis. *Remote Sens.* 10:1785. doi: 10.3390/rs10111785

Tremas, T. L., Dechoz, C., Lacherade, S., Nosavan, J., Petrucci, B. (2015). "Sentinel-2: presentation of the CAL/VAL commissioning phase," in *Proc. SPIE 9643, Image and Signal Processing for Remote Sensing XXI, 964309*. doi: 10.1117/12.2194847

Tseng, G., Kerner, H., Nakalembe, C., and Becker-Reshef, I. (2020). *Annual and In-Season Mapping of Cropland at Field Scale With Sparse Labels*. Tackling Climate Change with Machine Learning workshop at NeurIPS 2020. Available online at: https://www.climatechange.ai/papers/neurips2020/29/paper.pdf (accessed April 7, 2021).

Verde, N., Kokkoris, I. P., Georgiadis, C., Kaimaris, D., Dimopoulos, P., Mitsopoulos, I., et al. (2020). National scale land cover classification for ecosystem services mapping and assessment, using multitemporal Copernices EO data and Google Earth Engine. *Remote Sens.* 12:3303. doi: 10.3390/rs12203303

Wang, S., Di Tomasso, S., Deines, J. M., and Lobell, D. B. (2020). Mapping twenty years of corn and soybean across the US Midwest using the Landsat archive. *Nat. Sci. Data* 7:307. doi: 10.1038/s41597-020-00646-4

Conflict of Interest: The authors declare that the research was conducted in the absence of any commercial or financial relationships that could be construed as a potential conflict of interest.

frontiers in Climate

ORIGINAL RESEARCH
published: 09 August 2021
doi: 10.3389/fclim.2021.663444

Dynamics of Green and Blue Water Supply Stress Index Across Major Global Cropland Basins

Kul Khand[1], Gabriel B. Senay[2], Stefanie Kagone[1] and Gabriel Edwin Lee Parrish[3]*

[1] Arctic Slope Regional Corporation Federal Data Solutions, Contractor to the U.S. Geological Survey Earth Resources Observation and Science Center, Sioux Falls, SD, United States, [2] U.S. Geological Survey Earth Resources Observation and Science Center, North Central Climate Adaptation Science Center, Boulder, CO, United States, [3] Innovate! Inc., Contractor to the U.S. Geological Survey Earth Resources Observation and Science Center, Sioux Falls, SD, United States

Global food and water insecurity could be serious problems in the upcoming decades with growing demands from the increasing global population and more frequent effect of climatic extremes. As the available water resources are diminishing and facing continuous stress, it is crucial to monitor water demand and water availability to understand the associated water stresses. This study assessed the water stress by applying the water supply stress index (WaSSI) in relation to green ($WaSSI_G$) and blue ($WaSSI_B$) water resources across six major cropland basins including the Mississippi (North America), San Francisco (South America), Nile (Africa), Danube (Europe), Ganges-Brahmaputra (Asia), and Murray-Darling (Australia) for the past 17-years (2003–2019). The $WaSSI_G$ and $WaSSI_B$ results indicated that the Murray-Darling Basin experienced the most severe (maximum $WaSSI_G$ and $WaSSI_B$ anomalies) green and blue water stresses and the Mississippi Basin had the least. All basins had both green and blue water stresses for at least 35% (6 out of 17 years) of the study period. The interannual variations in green water stress were driven by both crop water demand and green water supply, whereas the blue water stress variations were primarily driven by blue water supply. The $WaSSI_G$ and $WaSSI_B$ provided a better understanding of water stress (blue or green) and their drivers (demand or supply driven) across cropland basins. This information can be useful for basin-specific resource mobilization and interventions to ensure food and water security.

Keywords: evapotranspiration, green and blue water, water stress, drought, food security

OPEN ACCESS

Edited by:
Andrew Hoell, Earth System Research Laboratory (NOAA), United States

Reviewed by:
Nicholas Christopher Mbangiwa, University of Botswana, Botswana
Tamuka Magadzire, University of California Santa Barbara, United States

****Correspondence:***
Kul Khand
kkhand@contractor.usgs.gov

Specialty section:
This article was submitted to Climate Services, a section of the journal Frontiers in Climate

Received: *02 February 2021*
Accepted: *15 July 2021*
Published: *09 August 2021*

Citation:
Khand K, Senay GB, Kagone S and Parrish GEL (2021) Dynamics of Green and Blue Water Supply Stress Index Across Major Global Cropland Basins. Front. Clim. 3:663444. doi: 10.3389/fclim.2021.663444

INTRODUCTION

Water resources are critical for providing human needs of water, energy, and food, and preserving healthy ecosystems (Bhaduri et al., 2016; Vanham, 2016). Increasing water demands from the growing population and shifting lifestyles are increasing competition within and among water use sectors (Molden, 2007). Additionally, climate change is deteriorating water resources (Scanlon et al., 2007) and fueling more stress on water resources (Hanjra and Qureshi, 2010; Siegfried et al., 2012), resulting in conflicts during water shortages (Eriksen and Lind, 2009; Theisen et al., 2012; Tang et al., 2018). Water stress assessments at local to regional scale are increasingly crucial to understand the vulnerability and resiliency of water resources. In particular, assessing water stress associated with crop water use (or evapotranspiration) and its relationship with green water (precipitation) or blue water (surface water and groundwater) sources provides integrated information on food and water status.

Global water supply is declining but the water demand has tripled since the 1950s (Gleick, 2003). Approximately 1.4 billion people live in river basins where water use is larger than water recharge rates (UNDP, 2006) with the projection that more than half of the global population will live in areas that suffer water scarcity at least a month each year by 2050 (WWAP, 2018). Several river basins and regions with large cropland areas that are heavily dependent on blue water irrigation could face critical challenges for food and water security because irrigation is the first sector to lose water when the water scarcity increases (Molden, 2007). For example, the Ganges-Brahmaputra, the largest basin in Asia with ∼32% of its total area as irrigated croplands (Thenkabail et al., 2016), may face reductions in blue water availability for irrigation due to increasing competition among the water use sectors (Flörke et al., 2018). The southern High Plains of the United States (U.S.), a heavy blue water-dependent irrigated region, is diminishing due to unsustainable groundwater withdrawal (Scanlon et al., 2012). The continuous depletion of groundwater level would result in more than a third of the region being unable to support irrigation within the next 30 years (Scanlon et al., 2012). With the continuous effects of frequent and severe droughts in agriculture and its projected effects in the future (Li et al., 2009; van Asten et al., 2011; Howitt et al., 2014), the irrigated croplands (∼20% of the global cropland area) may undergo severe water stress due to blue water shortages and could cause significant reduction to food production (Siebert and Döll, 2010; Leng and Hall, 2019).

Conversely, rainfed agriculture (∼80% of the global cropland) is dependent on green water, which contributes to more than half of the global food production (Rosegrant et al., 2002). Food production in some regions is completely dependent on green water-supplied rainfed agriculture such as in Sub-Saharan Africa (Alexandratos, 1995). River basins with large portion as rainfed croplands are also under food and water security threat due to climate change-induced variabilities in precipitation (Kang et al., 2009). For example, the largest basins in Europe—the Danube Basin has almost two-third (∼64%) of its area as rainfed croplands and several sub-regions could face severe water stress due to the shortage of green water availability from the projected reduction in precipitation (Bisselink et al., 2018; ICPDR, 2018). For such green water-dependent cropland basins, indicators for monitoring the crop water use and green water availability provide useful information to detect the associated water stress. Similarly, for the basins with blue water-dependent cropland, indicators that monitor blue water use and availability are more useful than other water stress indicators for better decision making. Thus, the stress indicators that integrate the water use and water availability information relating to the type of water resources (i.e., blue and green) will help to better characterize water stresses.

Water stress at a basin scale is commonly quantified as a ratio of water demand (or water use) to water availability (Falkenmark et al., 2007; Sun et al., 2008; Richey et al., 2015). One of the several water stress indices to detect water stress at basin scale is the water supply stress index (WaSSI) (Sun et al., 2008), originally developed to simulate water stress based on water demand and water supply on an annual time-step (Sun et al., 2015). The WaSSI has been applied to model and predict water stress caused by increasing human population, land-use change, and climate change (Sun et al., 2008, 2015; Caldwell et al., 2012; Duan et al., 2019) across several basins worldwide (Ji et al., 2012; Eldardiry et al., 2016; McNulty et al., 2016; Tang et al., 2018; Zhang et al., 2018). However, only a few studies have applied the WaSSI to understand the contribution of different water use sectors to basin water stress. Averyt et al. (2013) assessed the contribution of different water use sectors across the 8-digit Hydrological Unit Code (HUC8) (Seaber et al., 1987) scale basins in the U.S. The study reported agriculture as the main sector contributing to water stress at about two-thirds of the water-stressed HUC8 basins in the U.S. Larger contributions to water stress from the agricultural sector were observed across HUC8 basins in the western U.S., where there are fewer surface water resources compared to the eastern U.S. (Averyt et al., 2013). Similar studies with further investigation of green and blue water use and availability across agricultural regions would help to understand the vulnerability and resiliency of those regions for food and water security.

This study aims to assess water stress of six major cropland-dominated basins from six continents (Mississippi in North America, Sao Francisco in South America, Danube in Europe, Nile in Africa, Ganges-Brahmaputra in Asia, and Murray-Darling in Australia) by applying the WaSSI and by associating the index with green ($WaSSI_G$) and blue ($WaSSI_B$) water resources. The $WaSSI_G$ and $WaSSI_B$ were generated for the time period from 2003 to 2019 to investigate the significance of green or blue water resources and associated water stresses. The water stress information with integration to green and blue water resources is useful for resource mobilization and interventions to improve and ensure food and water security for human use and the environment.

MATERIALS AND METHODS

Study Site

The six major river basins from six continents were selected for this study (**Figure 1**). The selection of these basins was based on being one of the major basins in each continent that has large cropland areas facing challenges on water availability for food production. The basin sizes are between 52.0×10^4 km^2 (Sao Francisco Basin in South America) and 344.7×10^4 km^2 (Mississippi Basin in North America). These basins have croplands (rainfed and irrigated) varying between ∼20% (Nile Basin in Africa) and ∼72% (Danube Basin in Europe) of their basin area (**Table 1**). All basins have larger rainfed cropland areas than irrigated cropland areas except the Ganges-Brahmaputra in Asia, which has ∼30% of basin area irrigated and ∼22% rainfed. The study basins cover wide variations in climate from warm temperate humid in southeastern regions of the Mississippi Basin to arid desert in northern regions of the Nile Basin (Kottek et al., 2006). Among the basins, the Murray-Darling (Australia) had the lowest average annual precipitation of 436 mm/year and the Ganges-Brahmaputra had the highest average annual precipitation of 1,268 mm/year during the study period from 2003 to 2019 (**Table 1**).

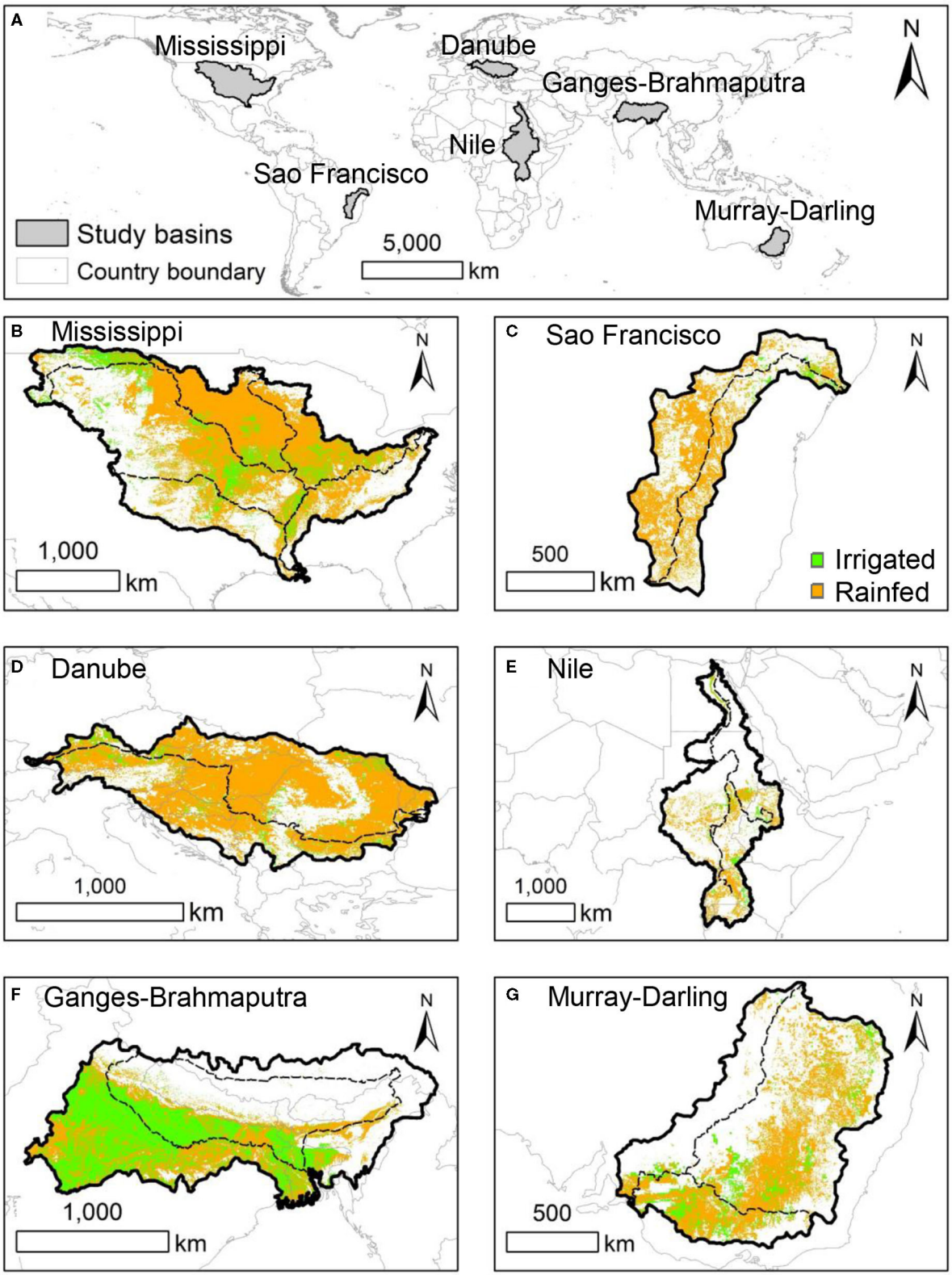

FIGURE 1 | The global map showing the location of six study basins **(A)**, including Mississippi **(B)**, Sao Francisco **(C)**, Danube **(D)**, Nile **(E)**, Ganges-Brahmaputra **(F)**, and Murray-Darling **(G)**. The dashed black color line inside the basins represents the major rivers. The croplands map is from the Global Food Security Support Analysis Data (https://lpdaac.usgs.gov/products/gfsad1kcmv001/) and basin boundaries are from World Resources Institute (https://www.wri.org/).

TABLE 1 | Study basins with respective continents, basin area, cropland area, irrigated area, and average (2003–2019) annual precipitation.

Basin	Continent	Basin area, $\times 10^4$ km^2	Cropland area, $\times 10^4$ km^2 (% of basin)	Irrigated area, $\times 10^4$ km^2 (% of basin)	Precipitation, mm/year
Mississippi	North America	344.7	200.8 (58%)	36.4 (11%)	817
Sao Francisco	South America	52.0	24.3 (47%)	1.1 (2%)	896
Danube	Europe	93.8	67.7 (72%)	5.2 (6%)	799
Nile	Africa	255.9	50.7 (20%)	8.5 (3%)	654
Ganges-Brahmaputra	Asia	151.0	78.2 (52%)	44.9 (30%)	1,268
Murray-Darling	Australia	100.1	37.8 (38%)	7.6 (8%)	436

The basin boundaries from World Resources Institute (https://www.wri.org/) were used to calculate zonal statistics aggregated over each basin. Cropland area and irrigated area were calculated using cropland maps from the Global Food Security Support Analysis Data (https://lpdaac.usgs.gov/products/gfsad1kcmv001/). Basin-averaged annual precipitation was calculated using precipitation maps from Oregon State University (https://prism.oregonstate.edu/).

Green and Blue WaSSI

Water demands from different water use sectors such as agriculture, industry, public supply, and others are primarily supplied by precipitation (green water) and surface water/groundwater (blue water). In this study, the water supply stress index (WaSSI), a ratio of water use to water available, was generated for croplands to evaluate the water stress associated with water use and water availability. The WaSSI was partitioned into green WaSSI ($WaSSI_G$) and blue WaSSI ($WaSSI_B$) based on the supply source for either green or blue water in the study basins. Because the green water is applied to all croplands regardless of rainfed or irrigated, all cropland area was used for computing $WaSSI_G$. But this could create an exaggerated $WaSSI_G$ over irrigated areas because part of the crop water use (or actual evapotranspiration, ETa) is met by irrigation. However, due to the difficulty of quantifying the partial contributions of precipitation and irrigation to the index, the inter-basin differences are driven by the supply source (precipitation or runoff) to meet the ETa, representing the total crop water demand that is met. In all basins, the relative proportion of rainfed areas is much larger than irrigated area except for the Ganges-Brahmaputra Basin (**Table 1**), thus the basin-scale estimates are in proportion to the relative area under rainfed or irrigation for $WaSSI_G$. For computing $WaSSI_B$, only ETa from the irrigated cropland area was used as the blue water is supplied to irrigated croplands only. Similar to $WaSSI_G$, the total ETa over the irrigated areas was used for $WaSSI_B$, but the supply is attributed to the runoff instead of precipitation. The $WaSSI_G$ and $WaSSI_B$ for each basin and year were computed as:

$$WaSSI_G = \frac{\frac{1}{n}\sum_1^n \text{All cropland water use (ETa)}}{\frac{1}{n}\sum_1^n \text{Green water available (precipitation)}} \quad (1)$$

$$WaSSI_B = \frac{\frac{1}{n}\sum_1^n \text{Irrigated cropland water use (ETa)}}{\frac{1}{n}\sum_1^n \text{Blue water available (runoff)}} \quad (2)$$

where n is the number cropland pixels at each basin, and ETa is the actual evapotranspiration.

The water used by crops or actual evapotranspiration (ETa) is driven by crop water demand and availability of supply. Thus, ETa represents the crop water demand that was met by available water from green and blue water sources. The separation of ETa for representing green and blue water components requires running a water balance model (including additional data) which will introduce additional uncertainties. Thus, the total ETa (both green and blue water), estimated using a surface energy balance model (detailed in the following section Data Preparation), from the cropland and irrigated areas was assumed to represent the green and blue water demands to compute $WaSSI_G$ and $WaSSI_B$, respectively. Precipitation only over the cropland area (not for basin) was considered as the available green water to compute $WaSSI_G$. Not all precipitation is expected to have been available for crop water use due to various losses (e.g., canopy interception and runoff); however, to develop the index, total precipitation was used to minimize uncertainties associated to determining effective precipitation for soil moisture and ETa. The total runoff from the basin was assumed as the available blue water for irrigated area to compute $WaSSI_B$. The use of runoff as blue water instead of surface water and groundwater is due to the limitation of obtaining reliable data at the study basins, specifically for the groundwater that is declining in many places, and quality data on remaining volume and drawdown rates are limited (Reilly et al., 2008). The use of runoff as the blue water availability assumes that there is a strong hydraulic linkage between surface water and groundwater at basin scales.

The evaluation of $WaSSI_G$ and $WaSSI_B$ was made at an annual scale. The values of the indices vary from zero to infinity. The values closer to zero indicate lower stress and the larger values indicate higher water stress. Previous studies (Ji et al., 2012; Averyt et al., 2013) have applied a threshold of one (1) to represent no-stress (<1) and stress (>1) including the water demand from several water use sectors. However, as this study was focused on the water demand for croplands, anomalies (deviation from the average value) of $WaSSI_G$ and $WaSSI_B$ were used to detect the severity (magnitude) and duration of green and blue water stresses. The $WaSSI_G$ and $WaSSI_B$ anomalies larger than their average (2003–2019) values were considered stress and the anomalies equal to or smaller than their average values were considered no-stress.

$$\left.\begin{array}{l} WaSSI_G \text{ anomaly} = \\ \end{array}\right\} \frac{WaSSI_{G,\,i} - WaSSI_{G,\,avg.}}{WaSSI_{G,\,avg.}} \times 100$$

$$\frac{> 0\% \quad \text{stress (green water)}}{\leq 0\% \ \text{no} - \text{stress (green water)}} \quad (3)$$

$$\text{WaSSI}_\text{B} \text{ anomaly} = \left.\begin{array}{c} \dfrac{\text{WaSSI}_{\text{B},\,i} - \text{WaSSI}_{\text{B},\,avg.}}{\text{WaSSI}_{\text{B},\,avg.}} \times 100 \\ \\ \dfrac{> 0\% \quad \text{stress (blue water)}}{\leq 0\% \ \text{no} - \text{stress (blue water)}} \end{array}\right\} \quad (4)$$

where i in $\text{WaSSI}_{\text{G},i}$ and $\text{WaSSI}_{\text{B},i}$ represents the study years from 2003 to 2019. The $\text{WaSSI}_{\text{G},avg.}$ and $\text{WaSSI}_{\text{B},avg.}$ are the basin average (2003–2019) WaSSI_G and WaSSI_B, respectively. The responses of WaSSI_G and WaSSI_B were also evaluated during dry (lowest basin precipitation) and wet (highest basin precipitation) years both at pixel [following Equations (1, 2) for each pixel] and basin scales.

Data Preparation

For generating the WaSSI_G and WaSSI_B, four primary datasets were used: actual evapotranspiration (ETa), runoff, precipitation, and land cover. The ETa data were generated from the Operational Simplified Surface Energy Balance (SSEBop) model (Senay et al., 2013; Senay, 2018) using the Moderate Resolution Imaging Spectroradiometer (MODIS) imagery and global gridded weather datasets. The SSEBop model uses the surface energy balance approach to estimate daily ETa for the satellite overpass dates. The MODIS-scale (daily, 1-km) ETa maps were summed to generate annual ETa maps for the study basins from 2003 to 2019. These ETa datasets were validated with 12 flux tower sites across the six continents. The data are applied by the U.S. Geological Survey (USGS) Famine Early Warning Systems Network (FEWS NET) for drought monitoring and early warning purposes (Senay et al., 2020). The ETa data are freely available for download from the USGS FEWS NET Data Portal (https://earlywarning.usgs.gov/fews).

Runoff datasets were generated using the VegET water balance model (Senay, 2008). The VegET is a root-zone water balance model driven by precipitation and remotely sensed land surface phenology (Senay, 2008). Modeled runoff was used instead of observed runoff due to limitation of complete runoff observations for the study basins during the study period (2003–2019). For the calibration purpose, in the first step, the modeled runoff was compared with an observation-based global gridded runoff (GRUN) dataset (Ghiggi et al., 2019). In the second step, when the modeled runoff data was not within ±10% of the GRUN runoff, the modeled runoff was adjusted (by percentage) with the global composite runoff data (Fekete et al., 2002) from the global runoff data center (GRDC). The GRUN runoff was applied as reference data to filter the basins for the calibration of modeled runoff with GRDC runoff. Except for the Ganges-Brahmaputra Basin, where the modeled runoff was within ±10% of GRUN runoff, modeled runoff for all other basins was adjusted with the GRDC data.

Precipitation data were obtained from the Climate Hazards Group Infrared Precipitation with Stations (CHIRPS; https://www.chc.ucsb.edu/data/chirps). The CHIRPS rainfall data ($0.05^\circ \times 0.05^\circ$ spatial resolution) are generated by integrating infrared imagery, climatology, and observed rainfall records, and have global coverage (50°S−50°N, 180°E−180°W) ranging from 1981 to near-present (Funk et al., 2015). These rainfall data have been applied to support the drought monitoring efforts by FEWS NET, especially in areas where observed rainfall data are sparse. The land cover map to distinguish irrigated and rainfed croplands was obtained from the Global Food Security Support Analysis Data Crop Mask Global 1-km dataset (GFSAD1KCM; https://lpdaac.usgs.gov/products/gfsad1kcmv001/). The GFSAD1KCM map provides irrigated (major and minor) and rainfed (rainfed, minor fragments, and very minor fragments) croplands for the nominal year of 2010 (Teluguntla et al., 2015). All other globally consistent irrigated and rainfed maps were limited for all study years; thus, the GFSAD1KCM map was applied in this study.

RESULTS

Dynamics of Green and Blue WaSSI

The interannual variation of WaSSI_G and WaSSI_B of the six study basins is shown in **Figure 2**. Overall, WaSSI_G was greater than WaSSI_B for all basins except the Murray-Darling Basin indicating more water stresses associated with green water (precipitation) compared to blue water (runoff in this study). The average (2003–2019) WaSSI_G values were less than one (1) for all basins (**Table 1**). The WaSSI_G is the largest for Sao Francisco (0.91), followed by Nile (0.78), Mississippi (0.71), Murray-Darling (0.69), Ganges-Brahmaputra (0.69), and Danube (0.50) (**Table 2**). The larger interannual variation of WaSSI_G (max. WaSSI_G–min. WaSSI_G) was observed for the Murray-Darling Basin (**Figure 2**), indicating vulnerability to green water stress compared to other basins. In contrast, the smallest interannual variation of WaSSI_G was for the Mississippi Basin reflecting resiliency to green water stress.

Similar to the WaSSI_G values, the average WaSSI_B values were also less than one (1) for all basins with the exception for the Murray-Darling Basin (**Table 1**). The largest WaSSI_B was for Murray-Darling (1.59), followed by Ganges-Brahmaputra (0.52), Mississippi (0.41), Nile (0.22), Danube (0.09), and Sao Francisco (0.09). The largest interannual variation of WaSSI_B was at the Murray-Darling Basin. This basin also had the largest WaSSI_G variation, indicating greater vulnerability to both green and blue water stresses compared to other study basins. The smallest variation of WaSSI_B was at the Sao Francisco Basin showing more resilience to blue water stress.

The plots of WaSSI_G and WaSSI_B anomalies (percent deviation from the average value) show the blue and green water stress at study basins from 2003 to 2019 (**Figure 3**). In general, the WaSSI_G anomalies were within ±43% of their 2003–2019 average values for all basins. In contrast, WaSSI_B anomalies are relatively larger within ±103% of their average values except for a maximum of 224% for the year 2006, which was the driest year for the Murray-Darling Basin. During the study period, the most severe (maximum anomaly) green water stress was observed at the Murray-Darling Basin (average positive WaSSI_G anomaly of +16%) and the least severe (minimum anomaly) green water stress at the Mississippi Basin (average positive WaSSI_G anomaly

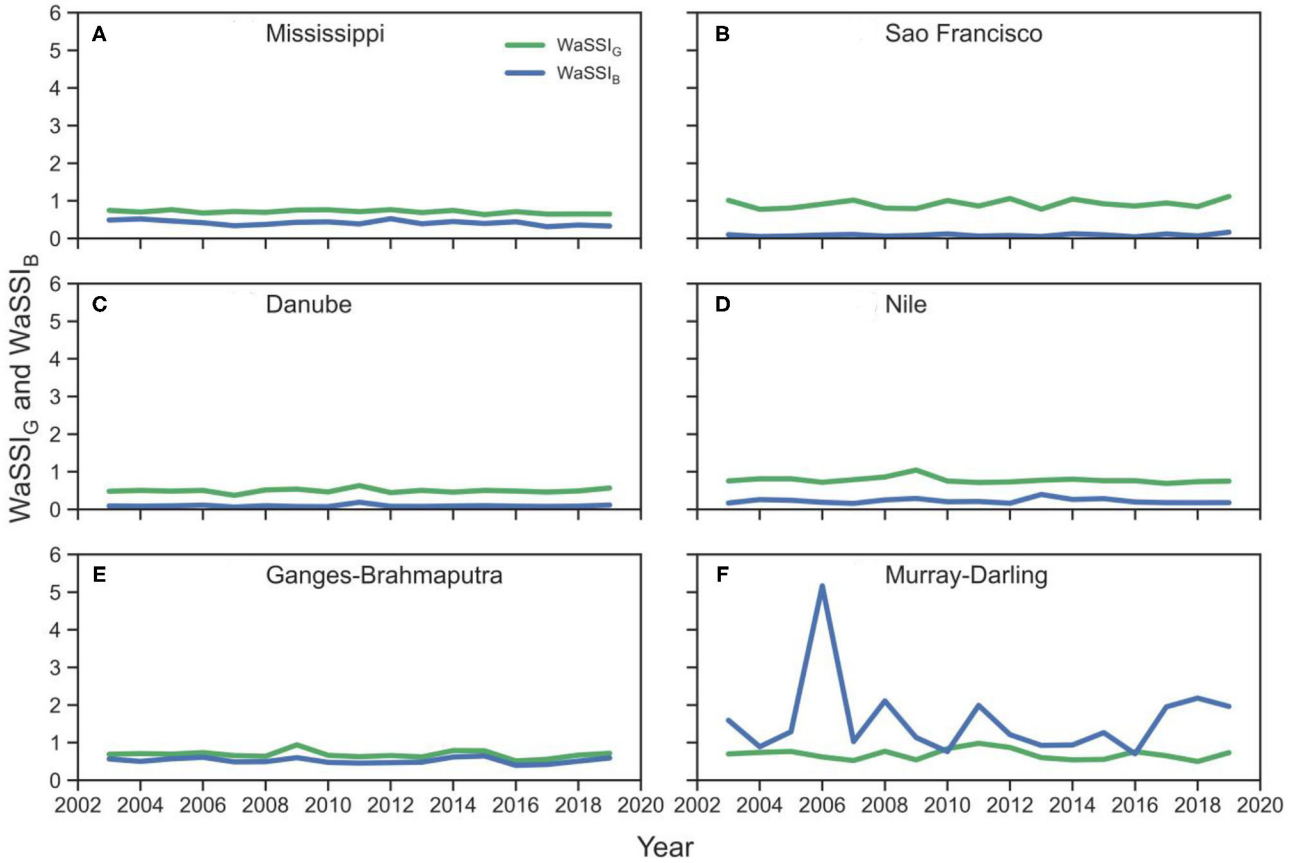

FIGURE 2 | Interannual variations of green (WaSSI$_G$) and blue (WaSSI$_B$) water supply stress indices across study basins including Mississippi **(A)**, Sao Francisco **(B)**, Danube **(C)**, Nile **(D)**, Ganges-Brahmaputra **(E)**, and Murray-Darling **(F)** from 2003 to 2019.

TABLE 2 | The average, minimum, maximum, and standard deviation of green (WaSSI$_G$) and blue (WaSSI$_B$) water supply stress indices of study basins from 2003 to 2019.

Basin	WaSSI$_G$				WaSSI$_B$			
	Avg.	Min.	Max.	Std. Dev.	Avg.	Min.	Max.	Std. Dev.
Mississippi	0.71	0.63	0.76	0.04	0.41	0.31	0.52	0.06
Sao Francisco	0.91	0.77	1.12	0.11	0.09	0.04	0.17	0.03
Danube	0.50	0.37	0.63	0.05	0.09	0.06	0.19	0.03
Nile	0.78	0.69	1.05	0.08	0.22	0.16	0.40	0.06
Ganges-Brahmaputra	0.69	0.51	0.94	0.09	0.52	0.40	0.65	0.07
Murray-Darling	0.69	0.50	0.98	0.13	1.59	0.70	5.16	1.02

of +5%). For the blue water stress, the most severe was also at the Murray-Darling Basin (+61%) and the least was at the Mississippi Basin (+12%). Thus, the most severe blue and green water stresses were observed at the Murray-Darling Basins and the least severe at the Mississippi Basin.

During the 17-year study period, the WaSSI$_G$ and WaSSI$_B$ anomalies were greater than zero (0) for at least six (6) years and >5% for at least two (2) years for all basins. In other words, these basins faced both green and blue water stresses for at least 35% of the study years from 2003 to 2019. The maximum number of years with WaSSI$_B$ anomalies greater than zero was observed for the Mississippi (9 years) and Murray-Darling (9 years) basins. Similarly, the maximum number of years with WaSSI$_G$ anomalies greater than zero was observed at the Mississippi Basin (9 years). These results indicate that the Mississippi Basin had the longest period (>50% of study years) of both green and blue water stresses. However, this basin had the least severe blue and green water stresses compared to other basins (**Figure 3**).

Responses of Green and Blue WaSSI During Dry and Wet Years

The WaSSI$_G$ and WaSSI$_B$ showed green and blue water stresses during the dry years (**Figure 4**; **Table 3**). The intensity of green and blue water stresses during dry years varied within and

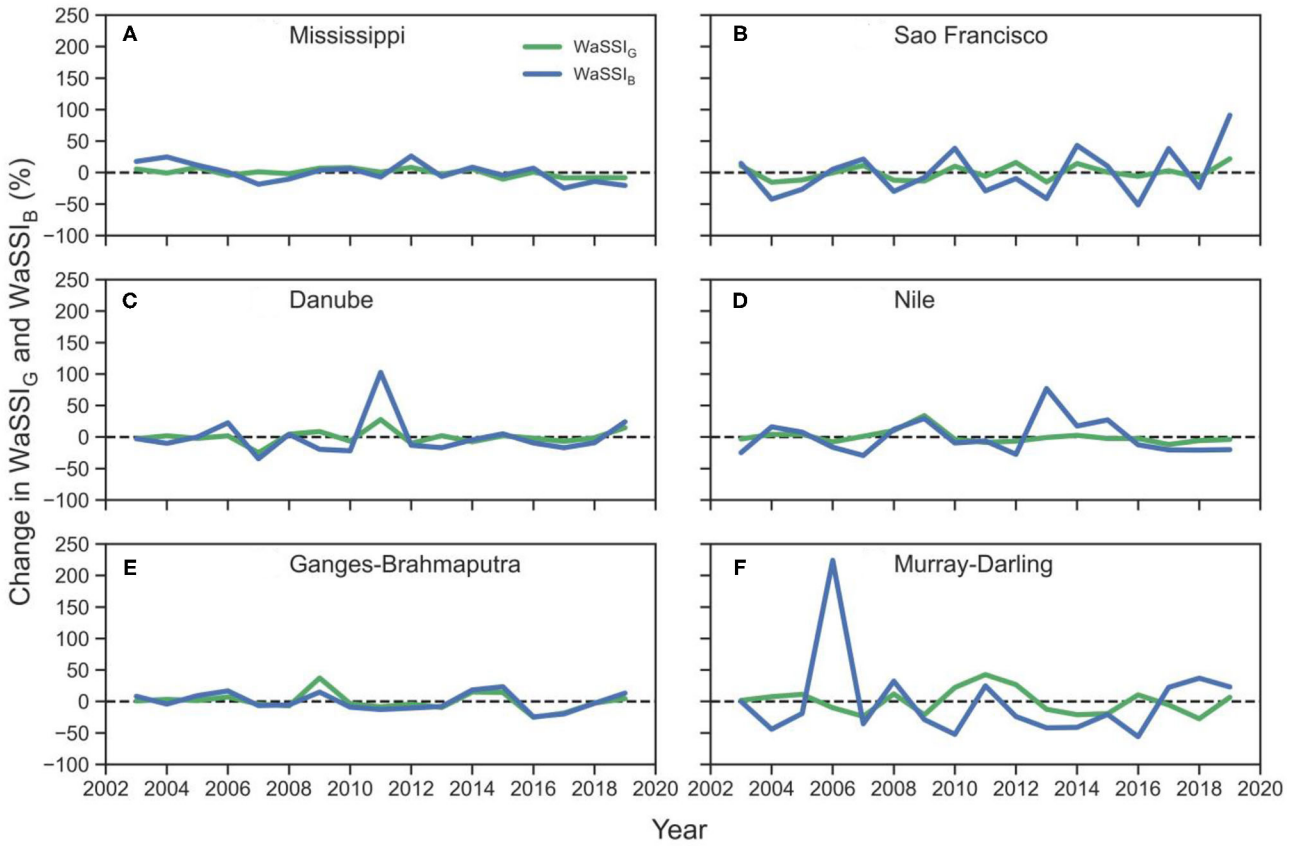

FIGURE 3 | Anomalies (percent deviation from average value) of green (WaSSI$_G$) and blue (WaSSI$_B$) water supply stress indices across study basins including Mississippi **(A)**, Sao Francisco **(B)**, Danube **(C)**, Nile **(D)**, Ganges-Brahmaputra **(E)**, and Murray-Darling **(F)** from 2003 to 2019.

across the study basins. For example, the western regions of the Mississippi Basin faced more green and blue stresses compared to the eastern regions of the basin (**Figure 4**) in the dry year of 2012. The central region of the Sao Francisco Basin had more stress than the northern or southern regions of the basin in the dry year 2012. Similarly, the central and eastern regions of Danube, southern region of the Nile Basin, central region of the Ganges-Brahmaputra Basin, and eastern region of the Murry-Darling Basin faced maximum stress during dry years (**Figure 4**). The spatially distributed maps of WaSSI$_G$ are visually clearer than WaSSI$_B$ maps showing several green water stress regions during the respective dry and wet years for all basins. In contrast, blue water stress indicated by WaSSI$_B$ maps for Sao Francisco, Danube, and Nile Basins is less evident due to the lower irrigated area (<6%) compared to other basins.

During the dry years across all basins, the largest green water stress (28% above average) was observed at the Ganges-Brahmaputra Basin for the dry year 2009 when the basin precipitation was 11% below the average precipitation. Similarly, the largest blue water stress (224% above average) was at the Murray-Darling Basin for the dry year 2006 when the precipitation was 35% below average. For wet years, the least green water stress (15% below average) was at the Sao Francisco Basin when the precipitation was 24% above average and the least blue water stress (52% below average) was for the Murray-Darling Basin when the precipitation was 35% above average. These results show that WaSSI$_G$ and WaSSI$_B$ variations followed the trends of basin precipitation; however, the magnitudes of green and blue water stresses varied across and within basins. Thus, WaSSI$_G$ and WaSSI$_B$ indices can be applied for monitoring green and blue water stresses at basin scales. For basins with the potential spatial disconnect between the available water (runoff and precipitation) and the point of water use (irrigation), pixel-scale applications of WaSSI$_G$ and WaSSI$_B$ may benefit from additional *in-situ* information before decisions can be made.

DISCUSSION

Drivers of Green and Blue Water Stresses

The interannual plots of WaSSI$_G$ and WaSSI$_B$ indicate the large variations of green and blue water stresses within and across the study basins (**Figures 2**, **3**). These variations are primarily driven by either demand or supply of green and blue water at the basins. Based on the water demand and water available for crops applied in this study, the interannual variations of green water stresses were driven by both the demand (ETa) and supply (precipitation)

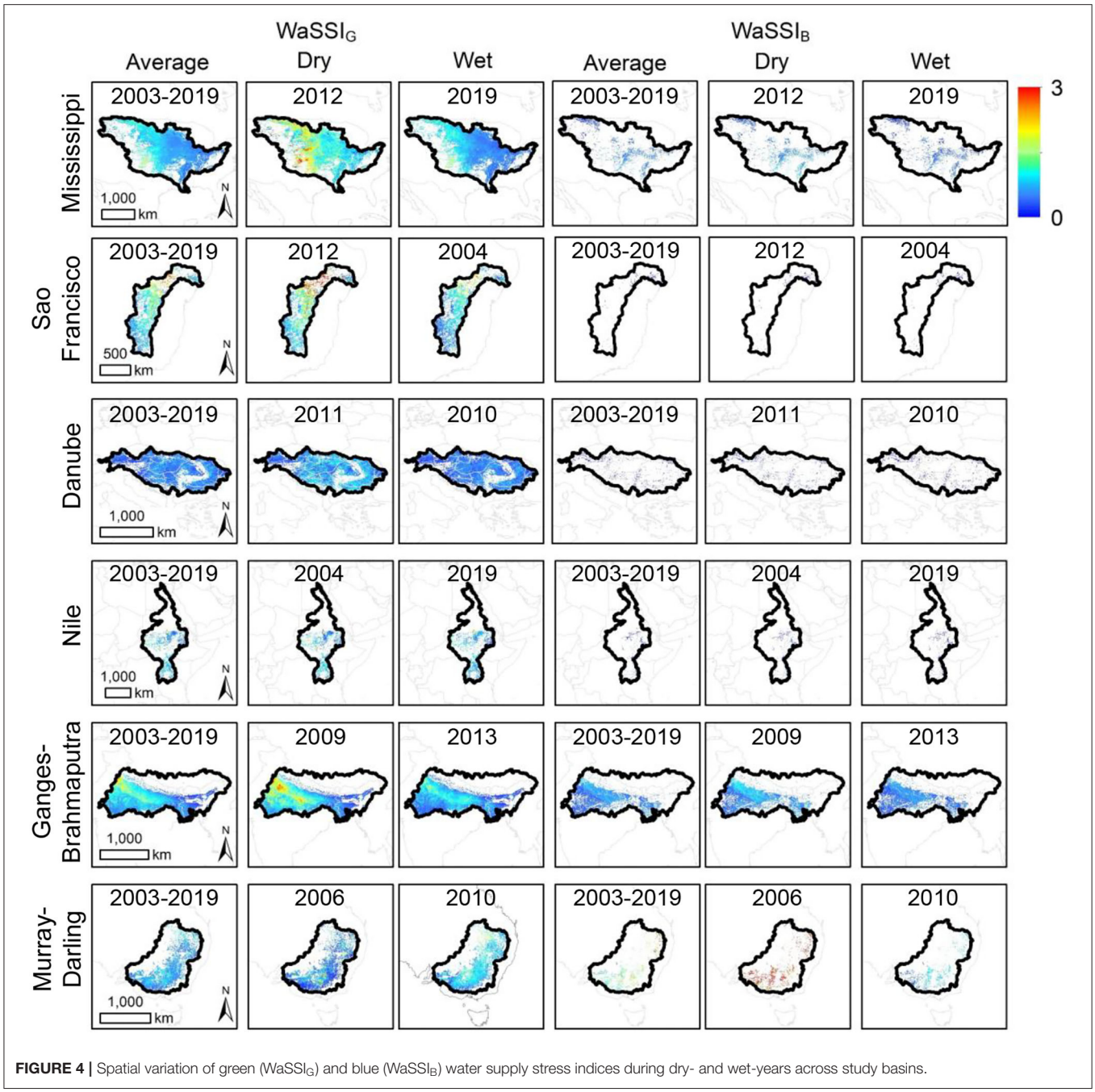

FIGURE 4 | Spatial variation of green (WaSSI$_G$) and blue (WaSSI$_B$) water supply stress indices during dry- and wet-years across study basins.

for most of the basins. The differences of the percent coefficient of variation (CV) between the green water demand and the green water supply were within ±7% for all basins except for the Murray-Darling Basin (**Supplementary Table 1**). The Murray-Darling Basin is the basin with the largest interannual variations in green water stress (**Figure 3**). The basin had the percent CV of green water demand that was 16% greater than that of green water supply, indicating the larger influence of water demand for green water stress variations. For the blue water stress, the percent CV of blue water supply (runoff) was larger than the percent CV of demand (ETa) for all basins (**Supplementary Table 1**). The smallest difference between the percent CVs of water demand and supply was for the Ganges-Brahmaputra Basin (4% larger CV for supply) and the largest difference was for the Murry-Darling basin (29% larger CV for supply). Thus, the variation in blue water stress was driven more by water supply than by water demand.

The cropland area within a basin can affect green and blue water stresses. Basins with large cropland areas tend to have higher green and blue (when irrigated) water demands and

TABLE 3 | Summary of green ($WaSSI_G$) and blue ($WaSSI_B$) water supply stress indices during dry and wet years across study basins.

Basin	Dry year				Wet year			
	Year	Precipitation mm/year	$WaSSI_G$	$WaSSI_B$	Year	Precipitation mm/year	$WaSSI_G$	$WaSSI_B$
Mississippi	2012	646	0.71	0.52	2019	989	0.65	0.33
Sao Francisco	2012	682	1.06	0.08	2004	1,120	0.77	0.05
Danube	2011	613	0.63	0.19	2010	950	0.46	0.07
Nile	2004	548	0.81	0.26	2019	747	0.75	0.18
Ganges-Brahmaputra	2009	1,128	0.94	0.60	2013	1,384	0.62	0.48
Murray-Darling	2006	283	0.62	5.16	2010	708	0.84	0.76

therefore are more prone to water stress when the water supply is limited. Among the study basins, the Danube Basin had the largest cropland (∼72%); however, the maximum magnitude of water stress (both green and blue water) was observed at the Murray Darling Basin. Similarly, the Nile Basin had the smallest cropland (∼20%) but the minimum water stress magnitude was observed at the Mississippi Basin. Although the Mississippi Basin had the least water stress magnitude, this basin had the longest duration of both green and blue water stresses (9 out of 17 years). These results indicate the percent area of cropland is not the primary factor to drive green and blue water stresses (magnitude and duration) at these studied basins. However, the spatial distribution of cropland within the basins can affect the green and blue water stresses. For example, irrigated cropland with easy access to available water may not suffer more blue water stress during droughts compared to cropland that is far from the available water within a basin. Other factors such as climate, crop types (high or low water demand), infrastructure development for irrigation systems (high or low water use efficiency), and local and regional water management policies can influence variations in green and blue water stresses across the basins.

Limited studies have applied the WaSSI approach for assessing water stress across basins considered in this study. A study by Averyt et al. (2013) in the U.S. reported about 9% (193 out of 2103) of the HUC8 basins were stressed in 2013. The agricultural sector was the main contributor to the water stress, mostly in the lower Mississippi Basin and most of the western U.S. Although our study was further extended to link with green and blue water resources, the spatial distribution of water stress regions in the Mississippi Basin (**Figure 4**) is consistent with Averyt et al. (2013). Several other studies have accounted blue and green water availability and consumption (Schuol et al., 2008; Wada et al., 2011; Hoekstra et al., 2012), and the potential factors that can affect water availability for croplands (Rost et al., 2008; Liu and Yang, 2010). For example, Ferrarini et al. (2020) reported the potential expansion of irrigated areas in the upper and middle regions of Sao Francisco Basin due to water availability. Our study shows that the blue water stress at the Sao Francisco Basin is among the lowest (**Table 2**); however, expansion of irrigated areas may add stress on blue water resources in the basin. The larger blue water stress in the Ganges-Brahmaputra Basin and Murray-Darling Basins (**Table 2**) indicates the higher vulnerability of croplands in the basin to extreme water stress, especially during the dry seasons/years, that may lead to complete desiccation and substantial economic disruption (Hoekstra et al., 2012).

Model Parameter Estimation Uncertainties

Three primary parameters (precipitation, ETa, and runoff) were applied to assess green and blue water stresses across the study basins. The precipitation data were obtained from the gauge-adjusted CHIRPS datasets. The CHIRPS precipitation data have been widely validated across the globe (Paredes-Trejo et al., 2017; Prakash, 2019; Tarek et al., 2020). A recent global-scale evaluation of CHIRPS monthly precipitation from 2000 to 2016 with the Global Precipitation Climatology Center gauge-based precipitation data reported error (including random and bias components) within ±2.5% across Europe, Africa, Australia, United States, and South America (Shen et al., 2020). The Southeast China region had a relatively larger error at 5.6% (Shen et al., 2020); however, this region does not cover the large cropland areas included in this study. Additionally, these errors are at a monthly scale and the annual scale error is smaller at −0.06% (Shen et al., 2020).

ETa data were from the surface energy balance based SSEBop model. The SSEBop ETa products have been applied across different climates and land covers for monitoring water use from a field to regional scales (Singh et al., 2014; Alemayehu et al., 2017; da Motta Paca et al., 2019; Schauer and Senay, 2019). The continental-scale validated ETa maps across several land covers (Senay et al., 2020) were applied in this study which captured seasonal and interannual variations when compared with flux tower observations. For croplands, the SSEBop tends to underestimate ETa at a monthly scale in North America and Europe (up to −33%) compared to flux tower observations without energy balance closure (Senay et al., 2020). Considering the energy balance closure issue with flux towers, which often lag in the order of 20% (Wilson et al., 2002), errors from SSEBop ETa would be lower when aggregated to longer temporal scales such as monthly and annual scales (Senay et al., 2016). Further, green and blue water stresses in this study are evaluated at a basin-scale (unlike a few 100 m in the flux tower footprint) and therefore these ETa-related errors are expected to be lower for monitoring interannual water stress variations at basin scales.

Runoff estimations from the water balance VegET model were calibrated with the observation-based GRUN and the climatology runoff data from GRDC. Although the VegET model was calibrated when the differences in annual runoff values

were $> \pm 10\%$, the runoff estimation uncertainty may still exist when applying the model for evaluating blue waters stress for basins with relatively low percent cover of irrigated croplands (for example, the Sao Francisco and Nile Basins). However, the evaluation of green and blue water stresses severity (magnitude) and duration with the baseline of 17-year (2003–2019) average values, rather than the absolute values of $WaSSI_G$ and $WaSSI_B$ for each year, would minimize the potential uncertainties from the model parameter estimations.

Advantages and Limitations of Partitioning Green and Blue Water Stresses

The idea of partitioning water consumed by crops into green and blue water sources is a fairly new approach (Falkenmark and Rockström, 2006; Rost et al., 2008; Liu and Yang, 2010; Velpuri and Senay, 2017). The assessment of green and blue water use at varying scales helps to identify the areas to efficiently manage and use the available water. This study demonstrated an approach for monitoring green and blue water stresses for croplands, which is directly associated with food and water status. The current study of green and blue water stresses across the six major cropland basins provides an insight on how green and blue water stresses vary (demand vs. supply driven) with time and space, and identified the basins that need to address the associated water stresses. For example, most basins had green water stress larger than the blue water stresses highlighting the uncertainty in food production as most of the global food production comes from green water-dependent rainfed systems. Similarly, the Murray-Darling Basin had the most severe (maximum $WaSSI_G$ and $WaSSI_B$ anomalies) green and blue water stress, which indicates that adoption of measures to improve the overall water use efficiency for sustaining food production may be beneficial. Proven methods and technologies can help to efficiently manage the available water. For example, Chukalla et al. (2015) reported that change in irrigation and mulching strategies in irrigated agriculture can reduce the green and blue water footprint up to 28%. Identification of regions or basins with green and blue water stresses could be useful for specific resource allocation and potential infrastructure development for improving green water and blue water use efficiency. Additionally, while blue water-based policies have been focused in the past (Sulser et al., 2010), the basin-specific green and blue water integrative plans and polices would help to minimize water stress and increase food production.

Besides the advantages of partitioning green and blue water resources, limitations exist when implementing the partitioning approach in this study. Our study is primarily focused on identifying an index to account for both green and blue water stress and their variations across time and space, rather than to accurately quantify green and blue water use as explored in previous studies (Siebert and Döll, 2010; Hoekstra, 2019). Thus, the equations used to compute $WaSSI_G$ and $WaSSI_B$ and assumptions made in this study must be considered before making decisions. For example, effective precipitation would have applied to compute $WaSSI_G$ for an ideal condition. However, due to additional data required for partitioning precipitation to canopy interception, runoff, soil moisture, and effective precipitation, and additional uncertainties associated with these estimations, total precipitation was applied to compute $WaSSI_G$. The use of total precipitation may have exaggerated $WaSSI_G$, especially for irrigated areas due to the contribution of blue water and reached the basin-scale $WaSSI_G$ more than one (1). Basin-scale $WaSSI_G$ values were less than 1 for most basins but a year (2009) in the Nile Basin and 6 years (2003, 2007, 2010, 2012, 2014, and 2019) in the Sao Francisco Basin. The frequent $WaSSI_G$ values of more than 1 in the Sao Francisco Basin may indicate a larger contribution of blue water across irrigated croplands. For computing $WaSSI_B$, reliable groundwater data was not available. For this reason, surface runoff was considered available blue water with the assumption of interconnections between the surface water and groundwater at a basin-scale analysis. This assumption may add bias to the blue water stress estimations. For example, $WaSSI_B$ for the dry year 2006 in the Murray-Darling Basin was relatively high, compared to other years (**Figure 2**), primarily due to a substantial reduction (87% below average) in the modeled runoff. The exclusion of groundwater may have exaggerated the blue water stress for the dry year in this basin. However, the calculated blue water stress anomalies are based on the 17-year (2003–2019) average, and therefore, the biases on the anomalies were not influenced primarily by the unavailability of groundwater data. The green and blue water stress anomalies are presented at an annual scale to capture water used by all crops including main crops grown during the growing season and other crops (e.g., cover crops, secondary crops) grown during the non-growing season. Thus, the annual scale analysis does not reflect monthly or seasonal stresses. The potential water transfer (blue water) from a year to the following year that is stored in reservoirs is not accounted for by WaSSI indices. Another limitation included the unavailability of consistent land cover data for all years during the study period. Therefore, this study used the cropland data for the nominal year 2010 based on several studies from 2007 to 2012 (Thenkabail et al., 2016). The cropland area may have changed in the other years, which could change the water stresses. However, the water stresses are generalized at a basin-scale and may have minimal effects on the overall outcome of this study. Additionally, previous studies have suggested refinement of green and blue water estimation in croplands such as by computing soil water balance components (Siebert and Döll, 2010), which could improve the spatiotemporal accuracy and further enhancement of similar green and blue water stress indices. With the availability of consistent finer scale land cover data, groundwater data, and associated dataset, the $WaSSI_G$ and $WaSSI_B$ indices can be improved and implemented for monitoring water stress and have potential applications for creating and implementing basin-specific adaptive decision support systems to ensure food and water security.

CONCLUSION

An approach to assess the water stress across croplands based on green and blue water resources is demonstrated by applying

the water supply stress index across six large cropland basins across the globe. The results from the 17-year (2003–2019) study show that all basins had both green and blue water stresses for at least 35% (6 out of 17 years) of the study period. The most severe (maximum $WaSSI_G$ and $WaSSI_B$ anomalies) green and blue water stresses were observed for the Murray-Darling Basin in Australia and the least severe (minimum $WaSSI_G$ and $WaSSI_B$ anomalies) stress for the Mississippi Basin in North America. The interannual variations in green water stress were driven by both crop water demand and green water supply, whereas the blue water stress variations were primarily driven by blue water supply. This study identified the basins and regions that may benefit from basin-specific adaptive measures and policies for the efficient use and management of available water. Similar studies can be implemented to monitor the green and blue water stresses at varying scales for developing decision support systems to ensure food and water security.

DATA AVAILABILITY STATEMENT

The datasets presented in this study can be found in online repositories. The names of the repository/repositories are provided in the methods section of the article.

AUTHOR CONTRIBUTIONS

GS and KK: conceptualization. KK, GS, SK, and GP: methodology, formal analysis, and writing—review and editing. SK and GP: software. KK: writing—original draft preparation. GS: project administration. All authors contributed to the article and approved the submitted version.

FUNDING

This research was funded by the USGS Land Change Science program.

ACKNOWLEDGMENTS

The authors would like to acknowledge the USGS Land Change Science program and FEWS NET for supporting remote sensing-based ET research and applications. Any use of trade, firm, or product names is for descriptive purposes only and does not imply endorsement by the U.S. Government.

SUPPLEMENTARY MATERIAL

The Supplementary Material for this article can be found online at: https://www.frontiersin.org/articles/10.3389/fclim.2021.663444/full#supplementary-material

REFERENCES

Alemayehu, T., Griensven, A. V., Senay, G. B., and Bauwens, W. (2017). Evapotranspiration mapping in a heterogeneous landscape using remote sensing and global weather datasets: application to the Mara Basin, East Africa. *Remote Sens.* 9:390. doi: 10.3390/rs9040390

Alexandratos, N. (1995). *World Agriculture: Towards 2010: An FAO Study*. New York, NY: John Wiley.

Averyt, K., Meldrum, J., Caldwell, P., Sun, G., McNulty, S., Huber-Lee, A., et al. (2013). Sectoral contributions to surface water stress in the coterminous United States. *Environ. Res. Lett.* 8:035046. doi: 10.1088/1748-9326/8/3/035046

Bhaduri, A., Bogardi, J., Siddiqi, A., Voigt, H., Vörösmarty, C., Pahl-Wostl, C., et al. (2016). Achieving sustainable development goals from a water perspective. *Front. Environ. Sci.* 4:64. doi: 10.3389/fenvs.2016.00064

Bisselink, B., De Roo, A., Bernhard, J., and Gelati, E. (2018). Future projections of water scarcity in the Danube River Basin due to land use, water demand and climate change. *J. Environ. Geogr.* 11, 25–36. doi: 10.2478/jengeo-2018-0010

Caldwell, P. V., Sun, G., McNulty, S. G., Cohen, E. C., and Myers, J. A. M. (2012). Impacts of impervious cover, water withdrawals, and climate change on river flows in the conterminous US. *Hydrol. Earth Syst. Sci.* 16, 2839–2857. doi: 10.5194/hess-16-2839-2012

Chukalla, A. D., Krol, M. S., and Hoekstra, A. Y. (2015). Green and blue water footprint reduction in irrigated agriculture: effect of irrigation techniques, irrigation strategies and mulching. *Hydrol. Earth Syst. Sci.* 19, 4877–4891. doi: 10.5194/hess-19-4877-2015

da Motta Paca, V. H., Espinoza-Dávalos, G. E., Hessels, T. M., Moreira, D. M., Comair, G. F., and Bastiaanssen, W. G. (2019). The spatial variability of actual evapotranspiration across the Amazon River Basin based on remote sensing products validated with flux towers. *Ecol. Proces.* 8, 1–20. doi: 10.1186/s13717-019-0158-8

Duan, K., Caldwell, P. V., Sun, G., McNulty, S. G., Zhang, Y., Shuster, E., et al. (2019). Understanding the role of regional water connectivity in mitigating climate change impacts on surface water supply stress in the United States. *J. Hydrol.* 570, 80–95. doi: 10.1016/j.jhydrol.2019.01.011

Eldardiry, H., Habib, E. H., and Borrok, D. M. (2016). Small-scale catchment analysis of water stress in wet regions of the US: an example from Louisiana. *Environ. Res. Lett.* 11:124031. doi: 10.1088/1748-9326/aa51dc

Eriksen, S., and Lind, J. (2009). Adaptation as a political process: adjusting to drought and conflict in Kenya's drylands. *Environ. Manage.* 43, 817–835. doi: 10.1007/s00267-008-9189-0

Falkenmark, M., Berntell, A., Jägerskog, A., Lundqvist, J., Matz, M., and Tropp, H. (2007). *On the Verge of a New Water Scarcity: A Call for Good Governance and Hyman Ingenuity*. Stockholm: Stockholm International Water Institute.

Falkenmark, M., and Rockström, J. (2006). The new blue and green water paradigm: breaking new ground for water resources planning and management. *J. Water Resour. Plann. Manag.* 132, 129–132. doi: 10.1061/(ASCE)0733-9496(2006)132:3(129)

Fekete, B. M., Vörösmarty, C. J., and Grabs, W. (2002). High-resolution fields of global runoff combining observed river discharge and simulated water balances. *Global Biogeochem. Cycles* 16, 15–11. doi: 10.1029/1999GB001254

Ferrarini, A. D. S. F., Ferreira Filho, J. B. D. S., Cuadra, S. V., and Victoria, D. D. C. (2020). Water demand prospects for irrigation in the São Francisco River: Brazilian public policy. *Water Policy* 22, 449–467. doi: 10.2166/wp.2020.215

Flörke, M., Schneider, C., and McDonald, R. I. (2018). Water competition between cities and agriculture driven by climate change and urban growth. *Nat. Sustain.* 1, 51–58. doi: 10.1038/s41893-017-0006-8

Funk, C., Peterson, P., Landsfeld, M., Pedreros, D., Verdin, J., Shukla, S., et al. (2015). The climate hazards infrared precipitation with stations—a new environmental record for monitoring extremes. *Sci. Data* 2, 1–21. doi: 10.1038/sdata.2015.66

Ghiggi, G., Humphrey, V., Seneviratne, S. I., and Gudmundsson, L. (2019). GRUN: an observation-based global gridded runoff dataset from 1902 to 2014. *Earth Syst. Sci. Data* 11, 1655–1674. doi: 10.5194/essd-11-1655-2019

Gleick, P. H. (2003). Water use. *Annu. Rev. Environ. Resour.* 28, 275–314. doi: 10.1146/annurev.energy.28.040202.122849

Hanjra, M. A., and Qureshi, M. E. (2010). Global water crisis and future food security in an era of climate change. *Food Policy* 35, 365–377. doi: 10.1016/j.foodpol.2010.05.006

Hoekstra, A. Y. (2019). Green-blue water accounting in a soil water balance. *Adv. Water Resour.* 129, 112–117. doi: 10.1016/j.advwatres.2019.05.012

Hoekstra, A. Y., Mekonnen, M. M., Chapagain, A. K., Mathews, R. E., and Richter, B. D. (2012). Global monthly water scarcity: blue water footprints versus blue water availability. *PLoS ONE* 7:e32688. doi: 10.1371/journal.pone.0032688

Howitt, R., Medellín-Azuara, J., Macewan, D., Lund, J. R., and Sumner, D. (2014). *Economic Analysis of the 2014 Drought for California Agriculture.* Davis, CA: Center for Watershed Sciences University of California. Available online at: https://watershed.ucdavis.edu/2014-497 drought-report (accessed March 19, 2021).

ICPDR (2018). *Danube River Basin Climage Change Adaptation. Update of the Danube Study. International Commission for the Protection of the Danube River*. Available online at: http://www.icpdr.org/main/resources/climate-change-adaptation-update-danube-study (accessed March 19, 2021).

Ji, Y., Chen, L., and Sun, R. (2012). Temporal and spatial variability of water supply stress in the Haihe River Basin, Northern China. *J. Am. Water Resour. Assoc.* 48, 999–1007. doi: 10.1111/j.1752-1688.2012.00671.x

Kang, Y., Khan, S., and Ma, X. (2009). Climate change impacts on crop yield, crop water productivity and food security–a review. *Prog. Nat. Sci.* 19, 1665–1674. doi: 10.1016/j.pnsc.2009.08.001

Kottek, M., Grieser, J., Beck, C., Rudolf, B., and Rubel, F. (2006). World map of the Köppen-Geiger climate classification updated. *Meteorol. Zeitschrift* 15, 259–263. doi: 10.1127/0941-2948/2006/0130

Leng, G., and Hall, J. (2019). Crop yield sensitivity of global major agricultural countries to droughts and the projected changes in the future. *Sci. Total Environ.* 654, 811–821. doi: 10.1016/j.scitotenv.2018.10.434

Li, Y., Ye, W., Wang, M., and Yan, X. (2009). Climate change and drought: a risk assessment of crop-yield impacts. *Clim. Res.* 39, 31–46. doi: 10.3354/cr00797

Liu, J., and Yang, H. (2010). Spatially explicit assessment of global consumptive water uses in cropland: green and blue water. *J. Hydrol.* 384, 187–197. doi: 10.1016/j.jhydrol.2009.11.024

McNulty, S., Mack, E. C., Sun, G., and Caldwell, P. (2016). "Hydrologic modeling for water resource assessment in a developing country: the Rwanda case study," in *Forest and the Water Cycle: Quantity, Quality, Management*, eds P. Lachassagne and M. Lafforgue (Newcastle upon Tyne: Cambridge Scholars Publishing), 198–203.

Molden, D. (2007). Water responses to urbanization. *Paddy Water Environ.* 5, 207–209. doi: 10.1007/s10333-007-0084-8

Paredes-Trejo, F. J., Barbosa, H., and Kumar, T. L. (2017). Validating CHIRPS-based satellite precipitation estimates in Northeast Brazil. *J. Arid Environ.* 139, 26–40. doi: 10.1016/j.jaridenv.2016.12.009

Prakash, S. (2019). Performance assessment of CHIRPS, MSWEP, SM2RAIN-CCI, and TMPA precipitation products across India. *J. Hydrol.* 571, 50–59. doi: 10.1016/j.jhydrol.2019.01.036

Reilly, T. E., Dennehy, K. F., Alley, W. M., and Cunningham, W. L. (2008). *Ground-Water Availability in the United States*. Reston, VA: U.S. Geological Survey.

Richey, A. S., Thomas, B. F., Lo, M. H., Reager, J. T., Famiglietti, J. S., Voss, K., et al. (2015). Quantifying renewable groundwater stress with GRACE. *Water Resour. Res.* 51, 5217–5238. doi: 10.1002/2015WR017349

Rosegrant, M. W., Cai, X., Cline, S. A., and Nakagawa, N. (2002). *The Role of Rainfed Agriculture in the Future of Global Food Production*. Washington, DC: Food Policy Research Institute.

Rost, S., Gerten, D., Bondeau, A., Lucht, W., Rohwer, J., and Schaphoff, S. (2008). Agricultural green and blue water consumption and its influence on the global water system. *Water Resour. Res.* 44:W09405. doi: 10.1029/2007WR006331

Scanlon, B. R., Faunt, C. C., Longuevergne, L., Reedy, R. C., Alley, W. M., McGuire, V. L., et al. (2012). Groundwater depletion and sustainability of irrigation in the US High Plains and Central Valley. *Proc. Natl. Acad. Sci. U.S.A.* 109, 9320–9325. doi: 10.1073/pnas.1200311109

Scanlon, B. R., Jolly, I., Sophocleous, M., and Zhang, L. (2007). Global impacts of conversions from natural to agricultural ecosystems on water resources: quantity versus quality. *Water Resour. Res.* 43:W03437. doi: 10.1029/2006WR005486

Schauer, M., and Senay, G. B. (2019). Characterizing crop water use dynamics in the central valley of california using landsat-derived evapotranspiration. *Remote Sens.* 11:1782. doi: 10.3390/rs11151782

Schuol, J., Abbaspour, K. C., Yang, H., Srinivasan, R., and Zehnder, A. J. (2008). Modeling blue and green water availability in Africa. *Water Resour. Res.* 44:W07406. doi: 10.1029/2007WR006609

Seaber, P. R., Kapinos, F. P., and Knapp, G. L. (1987). *"Hydrologic Unit Maps". U. S. Geological Survey Water Supply Paper 229*. Reston, VA: U.S. Geological Survey.

Senay, G. B. (2008). Modeling landscape evapotranspiration by integrating land surface phenology and a water balance algorithm. *Algorithms* 1, 52–68. doi: 10.3390/a1020052

Senay, G. B. (2018). Satellite psychrometric formulation of the operational Simplified Surface Energy Balance (SSEBop) model for quantifying and mapping evapotranspiration. *Appl. Eng. Agirc.* 43, 555–566. doi: 10.13031/aea.12614

Senay, G. B., Bohms, S., Singh, R. K., Gowda, P. H., Velpuri, N. M., Alemu, H., et al. (2013). Operational evapotranspiration mapping using remote sensing and weather datasets: a new parameterization for the SSEB approach. *JAWRA J. Am. Water Resour. Assoc.* 49, 577–591. doi: 10.1111/jawr.12057

Senay, G. B., Friedrichs, M., Singh, R. K., and Velpuri, N. M. (2016). Evaluating Landsat 8 evapotranspiration for water use mapping in the Colorado River Basin. *Remote Sens. Environ.* 185, 171–185. doi: 10.1016/j.rse.2015.12.043

Senay, G. B., Kagone, S., and Velpuri, N. M. (2020). Operational global actual evapotranspiration: development, evaluation, and dissemination. *Sensors* 20:1915. doi: 10.3390/s20071915

Shen, Z., Yong, B., Gourley, J. J., Qi, W., Lu, D., Liu, J., et al. (2020). Recent global performance of the Climate Hazards group Infrared Precipitation (CHIRP) with Stations (CHIRPS). *J. Hydrol.* 591:125284. doi: 10.1016/j.jhydrol.2020.125284

Siebert, S., and Döll, P. (2010). Quantifying blue and green virtual water contents in global crop production as well as potential production losses without irrigation. *J. Hydrol.* 384, 198–217. doi: 10.1016/j.jhydrol.2009.07.031

Siegfried, T., Bernauer, T., Guiennet, R., Sellars, S., Robertson, A. W., Mankin, J., et al. (2012). Will climate change exacerbate water stress in Central Asia? *Clim. Change* 112, 881–899. doi: 10.1007/s10584-011-0253-z

Singh, R., Senay, G., Velpuri, N., Bohms, S., Scott, R., and Verdin, J. (2014). Actual evapotranspiration (water use) assessment of the Colorado River Basin at the Landsat resolution using the Operational Simplified Surface Energy Balance Model. *Remote Sens.* 6, 233–256. doi: 10.3390/rs6010233

Sulser, T. B., Ringler, C., Zhu, T., Msangi, S., Bryan, E., and Rosegrant, M. W. (2010). Green and blue water accounting in the Ganges and Nile basins: implications for food and agricultural policy. *J. Hydrol.* 384, 276–291. doi: 10.1016/j.jhydrol.2009.10.003

Sun, G., McNulty, S. G., Moore Myers, J. A., and Cohen, E. C. (2008). Impacts of multiple stresses on water demand and supply across the Southeastern United States 1. *JAWRA J. Am. Water Resour. Assoc.* 44, 1441–1457. doi: 10.1111/j.1752-1688.2008.00250.x

Sun, S., Sun, G., Caldwell, P., McNulty, S. G., Cohen, E., Xiao, J., et al. (2015). Drought impacts on ecosystem functions of the US National Forests and Grasslands: part I evaluation of a water and carbon balance model. *For. Ecol. Manage.* 353, 260–268. doi: 10.1016/j.foreco.2015.03.054

Tang, L.-L., Cai, X.-B., Gong, W.-S., Lu, J.-Z., Chen, X.-L., Lei, Q., et al. (2018). Increased vegetation greenness aggravates water conflicts during lasting and intensifying drought in the Poyang Lake watershed, China. *Forests* 9:24. doi: 10.3390/f9010024

Tarek, M., Brissette, F. P., and Arsenault, R. (2020). Large-scale analysis of global gridded precipitation and temperature datasets for climate change impact studies. *J. Hydrometeorol.* 21, 2623–2640. doi: 10.1175/JHM-D-20-0100.1

Teluguntla, P., Thenkabail, P., Xiong, J., Gumma, M. K., Giri, C., Milesi, C., et al. (2015). *Global Food Security Support Analysis Data (GFSAD) at Nominal 1 km (GCAD) Derived From Remote Sensing in Support of Food Security in the Twenty-First Century: Current Achievements and Future Possibilities.* Boca Raton, FL: CRC Press.

Theisen, O. M., Holtermann, H., and Buhaug, H. (2012). Climate wars? assessing the claim that drought breeds conflict. *Int. Secur.* 36, 79–106. doi: 10.1162/ISEC_a_00065

Thenkabail, P., Knox, J., Ozdogan, M., Gumma, M., Congalton, R., Wu, Z., et al. (2016). *NASA Making Earth System Data Records for Use in Research*

Environments (MEaSUREs) Global Food Security Support Analysis Data (GFSAD) CROP Dominance 2010 Global 1 km V001. Reston, VA: U.S. Geological Survey.

UNDP (2006). *Beyond Scarcity: Power, Poverty, and the Global Water Crisis*. London: Palgrave Macmillan.

van Asten, P. J., Fermont, A., and Taulya, G. (2011). Drought is a major yield loss factor for rainfed East African highland banana. *Agric. Water Manag.* 98, 541–552. doi: 10.1016/j.agwat.2010.10.005

Vanham, D. (2016). Does the water footprint concept provide relevant information to address the water–food–energy–ecosystem nexus? *Ecosyst. Serv.* 17, 298–307. doi: 10.1016/j.ecoser.2015.08.003

Velpuri, N. M., and Senay, G. B. (2017). Partitioning evapotranspiration into green and blue water sources in the conterminous United States. *Sci. Rep.* 7, 1–12. doi: 10.1038/s41598-017-06359-w

Wada, Y., Van Beek, L., and Bierkens, M. F. (2011). Modelling global water stress of the recent past: on the relative importance of trends in water demand and climate variability. *Hydrol. Earth Syst. Sci.* 15, 3785–3808. doi: 10.5194/hess-15-3785-2011

Wilson, K., Goldstein, A., Falge, E., Aubinet, M., Baldocchi, D., Berbigier, P., et al. (2002). Energy balance closure at FLUXNET sites. *Agric. For. Meteorol.* 113, 223–243. doi: 10.1016/S0168-1923(02)00109-0

WWAP (2018). *The United Nations World Water Development Report 2018: Nature-Based Solutions for Water*. Paris: UNESCO.

Zhang, L., Sun, G., Cohen, E., McNulty, S. G., Caldwell, P. V., Krieger, S., et al. (2018). An improved water budget for the El Yunque National Forest, Puerto Rico, as Determined by the Water Supply Stress Index Model. *For. Sci.* 64, 268–279. doi: 10.1093/forsci/fxx016

Conflict of Interest: KK and SK were employed by company ASRC Federal Data Solutions. GP was employed by Innovate! Inc. The affiliations listed as Innovate! Inc. and ASRC Federal Data Solutions are contractors for the USGS EROS Center.

The remaining authors declare that the research was conducted in the absence of any commercial or financial relationships that could be construed as a potential conflict of interest.

Publisher's Note: All claims expressed in this article are solely those of the authors and do not necessarily represent those of their affiliated organizations, or those of the publisher, the editors and the reviewers. Any product that may be evaluated in this article, or claim that may be made by its manufacturer, is not guaranteed or endorsed by the publisher.

frontiers in Climate

ORIGINAL RESEARCH
published: 24 August 2021
doi: 10.3389/fclim.2021.716568

An Agro-Pastoral Phenological Water Balance Framework for Monitoring and Predicting Growing Season Water Deficits and Drought Stress

Chris Funk[1]*, *Will Turner*[1], *Amy McNally*[2,3,4], *Andrew Hoell*[5], *Laura Harrison*[1], *Gideon Galu*[1], *Kim Slinski*[3], *Juliet Way-Henthorne*[1] *and Gregory Husak*[1]

[1] Climate Hazards Center, Department of Geography, University of California, Santa Barbara, Santa Barbara, CA, United States, [2] United States Agency for International Development, Washington, DC, United States, [3] Goddard Space Flight Center, National Aeronautics and Space Administration, Greenbelt, MD, United States, [4] SAIC Inc., McLean, VA, United States, [5] NOAA Physical Sciences Laboratory, Boulder, CO, United States

OPEN ACCESS

Edited by:
Riddhi Singh,
Indian Institute of Technology Bombay, India

Reviewed by:
Udit Bhatia,
Indian Institute of Technology Gandhinagar, India
Ladislaus Benedict Chang'A,
Tanzania Meteorological Agency, Tanzania

***Correspondence:**
Chris Funk
chris@geog.ucsb.edu

Specialty section:
This article was submitted to Climate Services, a section of the journal Frontiers in Climate

Received: *28 May 2021*
Accepted: *13 July 2021*
Published: *24 August 2021*

Citation:
Funk C, Turner W, McNally A, Hoell A, Harrison L, Galu G, Slinski K, Way-Henthorne J and Husak G (2021) An Agro-Pastoral Phenological Water Balance Framework for Monitoring and Predicting Growing Season Water Deficits and Drought Stress. Front. Clim. 3:716568. doi: 10.3389/fclim.2021.716568

Sharing simple ideas across a broad community of practitioners helps them to work together more effectively. For this reason, drought early warning systems spend a considerable effort on describing how hazards are detected and defined. Well-articulated definitions of drought provide a shared basis for collaboration, response planning, and impact mitigation. One very useful measure of agricultural drought stress has been the "Water Requirement Satisfaction Index" (WRSI). In this study, we develop a new, simpler metric of water requirement satisfaction, the Phenological Water Balance (PWB). We describe this metric, compare it to WRSI and yield statistics in a food-insecure region (east Africa), and show how it can be easily combined with analog-based rainfall forecasts to produce end-of-season estimates of growing season water deficits. In dry areas, the simpler PWB metric is very similar to the WRSI. In these regions, we show that the coupling between rainfall deficits and increased reference evapotranspiration amplifies the impacts of droughts. In wet areas, on the other hand, our new metric provides useful information about water excess—seasons that are so wet that they may not be conducive to good agricultural outcomes. Finally, we present a PWB-based forecast example, demonstrating how this framework can be easily used to translate assumptions about seasonal rainfall outcomes into predictions of growing season water deficits. Effective humanitarian relief efforts rely on early projections of these deficits to design and deploy appropriate targeted responses. At present, it is difficult to combine gridded satellite-gauge precipitation forecasts with climate forecasts. Our new metric helps overcome this obstacle. Future extensions could use the water requirement framework to contextualize other water supply indicators, like actual evapotranspiration values derived from satellite observations or hydrologic models.

Keywords: agriculture, agricultural monitoring, early warning, food security, early action, forecasting, drought, drought monitoring

INTRODUCTION

A central and successful tenet of the famine early warning community is the fact that impacts of water deficits are predictable—water deficits anticipate reductions in food access and availability. In the late 1970s and 1980s, plot-based studies by the Food and Agricultural Organization (FAO) identified crop water requirements (Doorenbos and Pruitt, 1977) and created the Water Requirement Satisfaction Index (WRSI) model (Frère and Popov, 1986) to estimate yield reductions based on the crop water balance and accumulated deficits. The WRSI framework quantifies the water required for optimal plant growth during four main growth stages, with the vegetative and grain-filling stages occurring when the crop water requirements are highest. The WRSI tracks increased crop water use—and crop water stress—, which occurs when the available soil moisture is less than the crop's water requirement. For regional crop monitoring, an important step forward in operational application of the WRSI was the combination of the WRSI formulation with gridded rainfall, reference evapotranspiration, and soil property data sets (Senay and Verdin, 2001, 2003; Verdin and Klaver, 2002). These models now provide a widely used foundation for tracking agricultural shocks in food-insecure countries. WRSI is actively used to support the Famine Early Warning Systems Network (FEWS NET) Food Security Outlook (FSO) process (Magadzire et al., 2017), in which FEWS NET scientists provide forward-looking assumptions that food security analysts use to estimate food-insecure populations (Funk et al., 2019b). In this study, we draw from some of the most useful aspects of the WRSI framework and consider how advancements in forecast weather and climate data can support new types of forward-looking crop and rangeland monitoring applications.

Over the past few decades, the food security community has increasingly taken advantage of the opportunities provided by climate science (Verdin et al., 2005). FEWS NET scientists use "staged" early warning systems that combine long-lead and short-lead climate and weather forecasts with high-resolution satellite observations, and hydrology and crop model simulations. The staged system accommodates the benefits and challenges from weather and climate information being produced by different communities, with disparate scales and statistical distributions, as well as the skill in long-lead time climate forecasts associated with major climate modes like the El Niño-Southern Oscillation and at short-lead time weather forecasts.

At the forefront of such efforts are climate services focused on producing "seamless" or "interoperable" sets of precipitation estimates that combine satellite observations, rain gauge archives, weather forecasts and climate outlooks—high-resolution grids that extend from the past into the future. A key aspect of such systems is that the statistical distributions of the rainfall predictions are similar to those of the observations. At weather time scales, the Climate Hazards Center (CHC) uses quantile mapping to produce high-resolution forecasts at weather time scales. At climate time scales, it is also common practice to identify analog seasons, which can also be used to generate high-resolution "forecasts" of future rainfall based on averages of observed blended satellite-gauge data. For example, in early November 2020, combinations of satellite-gauge observations, downscaled weather forecasts, and expectations based on climate analogs, were combined and presented in a Crop Monitor Alert[1] While these "Early Estimates" were fairly accurate[2], they only presented likely precipitation outcomes. To move closer to impacts associated with crop and rangeland water deficits, we explore simple combinations of Growing Season Precipitation (GSP) and estimates of crop and rangeland Water Requirements (WR). We use GSP and WR to define a simple "Phenological Water Balance" (PWB) metric.

WRSI tracking involves estimating, in mm, the amount of evapotranspiration required by the crop at each time step, which is typically a dekad, or 10-day increment[3]. This is the Water Requirement (WR). The WRSI estimates water supply, in mm per dekad, by using a "bucket" model of the soil column, parameterized using assumptions about crop phenology (e.g., rooting depth) and water holding capacity, to track soil moisture conditions throughout the growing season. The WRSI is the ratio of growing season actual evapotranspiration (AET) to the crop's water requirements (WR). This ratio quantifies the degree of crop water stress, ranging from no stress to enough stress to cause wilting (Smith, 1992; Senay and Verdin, 2003). The dekad is the most common time step used in WRSI modeling, and we use it here. Each month is divided into two 10-day dekads and a final dekad that contains the remainder of the days in each month.

The start of the growing season (SOS) commences when a location receives more than 25 mm of rain, and is followed by two dekads that total more than 20 mm of rain combined (AGRHYMET, 1996). Beginning with that first dekad, the WR component of the WRSI uses Length of Growing Period (LGP) assumptions and crop-stage-dependent coefficients (K_c) to adjust the Reference EvapoTranspiration (RefET) corresponding to the phenological cycle of healthy plant growth and photosynthesis during a growing season ($WR = RefET \times K_c$). For context, Kc values greater than one indicate periods of the phenological cycle in which the crop has a greater upper limit to its atmospheric demand of moisture than the *reference* green-grass crop used in the calculation of the RefET data. This will be shown formulaically in Methods section, but can be described generally as follows. Plants emerge, and WR increases as they add biomass during their vegetative stage. Then, after a fixed fraction of the LGP, cereals enter a grain-filling phase. The energy, carbohydrates, and sugars obtained via photosynthesis are used to increase the size and quantity of grains. Finally, cereal crops enter a senescent stage associated with decreasing WR. The bucket model, driven with observed precipitation and RefET, estimates the amount of water available for extraction as AET. When there is always sufficient moisture available to meet the WR, the WRSI (AET÷WR) will be 100%, and there is no water deficit-related yield reduction. Large (∼50%) seasonal water deficits will be associated with crop failure (Smith, 1992).

[1] http://cropmonitor.org/documents/EWCM/reports/EarlyWarning_CropMonitor_202011.pdf.

[2] https://blog.chc.ucsb.edu/?p=937.

[3] Dekads break each month into two 10 day periods and one final dekad containing the remaining days in each month.

The PWB is simpler to calculate than the WRSI, easier to integrate with climate observations and forecasts, less impacted by potential biases associated with the input rainfall and RefET data sets, and unaffected by potential errors in the specification of soil conditions. Furthermore, unlike the WRSI, the PWB is not capped at 100%, and therefore provides more information about exceptionally wet conditions. This feature may support better assessments of adverse precipitation impacts in productive agriculture areas and could mean that PWB is better equipped for monitoring impacts of extreme precipitation events and destructive storms related to global climate change (Trenberth et al., 2003; Donat et al., 2016). Sub-Saharan Africa may be experiencing more extreme precipitation events, yet information is heavily under observed (Harrison et al., 2019).

The PWB indicator can be seen as a plant-smart form of Aridity Index (Zucca et al., 2012) or Standardized Precipitation Evaporation Index (SPEI) (Vicente-Serrano et al., 2010; Peng et al., 2020). We will explore the utility of the PWB framework for seasonal monitoring, scenario development (Husak et al., 2013), yield estimation, trend analyses, and national agricultural risk management. We will use seasonal precipitation as our water supply indicator, but the approach used here could easily be expanded to incorporate alternative variables, such as satellite or model-based estimates of AET or soil moisture, Normalized Difference Vegetation Index (NDVI) Values, etc. The temporal filtering provided by the WR framework could be used in conjunction with myriad supply-related inputs. These filtered inputs, furthermore, could then feed into more complex statistical or machine-learning-based estimation processes (e.g., Laudien et al., 2020).

This study seeks to demonstrate the utility of the PWB framework for seasonal monitoring, prediction, trend analyses, and risk management. In the sections below, we examine the following questions:

- Can the PWB be used, like the WRSI, to effectively detect agricultural and pastoral droughts? Can it provide insights into areas with high drought risk?
- How does the PWB compare with WRSI as a basis for estimating national and sub-national crop production in Kenya?
- Can the PWB framework be used to combine gridded satellite observations with weather and climate forecasts to produce mid-season outlooks of plant water stress?

The case study presented here focuses on east Africa during the boreal spring Long/Gu/Belg rainy season, providing an important context for our analyses. This region, which includes parts of Kenya, Somalia, and Ethiopia, is extremely food insecure, and prone to both severe droughts and flooding. While March–April–May is the core of this season, some regions may start earlier or end later. Data and Study Region section describes the data used and our study region, and Methods section lays out our methods. Examining the Utility of the PWB Framework for Monitoring Water Stress section, Examining the Utility of the PWB Framework as a Basis for Estimation of National and Sub-national Yields in Kenya section and, Examining the Utility of the PWB Framework as a Basis for Translating Integrated Rainfall Early Estimates into Assessments of Agro-pastoral Hazards section, then examine: (1) The utility of the PWB Framework for monitoring agro-pastoral drought; (2) The utility of the PWB framework as a basis for estimation national and sub-national yields in Kenya; and (3) The utility of the PWB framework as a basis for translating integrated rainfall observations and forecasts into assessments of agro-pastoral hazards. Discussion and Conclusion sections present some discussion and conclusions.

DATA AND STUDY REGION

This study uses 1981–2020 0.1° Climate Hazards InfraRed Precipitation with Stations (CHIRPS) rainfall data (Funk et al., 2015b) and 0.1° Penman-Monteith-based RefET estimates produced by Michael Hobbins (Hobbins et al., 2016)[4] Focusing on the east Africa boreal spring rainy season, the study uses the land cover designations, LGP, and crop types commonly used by the United States Geological Survey (USGS)'s Early Warning team[5] to support FEWS NET. Three WRSI modeling frameworks have been combined to provide one synoptic overview of east Africa (**Figure 1A**). A "long rains" maize modeling framework describes crop-growing conditions across the general region. Within Ethiopia, settings for the "Belg" growing season augment this default. Finally, in drier regions, settings for rangeland are used to quantify outcomes in pastoral regions. This corresponds with the USGS's "Long rains, maize" WRSI framework[6], "Croplands Belg"[7], and "Long rains, rangeland" WRSI[8] The long rains and Belg maize simulations use the same crop coefficients, but the Belg season has been customized for Ethiopia, with a different mask, LGP, and SOS values. Where available, Belg cropland parameters were used in place of the long rains values. In highland areas, the Belg LGP values can be long, 15+ dekads, representing the slow development of crops in cool high-elevation locations. The resulting composite map provides a snapshot of conditions over the entire region in a single view, aiding in the interpretation of individually modeled growing conditions and identification of conditions which may present food-insecurity issues.

The rangeland WRSI parameters are very different from the maize parameters. The SOS calculation uses a much-less stringent threshold: 10 mm in dekad one, followed by a total of just 5 mm in the next two dekads. The maximum Kc coefficients are substantially lower (0.75 as opposed to 1.2), and the LGP is set to a universal 7 dekads.

The next key modeling parameters used are modal estimates of SOS. Using 40 years of CHIRPS data, onset dates were calculated for each pixel, and then the most frequent SOS dekad (i.e., the mode) was identified (**Figure 1B**). In this pilot study, we use these fixed dates to begin every year's growing season. In practice, different dates could be identified every year. Implicit

[4]https://psl.noaa.gov/eddi/globalrefet/.
[5]https://earlywarning.usgs.gov/fews/.
[6]https://earlywarning.usgs.gov/fews/product/125.
[7]https://earlywarning.usgs.gov/fews/product/124.
[8]https://earlywarning.usgs.gov/fews/product/130.

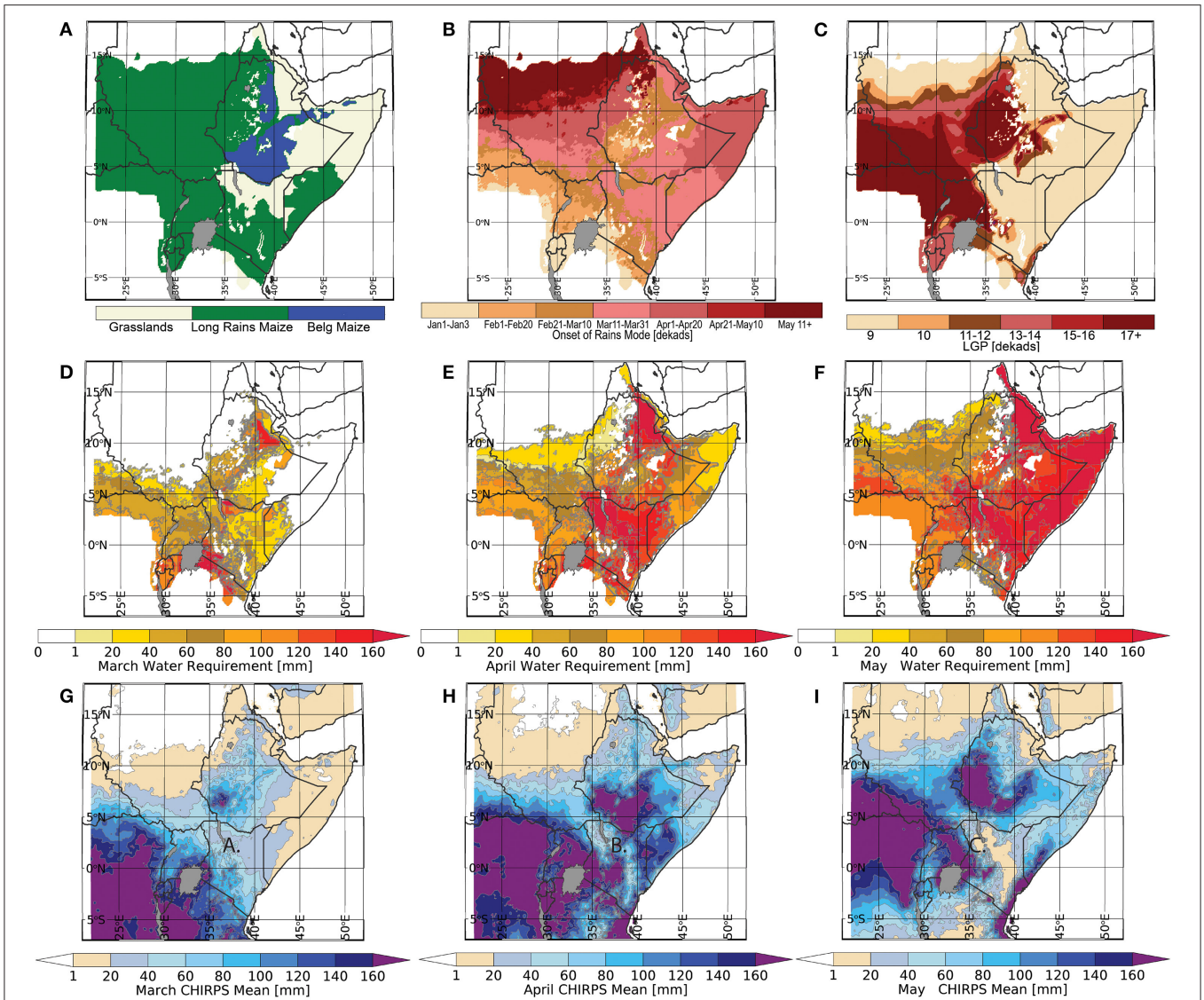

FIGURE 1 | (A) The three crop classes used to calculate Water Requirements. **(B)** The most frequent (modal) SOS dekad used to define the start of the season. **(C)** Mean LGP values, in dekads. **(D–F)** Average monthly crop WR totals in mm. **(G–I)** Average monthly CHIRPS precipitation totals in mm.

in the WRSI simulation system developed by the U.S. Geological Survey FEWS NET team[9] This framework provides spatially detailed information about the dominant crop or pasture type, when we can expect the season to begin, and how the plant water requirements are expected to evolve over time.

Commencing with the SOS dekad, LGP values (**Figure 1C**) are then used to identify the end of a growing season. Static LGP values were originally developed by WRSI modelers at the U.S. Geological Survey (Senay and Verdin, 2001, 2003; Verdin and Klaver, 2002) based on climatological (long-term average) precipitation and RefET. Note that LGP will vary dramatically depending on geographical location. A common metric for estimating LGP is the number of consecutive dekads in which the precipitation is greater than one half of the reference evapotranspiration[10] (FAO, 1978). In arid areas with low rainfall and high RefET, LGP values will be low (∼7 dekads or 70 days). In these regions, plants have a very short window through which to receive adequate moisture to support growth. In moist, cool areas with high rainfall and low RefET, LGP values can be much larger. Corresponding growing seasons can extend beyond 18 dekads (180 days). In east Africa, longitude and altitude play a huge role in determining LGP. As seen in **Figure 1C**, many critical crop-growing regions tend to be located in spatially limited, high-mountain areas associated with the Rift Valley escarpments. Meanwhile, in most of Kenya, all of Somalia, and most of Ethiopia east of 38°E, the growing season is very short.

[9]https://earlywarning.usgs.gov/fews.

[10]http://www.fao.org/nr/climpag/cropfor/lgp_en.asp.

Taken together, the SOS, LGP, and K_c coefficients provide a simple yet powerful way to automatically filter environmental information in time. In data-sparse environments, such filtering can be extremely useful in a food-security setting. While we are often interested in the ultimate drivers of food access and availability shocks, such as food production deficits, in practice, we only have proximate indicators like precipitation, RefET, etc. The WR framework gives us a physically plausible way to interpret this information. This filtering can be used to augment statistical and machine-learning-based estimation approaches and support easy-to-implement decision support informatics.

As previously noted (**Figure 1C**), most of Kenya, all of Somalia, and most of Ethiopia east of 38°E have very short growing seasons. In many of these areas, RefET and WR increases substantially in April and May (**Figures 1E,F**), and precipitation drops in May (**Figure 1I**). This results in a short window for crop and pasture growth.

A few high-elevation areas with high rainfall and low RefET provide limited areas that can support highly productive crops. The interplay of water demand and water supply can be visualized using long-term averages for March, April, and May (**Figures 1D–I**). In March, both WR and GSP totals tend to be relatively low, as the season becomes established and the growing season begins. WR values increase dramatically in April, as K_c values increase and crops typically enter their vegetative stage. April typically represents the month of maximum rains in most eastern regions (east of 38°E). In May, WR values remain high, or even increase in this eastern region, as rains begin to subside and climatological RefET values intensify. This intensification and the inherently short eastern African March-April-May rainy season can make it hard to recover from late starts or early-to-mid season deficits.

METHODS

Building on the standard FEWS NET crop phenology framework (**Figures 1A–C**), we introduce a simple agro-pastoral Phenological Water Balance (PWB), which is a form of tailored Aridity Index that takes into account the total amount of Growing Season Precipitation (GSP) and crop Water Requirements (WR) based on standard WRSI modeling practices. In this study, we use fixed SOS dates (**Figure 1B**). Beginning with each location's SOS date, and assuming a fixed LGP value at each pixel (**Figure 1C**), GSP values can be accumulated over each year's growing season's dekadal precipitation in mm (P_i).

$$GSP = \sum_{i=SOS}^{SOS+LGP} P_i \tag{1}$$

Equation (1) represents a simple measure of water supply. Borrowing directly from the WRSI framework, we can then estimate seasonal plant-specific WR values based on time-varying crop coefficients (K_c) and time-varying dekadal RefET values—equation (2). The WR values represent the amount of AET required by crops or fields to maintain maximum "water satisfaction." As atmospheric water demand (RefET) increases, the optimal amount of AET increases as well. But WR also changes as plants grow. RefET formulations typically assume a well-watered, well-developed "reference" crop, like alfalfa, that efficiently transports water into the atmosphere. At the start of the season, at emergence, WR values will be much lower than this upper limit. Hence, K_c terms start low and increase during the vegetative stage. In cereal crops, the K_c terms typically stay high during grain filling, then drop rapidly as the plants senesce. Rangeland K_c terms typically stay high throughout the plant's short (70-day) growing season (**Figure 1C**). The time-varying K_c and RefET values can be combined to calculate season WR totals in mm.

$$WR = \sum_{i=SOS}^{SOS+LGP} Kc_i \times RefET_i \tag{2}$$

While powerful, WRSI results can be problematic when any of the core inputs are biased. Furthermore, because the WRSI requires sub-monthly rainfall data, it can be difficult to connect the WRSI framework with climate forecasts, climate change simulations, or historical gridded rainfall archives. Finally, WRSI does not provide information about extremely wet conditions.

Hence, we examine here the utility of combining the WR framework of the WRSI with a simpler PWB formulation:

$$PWB = 100 \times \frac{GSP + \varepsilon}{WR + \varepsilon} \tag{3}$$

Whereas the WRSI estimates the ratio of AET and WR values, PWB examines the ratio of GSP and WR. A small value (10 mm in this study) is added to both the numerator and denominator to increase numerical stability in arid regions. This study will compare PWB results with those produced using the WRSI model, asking whether we can get reasonably comparable results using the simpler PWB framework.

Note also that the rainfall accumulations in the numerator of eq. 3 could be replaced by a host of other indicators, such as AET values from hydrologic models, like the FEWS NET Land Data Assimilation System (FLDAS) (McNally et al., 2017), hydrologic forecast systems (Arsenault et al., 2020), satellite-based energy balances (Senay et al., 2007, 2011; Anderson et al., 2011), or satellite-based vegetation or soil moisture observations (McNally et al., 2015). The WR framework, therefore, could be used to search for consilience across multiple data sets that relate to crop water supply.

RESULTS

Examining the Utility of the PWB Framework for Monitoring Water Stress

This section begins by comparing PWB and WRSI values over east Africa. As **Figures 2A**,**B** reveal, the variance structure of WRSI and PWB is quite similar in drier, water-limited areas, where WR > GSP, but quite different in wetter areas, where WR < GSP. In the latter, the WRSI tends to saturate at or just below

100%, and the WRSI standard deviation rapidly tends to zero. In these regions, the PWB is allowed to have large values >100, and hence, has a larger amount of variability. In many water-limited areas, however, we find moderate-to-high correlations between the WRSI and PWB (**Figure 2C**).

Note that there are potential advantages to both approaches. If the WRSI is perfectly calibrated with the correct soil properties, crop coefficients, plant phenology, and driven by accurate and low-bias precipitation and RefET data, then, presumably, WRSI values near 100 will be a reliable indicator of good yields. There are times and places, however, where these conditions are not met. In such cases, the simpler PWB approach might actually be more representative. Another interesting potential application of the PWB might be to explore *negative* impacts associated with very high PWB values. It seems plausible that when PWB values become very large, crops may experience waterlogging, reduced photosynthesis due to reduced sunlight, or other detrimental influences associated with extremely wet conditions. Extremely wet conditions will not register in WRSI simulations.

As one might expect, the overall correlation between the end-of-season WRSI and PWB is quite high in water-limited areas, where the standard deviation of the WRSI is high (**Figure 2A**). Stratifying these correlation grids by the standard deviation of the WRSI, we find that the mean WRSI-PWB correlations are 0.28, 0.59, 0.71, 0.83, and 0.87 when σ_{WRSI} ranges from >0 to <5, >5 to <10, >10 to <15, >15 to < 20, and >20, respectively. Hence, the PWB and WRSI results are quite similar in water-limited regions.

The simplicity of the PWB framework makes it easy to explore and quantify the covariability of the supply (GSP) and demand terms (WR). This is valuable, because the Bouchet–Morton Complementary Relationship suggests that water-limited arid regions will exhibit a negative relationship between RefET and AET (Hobbins et al., 2012). Under arid conditions, reductions in AET drive increase in RefET through energy exchanges across the land-atmosphere interface (Hobbins et al., 2016). In contrast, in humid regions, radiation, not water availability, limits AET, and RefET will equal AET. In dry regions, the lack of AET means that the Earth's surface will need to rely on upward radiative and sensible heat energy fluxes. So as radiation increases, surface temperatures and RefET increase, and as RefET increases, AET tends to decrease. And as AET decreases, RefET increases.

Figure 2D displays an empirical regression slope grid, with GSP predicting WR. While we might expect an inverse relationship from first principles, the strong spatial coherence of these slope values is nonetheless striking. Particularly in arid pastoral regimes, we find slopes as low as -0.5 mm·mm^{-1}. This slope implies that a 50-mm rainfall deficit might be exacerbated by a 25 mm increase in WR. The magnitude of the plant water deficits would be magnified by 50%, from 50 to 75 mm. On a year-to-year basis, this helps explain why pasture conditions can collapse so rapidly in arid and semi-arid areas like southern and eastern Ethiopia, northern and eastern Kenya, and all of Somalia, where RefET or WR often increase with rainfall deficits.

According to the Complementary Relationship, one expects that the mean AET and RefET will converge in humid areas and diverge in water-limited areas, where AET decreases and RefET increases. What we see in **Figure 2D** is an important temporal expression of these interdependencies. In humid areas, AET should follow RefET, and we do not expect precipitation to strongly influence RefET. Regression coefficients in these regions are very low. In dry areas, wet and dry seasons will be associated with more or less clouds and cooler or warmer land surface conditions, which in turn strongly modulate RefET and WR.

In **Figures 3**, **4** we have plotted PWB and WRSI anomalies for four boreal spring seasons, as well as four prior signature drought years. While not identical, there is a high level of agreement between the PWB and WRSI anomaly figures. This suggests that very WRSI-like results may be derived from GSP and WR. The 2017, 2018, 2019, and 2020 seasons were selected because they provide a "whip-saw" example, with dramatic swings between dry and wet seasons. Both the PWB and WRSI display this sequence. But by construction, the unbounded PWB indicator provides more information about very wet conditions in humid areas. It is interesting to note that the PWB dry anomalies in 2017 and 2019 indicate more stress in some important areas, such as southern Somalia, the south-central highlands of Ethiopia, and central-western Kenya. The stronger and more extensive drought response of the PWB index maps can be seen even more clearly in plots of four very dry seasons: 1984, 1993, 2000, and 2009. In 1984 and 1993, tragic famines struck Ethiopia and Somalia, respectively. In 2000 and 2009, strong La Niña conditions and extremely warm west Pacific sea surface temperatures produced widespread droughts (Funk et al., 2018b). For these very dry years, in humid regions, the PWB anomalies suggest more widespread water deficits than the WRSI.

Examining the Utility of the PWB Framework as a Basis for Estimation of National and Sub-national Yields in Kenya

We next turn to a comparison of WRSI and PWB values with national and sub-national maize yields for Kenya. Kenya has been selected because of its abundant crop data compared to other countries in the region. It should be noted, however, that this data is imperfect, given limited and changing crop survey capacities. Two sources of yield statistics were examined: (1) sub-national (county) level yields, obtained via the FEWS NET Data Warehouse, and (2) national yields obtained from the FAO's statistical archive (FAOSTAT). At the sub-national scale, we focused on 18 key agricultural counties[11]. The PWB and WRSI time-series were very similar in 12 of these counties ($R > 0.8$). In four counties, correlations were 0.5–0.79. The remaining two counties had saturated WRSI (mean of >99%), resulting in no relationship between the two metrics.

Overall, the correlations between county-level yields and WRSI and PWB were relatively poor, with median correlations of 0.36 and 0.37, respectively. While far from impressive, these results do indicate that the performance of the WRSI and PWB

[11]Baringo, Elgeyo-Marakwet, Kajiado, Kiambu, Kirinyaga, Kwale, Laikipia, Lamu, Murang'a, Nakuru, Narok, Nyandarua, Nyeri, Taita Taveta, Tana River, Trans Nzoia, Uasin Gishu, Kilifi.

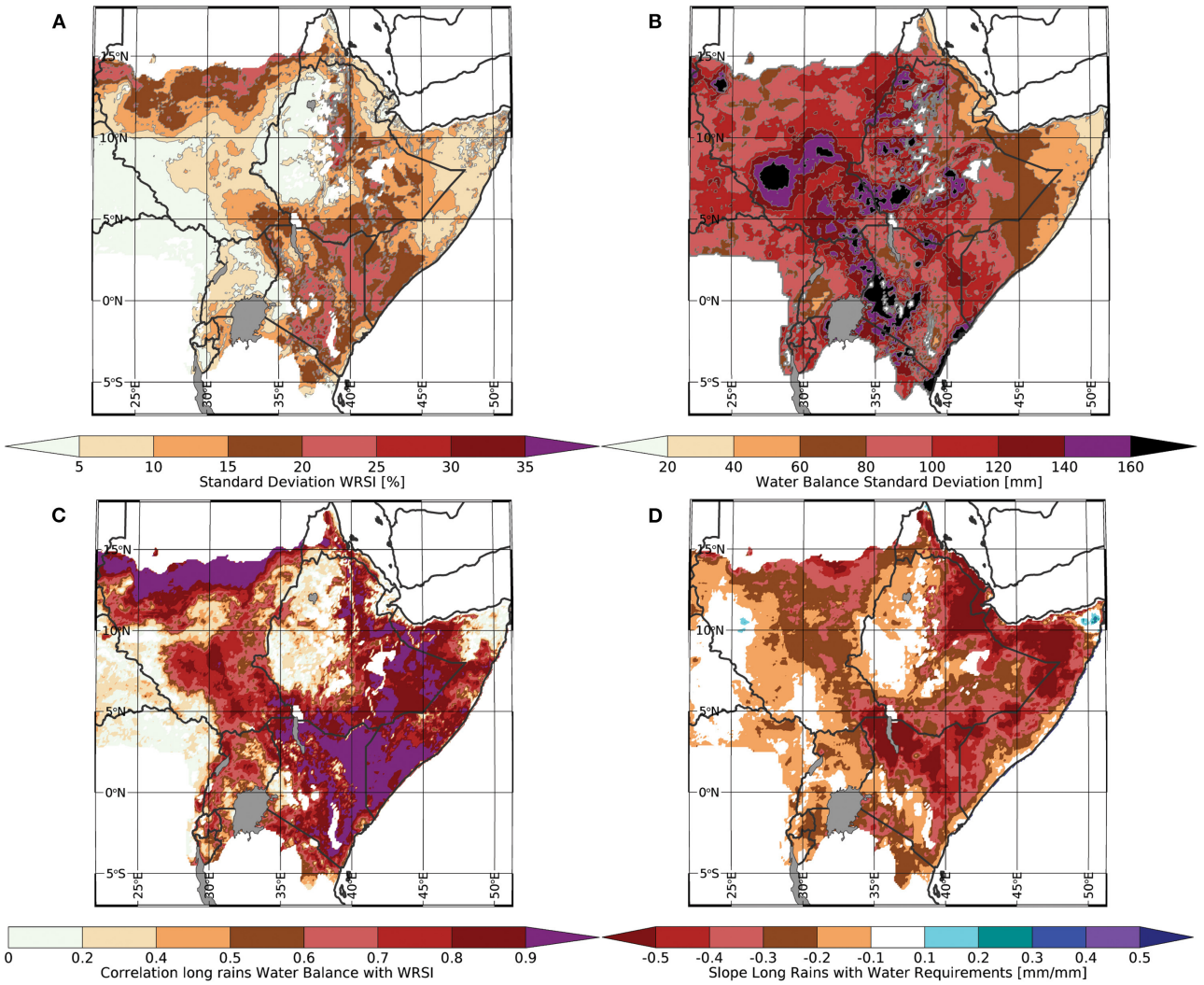

FIGURE 2 | (A) Interannual WRSI standard deviation. **(B)** Interannual PWB standard deviation. **(C)** Interannual correlation between end-of-season WRSI and WB **(D)**. Slope coefficients from regression between GSP and WR in units of mm per mm.

were not statistically distinguishable. The WRSI did not perform better than the PWB.

We next turn to comparisons with national Kenyan FAOSTAT yields and spatially aggregated sub-national yields (**Figure 5**). For these comparisons, the PWB and WRSI were averaged over key cropping counties[9]. Scatterplots with national yields are shown in panels A and B, and sub-national results are plotted in C and D. Again, the statistical relationships are fairly weak, with national R^2 values ranging from 25 to 41%[12] In general, the scatterplots reveal more discrimination when PWB and WRSI averages are low. When PWB and WRSI are high, the values' relationships with yields are weak. But, when PWB and WRSI are <90 and 60%, respectively, we do find consistent below-normal yield outcomes. These seasons (1984, 1993, 2000, and 2009) are noted in **Figure 5** and are mapped in **Figure 3**, **Figure 4**. The relationships with sub-national yields are somewhat stronger, with R^2 values of 41 and 37 percent. For both national and sub-national yields, there are low-yield seasons that have average WRSI and PWB values. It is not clear whether this is an issue with the yield statistics or a function of non-weather-related factors, such as conflict. While the PWB and WRSI performance is very similar, the PWB is substantially less complex to calculate, and less sensitive to parameterization.

Figure 6 presents a time-series of national yields and standardized PWB values from Kenya's key cropping counties. One striking aspect of this time-series is the incredibly wet outcomes in 2018 and 2020. The actual PWB values for Kenya were 269 and 232%. The GSP totals far exceeded crop water requirements. The average WRSI time-series (not shown)

[12]Please note that, in general, very few counties exhibited positive yield trends. In general, yield growth in Kenya is stagnant, and per capita cereal production is declining. https://www.usaid.gov/documents/1867/contrasting-kenyan-resilience-drought-2011-2017-full-report.

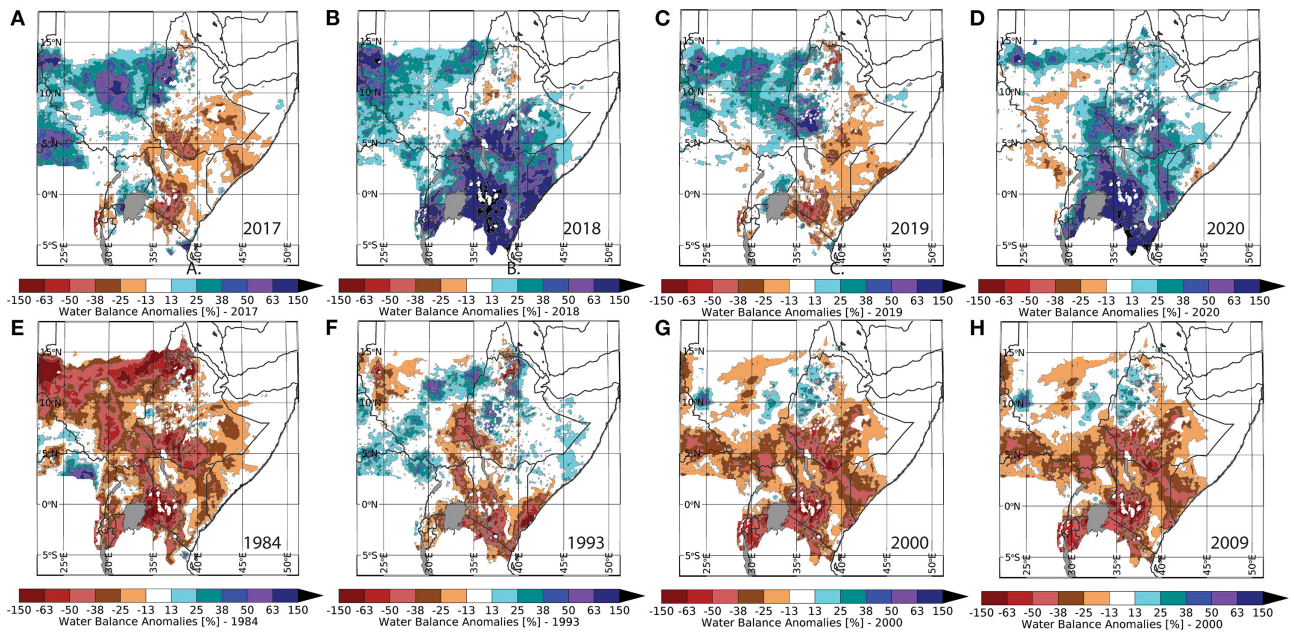

FIGURE 3 | Seasonal PWB maps, expressed as percent anomalies from the long-term average, for the four most recent years (**A** 2017, **B** 2018, **C** 2019, **D** 2020) and four extremely dry prior years (**E** 1984, **F** 1993, **G** 2000, **H** 2009).

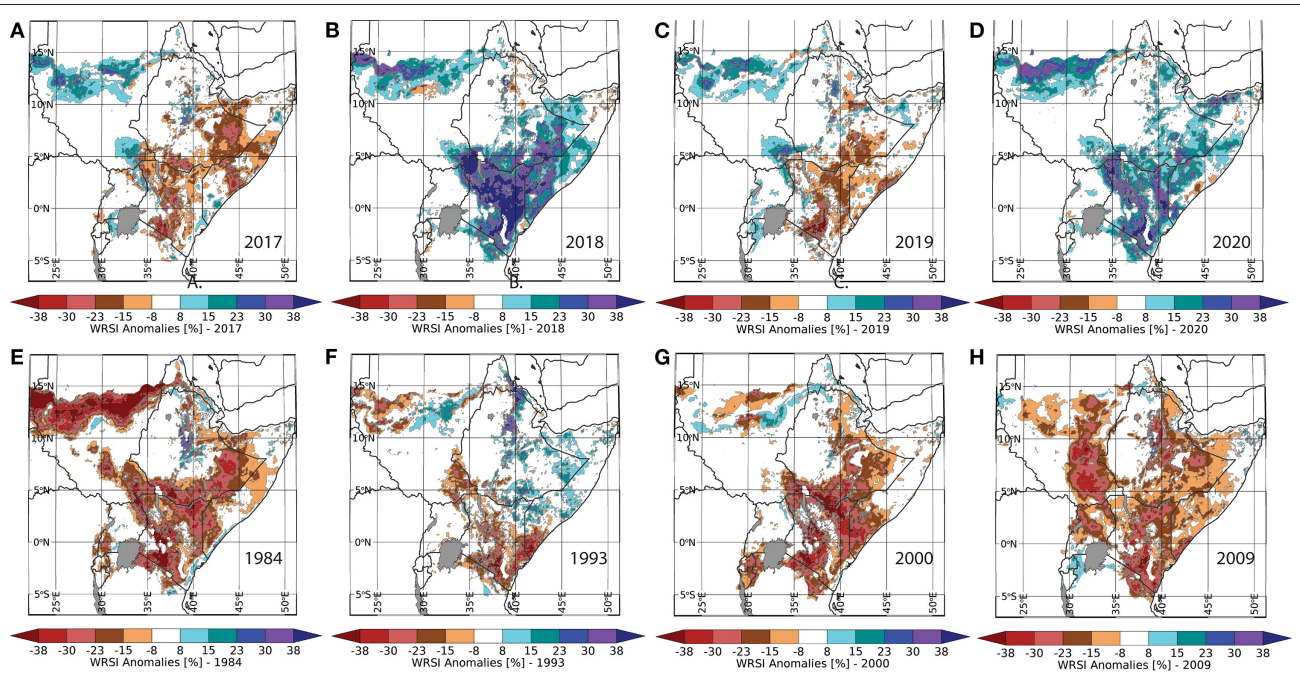

FIGURE 4 | End-of-season WRSI anomalies for the four most recent years (**A** 2017, **B** 2018, **C** 2019, **D** 2020) and four extremely dry prior years (**E** 1984, **F** 1993, **G** 2000, **H** 2009).

presents a very different story, with 2018 and 2020 values of 89 and 87. While these values are extremes in both time-series, the physical implications of these values are quite distinct. A WRSI value of about 88 indicates good cropping conditions. A PWB value of about 250% may indicate issues associated with extremely wet conditions. Again, PWB and WRSI maps of these wet seasons (**Figures 3**, **4**) demonstrate that the PWB better reflects the dynamic range of these extremely wet seasons. Plots of

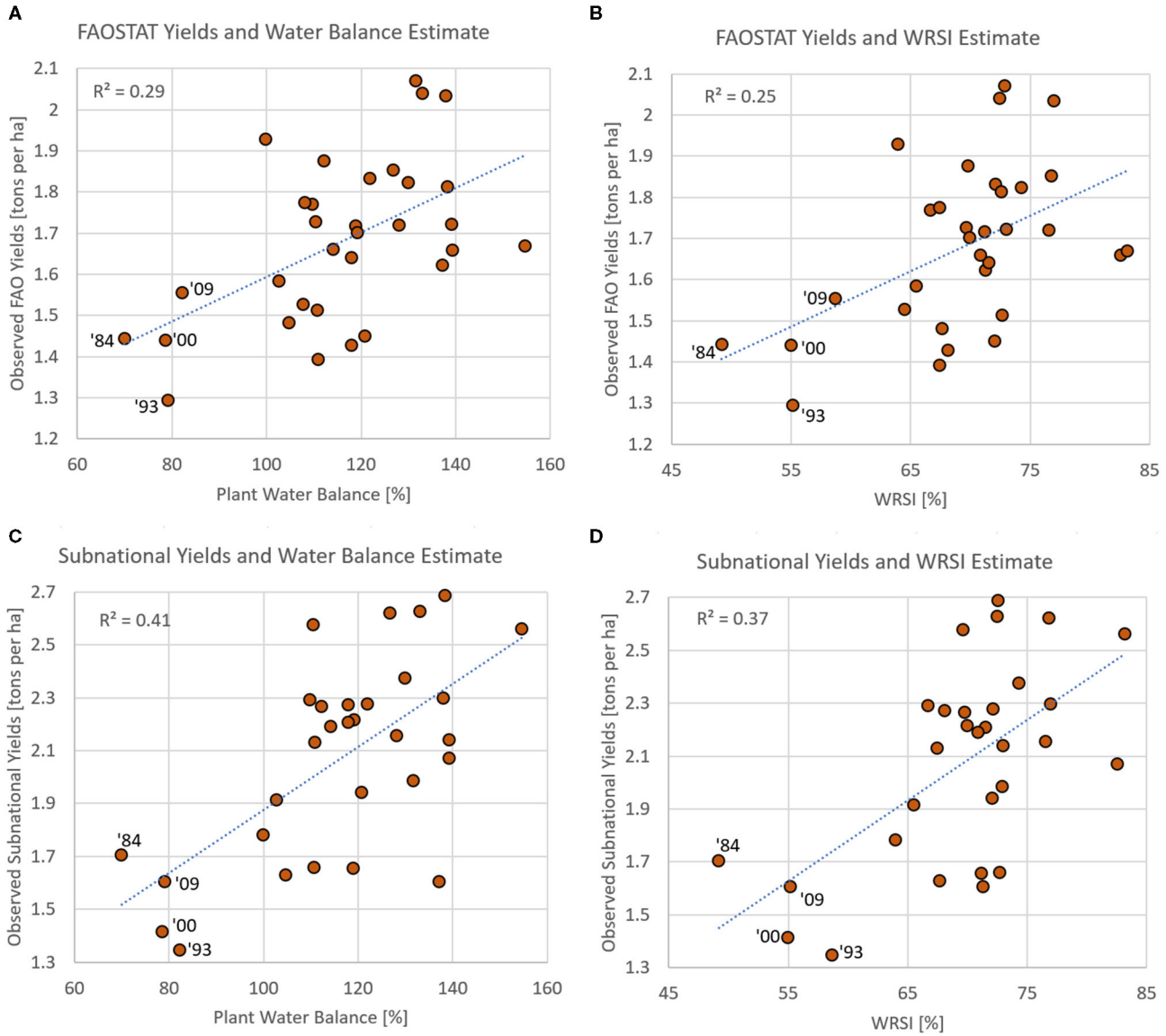

FIGURE 5 | Comparisons (scatterplots) showing Kenyan FAOSTAT national yields (y-axis) and Plant Water Balance **(A)** and WRSI **(B)** (x-axis) in key crop-growing counties in Kenya. **(C, D)** Show similar results based on sub-national yields from these counties. The FAOSTAT time-series extends from 1982 to 2019, the sub-national yields extend from 1982 to 2016.

the GSP minus WR differences (not shown) are also useful from this perspective.

It is worth noting that national yields appear quite static, i.e., they are not trending upward. At the same time, the population has grown rapidly, at about 3% per year. As we will explore, this has resulted in exceptionally low per-capita maize production values. But another striking feature of **Figure 6** is the lack of extreme agro-hydrological deficits over the last 10 years—a period in which the number of people facing acute food insecurity has climbed dramatically. While 2011, 2014, 2016, 2017, and 2019 had below-average PWB values, the magnitude of these PWB deficits were relatively mild given the historical record, with standardized anomalies of about −0.7. Given that many of these seasons were associated with large humanitarian crises (Funk et al., 2018a), these results appear to indicate that non-weather drivers may be decreasing Kenyan resilience and adaptive capacity, so that relatively modest droughts appear associated with rather large increases in food insecurity.

What will happen when Kenya experiences another severe drought, a drought similar to 1984, 1993, 2000, or 2009? We will explore this question in more detail in Examining the Utility

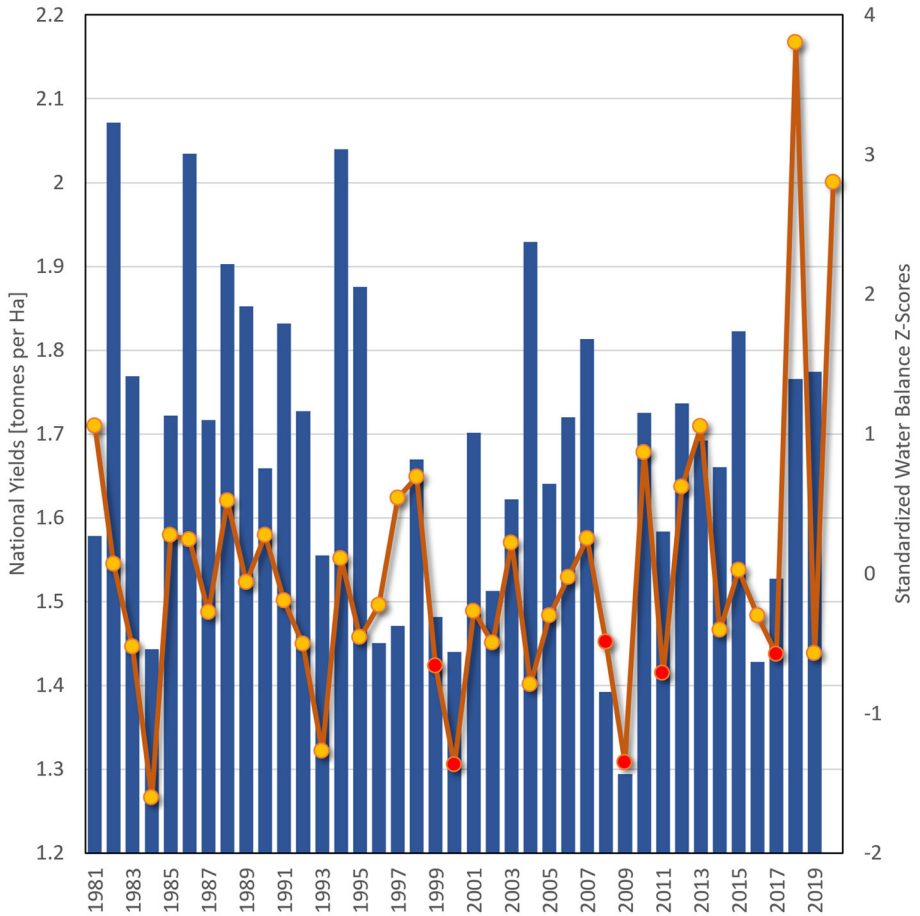

FIGURE 6 | Time-series of FAOSTAT national Kenyan maize yields (blue bars) and PWB Z-scores for key crop-growing counties (orange line with dots).

of the PWB Framework as a Basis for Translating Integrated Rainfall Early Estimates into Assessments of Agro-pastoral Hazards section.

Examining the Utility of the PWB Framework as a Basis for Translating Integrated Rainfall Early Estimates Into Assessments of Agro-Pastoral Hazards

We next describe how the PWB framework can be used to take advantage of integrated monitoring-forecast systems. For many years, the Climate Hazards Center has worked toward methods that support the combination of high-resolution gridded rainfall estimates (like CHIRPS) with weather and climate forecasts. The basic idea is that coarse resolution weather and climate information can be transformed such that it has statistical distributions similar to high-resolution, rapidly updated data streams, like CHIRPS. This makes these forecasts *inter-operable* with the observations. The ability to combine observations and predictions can be very powerful. In terms of hydrologic modeling, the NASA Hydrologic Forecast System (NHyFAS) (Arsenault et al., 2020) provides one good example of linking to-date conditions and forecasts to assess hydrologic conditions in the future. Here, we demonstrate how the PWB framework can be used to generate forecasts of agro-pastoral water deficits. This framework builds on two existing forecasting resources: (1) high-resolution CHIRPS-GEFS 1–15-day precipitation forecasts and (2) east African climate analog-based rainfall and RefET predictions.

CHIRPS-GEFS is a bias-corrected and downscaled version of National Center for Environmental Prediction Global Ensemble Forecast System (GEFS) precipitation forecasts (Hamill et al., 2013). Quantile matching is used to make GEFS forecasts spatially compatible with various CHIRPS products[13] Daily rainfall forecasts are accumulated to create 5-, 10-, and 15-day totals. The rank-based quantile of these totals is then quantile-matched to the empirical distribution of CHIRPS rainfall for the corresponding period. The result of this quantile-matching scheme is that the average and variance of the CHIRPS data is approximately retained in the resulting CHIRPS-GEFS values.

[13]https://chc.ucsb.edu/data/chirps-gefs.

The CHIRPS-GEFS forecast data product is a valuable resource for CHIRPS users, since it provides GEFS precipitation totals and anomalies that are compatible with the historical CHIRPS. This feature allows for the timely assessment of how the latest forecast could alter the current agro-climatological situation. The CHC Early Estimates provide routinely updated analyses that combine CHIRPS and CHIRPS-GEFS.

Climate analogs can provide longer lead (1–8 months) climate forecasts. Typically based on diagnostic drought analyses, the identification of analog seasons (historical seasons that may resemble current/predicted conditions) provides a simple but powerful means of leveraging the power and detail of high-resolution data sets and hydrologic and crop simulations. This can be especially powerful when combined with skillful long-lead climate forecasts of Pacific Sea surface temperatures, as exemplified by FEWS NET long-lead forecasts for eastern Africa. To support the FEWS NET FSO process, FEWS NET uses a staged approach (Funk et al., 2019b) that combines tailored 1–8 month climate forecasts, down-scaled weather predictinos, satellite observations and hydrologic simulations (McNally et al., 2017) and forecasts (Arsenault et al., 2020).

Following the disastrous 2011 famine in Somalia (Checchi and Robinson, 2013), the FEWS NET team carried out extensive research that focused on understanding and predicting east African droughts (Hoell and Funk, 2013a; Funk et al., 2014; Hoell et al., 2014; Shukla et al., 2014). While a full description of this work is beyond the scope of this paper, this research links climate change-enhanced La Niña conditions to sequential dry east African conditions in the October-to-December and March-to-May rainy seasons (Funk et al., 2018a, 2019a). While the best analog definitions vary by season, timing, and data source, variations of the West Pacific Gradient (WPG) (Hoell and Funk, 2013b) are used to identify strong-gradient La Niña seasons.

In eastern Africa, this approach, combined with the latest generation of climate forecast models, can provide surprisingly skillful forecasts at very long leads of 6 or more months. For the October-to-December season, many La Niña-related dry seasons can be identified as early as June[14,15] For the March-to-May season, September forecasts of strong La Niña-like Pacific Sea surface temperature gradients can be robust indicators of eastern east Africa droughts[16] While these forecasts explain a relatively low amount of the overall variance (∼40%), they do provide valuable advance notice of many sequential droughts. The September 2020 analysis identified 2017, 1999, 2011, 2008, 2014, and 2009 as analogs. The final update[17] identified 1999, 2000, 2001, 2008, 2009, 2011, 2012, and 2017.

In May of 2021 (as we write), the eastern Horn faces a severe food crisis associated with poor late 2020 and early 2021 rainy seasons. The food security situation, already dire due to the combined influences of conflict in Ethiopia and Somalia, recurrent drought and flood shocks since 2016, persistently high inflation in Ethiopia, the COVID-19 pandemic, and the desert locust upsurge, is becoming worse.

Our focus here is to show how the PWB framework makes it relatively simple to "stack" three sources of information to provide spatially detailed forecasts of agro-pastoral risk—CHIRPS observations, CHIRPS-GEFS forecasts, and analog-based climate forecasts. In this example, we use CHIRPS observations through the 1st dekad of April (dekad 10), CHIRPS-GEFS forecasts for the second dekad of April, and then analog and average CHIRPS rainfall through the remainder of the season. In this last step, we use two different assumptions to finish out the season. We explore one scenario that assumes performance similar to the recent La Niña-like seasons, using the average of our analog seasons. We also examine a "normal" scenario that uses the 40-year (1981–2020) average of the CHIRPS archive.

Figure 7A shows the observed+CHIRPS-GEFS precipitation anomalies for the beginning of the 2021 growing season (dekads 1–10). To harmonize our results with those already presented, in this example, we have used, as above, a fixed climatological start of season (**Figure 1B**). Onset dates could vary from year to year in a more sophisticated operational implementation. Through dekad 10, much of the region had experienced rainfall deficits ranging from about −15 to more than −90 mm, with the largest deficits occurring in the Ethiopian highlands, northeastern Kenya, and southern Somalia. While these types of anomalies are known to frequently occur during recent La Niña-like seasons, the impact of elevated WR values during these events has not been examined. Growing season analog WR anomalies (**Figure 7B**) are actually fairly large (up to ∼+50 mm), and, more importantly, the location of many of these increases are often in exceptionally dry areas of Kenya, Somalia, and Ethiopia. We can finish out the season by either assuming rainfall performance similar to our set of analogs (**Figure 7C**) or simple climatological averages (**Figure 7D**). The analog scenario is substantially more pessimistic, particularly for Kenya and Somalia, where late April and early May rains play a critical role in providing moisture for crops.

Combining the analog-based GSP precipitation totals with analog season WR totals allows us to generate a mid-season analog PWB anomaly map (**Figure 7E**). We can use a similar calculation based on climatological WR calculations to create an "average" PWB projection (**Figure 7F**). While more sophisticated bootstrapping approaches could be used to generate scenarios (Husak et al., 2013), **Figure 7E**, **F** represent a reasonable way to transform CHIRPS-GEFS and climate analog assumptions into results bracketing likely agro-pastoral outcomes. Contrasting the pessimistic analog with the less-presumptive average scenario suggests that outcomes in Kenya and Somalia may be substantially less certain than in Ethiopia. In Ethiopia, in both the analog and average scenarios, substantial water stress appears across much of the country.

While space limitations prevent further elaboration here, the PWB framework does seem promising as a basis for developing predictive agro-pastoral outlooks. In addition to growing-season precipitation totals derived from observations, weather, and climate conditions, similar interoperable seamless

[14]https://blog.chc.ucsb.edu/?p=937.
[15]https://blog.chc.ucsb.edu/?p=757.
[16]https://blog.chc.ucsb.edu/?p=880.
[17]https://blog.chc.ucsb.edu/?p=946.

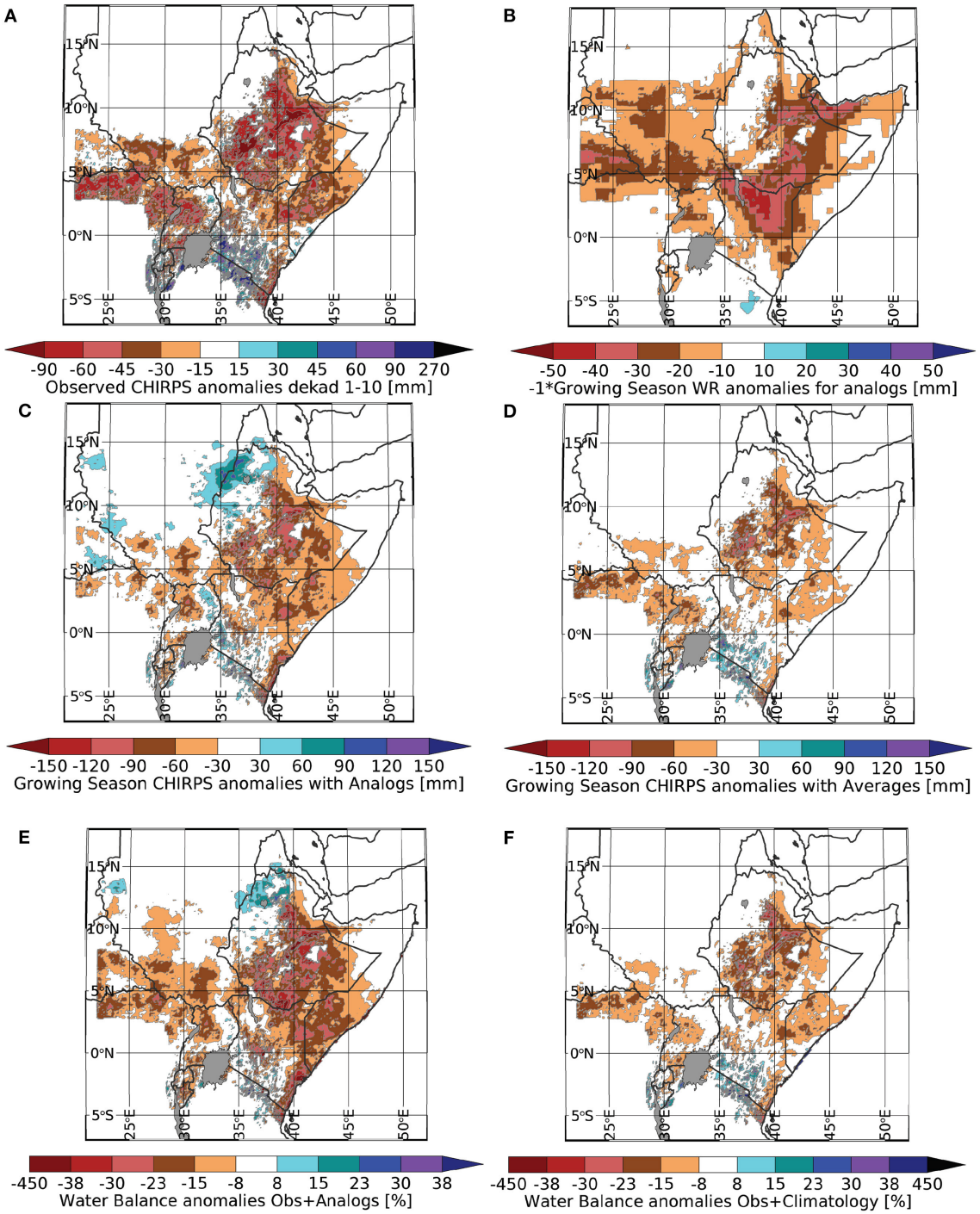

FIGURE 7 | An Agro-Pastoral Outlook example for 2021. **(A)** Early season rainfall anomalies through dekad 10. **(B)** Average growing season WR anomalies for analog seasons. **(C)** 2021 GSP CHIRPS anomalies based on analogs for dekads 11–36. **(D)** Same but based on long-term averages. **(E)** The predicted end-of-season WB anomalies associated with the analog forecast assumption shown in **(C)**. **(F)** The predicted end-of-season WB anomalies associated with the climatological forecast shown in **(D)**. **(C, D)** All anomalies based on a 1981–2020 period of record.

RefET observations/prediction data streams could be developed. One-to-fifteen-day forecasts could be derived from the GEFS (Hamill et al., 2013). At climatic timescales, these forecasts could be derived from coupled ocean-atmosphere models (Shukla et al., 2017), predictive hydrologic modeling systems (Arsenault et al., 2020), or via constructed analogs (Pierce et al., 2014). Finally, it should be noted that these outlooks could also help capture potential disruptions associated with extreme precipitation. Using the WRSI phenology stages, for example, one can identify regions in the grain-filling stage and the associated optimal WR values. When the observed precipitation far exceeds these WR values, that may be a clear indicator of potential negative influences (e.g., flooding).

DISCUSSION

In his classic book on Cultural Anthropology, Clifford Geertz explained how societies produce cultures that allow for coordinated behavior by effectively combining "*models of*" the world and "*models for*" the world (Geertz, 1973). Models "*of*" the world imitate or simulate the world as it is; they resemble our numerical models. Models "*for*" the world, however, are models "*for*" human behavior, behaviors that imply specific and coherent actions, actions informed by our models "*of*" the world. This distinction was first introduced by Geertz (1973) as he described how conceptual frameworks supported coherent behavior among tribes in Southeast Asia (Geertz, 1973). Such considerations are relevant here because agricultural early warning systems, like the FEWS NET (www.fews.net) (Brown, 2008; Funk et al., 2019b) or the United States Drought Monitor (Svoboda et al., 2002) are also "cultures" — cultures, furthermore, distributed across space, multiple institutions, and even nations. Coherent, intelligent behavior in these systems requires shared and crisply defined "search patterns." These patterns describe hazards, supporting consensus and early action, leading to emergent collaboration across a wide variety of factors. In this setting, models "of" the world provide information, while models "for" the world describe impacts and (re)actions (Funk et al., 2021).

Models "of" the world may provide synoptic observations of precipitation (Funk et al., 2015b; Huffman et al., 2020), soil moisture (Karthikeyan et al., 2017a,b), or actual evapotranspiration (Anderson et al., 2011; Senay et al., 2011, 2013). Complex numerical models "of" the world may offer detailed simulations and forecasts of land (Nijssen et al., 1997, 2014; McNally et al., 2017; Arsenault et al., 2020) and atmospheric (Hamill et al., 2013; Gelaro et al., 2017) conditions. In fact, every day, an ever-increasing torrent of such sources output more and more information.

Ironically, filtering and assimilating all of this information is increasingly challenging. But one long-standing and very effective "model for" impact assessment, which we have explored in this study, is crop WR. Here, we have revisited this widely used and effective concept, using an example situated in the boreal spring rain season of eastern Africa. We have described how this simple yet powerful framework can guide monitoring and prediction, providing "WRSI-like" results that are easier to calculate, more interoperable with rainfall forecasts, and potentially less sensitive to parameterization and potential biases and timing issues.

Clearly communicated definitions of drought (Wilhite and Glantz, 1985; Svoboda and Fuchs, 2016) provide a shared basis for collaboration, response planning, and impact mitigation. In the context of food security, the Integrated Phase Classification (IPC) system supports the evaluation of food security status across diverse cultural and socio-economic settings (Frankenberger and Verduijn, 2011). More specifically, FEWS NET uses a household food economy approach to develop food security scenarios[18] that take into account a complex tableau of drivers. Many social factors—conflict, price shocks, micro and macro-economic conditions—drive food insecurity. But, especially in many arid and semi-arid regions, agricultural and pastoral water deficits create shocks to food access and availability.

In this paper, we have used the PWB framework to demonstrate WRSI-like performance across several important decision support contexts. In general, we found that the easy-to-calculate PWB index appears to perform very similarly to the WRSI in most locations. More detailed analyses based on crop stages could certainly be of value, and the WR framework could be used to filter other indicators of water supply or water stress. Satellite-observed soil moisture (Karthikeyan et al., 2017a,b) or actual evapotranspiration (Anderson et al., 2011; Senay et al., 2011, 2013) could be processed with WR framing, as could hydrologic model outputs (McNally et al., 2017; Arsenault et al., 2020) .

The simplicity of the PWB makes it relatively straightforward to combine observations, weather forecasts, and climate analog predictions, as demonstrated in Examining the Utility of the PWB Framework as a Basis for Translating Integrated Rainfall Early Estimates into Assessments of Agro-pastoral Hazards section. Producing reasonably interoperable rainfall and RefET estimates, at high resolutions, based on satellite and station observations, reanalyses, weather models, and coupled global climate models is challenging on its own. The PWB provides a defensible way to combine such outputs, resulting in forward-looking assessments of crop water satisfaction. The example provided here focuses on combining Early Estimates and climate analog predictions (Examining the Utility of the PWB Framework as a Basis for Translating Integrated Rainfall Early Estimates into Assessments of Agro-Pastoral Hazards Section), but similar framing could be used with outputs from hydrologic forecast systems like NHyFAS. NHyFAS forecasts of AET and RefET could be translated into PWB forecasts, for example.

In addition to an expected opportunity to describe PWB-based impact assessments, we were also surprised by two specific aspects of this study: the very high level of covariability of WR and GSP in arid regions (**Figure 2D**) and the extremely high positive Kenyan PWB values in 2018 and 2020 (**Figure 6**). Both results indicate forms of climatic hazards. During dry seasons in arid regions, positive land surface feedbacks associated with low

[18]https://fews.net/sites/default/files/documents/reports/Guidance_Document_Scenario_Development_2018.pdf.

precipitation enhance RefET and WR values, increasing plant water stress. But during extremely wet seasons, like 2018 and 2020, the available water may far exceed plant needs in many areas, leading to increased runoff and potential waterlogging and flooding.

CONCLUSIONS

Simplicity can, at times, be revealing. Because the PWB simply uses accumulations of CHIRPS rainfall and WR, this framework makes it very easy to assess the covariability and relative contributions of water supply and atmospheric demand. Explicitly calculating and analyzing the WR provides valuable insights. Climatologically, late-season WR values make it hard to catch up from early season rainfall deficits (**Figure 1**). Interannually, the magnitude of WR increases and decreases in dry and wet seasons can be relatively large in arid regions, amplifying rainfall anomalies, and helping to support extreme outcomes (**Figure 2D**).

In conclusion, the PWB framework seems very useful for monitoring, prediction, trend analyses, and risk management applications. Future work will expand our analysis to more regions and develop more decision support-related analyses. In general, analyzing WR along with GSP provides valuable information by answering a simple question—was growing season precipitation inadequate, adequate, or much more than adequate? Spatially, this provides a picture of eastern east Africa as a relatively small set of cool, moist highland areas with seasons long enough to support agriculture.

Finally, we return to a simple but important result: the PWB provides results that are, for most water-limited areas, very similar to the WRSI. At the pixel scale, correlations were greater than 0.8 for all regions in which the standard deviation of WRSI was greater than 15. At the sub-national administrative unit, the median 1981–2020 PWB/WRSI correlations were 0.8, 0.93, and 0.82 in Kenya, Somalia, and Ethiopia, respectively. For our Kenya crop-growing counties, the correlation between regionally averaged PWB and WRSI was 0.85. These results suggest that the PWB can be a useful supplement to the more intensive WRSI modeling. When parameterized with accurate soil information and driven with accurate climate data, the WRSI should provide more accurate estimates that take into account soil moisture and sub-seasonal weather variability. But WRSI-like results can be obtained using GSP and WR. Similar analyses could incorporate other metrics of water supply, such as satellite or model-based estimates of AET. Both satellite and model-based estimates are likely to capture the complementary transitions as AET decreases and WR increases during periods of severe water stress.

In a world with increasingly extreme precipitation (Emori and Brown, 2005; Allan and Soden, 2008) and Indo-Pacific sea surface temperature volatility (Cai et al., 2013, 2015), East African agricultural advances are struggling to cope with climate change (Davenport et al., 2018). As the combination of population growth, declining rainfall and climate volatility create increasing food stress (Funk et al., 2005, 2015a; Funk and Brown, 2009), improved integrated drought early warning systems (Funk et al., 2007; Thomas et al., 2019, 2020; Funk and Shukla, 2020; Shukla et al., 2021) and improved drought risk management practices and policies (Pulwarty and Sivakumar, 2014; Wilhite and Pulwarty, 2017) can help east Africa manage risk and boost productivity. The PWB framework, discussed here, will provide a relatively simple means of connecting satellite observations with climate, weather and land surface model simulations, helping to support integrated early warning systems.

DATA AVAILABILITY STATEMENT

The original contributions presented in the study are included in the article/supplementary materials, further inquiries can be directed to the corresponding author.

AUTHOR CONTRIBUTIONS

All authors listed have made a substantial, direct and intellectual contribution to the work, and approved it for publication.

FUNDING

Primary support for this work came from the National Aeronautics and Space Administration (NASA) GPM mission grant #80NSSC19K0686 and the United States Agency for International Development (USAID) cooperative agreement #72DFFP19CA00001 and the Famine Early Warning Systems Network.

REFERENCES

AGRHYMET (1996). *Méthodologie de suivi des zones à risque*. Niamey: AGRHYMET FLASH, Bulletin de Suivi de la Campagne Agricole au Sahel, Centre Regional AGRHYMET

Allan, R. P., and Soden, B. J. (2008). Atmospheric warming and the amplification of precipitation extremes. *Science* 321, 1481–1484. doi: 10.1126/science.1160787

Anderson, M. C., Kustas, W. P., Norman, J. M., Hain, C. R., Mecikalski, J. R., Schultz, L., et al. (2011). Mapping daily evapotranspiration at field to continental scales using geostationary and polar orbiting satellite imagery. *Hydrol. Earth Syst. Sci.* 15, 223–239. doi: 10.5194/hess-15-223-2011

Arsenault, K. R., Shukla, S., Hazra, A., Getirana, A., McNally, A., Kumar, S. V., et al. (2020). The NASA hydrological forecast system for food and water security applications. *Bull. Am. Meteorol. Soc.* 101, E1007–E1025. doi: 10.1175/BAMS-D-18-0264.1

Brown, M. E. (2008). *Famine Early Warning Systems and Remote Sensing Data*. Berin: Springer Science and Business Media.

Cai, W., Santoso, A., Wang, G., Yeh, S. W., An, S. I., Cobb, K. M., et al. (2015). ENSO and greenhouse warming. *Nat. Clim. Change* 5, 849–859. doi: 10.1038/nclimate2743

Cai, W., Zheng, X. T., Weller, E., Collins, M., Cowan, T., Lengaigne, M., et al. (2013). Projected response of the Indian Ocean Dipole to greenhouse warming. *Nat. Geosci.* 6, 999–1007. doi: 10.1038/ngeo2009

Checchi, F., and Robinson, W. C. (2013). Mortality among populations of southern and central Somalia affected by severe food insecurity and famine during 2010–2012. Washington, DC: FEWS NET.

Davenport, F., Funk, C., and Galu, G. (2018). How will East African maize yields respond to climate change and can agricultural development mitigate this response? *Clim. Change* 147, 491–506. doi: 10.1007/s10584-018-2149-7

Donat, M. G., Lowry, A. L., Alexander, L. V., O'Gorman, P. A., and Maher, N. (2016). More extreme precipitation in the world's dry and wet regions. *Nat. Clim. Change* 6:508. doi: 10.1038/nclimate2941

Doorenbos, J., and Pruitt, W. O. (1977). *Crop Water Requirements*. Rome: FAO.

Emori, S., and Brown, S. (2005). Dynamic and thermodynamic changes in mean and extreme precipitation under changed climate. *Geophys. Res. Lett.* 32:1–5. doi: 10.1029/2005GL023272

FAO (1978). *World Soil Resources Report 48/1*. Rome: FAO.

Frankenberger, T. R., and Verduijn, R. (2011). *Integrated Food Security Phase Classification* (IPC). Rome: The Food and Agriculture Organization of the United Nations.

Frère, M., and Popov, G. (1986). *Early Agrometeorological Crop Yield Forecasting*. Rome: The Food and Agriculture Organization of the United Nations.

Funk, C., Davenport, F., Eilerts, G., Nourey, N., and Galu, G. (2018a). *Contrasting Kenyan Resilience to Food Insecurity: 2011 and 2017*. USAID Special Report.

Funk, C., Harrison, L., Shukla, S., Pomposi, C., Galu, G., and Korecha, D. (2018b). Examining the role of unusually warm Indo-Pacific sea surface temperatures in recent African droughts. *Quart J Roy Meteor Soc* 144, 360–383. doi: 10.1002/qj.3266

Funk, C., Hoell, A., Shukla, S., Bladé, I., Liebmann, B., Roberts, J. B., and Husak, G. (2014). Predicting East African spring droughts using Pacific and Indian Ocean sea surface temperature indices. *Hydrol. Earth Syst. Sci. Discuss.* 11, 3111–3136. doi: 10.5194/hessd-11-3111-2014

Funk, C., Nicholson, S. E., Landsfeld, M., Klotter, D., Peterson, P., and Harrison, L. (2015a). The Centennial Trends Greater Horn of Africa precipitation dataset. *Sci. Data* 2:150050. doi: 10.1038/sdata.2015.50

Funk, C., Pedreros, D., Nicholson, S., Hoell, A., Korecha, D., Galu, G., et al. (2019a). Examining the potential contributions of extreme 'Western V' sea surface temperatures to the 2017 March–June East African Drought. *Bull. Am. Meteor. Soc.* 100, S55–S60. doi: 10.1175/BAMS-D-18-0108.1

Funk, C., Peterson, P., Landsfeld, M., Pedreros, D., Verdin, J., Shukla, S., et al. (2015b). The climate hazards infrared precipitation with stations—a new environmental record for monitoring extremes. *Sci. Data* 2:150066. doi: 10.1038/sdata.2015.66

Funk, C., Senay, G., Asfaw, A., Verdin, J., Rowland, J., Michaelson, J., et al. (2005). *Recent drought tendencies in Ethiopia and equatorial-subtropical eastern Africa*. Vulnerability to Food Insecurity: Factor Identification and Characterization Report, F. NET, Ed., US Agency for International Development, 12.

Funk, C., and Shukla, S. (2020). *Drought Early Warning and Forecasting: Theory and Practice. Elsevier*. doi: 10.1016/B978-0-12-814011-6.00003-8

Funk, C., Shukla, S., Thiaw, W. M., Rowland, J., Hoell, A., McNally, A., et al. (2019b). Recognizing the famine early warning systems network (FEWS NET): over 30 years of drought early warning science advances and partnerships promoting global food security. *Bull. Am. Meteor. Soc.* 14:13.

Funk, C., Verdin, J. P., and Husak, G. (2007). Integrating observation and statistical forecasts over sub-Saharan Africa to support Famine Early Warning. *87th American Meteorological Society Annual Meeting*, San Antonio, TX.

Funk, C. C., and Brown, M. E. (2009). Declining global per capita agricultural production and warming oceans threaten food security. *Food Sec.* 1, 271–289. doi: 10.1007/s12571-009-0026-y

Funk, C. C., Hoell, A., and Mitchell, D. (2021). Climate science advances to address 21st century weather and climate extremes. *Front. Clim.* 3:59. doi: 10.3389/fclim.2021.680291

Geertz, C. (1973). *The Interpretation of Cultures, Vol. 5019*. New York, NY: Basic Books.

Gelaro, R., McCarty, W., Suárez, M. J., Todling, R., Molod, A., Takacs, L., et al. (2017). The modern-era retrospective analysis for research and applications, version 2 (MERRA-2). *J. Clim.* 30, 5419–5454. doi: 10.1175/JCLI-D-16-0758.1

Hamill, T. M., Bates, G. T., Whitaker, J. S., Murray, D. R., Fiorino, M., Galarneau Jr, T. J., et al. (2013). NOAA's second-generation global medium-range ensemble reforecast dataset. *Bull. Am. Meteorol. Soc.* 94, 1553–1565. doi: 10.1175/BAMS-D-12-00014.1

Harrison, L., Funk, C., and Peterson, P. (2019). Identifying changing precipitation extremes in Sub-Saharan Africa with gauge and satellite products. *Environ. Res. Lett.* 14:085007. doi: 10.1088/1748-9326/ab2cae

Hobbins, M., Wood, A., Streubel, D., and Werner, K. (2012). What drives the variability of evaporative demand across the conterminous United States? *J. Hydrometeorol.* 13, 1195–1214. doi: 10.1175/JHM-D-11-0101.1

Hobbins, M. T., Wood, A., McEvoy, D. J., Huntington, J. L., Morton, C., Anderson, M., and Hain, C. (2016). The evaporative demand drought index. Part I: Linking drought evolution to variations in evaporative demand. *J. Hydrometeorol.* 17, 1745–1761. doi: 10.1175/JHM-D-15-0121.1

Hoell, A., and Funk, C. (2013a). Indo-Pacific sea surface temperature influences on failed consecutive rainy seasons over eastern Africa. *Clim. Dyn.* 43, 1645–1660. doi: 10.1007/s00382-013-1991-6

Hoell, A., and Funk, C. (2013b). The ENSO-related west pacific sea surface temperature gradient. *J. Clim.* 26, 9545–9562. doi: 10.1175/JCLI-D-12-00344.1

Hoell, A., Funk, C., and Barlow, M. (2014). La Nina diversity and the forcing of Northwest Indian Ocean Rim teleconnections. *Clim. Dyn.* 42, 3289–3311. doi: 10.1007/s00382-013-1799-4

Huffman, G. J., Bolvin, D. T., Braithwaite, D., Hsu, K. L., Joyce, R. J., Kidd, C., et al. (2020). "Integrated multi-satellite retrievals for the global precipitation measurement (GPM) mission (IMERG)," in *Satellite Precipitation Measurement*, eds K. C. Levizzani, D. Kirschbaum, C. Kummerow, K. Nakamura, and F. Turk (Cham: Springer), 343–354. doi: 10.1007/978-3-030-24568-9_19

Husak, G. J., Funk, C. C., Michaelsen, J., Magadzire, T., and Goldsberry, K. P. (2013). Developing seasonal rainfall scenarios for food security early warning. *Theor. Appl. Climatol.* 114, 291–302. doi: 10.1007/s00704-013-0838-8

Karthikeyan, L., Pan, M., Wanders, N., Kumar, D. N., and Wood, E. F. (2017a). Four decades of microwave satellite soil moisture observations: Part 1. A review of retrieval algorithms. *Adv. Water Resour.* 109, 106–120. doi: 10.1016/j.advwatres.2017.09.006

Karthikeyan, L., Pan, M., Wanders, N., Kumar, D. N., and Wood, E. F. (2017b). Four decades of microwave satellite soil moisture observations: Part 2. Product validation and inter-satellite comparisons. *Adv. Water Resour.* 109, 236–252. doi: 10.1016/j.advwatres.2017.09.010

Laudien, R., Schauberger, B., Makowski, D., and Gornott, C. (2020). Robustly forecasting maize yields in Tanzania based on climatic predictors. *Sci. Rep.* 10, 1–12. doi: 10.1038/s41598-020-76315-8

Magadzire, T., Galu, G., and Verdin, J. (2017). *How Climate Forecasts Strengthen Food Security*. World Meteorological Organisation Bulletin—Special Issue on Water, World Meteorological Organisation.

McNally, A., Arsenault, K., Kumar, S., Shukla, S., Peterson, P., Wang, S., et al. (2017). A land data assimilation system for sub-Saharan Africa food and water security applications. *Sci. Data* 4:170012. doi: 10.1038/sdata.2017.12

McNally, A., Husak, G. J., Brown, M., Carroll, M., Funk, C., Yatheendradas, S., et al. (2015). Calculating crop water requirement satisfaction in the West Africa Sahel with remotely sensed soil moisture. *J. Hydrometeorol.* 16, 295–305. doi: 10.1175/JHM-D-14-0049.1

Nijssen, B., Lettenmaier, D. P., Liang, X., Wetzel, S. W., and Wood, E. F. (1997). Streamflow simulation for continental-scale river basins. *Water Resour. Res.* 33, 711–724. doi: 10.1029/96WR03517

Nijssen, B., Shukla, S., Lin, C., Gao, H., Zhou, T., Sheffield, J., et al. (2014). A prototype global drought information system based on multiple land surface models. *J. Hydrometeorol.* 15, 1661–1676. doi: 10.1175/JHM-D-13-090.1

Peng, J., Dadson, S., Hirpa, F., Dyer, E., Lees, T., Miralles, D. G., et al. (2020). A pan-African high-resolution drought index dataset. *Earth Syst. Sci. Data* 12, 753–769. doi: 10.5194/essd-12-753-2020

Pierce, D. W., Cayan, D. R., and Thrasher, B. L. (2014). Statistical downscaling using localized constructed analogs (LOCA). *J. Hydrometeorol.* 15, 2558–2585. doi: 10.1175/JHM-D-14-0082.1

Pulwarty, R. S., and Sivakumar, M. V. (2014). Information systems in a changing climate: early warnings and drought risk management. *Weather Clim. Extremes* 3, 14–21. doi: 10.1016/j.wace.2014.03.005

Senay, G., and Verdin, J. (2001). "Using a GIS-based water balance model to assess regional crop performance," in *Proceedings of the Fifth International Workshop on Application of Remote Sensing in Hydrology*.

Senay, G. B., Bohms, S., Singh, R. K., Gowda, P. H., Velpuri, N. M., Alemu, H., and Verdin, J. P. (2013). Operational evapotranspiration mapping using remote

sensing and weather datasets: a new parameterization for the SSEB approach. *JAWRA J. Am. Water Resour. Assoc.* 49, 577–591. doi: 10.1111/jawr.12057

Senay, G. B., Budde, M., Verdin, J. P., and Melesse, A. M. (2007). A coupled remote sensing and simplified surface energy balance approach to estimate actual evapotranspiration from irrigated fields. *Sensors* 7, 979–1000. doi: 10.3390/s7060979

Senay, G. B., Budde, M. E., and Verdin, J. P. (2011). Enhancing the simplified surface energy balance (SSEB) approach for estimating landscape ET: validation with the METRIC model. *Agric. Water Manag.* 98, 606–618. doi: 10.1016/j.agwat.2010.10.014

Senay, G. B., and Verdin, J. (2003). Characterization of yield reduction in Ethiopia using a GIS-based crop water balance model. *Can. J. Remote Sens.* 29, 687–692. doi: 10.5589/m03-039

Shukla, S., Funk, C., and, Hoell A. (2014). Using constructed analogs to improve the skill of March-April-May precipitation forecasts in equatorial East Africa. *Environ. Res. Lett.* 9:094009. doi: 10.1088/1748-9326/9/9/094009

Shukla, S., Husak, G., Turner, W., Davenport, F., Funk, C., Harrison, L., and Krell, N. (2021). A slow rainy season onset is a reliable harbinger of drought in most food insecure regions in Sub-Saharan Africa. *PLos ONE* 16:e0242883. doi: 10.1371/journal.pone.0242883

Shukla, S., McEvoy, D., Hobbins, M., Husak, G., Huntington, J., Funk, C., et al. (2017). Examining the value of global seasonal reference evapotranspiration forecasts to support FEWS NET's food insecurity outlooks. *J. Appl. Meteorol. Climatol.* 56, 2941–2949. doi: 10.1175/JAMC-D-17-0104.1

Smith, M. (1992). *Expert Consultation on Revision of FAO Methodologies for Crop Water Requirements*. Rome: FAO

Svoboda, M., and Fuchs, B. (2016). Handbook of drought indicators and indices. Geneva: World Meteorological Organization. doi: 10.1201/b22009-11

Svoboda, M., LeComte, D., Hayes, M., Heim, R., Gleason, K., Angel, J., et al. (2002). The drought monitor. *Bull. Am. Meteorol. Soc.* 83, 1181–1190. doi: 10.1175/1520-0477-83.8.1181

Thomas, E., Jordan, E., Linden, K., Mogesse, B., Hailu, T., Jirma, H., et al. (2020). Reducing drought emergencies in the Horn of Africa. *Sci. Total Environ.* 727:138772. doi: 10.1016/j.scitotenv.2020.138772

Thomas, E. A., Needoba, J., Kaberia, D., Butterworth, J., Adams, E. C., Oduor, P., et al. (2019). Quantifying increased groundwater demand from prolonged drought in the East African Rift Valley. *Sci. Total Environ.* 666, 1265–1272. doi: 10.1016/j.scitotenv.2019.02.206

Trenberth, K. E., Dai, A., Rasmussen, R. M., and Parsons, D. B. (2003). The changing character of precipitation. *Bull. Am. Meteorol. Soc.* 84, 1205–1217. doi: 10.1175/BAMS-84-9-1205

Verdin, J., Funk, C., Senay, G., and Choularton, R. (2005). Climate science and famine early warning. *Philos. Trans. R. Soc. B* 360, 2155–2168. doi: 10.1098/rstb.2005.1754

Verdin, J., and Klaver, R. (2002). Grid-cell-based crop water accounting for the famine early warning system. *Hydrol. Process.* 16, 1617–1630. doi: 10.1002/hyp.1025

Vicente-Serrano, S. M., Beguería, S., and López-Moreno, J. I. (2010). A multiscalar drought index sensitive to global warming: the standardized precipitation evapotranspiration index. *J. Clim.* 23, 1696–1718. doi: 10.1175/2009JCLI2909.1

Wilhite, D., and Glantz, M. (1985). Understanding: the Drought Phenomenon: The Role of Definitions. *Water Int.* 10, 111–120. doi: 10.1080/02508068508686328

Wilhite, D., and Pulwarty, R. S. (2017). *Drought and Water Crises: Integrating Science, Management, and Policy*. Boca Raton: CRC Press.

Zucca, C., Della Peruta, R., Salvia, R., Sommer, S., and Cherlet, M. (2012). Towards a World desertification atlas. Relating and selecting indicators and data sets to represent complex issues. *Ecol. Indic.* 15, 157–170. doi: 10.1016/j.ecolind.2011.09.012

Conflict of Interest: AM was employed by company SAIC Inc.

The remaining authors declare that the research was conducted in the absence of any commercial or financial relationships that could be construed as a potential conflict of interest.

Publisher's Note: All claims expressed in this article are solely those of the authors and do not necessarily represent those of their affiliated organizations, or those of the publisher, the editors and the reviewers. Any product that may be evaluated in this article, or claim that may be made by its manufacturer, is not guaranteed or endorsed by the publisher.

frontiers in Climate

PERSPECTIVE
published: 17 September 2021
doi: 10.3389/fclim.2021.710625

Development of Tailored Early Warning Agromet Advisories for Farmers in Zambia, Indonesia, and South Africa

Sue Walker[1,2]*

[1] Agricultural Research Council—Natural Resources and Engineering, Pretoria, South Africa, [2] Department of Soil, Crop, and Climate Sciences, University of the Free State, Bloemfontein, South Africa

Farmers do not often use climate and weather information on a regular basis, as the specific influence of weather parameters on farm-level decision making is not well-known. Agromet advisories are needed for local farming systems. Effective agrometeorological advisory systems, need tailored agricultural weather forecasts, and two-way communication. Transdisciplinary teams together with farmers can co-develop early warning Agromet advisory systems to address farmers' needs. Three examples of Agromet advisories are discussed- CAPES in Zambia, Science Field Shops in Indonesia, and the AgriCloud mobile App in South Africa. Community Agrometeorological Participatory Extension Service (CAPES) began in Monze, Zambia to communicate seasonal climate forecasts to farmers through researchers and extension interactions. Participatory groups collected spatial and temporal data about local farming systems to highlight opportunities. Communication methods used were local radio, farmers' days, trials, with farm visits. CAPES resulted in lifelong learning about climate and co-development of tailored Agromet advisories to improve climate resilience. In Science Field Shops (SFS) groups of Indonesian farmers meet experts regularly to exchange information about climate and farming activities. Farmers measure rainfall and observe their agroecological systems each day. At monthly meetings, the seasonal forecasts are discussed using dialogue-discussion methods. Agrometeorological learning is trans-disciplinary through interaction between anthropologists, agrometeorologist, and extension personnel. SFS includes eight climate services that empower farmers to address challenges and sustain their productivity. AgriCloud is an online weather-based agricultural advisory system enriching weather forecasts with agricultural information and local knowledge. Real-time overviews and warnings are tailored to farmer's needs. AgriCloud provides farmers, extension staff, and advisors daily updated weather-related farm-specific advice in 11 South African official languages. AgriCloud is available as an android mobile App, or API to use via a platform. These examples illustrate the use of weather forecasting together with tailored forecasts and communication systems to deliver Agromet advisories, showing different aspects of the incorporation of local knowledge in co-developing advisories for the farmers. In the future, various combinations can be used around the world when co-developing with the farmers.

Keywords: agromet advisories, co-development, community participation, Zambia, Indonesia, South Africa

OPEN ACCESS

Edited by:
Tamuka Magadzire, University of California, Santa Barbara, United States

Reviewed by:
Peter Johnston, University of Cape Town, South Africa
Bridget Bwalya Umar, University of Zambia, Zambia
Robert Stefanski, World Meteorological Organization, Switzerland

***Correspondence:**
Sue Walker
WalkerS@arc.agric.za

Specialty section:
This article was submitted to Climate Services, a section of the journal Frontiers in Climate

Received: *16 May 2021*
Accepted: *27 August 2021*
Published: *17 September 2021*

Citation:
Walker S (2021) Development of Tailored Early Warning Agromet Advisories for Farmers in Zambia, Indonesia, and South Africa. Front. Clim. 3:710625. doi: 10.3389/fclim.2021.710625

INTRODUCTION

Effective practical local early warning agromet advisories can be developed using participatory approaches in order to incorporate local knowledge to farmers on a routine basis. This local and indigenous knowledge is then used to refine the agricultural scientific information for the local conditions and provide information to farmers such as planting dates and suitable crop selections according to the current and expected weather conditions. Although farmers know about the general effects of weather and climate on their agricultural production, it is more difficult for them to extrapolate pertinent information relevant to their activities directly from a standard weather forecast (Stigter et al., 2013). Therefore, it is important that agrometeorologists use the available scientific evidence from research results to generate operational level agromet advisories. An agromet advisory is a message combining weather or climate information with specific information about the farming systems in the form of advice on farming activities. In South Africa, despite the existence of good historic climate datasets (ARC-Agromet database 2021) and good daily weather forecasts (www.weather.co.za) farmers do not often combine this information to use in their decision making. Many are not even aware of the detailed cumulative effects of the current and seasonal weather forecast on their agricultural enterprises. Therefore, it is important to formulate and operationalize routine Agromet advisories for each farming system and location including a range of options and management skills.

For an effective agrometeorological advisory system, aspects needed include

- scientific weather forecasting numerical models,
- monitoring systems,
- added agricultural value for tailored forecasts, and
- a good two-way communication system to deliver messages and receive feedback.

Some developed countries have been using especially tailored agromet advisories that were co-developed with the farming community for many years. Examples of such agromet services are in Australia under the FARMSCAPE approach to decision support where farmers, advisers, and researchers were involved in monitoring, simulation, communication and performance evaluation together (Carberry et al., 2002). The programme that developed and operated for over a decade, integrated farmer participation with the results particularly from the APSIM farming systems model to provide a scientific approach to decision support specifically using farmers information about their farming operations. Another example is in Florida, USA where a framework was developed with many activities integrated yet running parallel, including physical, biological, social, and economic aspects of agricultural systems (Jagtap et al., 2002). The framework included the generation of climate information from historic datasets and models, the communication though interactions with stakeholders, to the use, implementation and evaluation of the system which designed and developed agromet early warning advisories to assist the citrus farmers in receiving information about potential low temperatures that would adversely affect their trees. These are well-established, scientifically based and validated early warning services to specific parts of the agricultural sector (Walker and Stigter, 2010). These two examples, illustrate how the conventional weather forecast needs to be enhanced with additional information relevant to the farming operations in the area. However, in other countries such agromet advisory services are not operational on a routine basis.

Many times the direct and indirect influence of the weather on agricultural activities on a farm level and hence the decision-making processes of farmers for specific farming systems, are not well-defined and can include indigenous knowledge (Zuma-Netshiukhwi et al., 2013). Therefore, these aspects need to be part of co-investigation participatory projects, as farmers are not able to use the highly technical scientific information provided by the national meteorological and hydrological services (NMHS) in their day to day decisions or seasonal planning (Elhag and Walker, 2011). Typical conventional weather forecast only give expected values for weather parameters such as temperature and/or humidity and are often not related to the long-term means or variability experienced in past to put them in perspective. Agromet advisory services need to be co-developed together with the users, the farmers, farm managers and extension workers to formulate viable solutions (Walker et al., 2010). Transdisciplinary teams should co- develop effective integrated systems to interpret weather forecasts in relation to farming management decisions and then to develop systems to routinely deliver them to the farming community at the correct time. Such teams working together with the farmers can co-develop and design early warning and Agromet advisory systems to address the farmers' specific needs and questions according to their location and production systems (Stigter et al., 2014a,b,c). Three examples of development of such Agromet advisories are discussed, namely the CAPES in Zambia, the Science Field Shops in Indonesia, and the AgriCloud mobile App in South Africa. Important aspects needed during development of these advisory services are highlighted.

COMMUNITY AGROMETEOROLOGICAL PARTICIPATORY EXTENSION SERVICE

Community Agrometeorological Participatory Extension Services (CAPES) were established in some Mujika villages near Monze, Zambia to introduce and communicate seasonal climate forecast to farmers through interactions between the farmers, researchers and extension practitioners. This method was developed during Dr. Durton Nanja's Ph.D. study from 2007 to 2010 as he engaged the community and developed the methods to distribute the season forecast to the farmers in Mujika near Monze (Nanja, 2010). The process began with an interaction with the extension staff of the Zambia Department of Agriculture, the headmen of the villages to establish a good working relationship in order to obtain permissions to use the various participatory approaches to collect information from the farmers about the currently used farming systems and the natural resources. These interactions were typical focus group

meetings, similar to those used by Nyumba et al. (2018) to inform leaders in the community about the development of the agromet services and to arrange the community communications and interactions. During these meetings, participatory methods were used to identify the limiting factors in the local current farming systems (Nanja and Walker, 2009).

Prior to the community meetings, background information about the area for which the agromet services were being designed was obtained from secondary sources. Much of this information was obtained by a desktop study of the available natural resources and the current farming systems, being collected from the appropriate government departments archives and databases. However, as in many cases, the details needed were at a rather large scale without sufficient detail at the local scale of the actual farms. So the general topographic information about the contours or lie of the land and location of the rivers was obtained from topographic maps. The detailed soils information was not available at the time of the study that started in 2007, but is now accessible from the Soil Atlas of Africa (Jones et al., 2013) namely Chromic Luvisols (with clay subsoil), undifferentiated Acrisols (acid with clay rich subsoil) and Lithic Leptosols (shallow soils over rock) around Monze. The long-term climate information was obtained for two climate stations namely Magoye weather station and Moorings rainfall observing station from the Zambia Meteorological Department (ZMD) Provincial Meteorological Office with 29 and 86 years climate and rainfall records, respectively. These long-term data can be used together with the more recent reanalysis data available from NASA (POWER, https://power.larc.nasa.gov/) at a spatial resolution of 0.5° latitude by 0.5° longitude across the globe available from 1981. The other natural resources data was collected from the appropriate departments such as agriculture, water and environment. This information provided a background to the area and was supplemented with general information about the farming systems and the markets in the area. However, as the Agromet services are to serve the farmers themselves, one also needed to engage and interact with them and gather information directly from such farmers.

Participatory group activities include the collection of spatial and temporal data about the local farming systems and climatic conditions from the communities perspective. One of the best ways of doing this is using participatory techniques (Chambers, 2006, 2007). Such methods enable the farmers to also learn during the process, so that there can be joint ownership of the information together with empowerment, or enabling people to have what they need to solve their own problems. It was important to communicate the aims of such activities so that each group understood the reasons behind such activities. That helped to maintain focus during the sessions and later when prioritizing the information. The criteria were co-developed within some ground rules used during these activities.

Participatory techniques were used in a group context in each of the villages to enable them "to learn by doing" as they explore their own local resources. The techniques integrated community and farm mapping and transect walks (IFAD, 2009) to document the information about the lie of the land from stream or river through the flood plain to the cultivated fields and on toward the village and hills. Along the way during each transect walk in the three selected villages, each person took notice of the changes in vegetation and soils, which were then included in or provided complementary information to the specific map of that village. These community mapping exercises helped the villagers to articulate and express their spatial knowledge that was recorded by the researchers and archived local knowledge to assists in the crop modeling, land-use planning and resource management. These transect walks through the village and farmlands was a form of capacity building, as the people could explore the spatial dimension and integrate social aspects (e.g., taxi ranks and marketing opportunities) into the natural resources information. It is used to cross check with the other mapping activities and help the researchers with triangulation or confirmation of certain aspects. As a village group, they then drew a map and a transect on a large sheet of paper to represent the variety of aspects observed. Contributions from everyone were easily collated and added to the map that was then used later as a basis for planning interventions or services.

During the group discussion, the facilitator was able to highlight the issues discussed and how the climate and weather might affect each of them (Gandure et al., 2013). This opened the door for further discussion later about agromet services that were to be developed to address these locally pertinent questions. The participatory mapping exercises were integrated with the information from the desktop study to provide a base for further investigations. These included the siting of future developments, or location of a market or expansion of the agricultural activities.

Other participatory techniques used include the time lines at various scales. Timelines are a visualization tool build up by group contributions to show a list of sequential events that reflects their common history or activities. They helped to give context to the present conditions and situation so that the villagers could reflect on the trends and development and think strategically about a plan for the future. During the group discussions, the facilitator drew a time line of a flip chart and then filled it in as the farmers responded with suggestions. For the long-term time scale (years) information was collected about different aspects of past droughts and floods as well as highlighting historic milestones and other significant developments in the area. In the seasonal shorter-term (weeks or months) farmers gave details of their farming systems and typical operations like timing of land preparation (plowing), planting, weeding, fertilizer top-dressing and harvest time. All the results from these participatory activities helped the researchers to better understand cropping operations from the farmers point of view, and gave opportunity to highlight the critical times during the growing season. This information was later used in the crop modeling exercise. The daily time lines illustrated the difference between male and female daily routines and responsibilities of the typical complex life in the area. All this information was then used when planning and developing the agromet services, tailored and relevant to the specific seasonal activities in their local farming system and their daily routines. For example, the seasonal calendar represented the activities for the specific dryland maize cropping with integrated cattle livestock system and showed how the spread of their workload through the year

was related to the local climate (similar to Hall et al., 2017). Once the timelines were drawn by the farmers, then the critical periods were able to be identified together with the trigger weather parameters, such as the start of the rains. This then formed the basis of the agromet advisory that was be developed and distributed to the farmers on a routine basis. For example, they highlighted that they cannot begin plowing for land preparation and planting before they have received some rainfall, as the soil surface is too hard for the animal traction plow to break up the soil. This information, was then used to develop an algorithm based on the daily weather forecasts for a certain planting season, so as to formulate the added value agromet advisories.

Once the all the information was collected from the Mujika villages group interactions it was collated, highlighting the most important aspects identified by the farmers and other participants (like agricultural camp officers). It was then used to formulate responses to address problems and opportunities ranked by farmers using matrices as a preference ranking exercise according to their own cultural priorities (similar to Ager et al., 2010). Here the ranking method was used, where firstly the group brainstormed a list of the priority issues or problem areas that they wanted to see addressed. This formed a slightly different matrix for each group of participants, they then voted for the top three or four priority areas that they considered as priorities needing attention. Following the counting of the votes, there was further discussion to bring consensus about the highest priority issues. An ensuing analysis was then conducted to unpack the extent of each problem, the impacts on their farming systems and other associated effects. During this process the opportunities to address such issues was discussed with additional scientific perspective from the currently available information by the researcher and camp officer and how they could be packaged to form an agromet advisory for these specific villages.

In Mujika for CAPES, community engagement continued via the development of a community dissemination plan that was formulated by the farmers and extension staff, in order to develop and maintain a routine agromet services. This community information dissemination plan was designed specifically by these villages at this time, so it selected the appropriate communication methods that could be used in Monze district. The following methods to disseminate the agromet advisories were initiated–weekly local radio programmes that were listened to by farmer study "radio listening" groups; regular farmers' days to visit the "on-farm mother-baby" trials (see later) to investigate a variety of aspects of the farming systems (similar to methods used by Eldon et al., 2020; Périnelle et al., 2021); together with training activities; farm, field and home visits, based on much "farmer to farmer" communication techniques. This showed that the dissemination plan was not limited to a single method, but encompassed a variety of available methods and activities for this district. It also did not have a linear type of flow of information, as some of the activities were led by the researcher and extension officers, while others were led by the farmers themselves. This was possible as the mother-baby on-farm trials were situated at selected farmers own properties, usually near to their homestead (as described by Snapp et al., 2019). The idea was that the mother trial had all the treatments in a completely replicated statistical trial, but that each farmer with a "baby trial" only selects certain aspects for their four plots. These are not "demonstration plots" which are used in a top-down approach, but here the farmers were actually carrying out their own experiments under their own management style and environmental conditions. The mother-baby trials were developed during an intensive participatory engagement or focus group discussion. During that meeting, the Mujika farmers decided that the on-farm trials should address fertilizer, tillage practices and varieties. The treatments chosen to be tested were two maize varieties, two tillage practices and four fertility levels according to the forecast received (Nanja and Walker, 2010). Then each of the nominated farmers had only four plots to compare certain specific aspect, for example two varieties using two tillage methods. Thus, it was easy for them to show their visitors or fellow farmers the trials and explain the different treatments. This also provided an opportunity for the development of "transferable skills" amongst the farmers as part of the empowerment and capacity building effort. As they shared the detailed information about the on-farm trials, they were developing their confidence and communication skills. This proved to be a useful means of involving and stimulating the curiosity of the other farmers in the villages, as they became attentive in the trials and then would ask questions at the group meetings (Makuvaro et al., 2018). This was a good learning process for many of the farmers. Many of these activities provided opportunities and promoted discussion which resulted in lifelong learning about influence of climate on crop production.

The focus of these Agromet Advisories for the Mujika villages was on the use of the seasonal rainfall outlook regularly provided by the ZDM at the beginning of the rainfall season in spring or early summer. The researchers, together with the extension officers, then added pertinent farming information to the 3-month rainfall outlook. The type of information that was provided was for the maize crop as the main staple diet of that area. Some of the advisories included information for the planning of the planting of maize, such as which fields should receive priority according to the type of soil and amount of rain expected. Farmers then used that information to make their own decisions concerning their agronomic activities. These advisories included information about the selection of suitable varieties based on the relative amount of rainfall expected during the upcoming season, being formulated according to whether the rain would be above normal or near normal or below normal. Similarly, advice about application of fertilizer as basal pre-plant or top dressing was also given according to the expected rainfall. For example, if the rainfall outlook was for above normal rainfall, then they should not plant on the low lying areas near to the streams with heavy clay soils, but rather on the more gravelly soils on the slopes. Also they could plant longer growing season and later maturing varieties to make better use of the available rainfall and soil water, by applying good top dressing of fertilizers in the middle of the season. In contrast, for below normal rainfall seasons they could plant on the heavier soils with shorter maturing varieties and lower fertilizer applications. Therefore, these agromet advisories were addressing the high rainfall variability in this part of Zambia

(Nanja, 2010) and enabled the farmers to build their resilience to this climate variability.

These valuable interactions between the researchers, farmers and extension personnel through the whole cropping cycle resulted in co-development of tailored Agromet advisories. One of the challenges was how to encourage farmers to attend small group or large community meetings where the seasonal climate forecast was delivered. One method used was to have farmers explain the forecast to their fellow farmers. Another challenge was to maintain the on-farm baby trials, as each season 16 farmers began, during the first season 14 completed but during the last season only half managed to complete and harvest them. As the particular focus was on improving the climate resilience of the cropping component of the local farming systems, it was important that the on-farm baby trials were managed by the specific farmers themselves. One valuable lesson learnt was that as key farmers and extension were included in all the activities from the beginning of the process, they were later enthusiastic and willing to drive the dissemination of the information themselves, in a farmer to farmer process. It also became apparent that with the support from the researcher and extension, farmers gained self-confidence and independence in making changes and using the available information in their decision making.

SCIENCE FIELD SHOPS

Science Field Shops (SFS) are groups of farmers and experts meeting regularly to exchange information about interactions between weather/climate and farming activities in Indonesia (Stigter and Winarto, 2013). Farmers, in rainfall observer groups, measure rainfall each day, together with other observations of their agro-ecological systems (see list of climate services later). At regular monthly meetings the seasonal forecasts are discussed in relation to rainfall received and the farmers anticipate conditions and options for the upcoming season. These are two of the climate services for the farmers included in SFS, others will be mentioned later. This agrometeorological learning is trans-disciplinary thorough interaction with the farmers by anthropologists from Universitas Indonesia—Department of Anthropology, agrometeorologist from the University of Free State, South Africa and extension practitioners from the Indonesian Ministry of Agriculture (Winarto et al., 2018). The transdisciplinary learning is the exploration of a range of relevant concepts, issues or problems by integrating the perspectives of multiple disciplines in order to connect new knowledge and deeper understanding to real life experiences. The anthropologists contributed with their broad approach to understanding the many different aspects of the human experience, by seeking cultural and historical evidence, understand change, comparing and contrasting information, so as to make connections and insights about farmer social existence. The agrometorologist contributed information about the interactions between climate/weather and farming systems, and insights into possible adaptations to improve sustainability. Extension practitioners are intermediaries between researchers and farmers, helping farmers to use appropriate knowledge in their decision making for sustainable production.

SFS principles include dialogue-discussion methods with engagement and exchange of knowledge between farmers and scientists (Vaarst et al., 2011; Mohtar and Daher, 2016). Farmers, scientists, extension officers and students enter into a conversation and discussion that has value and content around the interrelationships between farming and the climate. This is the place where the internal and external knowledge sets meet and the dialogue occurs which then helps the knowledge to be translated into the framework of the farmers' own world (Vaarst, 2011). Thus, "new knowledge" (as one of the SFS climate services) appropriate to their farming systems is generated, to serve the local farmers under their current conditions. These dialogues serve as a platform of mutual support for the farmers of each other while allowing for interpersonal responsiveness resulting in a clear understanding of the situation. Therefore, everyone benefited from such dialogues and the farmers were able to interact and discuss the options available and evaluate the consequences for their own farm (Vaarst et al., 2011). These focused discussions are the process of talking about the current situation and weather conditions in order to exchange ideas and to reach a decision about the best possible farming actions. Both scientists and farmers are continually learning and applying their knowledge using climate information to think out logical recommendations for evidence-based decisions for optimal agricultural productivity. Therefore, the foundation of SFS is good rapport between farmers and scientists with a common goal of exchanging information about seasonal rainfall forecasts to improve farming decisions.

As the SFS discussions are based on the local farming systems, they are really a place where the farmers acquire knowledge and agromet advisories in a face-to-face manner from each other and the scientists. SFS include eight basic climate services (Winarto et al., 2018), namely daily rainfall measurements; agroecological observations in their fields; analysis/evaluation of yields amongst farmers from different locations, across different seasons, and different years; monthly rainfall scenario outlook discussions; problem-solving by farmer experimentation in their fields to develop strategies to sustain yields; exchange of scientific "new" knowledge; organization of SFS groups and storage and digital analysis of farmers' rainfall data (Winarto et al., 2019, 2020). Each of these is vital to the understanding of the farming system and the interactions with the environment as well as the local climate and weather phenomena.

The farmers must commit to make their own rainfall measurement each day at the same time and keep a good record of these measurements. This enables then to relate the conditions and experience on their own farm to the area as a whole and also to the seasonal forecasts. It helps them to have a good basis from which to understand climate variability, as they can experience first-hand that each day or week or year is not the same. They have developed a better comprehension of the fluctuations and even the extremes experienced in the rainfall between seasons. Following the input from the agrometeorologist scientists during the farmer facilitator training sessions, they could also relate their own rainfall records to the worldwide climate indicators

such as ENSO (El Niño—Southern Oscillation). This enables them to appreciate and comprehend the possibilities of what can occur in the upcoming season from the interaction of their own farming system with the global climate variability. So when they receive the monthly update about the current ENSO conditions, then they are able to discuss the options in their groups and make educated decisions about farm activities in the coming period. This process of anticipation of the future rainfall events and the knock-on effects on their farm as reported by Winarto et al. (2019), has been well-developed by the farmers themselves and shown many benefits being instrumental in improving their sustainability and productivity over the years since SFSs were organized in 2008.

The recording of the state of the agro-ecological conditions in their own fields, is also a learning process that had rewarded the farmers over the years. As they have documented the relationships between all the various aspects, they can consider these factors when planning for the following season. This feedback loop has proved to be a great learning process and provided the farmers with valuable insights into the cause and effect relationships on their own farms. For example, as they walked in the field every day, they observed the beginning of a pest breakout and were able to work proactively to prevent large-scale damage to their crops, in contrast to other farmers who may not enter their fields on a daily basis. In future they will also be more diligent to check for certain pests and disease according to the weather conditions they have been observing. Therefore, this transdisciplinary learning from farmers to scientists in varied fields brings a holistic view to the agricultural production system and promotes sustainability and productivity (Mubaya et al., 2015).

SFS are based on using transdisciplinary research principles in practice with the farming community. The scientist team was composed of anthropologists, agrometeorologist and extension practitioners as well as other agricultural experts as and when they are needed to answer specific questions from the farmers. As the world is not segregated into compartments according to disciplines, so to the research and applications should also be across disciplines. The principle of transdisciplinary research is explained as a broad concept including many ways of working itself out in reality but all "transcends the narrow scope of disciplinary worldviews" (Klein, 2013).

The concept of SFS has some overlapping aspects with the FFS (Farmer Field Schools) and CFS (Climate Field Schools) in that they are engagements between scientists and the farmers (Van Den Berg and Jiggins, 2007; Friis-Hansen and Duveskog, 2012), and CFS address climate aspects of agriculture (Siregar and Crane, 2011). However, the advantage of the Science Field Shops is that they become an institution in and of themselves within the community, led by the community members themselves. So, unlike the FFS and CFS, where the training may take place over a few weeks or a growing season (Van Den Berg and Jiggins, 2007), the SFS provide a continuing lifelong learning opportunity for the farmers and they are self-governing groups like an NGO (non-governmental organization) or a CBO (community based organization). This lifelong learning as the continued ongoing, voluntary, and self-motivated pursuit of knowledge by the farmers is due to the fact that they can see the continued benefit of the rainfall measurements groups. Therefore, as well as enhancing social inclusion and active citizenship, there are benefits of personal development, and farming self-sustainability, as well as some factors of competitiveness and employability for those engaging in these activities. These aspects of the SFS are in contrast to a more top-down approach in FFS which can result in the disappearance of the control group of farmers who continue with their own traditional practices (Van Den Berg and Jiggins, 2007). However, this presents a challenge to upscaling SFS, as it required intensive engagements with each different group of farmers in each new region. For this to be successful buy-in and support from the government structures is needed. The SFS focus on the local agricultural systems and market opportunities to address the complex issues and priorities of farming communities, as it is a bottom-up capacity building lifelong learning approach through whereby farmers enhance their analytic and problem-solving abilities as recommended by Van Den Berg and Jiggins (2007).

A lessons learnt was that as the farmer observers gained self-confidence in understanding their own rainfall records relationship to the season forecasts, they were confident to speak to the village leaders and gain their respect as advisors. So, farmers are now making their own agromet advisories based on their own experience and information from international climate centers. Farmers use their rainfall observations (represented in simple hand-drawn diagrammes) together with the scientific interpretation of seasonal forecasts to develop tailor-made climate services related to local farming systems. This enables farmers to use climate information for improved management decisions both for themselves and for their neighbors or to give advice to the village leaders. This learning process has empowered farmers to address challenges on their own, and sustain and improve their productivity. Such co-development of agromet advisories is highly beneficial and locally based, however, the concept can be transferred to other areas and regions as the foundation is firmly on good communication and good science and respect across the transdisciplinary groups.

AGRICLOUD

AgriCloud is an online weather-based agricultural advisory system that enriches weather and climate forecasts with pertinent agricultural information and local agricultural knowledge. Real-time personalized overviews, forecasts, and warnings are generated and tailored to the particular farmer's needs. This is achievable because the users select and mark their own specific location on a google map at registration on the smart phone mobile App. Then users can receive the information for this precise location from the 15×15 km grid used for the weather forecasts. AgriCloud provides farmers, extension staff and advisors in South Africa with daily updated weather-related farm specific advice. AgriCloud does not provide a weather forecast for the predicted rainfall and/or temperatures as on many weather Apps, but AgriCloud provides added value that it relevant to the dominant maize rainfed farming system.

AgriCloud information is available via an android mobile App; an API tailor-made for a client to use via their own platform. During the R4A project, a USSD system was also developed for farmers without smart mobile phones. Alternatively a client or reseller can connect by subscription for tailor-made advisories, information and maps delivering selected information for their selected region. On the mobile AgriCloud App users obtain forecasts of planting dates for rain-fed crops in the next 10 days and suitable spray conditions, for herbicides and pesticides, according to time of day. All advisories are available in 11 South African official languages. Advisories were based on real-time weather observations and forecasts from ECMWF (European Center for Medium-Range Weather Forecasts) or GFS (Global Forecast System) numerical models and locally developed agricultural knowledge engines with crop specific algorithms. The AgriCloud App was developed during the "Rain4Africa" (R4A) project funded by the Netherlands Space Office together with Dutch partners. Data and advisories from South African Agricultural Research Council (ARC), South African Weather Services (SAWS) and ECMWF include ground based automatic weather station observations, radar and satellite integrated rainfall surfaces. The process followed for the development of the AgriCloud agromet advisory messages was an approach including engagements with the farming community and applied science developments.

The science and IT developments included expansion to the HydroNet platform (https://www.hydronet.co.za/) from its water-climate focus to include some aspects of climate-agriculture interactions. HydroNet is used by the catchment management agencies as a web-based information and decision support system for water management. It combines weather, climate and water data and models with local knowledge to generate location specific information in the form of area overviews forecasts and warnings according to stakeholders needs. The water control room is used across South Africa by water resource managers and engineers at the Department of Water and Sanitation via specially formulated dashboards to generate hydrological reports. During the R4A project some of these aspects were expanded to include aspects important for agricultural water management as well.

Other scientific aspects included the development of algorithms or knowledge engines (Jahanshiri and Walker, 2015) specifically designed to address some of the critical aspects for optimal maize cultivation. As many losses in southern African maize production are weather related, it was important to include the weather forecast and then develop such relationships as explained by Myeni et al. (2019), Myeni and Moeletsi (2020). Aspects that are critical include the correct planting dates and control of pests and diseases. Therefore, algorithms, screening and trigger factors were developed to use the current weather parameters and their relationships with maize growth and development to generate agricultural advisories on a daily basis.

The principles of response farming (Stewart, 1988; Stigter et al., 2013) have been used in the development of the planting advisory for the rainfed maize in South Africa. This means that a certain amount of rainfall should be received within a stipulated time period before one can plant. This is based on the principle that water is needed around the seed to allow it to germinate, so following receiving this amount of rain it is deemed that sufficient moisture should be available in the top soil. In the AgriCloud app both the past observed and the rainfall expected from the medium-term weather forecast are used in this calculation (Walker, 2020). Then farmers can use this information to make plans for their planting activities by usually waiting for sufficient rainfall before planting the maize seeds (Moeletsi et al., 2013a; Makuvaro et al., 2014, 2017). The agromet advisory was presented in the AgriCloud App as a calendar block for the following 2 weeks with green shading to show that conditions are conducive for planting or a red shading to show that it would better not to plant on those days. This data is updated on a daily basis so can be available to the farmers for their own specific farm location when they open the app. An additional feature developed for AgriCloud was the crowd sourcing section. Here the user can give feedback to the app developers on the current extreme weather conditions. This is via a selection mode where one can select an icon that represents the current weather conditions and then earn some points for their contribution. At present the icons represent severe weather conditions, including hail, thunderstorms, frost, high winds, tornadoes, misty conditions, rain or floods. This provided a two-way communication channel on AgriCloud that can be further developed for other applications.

As a large part of the summer rainfall region in South Africa is in the Highveld on the South African inland plateau at altitudes above roughly 1500 m but below 2100 m, frost is a regular winter occurrence. As maize is sensitive to temperatures below 10°C, it must be planted where there is at least a 120 day frost free window (McMaster and Wilhelm, 1997). Therefore, a first screening of the long-term first and last frost dates was used to exclude planting dates within such time periods (Moeletsi et al., 2013b, Moeletsi and Walker, 2013). In this way certain dates for certain locations will be excluded from further calculations and will return a "do not plant" message to the farmers in those areas regardless of the amount of rainfall they have received, due to the danger of frost damage to the seedlings.

The farming community interactions during the R4A project included focus group discussions with training on the use of seasonal forecasts, and a survey through a pre-tested, structured questionnaire to assess farmers needs and understanding of climate change. The information collected highlighted the fact that many farmers in rural areas do not have smart phones and that the mobile network is poor in some locations. This hinders their use of such Apps. It also showed that most small-scale farmers only access the weather forecast via the TV or radio broadcasts, and that is only available for the main centers. So they need more detailed information for their own specific locality as they know that there are differences from the nearest city. Therefore, it was again highlighted that farmers need routinely updated weather information for their own areas that they could use when planning their farm activities. Therefore, it was vital to develop agromet advisories for specific farming systems in specific areas and to be able to deliver them on a routine basis.

Following the formulation of the agromet advisories, a series of meetings were held with the personnel from the departments of agriculture in selected provinces as a way of

testing the AgriCloud app with the users (with more than 540 attendees). These meeting were held between May and October 2018 and the comments received were integrated into a revised AgriCloud App. Further engagements were via the extension officers from October 2018 continuing into 2019, when a number of information training type meetings were held, with more than 1,000 extension officers attending across 6 provinces. These trainings sessions were held during the roll-out of the AgriCloud mobile app at the beginning of the 2018 rainy season in South Africa. It is estimated that these extension officers serve about 400,000 small-scale farmers. Some of the comments received from them include the following stumbling blocks encountered, such as poor access to mobile network or little data and not understanding the functions on the smart phones. Many extension officers also requested other functions on the AgriCloud App, particularly pertaining to livestock and vegetable production activities. However, by the end of the R4A project more than 1,500 people had downloaded the AgriCloud App from Google play store and about 70% of users were also returning on a regular basis. This illustrates that the agromet advisory information is being used as it has some unique aspects, namely that it is available in the 11 South African official languages, it is giving the information for one's own farm on one's own mobile smart phone with daily updated information for the upcoming 10-14 days.

Some of the lessons learnt during the R4A project, include the need for continued openness to listen to the clients, extension and farmers in this case, while maintaining regular communication and building credibility for the usefulness of the products. One of the big challenges was to try to evaluate the effect the increased availability of agromet information on the dryland cropping systems. As variation in yields is so large between years and dependent on the rainfall amount and distribution through the season, it was not possible to only compare production between years. This needs to be approached in a different manner in future, possibly by using crop modeling and historic weather datasets. But that would not include the essential element of the farmers decision making processes.

CONCLUSIONS

These three examples from three different countries, show how the scientific weather forecasts can be used together with especially co-developed tailored agricultural forecasts to inform farmers and supply them with updated information on a daily basis. Scientists from different disciplines were involved in all three examples, showing the importance of trans-disciplinary teams and how they complement each other by bringing different skills to the team. This is especially apparent in SFS where anthropologists were the initiator and team leaders, as during their exchanges with the farmers, they realized the need for expertise about climate change and adaptations. The anthropologists gained a deeper understanding of the interactions between weather/climate and crop production under a changing climate. The natural scientists learnt good social skills for interacting with farming communities during these co-development activities and the farmers benefited from the participatory team effort. Good communication systems are vital to deliver and receive feedback on Agromet advisories. The three examples highlighted different modes of stakeholder engagement and routine delivery of the agromet advisories. All used some form of focus group discussions, with close in-person interactions between the researchers and the farmers. This enabled the incorporation of local knowledge into the co-development of pertinent advisories suitable for the farmers and their own farming systems and situation. In SFS and CAPES farmers formed their own groups that met regularly to discuss the climate information and how it affected their farm level options and decisions. So these study groups became the made mode of regular information dissemination, as it allows immediate feedback and detailed discussions about the topics that arise. As AgriCloud is a mobile app, it does not offer such an opportunity, however, the crowd sourcing function is a step toward receiving feedback from the farmers. In future various combinations of these methods can be used to develop locally useful agromet advisories for other farmers and farming systems under a variety of climatic conditions around the world. It is vital that good weather forecasts are available and a co-development process with farmers uses local information about the agricultural systems to integrate into an acceptable and appropriate communication system. Such systems can then be used on a routine basis to reach as many farmers and farm managers provided that there are opportunities for two-way communication and continued refinement and co-developed of the agromet advisories with the farmer users.

DATA AVAILABILITY STATEMENT

The original contributions presented in the study are included in the article/supplementary material, further inquiries can be directed to the corresponding author.

AUTHOR CONTRIBUTIONS

The author confirms being the sole contributor of this work and has approved it for publication.

FUNDING

The following organizations were thanked for continued funding support over many years—University of the Free State, South African Agricultural Research Council, South African National Research Foundation, South African Water Research Commission, Universatas Indonesia, and for specific project funding from Canadian International Development Research Center (IDRC), Netherlands Space Office, G4AW (Geodata for Agriculture and Water), Indonesia Climate Change Trust Fund of the Ministry for Planning and Development and KONSEPSI Consortium for Study and Development Participations.

ACKNOWLEDGMENTS

The author thanks the Rain4Africa team members and organizations namely SAWS, HydroLogic and Weather Impact who made major contributions to development of AgriCloud. The Science Field Shops work was carried out together with Yunita Winarto and Rhino Ariefiansyah, from the Universatas Indonesia. CAPES was developed during Durton H. Nanja Ph.D. study in Zambia.

REFERENCES

Ager, A., Stark, L., and Potts, A. (2010). *Participative Ranking Methodology: A Brief Guide*. New York, NY: Columbia University, 18.

Carberry, P. S., Hochman, Z., McCown, R. L., Dalgliesh, N. P., Foale, M. A., Poulton, P. L., et al. (2002). The FARMSCAPE approach to decision support: farmers', advisers', researchers' monitoring, simulation, communication, and performance evaluation. *Agr. Syst*. 74, 141–177. doi: 10.1016/S0308-521X(02)00025-2

Chambers, R. (2006). Participatory mapping and geographic information systems: whose map? who is empowered and who is disempowered? who gains and who loses. *Electron. J. Inform. Syst. Dev. Countries* 25, 1–11. doi: 10.1002/j.1681-4835.2006.tb00163.x

Chambers, R. (2007). *From PRA to PLA and Pluralism: Practice and Theory. IDS Working Paper, no. 286*. Brighton: Institute of Development Studies, 41.

Eldon, J., Baird, G., Sidibeh, S., Dobasin, D., Rapaport, P., Cheng, W., et al. (2020). On-farm trials identify adaptive management options for rainfed agriculture in West Africa. *Agr. Syst*. 182:102819. doi: 10.1016/j.agsy.2020.102819

Elhag, M. M., and Walker, S. (2011). A decision support tool to assess desertification condition in arid and semi-arid regions. *Int. J. Water Resour. Arid Environ.* 1, 378–381. Available online at: http://www.integral-review.org/issues/vol_9_no_2_klein_the_transdiciplinary_moment(um).pdf

Friis-Hansen, E., and Duveskog, D. (2012). The empowerment route to well-being: an analysis of farmer field schools in East Africa. *World Dev*. 40, 414–427. doi: 10.1016/j.worlddev.2011.05.005

Gandure, S., Walker, S., and Botha, J. J. (2013). Farmers' perceptions of adaptation to climate change and water stress in a South African rural community. *Environ. Dev.* 5, 39–53. doi: 10.1016/j.envdev.2012.11.004

Hall, R., Brent, Z., Franco, J., Isaacs, M., and Shegro, T. (2017). *A Toolkit for Participatory Action Research*. Ottawa, ON: International Development Research Centre (IDRC), 16. Available online at: http://hdl.handle.net/10566/4112 (accessed May 11, 2021).

IFAD (2009). *Good Practices in Participatory Mapping*. Rome: International Fund for Agricultural Development, 59.

Jagtap, S. S., Jones, J. W., Hildebrand, P., Letson, D., O'Brien, J. J., Podest,à, G., et al. (2002). Responding to stakeholder's demands for climate information: from research to applications in Florida. *Agr. Syst*. 74, 415–430. doi: 10.1016/S0308-521X(02)00048-3

Jahanshiri, E., and Walker, S. (2015). Agricultural knowledge-based systems at the age of semantic technologies. *Int. J. Knowl. Eng.* 1, 64–67. doi: 10.7763/IJKE.2015.V1.11

Jones, A., Breuning-Madsen, H., Brossard, M., Dampha, A., Deckers, J., Dewitte, O., et al. (eds.). (2013). *Soil Atlas of Africa*. Luxenbourg: European Commission, Publ. Office European Union, 176.

Klein, J. T. (2013). The transdisciplinary moment(um). *Integ. Rev.* 9, 189–199.

Makuvaro, V., Walker, S., Munodawafa, A., Chagonda, I., Masere, P., Murew, C., et al. (2017). Constraints to crop production and adaptation strategies of smallholder farmers in semi-arid central and western Zimbabwe. *Afr. Crop Sci. J.* 25, 221–235. doi: 10.4314/acsj.v25i2.7

Makuvaro, V., Walker, S., Munodawafa, A., Masere, T. P., Murewi, C., et al. (2014). An overview of current agronomic practices of smallholder farmers in semi-arid Central and Western Zimbabwe. *Afr. J. Agric. Res*. 9, 2710–2720. doi: 10.5897/AJAR11.606

Makuvaro, V., Walker, S., Masere, T. P., and Dimes, D. (2018). Smallholder farmer perceived effects of climate change on agricultural productivity and adaptation strategies. *J. Arid Environ*. 152, 75–82. doi: 10.1016/j.jaridenv.2018.01.016

McMaster, G. S., and Wilhelm, W. W. (1997). Growing degree-days: one equation, two interpretations. *Agric. For. Meteorol.* 87, 291–300. doi: 10.1016/S0168-1923(97)00027-0

Moeletsi, M. E., Mellaart, E. A. R., Mpandeli, N. S., and Hamandawana, H. (2013a). The use of rainfall forecasts as a decision guide for small-scale farming in Limpopo Province, South Africa. *J. Agric. Educ. Exten*. 19, 133–145. doi: 10.1080/1389224X.2012.734253

Moeletsi, M. E., Moopisa, S. G., Walker, S., and Tsubo, M. (2013b). Development of an agroclimatological risk tool for dryland maize production in the Free State Province of South Africa. *Comput. Electron. Agric*. 95, 108–121. doi: 10.1016/j.compag.2013.04.006

Moeletsi, M. E., and Walker, S. (2013). Agroclimatological suitability mapping for dryland maize production in Lesotho. *Theor. Appl. Climat*. 114, 227–236. doi: 10.1007/s00704-012-0829-1

Mohtar, R. H., and Daher, B. (2016). Water-Energy-Food Nexus framework for facilitating multi-stakeholder dialogue. *Water Int.* 41, 655–661. doi: 10.1080/02508060.2016.1149759

Mubaya, C. P., Mugabe, F. T., and Walker, S. (2015). "Carving a niche for the social sciences in transdisciplinary research on climate change adaptation in Southern African agriculture," in *Global Sustainability Cultural Perspectives and Challenges for Transdisciplinary Integrated Research, Part II Knowledge Production and Action*, ed B. Werlen (Berlin: Springer), 107–117.

Myeni, L., Moeletsi, M., Thavhana, M., Randela, M., and Mokoena, L. (2019). Barriers affecting sustainable agricultural productivity of smallholder farmers in the eastern Free State of South Africa. *Sustainability* 11:3003. doi: 10.3390/su11113003

Myeni, L., and Moeletsi, M. E. (2020). Factors determining the adoption of strategies used by smallholder farmers to cope with climate variability in the Eastern Free State, South Africa. *Agriculture* 10:410. doi: 10.3390/agriculture10090410

Nanja, D. H. (2010). *Dissemination of climate information to small-holder farmers: A case study for Mujika area, Zambia* (Ph.D. in Agrometeorology). University of Free State, Bloemfontein, South Africa.

Nanja, D. H., and Walker, S. (2009). *Handbook for Community Agrometeorological Participatory Extension Service (CAPES)*. Bloemfontein: University of the Free State and Monze. Available online at: http://www.agrometeorology.org/files-folder/repository/HandbookCAPES.pdf (accessed May 11, 2021).

Nanja, D. H., and Walker, S. (2010). "Changes in farmer decision making under a variable Monze climate," in *Climate Change in Africa: Research Insights on Adaptation at Local and Regional/Sub-Regional Scales at the ACCFP Round I Culmination Conference, 8-10 December 2010* (Dakar).

Nyumba, T. O., Wilson, K., Derrick, C. J., and Mukherjee, N. (2018). The use of focus group discussion methodology: insights from two decades of application in conservation. *Meth. Ecol. Evol.* 9, 20–32. doi: 10.1111/2041-210X.12860

Périnelle, A., Meynard, J.-M., and Scopel, E. (2021). Combining on-farm innovation tracking and participatory prototyping trials to develop legume-based cropping systems in West Africa. *Agr. Syst*. 187:102978. doi: 10.1016/j.agsy.2020.102978

Siregar, P. R., and Crane, T. A. (2011). Climate information and agricultural practice in adaptation to climate variability: the case of Climate Field Schools in Indramayu, Indonesia. *Cult. Agric. Food Environ*. 33, 55–69. doi: 10.1111/j.2153-9561.2011.01050.x

Snapp, S. S., DeDecker, J., and Davis, A. S. (2019). Farmer participatory research advances sustainable agriculture: lessons from Michigan and Malawi. *Agron. J.* 111, 1–11. doi: 10.2134/agronj2018.12.0769

Stewart, J. I. (1988). *Response Farming in Rainfed Agriculture*. Davis, CA: The WHARF Foundation Press, 103.

Stigter, C. J., and Winarto, Y. T. (2013). Science Field Shops in Indonesia: a start of improved agricultural extension that fits a rural response to climate change. *J. Agric. Sci. Appl*. 2, 112–123. doi: 10.14511/jasa.2013.020210

Stigter, K., Walker, S., and Das, H. (2014c). Meeting farmers' needs for agrometeorological services: a review with case studies Part III: Context 2, the future. *Ital. J. Agrometeorol.* 2104, 45–52. Available online at: https://riviste.fupress.net/index.php/IJAm/issue/archive

Stigter, K., Walker, S., Das, H., Dominguez-Hurtado, I. M., and Nanja, D. (2014a). Meeting farmers' needs for agrometeorological services: a review with case studies Part I: Introduction and history. *Ital. J. Agrometeorol.* 1/2014, 59–65.

Stigter, K., Walker, S., Das, H., Huda, S., and Haasbroek, P. D. (2014b). Meeting farmers' needs for agrometeorological services: a review with case studies Part II: Context 1, the existing situation. *Ital. J. Agrometeorol.* 2/2014, 51–60.

Stigter, K., Winarto, Y. T., Ofori, E., Zuma-Netshiukhwi, G., Nanja, D., and Walker, S. (2013). Extension agrometeorology as the answer to stakeholder realities: response farming and the consequences of climate change. *Atmosphere* 4, 237–253. doi: 10.3390/atmos4030237

Vaarst, M. (2011). "Dialogue towards animal health and welfare planning," in *The Process of Minimising Medicine Use through Dialogue based Animal Health and Welfare Planning*, eds M. Vaarst and S. Roderick, (Tjele: International Centre for Research in Organic Food Systems (ICROFS)). 38–43.

Vaarst, M., Roderick, S., Smolders, G., Leeb, C., Walkenhorst, M., Winckler, C., et al. (2011). "The dialogue with farmers," in *The Process of Minimising Medicine Use through Dialogue based Animal Health and Welfare Planning*, eds M. Vaarst and S. Roderick, (Tjele: International Centre for Research in Organic Food Systems (ICROFS)) 64–79.

Van Den Berg, H., and Jiggins, J. (2007). Investing in farmers–the impacts of Farmer Field Schools in relation to integrated pest management. *World Dev.* 35, 663–686. doi: 10.1016/j.worlddev.2006.05.004

Walker, S. (2020). Value-added weather advisories for small-scale farmers in South Africa delivered via mobile apps. *Irrig. Drain.* 70, 505–511. doi: 10.1002/ird.2506

Walker, S., Ofori, E., Kyei-Baffour, N., and Stigter, K. (2010). "Problems and solutions in using and coping with weather phenomena in need of tactical decision making and challenges remaining for the use of science to contribute to problem analyses and designing viable solutions in this context: multiple cropping," in *Applied Agrometeorology*, ed K. Stigter (Heidelberg: Springer), 493–498.

Walker, S., and Stigter, K. (2010). "Designing and selecting early warning strategies and increasing their efficiencies: multiple cropping," in *Applied Agrometeorology*, ed K. Stigter (Heidelberg: Springer), 485–492.

Winarto, Y. T., Walker, S., and Ariefiansyah, R. (2019). People, clouds and roots: between the unseen, the seen, and the unforeseen. *Nat. Cult.* 14, 236–250. doi: 10.3167/nc.2019.140302

Winarto, Y. T., Walker, S., Ariefiansyah, R., Lisan, I. H., Bestari, M. Y., and Audina, T. (2020). "University's inclusion in providing climate services to farmers: Is it possible without agricultural agents and farmer facilitators?" in *Climate Change, Hazards and Adaptation Options: Handling the Impacts of a Changing Climate*, eds W. L. Filho, G. J. Nagy, M. Borga, P. D. Chávez Muñoz, and A. Magnuszewski (Berlin, Climate Change Management Series, Springer), 835–852.

Winarto, Y. T., Walker, S., Ariefiansyah, R., Prihandiani, A. F., Taqiuddin, M., and Nugroho, Z. C. (2018). *Institutionalizing Science Field Shops: Developing Response Farming to Climate Change*. Rome: Global Alliance for Climate Smart Agriculture. Available online at: http://www.fao.org/3/I8454EN/i8454en.pdf (accessed May 11, 2021).

Zuma-Netshiukhwi, G., Stigter, K., and Walker, S. (2013). Use of traditional weather/climate knowledge by farmers in the South-Western Free State of South Africa: agrometeorological learning by scientists. *Atmosphere* 4, 383–410. doi: 10.3390/atmos4040383

Conflict of Interest: The author declares that the research was conducted in the absence of any commercial or financial relationships that could be construed as a potential conflict of interest.

frontiers in Climate

ORIGINAL RESEARCH
published: 20 September 2021
doi: 10.3389/fclim.2021.716588

Phenological Water Balance Applications for Trend Analyses and Risk Management

Chris Funk, Juliet Way-Henthorne and Will Turner*

Climate Hazards Center, Department of Geography, University of California, Santa Barbara, Santa Barbara, CA, United States

The overarching goal of this work is to develop and demonstrate methods that support effective agro-pastoral risk management in a changing climate. Disaster mitigation strategies, such as the Sendai Framework for Disaster Risk Reduction (SFDRR), emphasize the need to address underlying causes of disaster risk and to prevent the emergence of new risks. Such assessments can be difficult, because they require transforming changes in meteorological outcomes into sector-specific impact. While it is common to examine trends in seasonal precipitation and precipitation extremes, it is much less common to study how these trends interact with crop and pasture water needs. Here, we show that the Water Requirement (WR) component of the widely used Water Requirement Satisfaction Index (WRSI) can be used to enhance the interpretation of precipitation changes. The WR helps answer a key question: was the amount of rainfall received in a given season enough to satisfy a crop or pasture's water needs? Our first results section focuses on analyzing spatial patterns of climate change. We show how WR values can be used to translate east African rainfall declines into estimates of crop and rangeland water deficits. We also show that increases in WR, during recent droughts, has intensified aridity in arid regions. In addition, using the PWB, we also show that precipitation increases in humid areas of western east Africa have been producing increasingly frequent excessive rainfall seasons. The second portion of our paper focuses on assessing temporal outcomes for a fixed location (Kenya) to support drought-management scenario development. Kenyan rainfall is decreasing and population is increasing. How can we translate this data into actionable information? The United Nations and World Meteorological Organization advise nations to proactively plan for agro-hydrologic shocks by setting aside sufficient grain and financial resources to help buffer inevitable low-crop production years. We show how precipitation, WR, crop statistics, and population data can be used to help guide 1-in-10 and 1-in-25-year low crop yield scenarios, which could be used to guide Kenya's drought management planning and development. The first and second research components share a common objective: using the PWB to translate rainfall data into more actionable information that can inform disaster risk management and development planning.

Keywords: climate change, East Africa, agriculture, risk management, climate extremes, drought, disaster risk management

OPEN ACCESS

Edited by:
Mphethe Tongwane, Zutari, South Africa

Reviewed by:
Alexandre S. Gagnon, Liverpool John Moores University, United Kingdom
Fadji Maina, National Aeronautics and Space Administration, United States

****Correspondence:***
Chris Funk
chris@geog.ucsb.edu

Specialty section:
This article was submitted to Climate Services, a section of the journal Frontiers in Climate

Received: *28 May 2021*
Accepted: *17 August 2021*
Published: *20 September 2021*

Citation:
Funk C, Way-Henthorne J and Turner W (2021) Phenological Water Balance Applications for Trend Analyses and Risk Management. Front. Clim. 3:716588. doi: 10.3389/fclim.2021.716588

BACKGROUND AND RATIONALE

In this study, we introduce a new Plant Water Balance (PWB) metric and demonstrate how it can be used to support trend analyses and risk management in east Africa (0–18°N, 20°E–51°E). Beginning in 2005 (Funk et al., 2005) and continuing to the present (Gebrechorkos et al., 2019), many studies have documented the decline in the eastern east Africa (east Africa east of 38°E and south of 8°N) boreal spring "Long" rains. This region experiences a bimodal seasonal cycle, with the boreal spring "Long" rainy season being longer and more copious than the boreal fall "Short" rainy season. More details on the crop phenology of the "Long" rains can be found in our accompanying paper, "An agro-pastoral phenological water balance framework" (Funk et al., 2021).

While it is generally accepted that this decline is associated with an intensification of the Indian Ocean branch of the Walker Circulation, as suggested in 2008 (Funk et al., 2008), the primary driver of that intensification is likely due to changes in the Pacific, and not Indian, Ocean (Williams and Funk, 2011; Lyon and DeWitt, 2012). These changes involve a combination of human-induced warming in the western Pacific and natural, La Niña-like, cool sea surface temperatures in the equatorial eastern Pacific (Hoell and Funk, 2013a,b; Liebmann et al., 2014). The relative contribution of natural variability to the observed declines in precipitation remains debated. Some studies have emphasized Pacific Decadal Variability (Lyon, 2014; Yang et al., 2014), while other papers have focused on anthropogenic warming in the western equatorial north-western Pacific (Funk et al., 2018, 2019b). Other studies, however, have focused on changes in the Indian Ocean. One study (Wainwright et al., 2019) suggested that the recent decline is strongly associated with a shorter rainy season, with warmer waters to the south of east Africa delaying the onset and decreasing surface pressures over Arabia, thus supporting an earlier cessation of the rainy season.

While decomposing the myriad potential drivers of the east African rainfall declines (Indian vs. Pacific, natural variability vs. climate change) is very difficult, it is not hard to identify the substantial increase in the frequency of poor eastern east African rains. Many of these dry seasons have been associated with strong Pacific sea surface temperature gradients, and the sea surface temperature gradients responsible for the decline, can be used as a basis for prediction (Funk et al., 2014; Shukla et al., 2014). At the same time, east Africa has also been impacted by extreme precipitation. According to the EM-Dat emergency database on natural and technological disasters (https://www.emdat.be/), since 2015, 119 flood events and extreme storms have impacted more than 11 million people. Climate science suggests a fairly straightforward explanation for at least some of these increases. As the atmosphere warms, saturation vapor pressures increase. A warmer atmosphere can hold more water vapor, which is expected to lead to more extreme precipitation events (Emori and Brown, 2005). While data limitations make assessments of extreme precipitation outcomes difficult in sub-Saharan Africa, recent assessments do suggest that in well-gauged areas, extreme events are becoming wetter, particularly in wet areas (Harrison et al., 2019).

To help contextualize the agricultural impacts associated with these extremes, it is useful to consider both crop water demand and crop water supply. In this study, we show how a new "Phenological Water Balance" (PWB) index can be used to (i) explore changes in both very dry and very wet growing seasons, and (ii) guide long-term risk management strategies by helping to identify plausible 1-in-10 and 1-in-25-year drought scenarios for Kenya. The focus of the first analysis section is spatial. Where are the hot spots of climate change? Where are crops and pastures experiencing more frequent water stress? Where is increased atmospheric water demand exacerbating the impact of rainfall deficits? In places where rainfall is increasing, where is it probably beneficial and where might it be harmful, in the sense that precipitation now often exceeds plant water requirements by a large amount? The focus of the second results section is temporal. For a given fixed region (Kenya), that has been experiencing rainfall declines, how bad might the next really low crop production year be? Answering such a question is central to the integrated drought management planning advocated by the World Meteorological Organization[1] and the United Nations (UN). In their 2021 special report on drought,[2] the UN Office of Disaster Risk Reduction discusses how the combination of climate change and population growth (Smirnov et al., 2016) is increasing drought exposure in many developing countries; understanding and managing these increasing drought risks will be central to meeting the objects enumerated in the Sendai Framework for Disaster Risk Reduction and 2030 Agenda for Sustainable Development. A key component of management involves quantifying drought impacts. This study uses precipitation, WR, population, and crop statistics to generate plausible near-term projections of low annual maize yields, maize production, and per capita maize production.

The PWB framework builds extensively on geospatial implementations of the "Water Requirement Satisfaction Index" (WRSI) (Verdin and Klaver, 2002; Senay and Verdin, 2003). In the results examined here, we use Start of Season (SOS) and Length of Growing Period (LGP) maps to define crop-growing seasons. Using these SOS dates and LGP, we can then calculate Growing Season Precipitation (GSP) and growing season Water Requirements (WR). The ratio of GSP and WR defines the PWB. In this paper, we explore how the PWB can be used to examine the following two questions:

1. Given the well-documented decline in the east African boreal spring rains, can the PWB framework be used to evaluate trends, thereby supporting monitoring at decadal time scales? Can we identify hot spots of elevated drought or flood risk?
2. Can the PWB framework be used with crop and population statistics to transform assumptions about precipitation into assumptions about national maize yields in Kenya, thereby supporting the development of plausible near-term low crop production scenarios? These scenarios can be used by Kenyan

[1] https://public.wmo.int/en/programmes/integrated-drought-management-programme.

[2] https://www.undrr.org/gar2021-drought.

planning agencies to inform national-scale planning and preparedness for agricultural shocks, leading to improved drought management policies.

The trend analyses cover the entire east African Long rains growing area. We show that the WR framing adds substantial value beyond just analyzing changes in rainfall. A given decrease in rainfall may have very different impacts depending on local water requirements. Rainfall declines in areas where precipitation exceeds plant water requirements may have no negative effects. On the other hand, a relatively modest decrease in precipitation in a water-stressed region may dramatically increase the frequency of poor crop and pasture conditions. Precipitation increases in such areas might be very beneficial. But precipitation increases in areas where seasonal rainfall substantially exceeds WR values may actually be detrimental to crop outcomes.

The agricultural shocks analysis focuses on Kenya. The first and second research components share a common objective: using the PWB to translate rainfall data into more actionable information that can inform disaster risk management and development planning. The first research section focuses on spatial patterns. Where are we seeing changes in risk? The second research section focuses on temporal distributions for a given country. How can we translate long time-series of rainfall into actionable near-term crop production deficit scenarios?

It should be noted that while the results presented here are regional and seasonal, the general approach taken could be extended to multiple seasons, and on continental or global scales; scales at which running more complicated models would be difficult.

DATA

Terminology

Before going into specifics about particular data sets, we present and discuss **Figure 1**, which schematically describes the PWB calculation. In this figure, we describe the typical seasonal progression of a rain-fed crop, such as maize, millet or sorghum. Farmers are well attuned to the typical seasonal progression of rains in their area, and these rains (shown with a solid blue curve) tend to begin with scattered showers, increase to a mid-season peak, and then taper off. In this paper, we break each growing season into "dekads." Each month is divided into three dekads—two 10-day dekads followed by a third dekad that contains the remaining days in the month. In agricultural modeling, dekads are often used to represent time-varying environmental variables, such as precipitation or RefET. RefET will increase when radiation, surface wind, or local vapor pressure deficits increase. It is a measure of atmospheric water demand. Early research by the Food and Agriculture Organization (FAO), based on plot-level crop observations, related RefET to the seasonal progression of crop-specific Water Requirements (WR) (Doorenbos and Pruitt, 1977), and created the Water Requirement Satisfaction Index (WRSI) model (Frère and Popov, 1986) to estimate crop water deficits. This framework breaks the crop season into emergence, vegetative, grain-filling, and senescing stages. The SOS begins when enough precipitation has fallen to stimulate crop growth. In this study, the SOS commences when a location receives more than 25 mm of rain in a dekad and then 20 mm of precipitation in the following two dekads (AGRHYMET, 1996). The plant begins to grow, adding biomass and leaves. As the photosynthesis increases, WR increases as well, typically plateauing during the vegetative and grain-filling stages. Then, once grain filling is complete, plants senesce, photosynthesis, and water requirements drop rapidly. These WR changes are shown with a thick red line in **Figure 1A**.

The PWB is based on the ratio of crop water supply and crop water demand, with supply and demand being based, respectively, on precipitation and RefET. To represent dekadal rainfall (P_i), this study uses 1981–2020 0.1° Climate Hazards InfraRed Precipitation with Stations[3] (CHIRPS) rainfall data (Funk et al., 2015c). CHIRPS is a widely used gridded precipitation data set that was explicitly designed for drought monitoring in food-insecure countries in Africa. One key input is the Climate Hazards Center Precipitation Climatology[4] (Funk et al., 2015b), which is constructed using moving window regressions, elevation, satellite observations and long-term in situ rain-gauge averages. At monthly and sub-monthly time scales, this climatology is combined with geostationary thermal infrared satellite observations and station data to produce gridded precipitation fields (Funk et al., 2015c). Several factors that make CHIRPS well suited to operational agro-meteorological drought monitoring are a long 40-year-plus period of record for historical context, low latency, low bias, and good performance in validation studies (Duan et al., 2016, 2019; Paredes Trejo et al., 2016; Agutu et al., 2017; Beck et al., 2017, 2019; Shrestha et al., 2017; Dinku et al., 2018; Gao et al., 2018; Retalis et al., 2018; Rivera et al., 2018; Harrison et al., 2019; Prakash, 2019; Gummadi et al., 2021). The CHIRPS product grows out of long-term efforts focused on representing orographic precipitation enhancements in data-sparse areas (Funk et al., 2003). In CHIRPS, these effects are represented by a high-resolution climatology and localized precipitation estimation parameters. This results in strong performance in east Africa's complex terrain (Dinku et al., 2018).

Dekadal RefET values ($RefET_i$) are represented by 0.1° Penman-Monteith-based RefET (Hobbins et al., 2016). [5] The RefET is calculated using MERRA-2 reanalysis data. Radiation and near-surface wind speeds, temperatures, and humidity are used to calculate the amount of evapotranspiration that would be expected if an alfalfa-like well-watered "reference" crop was grown in each grid cell. In general, increases in radiation, increases in temperature, and decreases in humidity make the atmosphere more "thirsty," increasing the associated crop water demand.

At each location, the start of the growing season (SOS) begins if a pixel receives more than 25 mm of rain, and is followed by two dekads that total more than 20 mm of

[3]https://data.chc.ucsb.edu/products/CHIRPS-2.0/.
[4]https://data.chc.ucsb.edu/products/CHPclim/.
[5]https://psl.noaa.gov/eddi/globalrefet/.

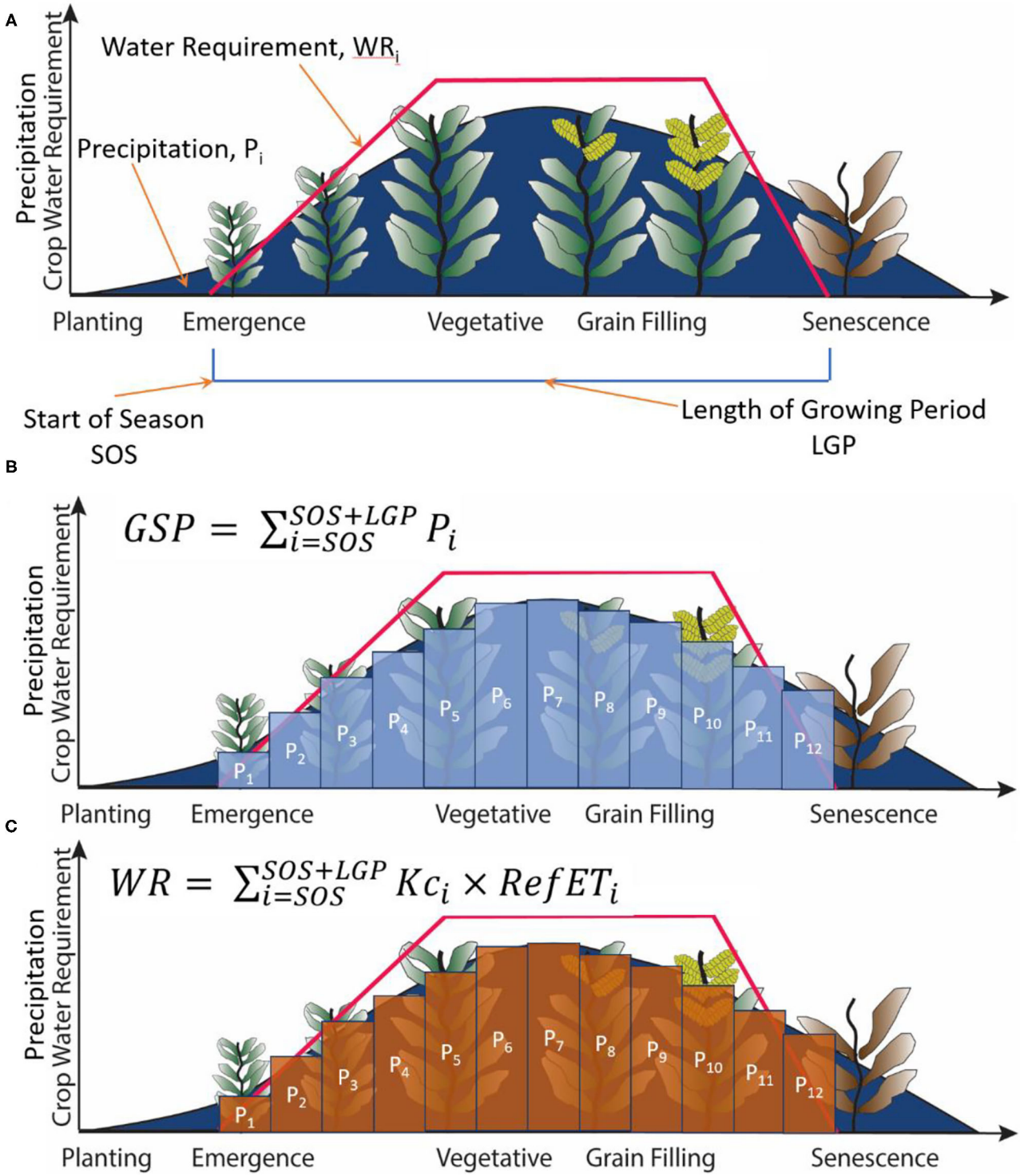

FIGURE 1 | A schematic representations of the seasonal progressions of precipitation and plant Water Requirements, **(B)** The calculation of Growing Season Precipitation, and **(C)** The calculation of seasonal Water Requirement totals.

rain combined (AGRHYMET, 1996). Time-varying crop-stage-dependent coefficients (K_c) are then used to modify RefET based on the phenological cycle of crop growth during a growing season ($WR_i = RefET_i \times K_c$).

The length of the growing period (LGP) is typically determined by the specific genotype of the specific crop, but farmers typically use longer LGP (more slowly maturing) crops when they can, since longer seasons support more photosynthesis, more production of biomass, and higher yields. More details regarding the specifications of SOS, LGP, and crop types can be found in our accompanying paper in this Frontiers collection (Funk et al., 2021).

METHODS

The core of the PWB is a comparison of the amount of water supply (precipitation) and plant water demand accumulated over the growing season, from the first dekad associated with SOS through to the end of season at a dekad corresponding to SOS+LGP. The dekadal totals of precipitation and WR are shown schematically in **Figures 1B,C**. Beginning with each location's SOS date, and assuming a fixed LGP value at each pixel, GSP values can be accumulated over each year's growing season's dekadal precipitation (P_i).

$$GSP = \sum_{i=SOS}^{SOS+LGP} P_i \tag{1}$$

GSP represents the amount of rainfall, in mm, between the beginning and end of the growing season (**Figure 1B**). GSP can be compared with WR, which estimates the total amount of growing season moisture, in mm, required by crops or fields to maintain maximum "water satisfaction." Each dekad's AET value is a function of that dekad's RefET and time-varying crop coefficients (K_c).

At the start of the season, at emergence, K_c values start low. They then increase during the vegetative and grain-filling stages. In cereal crops, Kc drops during senescence, while grassland K_c terms stay high throughout the short (7 dekad) growing season. The WR can be calculated from the beginning to the end of the growing season as follows (**Figure 1C**).

$$WR = \sum_{i=SOS}^{SOS+LGP} Kc_i \times RefET_i \tag{2}$$

The GSP and WR terms can then be combined to yield the PWB.

$$PWB = 100 \times \frac{GSP + \varepsilon}{WR + \varepsilon} \tag{3}$$

The epsilon term (10 mm in this study) is added to both the numerator and denominator to increase numerical stability in arid regions. Our companion article compares PWB with WRSI and Kenya crop yield data, exploring the utility of PWB in routine agro-meteorological monitoring and forecast settings. Here, we focus on the use of PWB as a basis for trend analyses and risk assessment.

EXAMINING THE UTILITY OF THE PWB FRAMEWORK AS A BASIS FOR EXAMINING TRENDS IN AGRO-PASTORAL HAZARDS?

Examining Changes in Mean Climate Conditions

Since the early 2000s, when the FEWS NET science team first identified the decline in the east African boreal rains (Funk et al., 2005), dozens of papers have studied the pattern, timing, and causes of these changes. While this is not the right venue for a review of that literature, we do wish to briefly show how the WR framework can provide a useful analytic foundation for exploring decadal variations in agro-pastoral hazard trends. Seasonal WR totals and PWB index values help to translate changes in precipitation into impacts on crop water availability.

There is almost universal agreement among experts that the eastern east Africa region has been substantially drier since about 1999. We contrast, therefore, changes between 1999 and 2020 and 1981–1998 (**Figure 2**). **Figure 2A** displays the well-documented declines in GSP. Central and coastal Kenya and eastern Ethiopia have seen substantial declines, which relate to 4 to 14% declines in WRSI (**Figure 2B**). Note that change shown here is in terms of the WRSI, which estimates the fraction (%) of the plant's water requirement that is satisfied. In some pastoral regions, recent rains have often failed to meet the criteria for season onset, and, therefore, we find large increases (i.e. delays) in the onset dates in these areas (**Figure 2C**). It is interesting to note that, in areas that rely on the boreal spring rains, we find little change in RefET (**Figure 2D**). While some increases are found in Sudan and South Sudan, that region tends to be associated with a boreal summer rainfall maxima. This is an important result. Warming temperatures do *not* appear to be associated with increasing WR trends, at least as represented via the Penman-Monteith calculation used in the Hobbins RefET data set. But we will return to this point momentarily, in the context of dry seasons, and reach a more nuanced, and more concerning, conclusion.

Figure 2E shows changes in PWB. While these maps closely follow the changes in precipitation, it is interesting to contrast these with the WRSI changes (panel 2B), which miss the substantial increases in western Kenya PWB values. Finally, PWB changes in terms of standardized anomalies (not shown) indicate that these declines are sufficient in magnitude to tilt the odds toward substantially more frequent droughts in central-eastern Kenya, southern Somalia, and eastern Ethiopia.

These results help demonstrate the value of WR framing. What we see is a tendency for TGP to increase in places where it is not generally needed (i.e., in wet areas) and decrease in arid regions where precipitation is desperately needed. One recent global Standardized Precipitation Evapotranspiration Index (SPEI) analysis (Funk et al., 2019a) found a robust global tendency toward higher RefET in arid regions, when SPI values were lower than −0.7. We find a similar result here. **Figure 2F** shows the difference between dry season (SPI < -0.7) WR averages over the 1999–2020 and 1981–1998 time periods. The +30 to +70 mm WR increases suggest that WR values, during

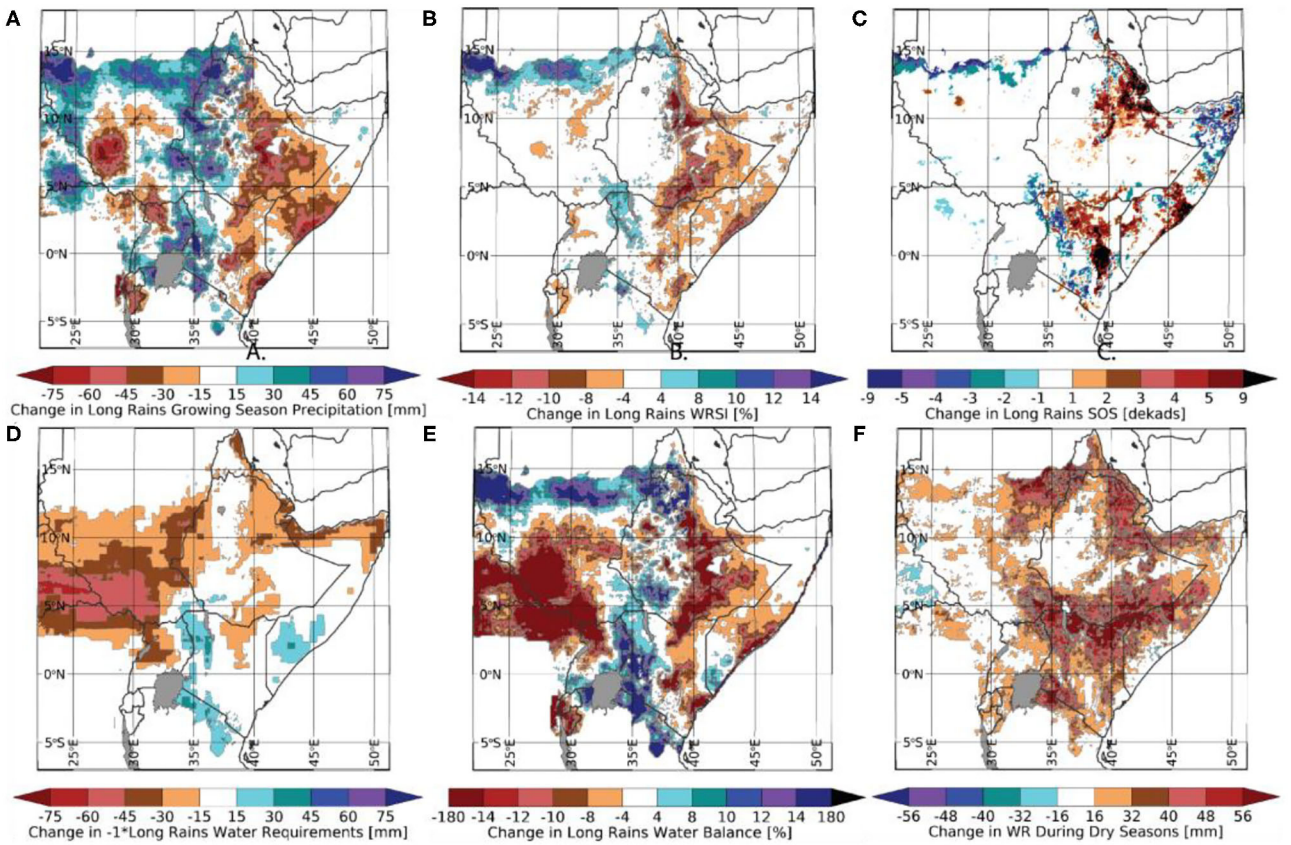

FIGURE 2 | Changes in 1999–2020 vs. 1981–1998 agro-climatic indicators. **(A)** Change in growing season precipitation. **(B)** Change in WRSI. Note that 'change in %' in this instance refers to changes in the fraction of the plant's water requirement satisfaction. **(C)** Change in Start of Season (SOS). **(D)** Change in growing season WR. Note that these WR changes have been inverted (multiplied by −1), to express the desiccating impacts of increasing WR. **(E)** Change in growing season PWB. **(F)** Change in 1999–2020 vs. 1981–1998 WR when SPI values are <-0.7.

meteorological droughts, are increasing. The spatial pattern of these increases, unfortunately, tends to align with some of the most food-insecure areas of eastern east Africa.

Examining Changes in Extreme Growing Season Precipitation

One interesting application of the PWB metric, not available with the WRSI, is to examine changes in the frequency of very wet seasons; seasons for which precipitation far exceeds WR. To demonstrate this, **Figure 3A** shows the change in frequency of the number of seasons for which GSP was more than twice the seasonal WR values. These results could suggest that the increases in PWB (**Figure 2E**), in areas that are already very wet (**Figure 3B**), might actually be detrimental. An example of this can be seen in the areas around Lake Victoria and across southwestern Ethiopia. In non-water-limited regions, increased cloudiness can reduce insolation and photosynthesis, while water logging, extreme precipitation, and flooding can have detrimental effects. In 2020, sites reporting flood impacts listed numerous crises in these regions.[6] While more detailed analyses can be carried out using hydrologic simulations from systems like the FLDAS (McNally et al., 2017), the PWB and PWB forecasts seem like a useful tool for interpreting hydrological extremes from a crop-water perspective. Simply put, above-normal rains are more likely to be detrimental when they occur in regions that have climatologically high PWB values. A map of the recent mean PWB values (**Figure 3B**) reveals quite stunning gradients. In Kenya, for example, mean PWB values exceed 200% near the shores of Lake Victoria, then drop to near 100% over the span of about 100 kilometers. The same steep gradients hold for the western highlands of Ethiopia. When rainfall increases in places that are very wet, that will increase the frequency of exceptionally wet growing seasons. Hence, increase precipitation could be associated with increased agricultural disruption.

While extreme precipitation and floods can happen anywhere, it is often very difficult to distinguish beneficial vs. hazardous above-normal rainfall amounts in arid regions. A reference to drought monitoring can help make this case. An experienced agricultural drought analyst will pay special attention to rainfall deficits in more marginal crop-growing regions. A 75 mm rainfall deficit (**Figure 2A**) will be much more impactful in regions with mean PWB values of <100 (**Figure 3A**). Conversely,

[6]http://floodlist.com/africa/.

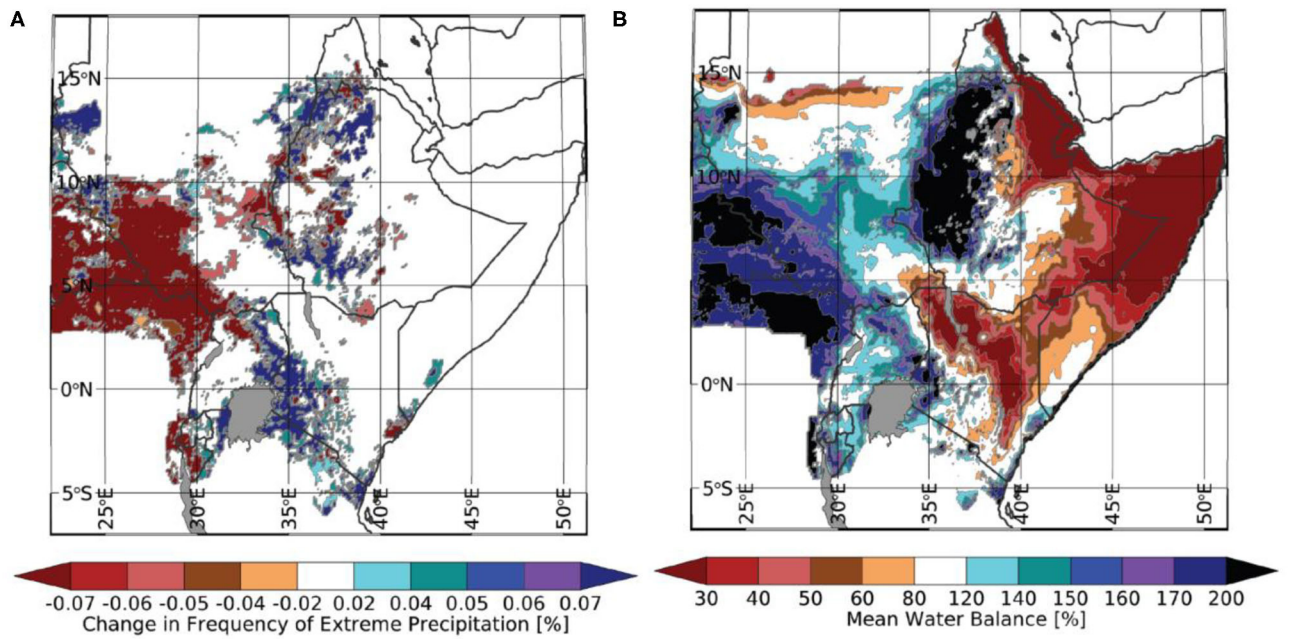

FIGURE 3 | (A) Change in the frequency of extreme PWB values (PWB > 200%). **(B)** Mean 1999–2020 east African boreal spring season PWB values.

exceptionally heavy rains are much less likely to be beneficial when they occur in a region in which precipitation almost always exceeds WR by a wide margin. Such considerations might be used to identify more probable risk areas in forecasts and observations.

Examining Long Time-Series of PWB Estimates

While the PWB and WRSI changes are quite similar, the simplicity of the PWB framework makes it easy to link with longer precipitation records, such as the Centennial Trends archive (Funk et al., 2015a), which are almost exclusively monthly. There are very few long-period-of-record sub-monthly rainfall archives in Africa. The Centennial Trends and CHIRPS data sets are built using the same high-resolution climatology and the same stations, and hence, tend to be quite similar on regional/seasonal time-scales. We can use the Centennial Trends data set to place recent PWB variations in a deeper historic context. We do so for two regions: Kenya's main crop growing regions[7] and "eastern east Africa," which is defined as Ethiopia, Kenya, and Somalia east and south of 38°E, 8°N. Strong linear relationships exist between regional March-April-May Centennial Trends and CHIRPS GSP, and CHIRPS GSP and WR. Hence, Centennial Trends PWB estimates that correlate well with the CHIRPS/Hobbins RefET values during their period of overlap can be constructed (R_{Kenya} =0.9, R_{EEA} =0.89). This allows us to plausibly extend the PWB back to the early 1900s (**Figure 4**). As discussed in our Centennial Trends paper, Kenya actually has quite a few stations during this time period. The eastern east Africa region has lower station densities, especially prior to the 1920s.

For Kenya (**Figure 4A**), we see juxtaposed both a tendency toward drier conditions and two exceptionally wet seasons (2018 and 2020). A deeper historical record reinforces how extremely wet 2018 and 2020 actually were. This deeper record, however, also suggests that recent (post-2009) droughts, like 2011, 2017, and 2019, really were not too severe, given the historical archive. These dry seasons had PWB values of around 110 percent. The historical archive has many examples of more severe droughts with PWB values on the order of 90 percent.

For eastern east Africa (**Figure 4B**), we find a much higher level of aridity, with a 1920-to-1989 Centennial Trends PWB mean of 59, which decreased to 52 over the 1999–2014 period—a 15% decrease. Between 1999 and 2020, 8 years were exceptionally dry (PWB < 46). The depth of drought during these dry seasons has also intensified as WR values increase (**Figure 2F**), resulting in frequent shocks that can erode resilience and increase vulnerability. These dry seasons can be contrasted with four very wet seasons (2010, 2013, 2018, 2020), with PWB values twice as large as dry seasons, i.e., 80 as opposed to 40. The skewed distribution of rain in this region, combined with the covariance of RefET and precipitation, sets the stage for volatile sequences of droughts and pluvials. As with Kenya, we note that the most recent dry seasons (2017, 2019) have not been as intense as prior severe droughts such as 1999, 2000, 2009, and 2011, which were associated with moderate-to-strong La Niña conditions. Disaster mitigation strategies, such as the Sendai Framework for Disaster Risk Reduction (SFDRR), emphasize the need to address underlying causes of disaster risk. Long time-series of historical

[7]The counties of Baringo, Elgeyo-Marakwet, Kajiado, Kiambu, Kirinyaga, Kwale, Laikipia, Lamu, Murang'a, Nakuru, Narok, Nyandarua, Nyeri, Taita Taveta, Tana River, Trans Nzoia, Uasin Gishu, Kilifi.

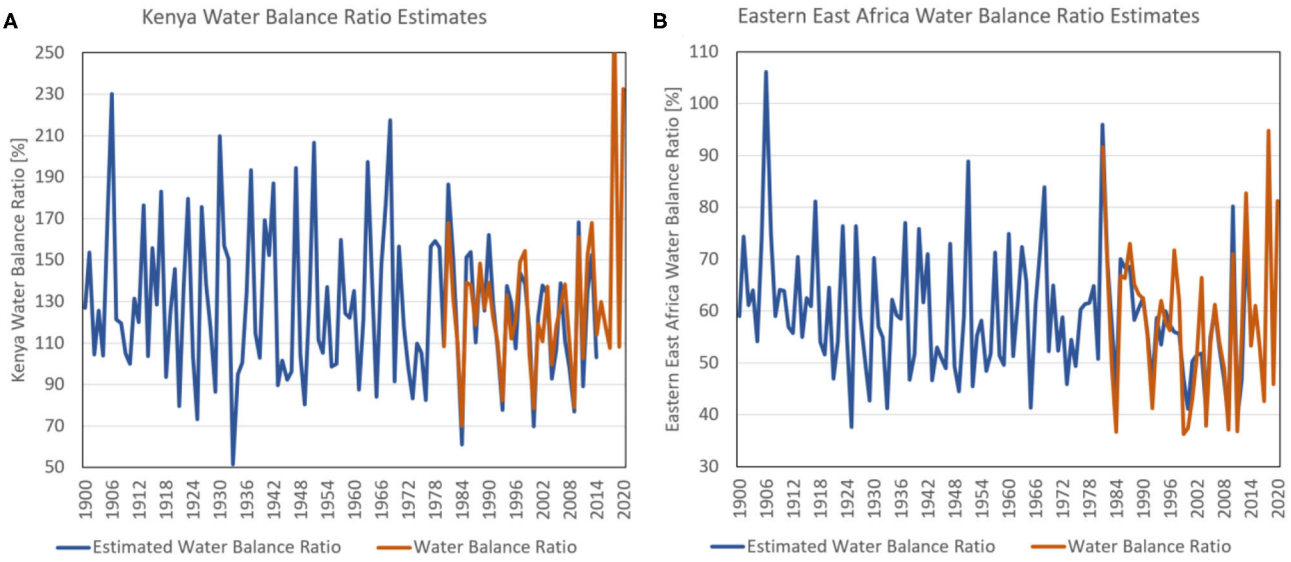

FIGURE 4 | Long time-series of **(A)** Kenyan and **(B)** Eastern east Africa PWB time-series.

PWB values (**Figure 4**) help inform drought management plans by helping us anticipate the magnitude of a "typical" drought sequence. What **Figure 4** tells us is that a) there have been many recent droughts—three out of the last five seasons (2017, 2019, and 2021[8])— but the actual magnitude of those droughts has been moderate in comparison to the longer-term record. DRR practices use past extremes as inputs into future disaster management plans. Hence, we should prepare for substantially more severe future droughts akin to 1999, 2000, 2009, and 2011.

EXAMINING THE UTILITY OF THE PWB FRAMEWORK AS A BASIS FOR ASSESSING 1-IN-10 AND 1-IN-25-YEAR CROP PRODUCTION DROUGHT RISKS

We next turn to the topic of disaster risk management, combining our PWB and Centennial Trends analyses with population and agricultural statistics to construct plausible near-term, low-yield scenarios. The intent is to demonstrate how the PWB can be used to inform national drought risk management planning, such as that advocated by the Sendai Framework for Disaster Risk Reduction and the United Nations Office for Disaster Risk Reduction.[9] The first priority of the Sendai Framework focuses on understanding risk. Agro-pastoral hydro-climatic risks arise through the interaction of exposure, vulnerability, and weather-related shocks. Here, we develop plausible 1-in-10 and 1-in-25-year Kenyan yield reduction scenarios. There are numerous actions that countries can take to prepare for agricultural shocks: store grain to offset crop production deficits, establish cash reserves that can be used to help smooth out grain price shocks, and fund social safety net programs that can help poor households cope with reductions in food availability and access. But investments in these risk reduction activities diverts funds from other potentially important sectors: health, education, transportation, etc. It is important, therefore, to provide quantitative assessment of drought risk. The 1-in-10 and 1-in-25-year Kenyan yield reduction scenarios explored here provide plausible scenarios that can be used to develop risk management planning.

As context, it is important to recognize that despite rapidly growing economies, countries like Kenya and Ethiopia still face serious levels of acute food insecurity. A growing wage gap may be one factor that helps drive such insecurity. While the annual per capita inflation-adjusted incomes of the poorest 20% of Ethiopians and Kenyans climbed dramatically between 1993 and 2019 (**Figure 5A**), the gap between these incomes and the national average income climbed even more rapidly (**Figure 5B**), such that the ratio between poor and middle incomes essentially tripled between 1993 and 2018. Poor households have to compete with the rest of society for access to goods and services. And countries like Kenya continue to see high food-price volatility. **Figure 5C** shows wholesale maize prices in Kenya. In 2008/09, 2011, and 2017, the region experienced sequential October-November-December and March-April-May droughts (Funk et al., 2018), and large spikes in maize prices.

One concerning result discussed above is the fact that the 2011 and 2017 Kenyan drought events were not actually all that extreme, based on the historical record (**Figure 4A**). Nevertheless, maize prices skyrocketed (**Figure 5C**). While a huge variety of factors influence prices, some insights can be gained from evaluating per capita maize cereal production. This metric can be composed into a yield term and per capita harvested area term (Funk and Brown, 2009). For

[8]https://fews.net/east-africa/alert/may-19-2021.
[9]https://www.undrr.org/implementing-sendai-framework/what-sendai-framework.

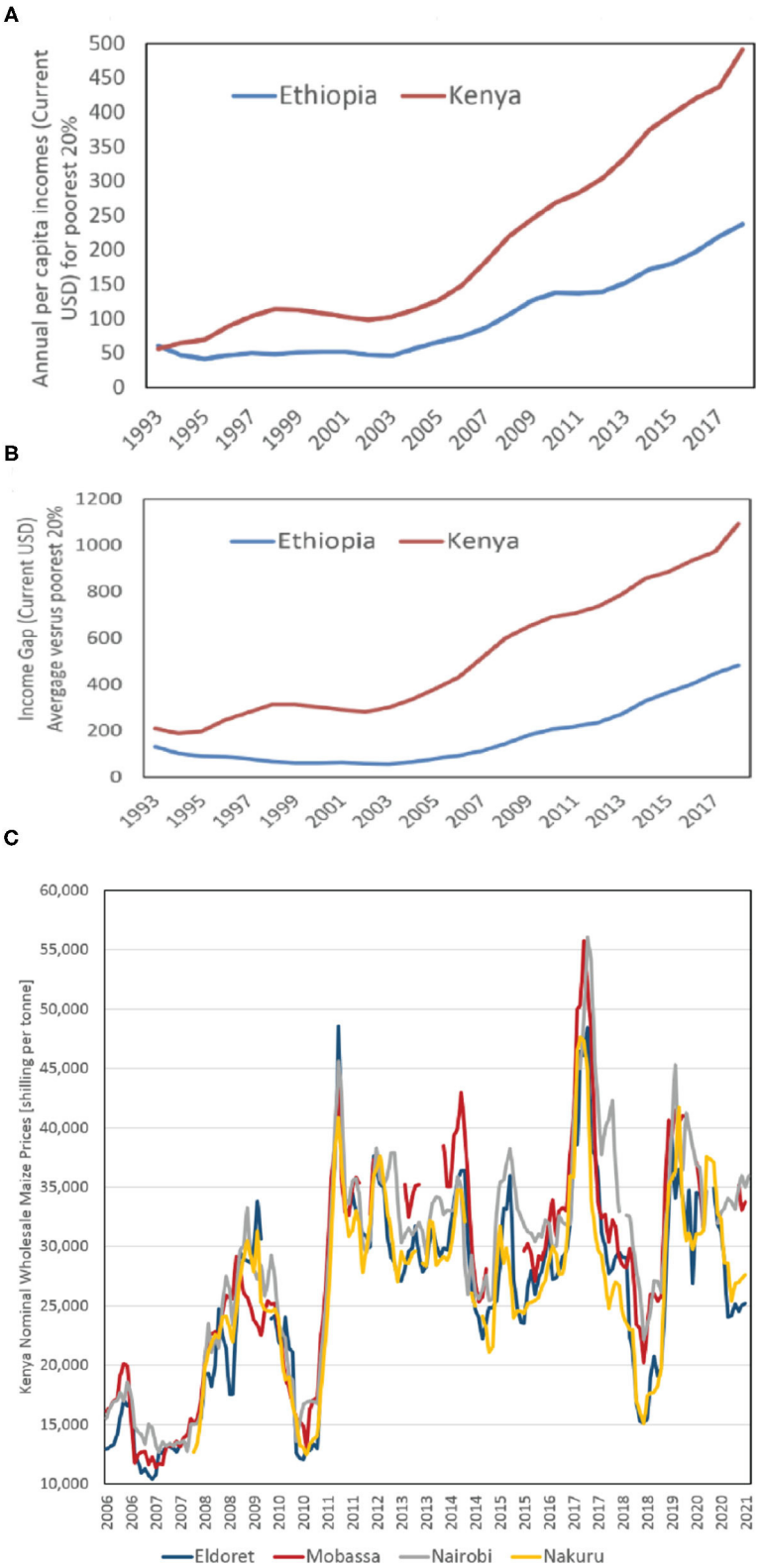

FIGURE 5 | (A) World Bank estimates of per capita income for the poorest 20% of Ethiopians and Kenyans. **(B)** The gap between the per capita incomes of average and poor Ethiopians and Kenyans. **(C)** Monthly nominal wholesale maize prices in Kenya. Price data obtained from the FAO price monitoring tool.

many countries, this decomposition tends to highlight opposing tendencies, with yields increasing and per capita harvested areas declining. For Kenya, however, maize yield statistics suggest stagnation around a fairly low baseline of about 1.7 tons per hectare (ha) (**Figure 6A**). Kenya has primarily relied on increases in cultivated area to increase production, with the area harvest increasing by about 70% since the early 1980s (**Figure 6B**). Since 2009, however, the rate of this increase appears to have slowed.

Combining maize harvested area statistics and projections with UN's population statistics and projections (**Figure 6C**) reveals declining per capita-harvested area. Since the 1960s, this value has fallen precipitously, and in 2019, per capita-harvested area was very low—just 0.042 ha person^{-1}. Expectations for the future trends are difficult to bracket, given the changing behavior in harvested area trends, which grew rapidly in the 2000s and then stagnated in the 2010s. Hence, the 2000–2019 downward trend in per capita HA is much smaller than the 2010–2019 trend (0.002 ha person^{-1} year^{-1} vs. −0.008 ha person^{-1} year^{-1}). In panel 6C, we have picked a value halfway between these trends to project out through 2050. This moderate assumption leads to a concerning 14% reduction between 2030 and 2019.

We can use this projection, along with yield assumptions, to generate per capita cereal projections (**Figure 6D**). For the average yield scenario, we have used the 2000–2019 FAOSTAT mean (1.71 tons ha^{-1}). The 1-in-10 and 1-in-25-year yield assumptions are largely guided by an analysis of long records of PWB time-series. There are 40 years of CHIRPS-driven PWB estimates, and in that record, 4 years stand out as substantially drier than the rest (1984, 1993, 2000, and 2008) (**Figure 4A**). Using the average yield of these four seasons (1.43 tons ha^{-1}) as a 1-in-10-year low yield value seems plausible. This value also matches closely with the 10th percentile value of the 1982–2019 FAOSTAT yields. Yields of 1.43 tons ha^{-1} would be associated with a ∼16% reduction in national yields. Kenya's relatively low variability seems realistic, given that many of the most productive crop-growing regions are in highland areas with high mean PWB values (**Figure 3B**). While vigorously defending any 1-in-25-year assumption is challenging, given substantial non-stationarity in both society and climate, we might select the low-2009 yield value (1.3 tons ha^{-1}) as a realistic worst-case scenario. This would correspond with a 24% reduction in yields.

When examining changes in per capita crop production (**Figure 6D**), it is important to recognize that the 10-year trend in per capita harvested area effect (∼14%) is on par with the 1-in-10-year yield shock (16%). This may help explain why many recent Kenyan food crises (2011, 2017, 2019) were induced by moderate, not extreme, drought and yield shocks. When the next 1-in-10-year drought comes, a drought event similar to 1984, 2000, or 2009, increases in population and slowing agricultural expansion will interact with, and likely amplify, the impact of water deficit-induced yield reductions. By 2028, for example, average per capita production may resemble the low value from the 2017 drought year (∼64 kg maize person^{-1}). A severe (1-in-10-year) drought in 2028 could result in per capita maize production of just 53 kg maize person^{-1}(**Figure 6D**), a value much lower than the 2009 value of ∼64 kg maize person^{-1}. It is very likely, therefore, that trends in population and harvested area, combined with typical year-to-year rainfall and RefET variability, will produce an unprecedented national-level food shock in the near future.

DISCUSSION

Our results emphasize that many climatologically dry areas in eastern east Africa (**Figure 3B**) have become drier (**Figures 2A,B,E**). For dry areas in the east, recent low-rainfall seasons have also been accompanied by larger positive WR anomalies (**Figure 2F**); WR acts to amplify precipitation deficits in eastern east Africa. While we did not find an upward tendency in most of east Africa (**Figure 2D**), we did find modest WR increases during low-rainfall seasons (**Figure 2F**).

Looking at longer time-series of PWB estimates (**Figure 4**), it is interesting to note that recent drought years like 2017 and 2019 were not actually as bad as the strong La Niña-related droughts in 2000, 2009, and 2011. It is not clear whether this represents a shift in the mean or a stochastic outcome. Perhaps recent combinations of large-scale forcing and random weather fluctuations have not combined to produce a really strong drought. When such a drought occurs, it will likely be exacerbated by WR increases (**Figure 2F**) and decreasing per capita-harvested areas (**Figure 6D**). Such an outcome would obviously be concerning, given the serious food-security concerns associated with 2017 and 2019 rainfall deficits.

The PWB analyses presented here also provides valuable insights into extreme seasonal precipitation outcomes. In general, we find a "wet-getting-wetter" and "dry-getting-drier" tendency—in climatologically humid regions in western Ethiopia and Kenya (**Figure 3B**), we find >14% increases in PWB (**Figure 2E**), which are also associated with an increased frequency of excessively wet rainy seasons (**Figure 3A**). Unlike the WRSI, the PWB lets us identify and explore "excessive" rainfall. The extreme Kenyan PWB values and increased frequencies of extreme PWB events found near Lake Victoria and in southwestern Ethiopia are quite concerning. To date, much more attention has been focused on the agricultural impacts of droughts. Relatively little work has focused on the potentially negative impacts of extreme growing season precipitation and associated reductions in radiation and RefET. Upward rainfall trends in areas with high climatological PWD are unlikely to improve crop production. This limit can also have a seasonal interpretation. In 2018 and 2020, we found extensive areas with PWB values of more than 200%. Even in an arid region, this "extra" water will be unlikely to enhance agricultural outcomes.

In both humid and arid regions, and wet and dry seasons, the complementary relationship between AET and RefET (Hobbins et al., 2016) provides a useful way to contextualize rainfall extremes and changes. **Figure 7** shows a schematic describing the complementary hypothesis. We have used "WR" in place of RefET to emphasize the phenological filtering associated with the time-varying KC coefficients.

In wet regions and seasons, where TGP > WR, AET is energy limited. Cloudiness and cool air temperatures will tend to reduce RefET, which acts as a cap on AET, and ultimately,

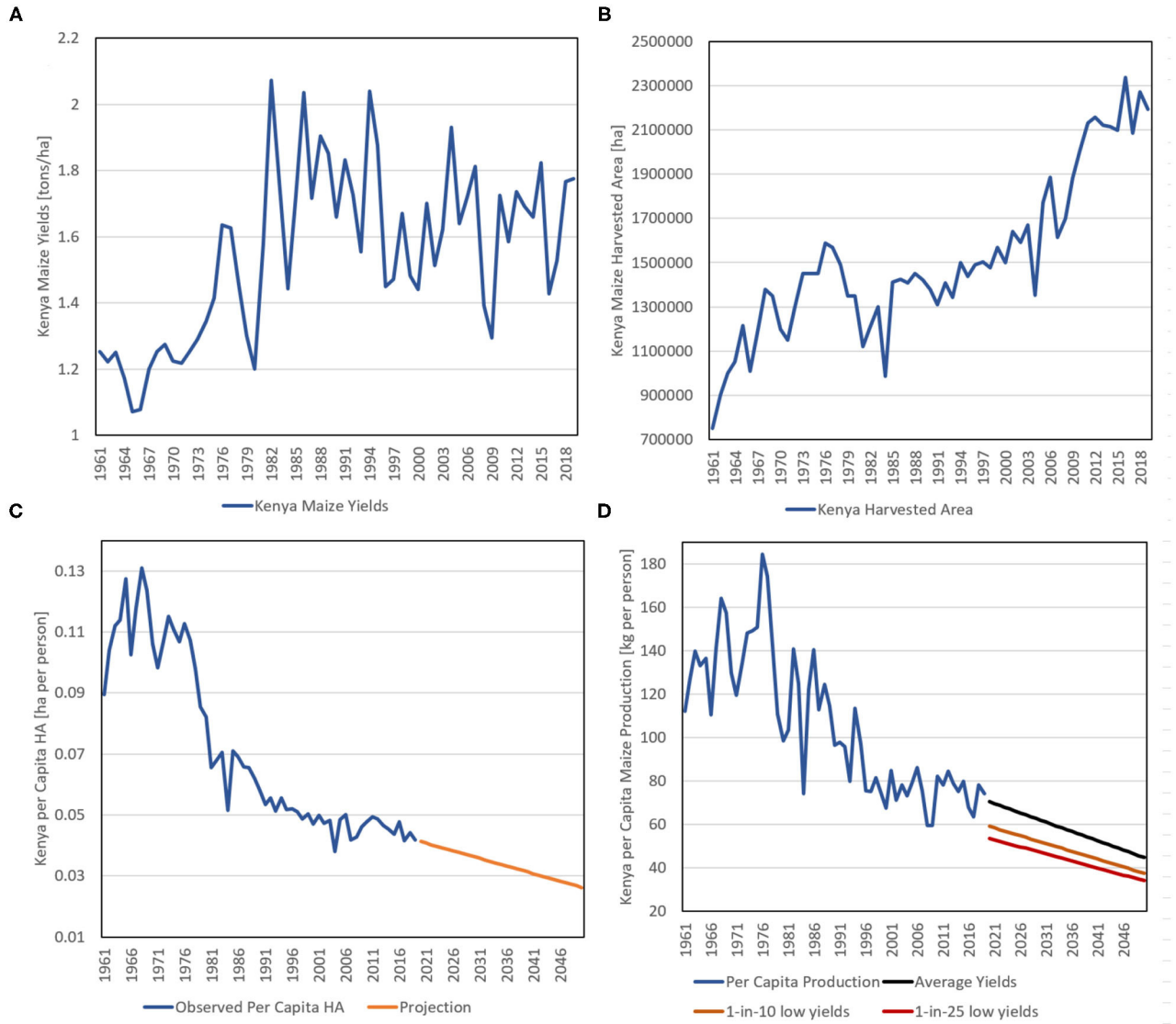

FIGURE 6 | (A) FAOSTAT Kenyan maize yields. **(B)** FAOSTAT maize harvested area. **(C)** Observed and projected per capita harvested area, based on an assumed decline of−0.0002 hectare per person per year for 2020 to 2050. **(D)** Observed and projected per capita maize production. Projections based on recent observed yield values, and 1-in-10 year and 1-in-25-year drought year estimate (1.71, 1.43, and 1.3 tons ha^{-1}).

photosynthesis. Furthermore, since a coarse approximation of the local water balance can be written as runoff = GSP – WR, when GSP is much greater than WR, runoff can increase dramatically, helping to set the stage for floods.

In dry regions and seasons, where TGP < WR, AET is water limited. Under such conditions, the PWB and WRSI are likely to perform similarly. Furthermore, as aridity increases, AET and WR are expected to be complementary, with WR increasing as AET decreases (**Figure 7**). Extraction and analysis of the WR component has really emphasized this relationship, as many of the driest regions and seasons exhibit the largest anomalous WR increases during below-normal rainfall seasons. In these regions and seasons, the PWB, WRSI, or hydrologic modeling systems like FLDAS are likely to perform better than simple rainfall observations, because they can capture WR/precipitation covariations in very dry regions.

The Bouchet-Morton complementary relationship (Hobbins et al., 2016) helps us understand the spatial and temporal covariations of RefET and precipitation. These covariations amplify the impacts of rainfall deficits in dry areas, as well as the impact of rainfall excesses in wet areas. Ironically, east Africa may be experiencing more crop water deficits in dry areas and more extreme growing season rainfall in some very wet areas.

In the literature discussing climate change and precipitation extremes, it is common to discuss dynamic and thermodynamic drivers (Emori and Brown, 2005). Thermodynamic controls

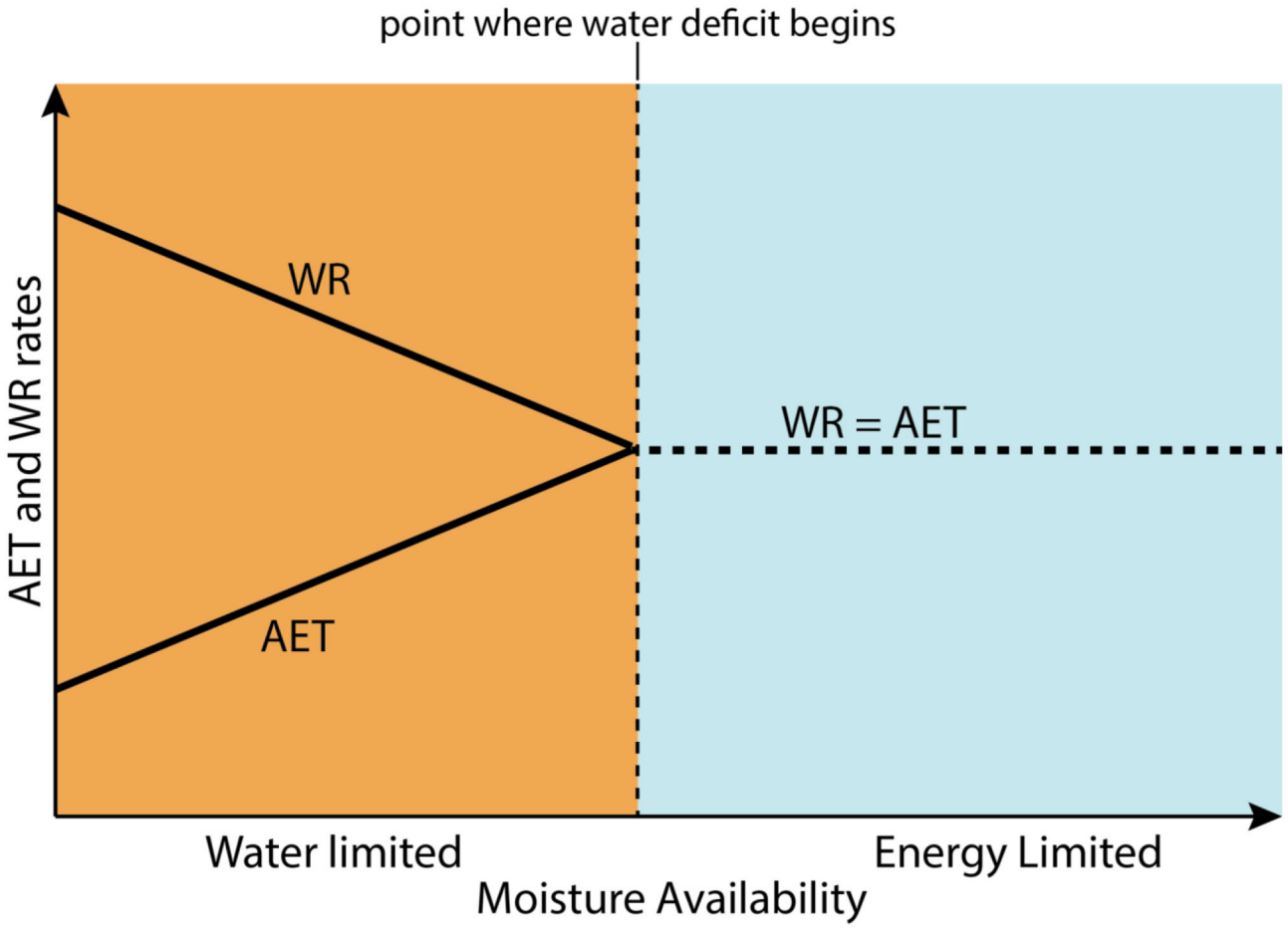

FIGURE 7 | A schematic diagram of the Bouchet-Morton complementary relationship.

relate to warming in the atmosphere, and the expectation that atmospheric saturation vapor pressure will increase with increasing temperatures at approximately 7% per degree Celsius of warming. Ironically, these increases can both increase the frequency and magnitude of extreme precipitation events (**Figure 3A**), while also exacerbating the intensity of droughts, especially in dry areas (**Figure 2F**).

Theoretically, at global scales, climate scientists expect mean precipitation to remain fairly stable, while extreme precipitation increases (Trenberth et al., 2003; Allan and Soden, 2008). Mean precipitation is fundamentally constrained by an energy balance that involves radiation, condensation/diabatic heating, and surface and latent heat fluxes. Because radiation changes are quite small, overall, changes in mean precipitation—both in models and observations—are quite small. This constraint does not hold at small and short spatial and temporal scales, scales in which experts expect both dynamic and thermodynamic exacerbation of extremes (Emori and Brown, 2005). Stable means and more extremes imply that the frequency of dry days would increase.

Globally (Donat et al., 2016), there is substantial evidence that extreme precipitation is becoming more frequent. In areas of sub-Saharan Africa with quality daily precipitation data, robust trends over 1950–2013 indicate that extreme events have become wetter, but that annual totals have decreased due to fewer rain days (Harrison et al., 2019). While this study has only examined seasonal totals, further analyses of sub-seasonal precipitation and temperature statistics, such as consecutive dry days and growing degree days, would be informative. For example, one recent study (Laudien et al., 2020) found that monitoring consecutive dry days was the best overall predictor for Tanzanian yields. Using the WR phenological framework, multiple statistics, arising from a host of potential data sources, could be examined during the vegetative and grain-filling stages. Compositing multiple crop scenarios, such as the combination of maize and grasslands analyzed here, seems useful from a decision analytics perspective.

In Kenya and Ethiopia, these highlands are densely populated. So, the increases in the frequency of extreme wet season precipitation (**Figure 3A**) are occurring in areas with millions of people. East of ∼38°E, densely populated highland areas in Kenya and Ethiopia are much more drought prone, and in these

regions, we find substantial increases in water stress (**Figure 2E**). Below and between the highlands, sparsely populated but very food-insecure pastoralists in eastern east Africa are seeing more frequent water deficits being exacerbated by increasing WR demands (**Figure 2F**).

Our deeper dive into Kenya crop conditions and per capita cereal production suggests that persistence of the current trends—stagnant yields and rapidly growing population—will likely lead, very soon, to unprecedented low levels of per capita cereal production. Intensification of agriculture through the adoption of improved seeds and fertilizer can help improve yields (Davenport et al., 2018). In addition, the results presented here point toward adaptation strategies that manage climate (**Figure 4**) and price volatility (**Figure 5C**). Kenyan climate is strongly impacted by the Indian Ocean Dipole and the El Niño Southern Oscillation, and climate projections anticipate that these drivers will become more extreme (Cai et al., 2013, 2015a,b).

In addition to planning for future food production shocks (**Figure 6D**), the results presented here provide hopeful evidence supporting improved water management as a path toward increased resilience and more stable agricultural production. In arid regions, well-maintained boreholes can provide access to water during droughts (Thomas et al., 2019), and "*drought emergencies can be mitigated by investing in resilience efforts that make safe water reliably available at strategic groundwater abstraction locations during cycles of water stress*" (Thomas et al., 2020). In humid areas, improved water storage and expanded irrigation could reduce risks during extremely wet seasons and provide supplemental water during dry seasons.

In closing, we note that, while this study has focused on an important season in an important food-insecure region, the general methods employed here could be expanded to multiple growing seasons and regions. This could then be used to further explore global increases in dryland RefET during drought (Funk et al., 2019a), as results similar to **Figure 2F** are explored across larger domains. Similarly, excessive precipitation amounts, as evaluated in **Figure 3A**, could be examined globally.

DATA AVAILABILITY STATEMENT

The original contributions generated for the study are included in the article/supplementary materials, further inquiries can be directed to the corresponding author/s.

AUTHOR CONTRIBUTIONS

All authors listed have made a substantial, direct and intellectual contribution to the work, and approved it for publication.

FUNDING

Primary support for this work came from the National Aeronautics and Space Administration (NASA) GPM mission grant #80NSSC19K0686 and the United States Agency for International Development (USAID) cooperative agreement #72DFFP19CA00001 and the Famine Early Warning Systems Network.

REFERENCES

AGRHYMET (1996). *Méthodologie de suivi des zones à risque*. Niamey: AGRHYMET FLASH, Bulletin de Suivi de la Campagne Agricole au Sahel, Centre Regional AGRHYMET.

Agutu, N., Awange, J., Zerihun, A., Ndehedehe, C., Kuhn, M., and Fukuda, Y. (2017). Assessing multi-satellite remote sensing, reanalysis, and land surface models' products in characterizing agricultural drought in East Africa. *Remote Sens. Environ.* 194, 287–302. doi: 10.1016/j.rse.2017.03.041

Allan, R. P., and Soden, B. J. (2008). Atmospheric warming and the amplification of precipitation extremes. *Science* 321, 1481–1484. doi: 10.1126/science.1160787

Beck, H. E., Pan, M., Roy, T., Weedon, G. P., Pappenberger, F., Van Dijk, A. I., et al. (2019). Daily evaluation of 26 precipitation datasets using Stage-IV gauge-radar data for the CONUS*Hydrology*. *Earth Syst. Sci.* 23, 207–224. doi: 10.5194/hess-23-207-2019

Beck, H. E., Vergopolan, N., Pan, M., Levizzani, V., Van Dijk, A. I., Weedon, G. P., et al. (2017). Global-scale evaluation of 22 precipitation datasets using gauge observations and hydrological modeling. *Hydrol. Earth Syst. Sci.* 21, 6201–6217. doi: 10.5194/hess-21-6201-2017

Cai, W., Santoso, A., Wang, G., Yeh, S. W., An, S. I., Cobb, K. M., et al. (2015a). ENSO and greenhouse warming. *Nat. Clim. Chang.* 5, 849–859. doi: 10.1038/nclimate2743

Cai, W., Wang, G., Santoso, A., McPhaden, M. J., Wu, L., Jin, F. F., et al. (2015b). Increased frequency of extreme La Niña events under greenhouse warming. *Nat. Clim. Chang.* 5, 132–137. doi: 10.1038/nclimate2492

Cai, W., Zheng, X. T., Weller, E., Collins, M., Cowan, T., Lengaigne, M., et al. (2013). Projected response of the Indian Ocean Dipole to greenhouse warming. *Nat. Geosci.* 6, 999–1007. doi: 10.1038/ngeo2009

Davenport, F., Funk, C., and Galu, G. (2018). How will East African maize yields respond to climate change and can agricultural development mitigate this response? *Clim. Change* 147, 491–506. doi: 10.1007/s10584-018-2149-7

Dinku, T., Funk, C., Peterson, P., Maidment, R., Tadesse, T., Gadain, H., et al. (2018). Validation of the CHIRPS satellite rainfall estimates over eastern of Africa. *Q. J. R. Meteorol. Soc.* 144, 292–312. doi: 10.1002/qj.3244

Donat, M. G., Lowry, A. L., Alexander, L. V., O'Gorman, P. A., and Maher, N. (2016). More extreme precipitation in the world's dry and wet regions. *Nat. Clim. Chang.* 6:508. doi: 10.1038/nclimate2941

Doorenbos, J., and Pruitt, W. O. (1977). *Crop Water Requirements. FAO Irrigation and Drainage Paper 24, Land and Water Development Division*. Rome: FAO.

Duan, Z., Liu, J., Tuo, Y., Chiogna, G., and Disse, M. (2016). Evaluation of eight high spatial resolution gridded precipitation products in Adige Basin (Italy) at multiple temporal and spatial scales. *Sci. Total Environ.* 573, 1536–1553. doi: 10.1016/j.scitotenv.2016.08.213

Duan, Z., Tuo, Y., Liu, J., Gao, H., Song, X., Zhang, Z., et al. (2019). Hydrological evaluation of open-access precipitation and air temperature datasets using SWAT in a poorly gauged basin in Ethiopia. *J. Hydrol.* 569, 612–626. doi: 10.1016/j.jhydrol.2018.12.026

Emori, S., and Brown, S. (2005). Dynamic and thermodynamic changes in mean and extreme precipitation under changed climate. *Geophys. Res. Lett.* 32:272. doi: 10.1029/2005GL023272

Frère, M., and Popov, G. (1986). *Early Agrometeorological Crop Yield Forecasting, The Food and Agriculture Organization of the United Nations*. Rome.

Funk, C., Dettinger, M. D., Michaelsen, J. C., Verdin, J. P., Brown, M. E., Barlow, M., et al. (2008). Warming of the Indian Ocean threatens eastern and southern African food security but could be mitigated by agricultural development. *Proc. Nat. Acad. Sci. USA* 105, 11081–11086. doi: 10.1073/pnas.0708196105

Funk, C., Harrison, L., Alexander, L., Peterson, P., Behrangi, A., and Husak, G. (2019a). Exploring trends in wet-season precipitation and drought indices in wet, humid and dry regions. *Environ. Res. Lett.* 14:115002. doi: 10.1088/1748-9326/ab4a6c

Funk, C., Harrison, L., Shukla, S., Pomposi, C., Galu, G., Korecha, D., et al. (2018). Examining the role of unusually warm Indo-Pacific sea surface temperatures in recent African droughts *Quart. J. Roy. Meteor. Soc.* 144, 360–383. doi: 10.1002/qj.3266

Funk, C., Hoell, A., Shukla, S., Blad,é I., Liebmann, B., Roberts, J. B., et al. (2014). Predicting East African spring droughts using Pacific and Indian Ocean sea surface temperature indices. *Hydrol. Earth Syst. Sci. Discuss.* 11, 3111–3136. doi: 10.5194/hessd-11-3111-2014

Funk, C., Michaelsen, J., Verdin, J., Artan, G., Husak, G., Senay, G., et al. (2003). The collaborative historical African rainfall model: description and evaluation. *Int. J. Climatol. J. Roy. Meteorol. Soc.* 23, 47–66. doi: 10.1002/joc.866

Funk, C., Nicholson, S. E., Landsfeld, M., Klotter, D., Peterson, P., and Harrison, L. (2015a). The centennial trends greater horn of Africa precipitation dataset. *Scien. Data* 2:50. doi: 10.1038/sdata.2015.50

Funk, C., Pedreros, D., Nicholson, S., Hoell, A., Korecha, D., Galu, G., et al. (2019b). Examining the potential contributions of extreme 'Western V' sea surface temperatures to the March-June East African Drought. *Bull. Amer. Meteor. Soc.* 100, S55–S60. doi: 10.1175/BAMS-D-18-0108.1

Funk, C., Peterson P., Landsfeld, M., Pedreros, D., Verdin, J., Shukla, S., et al. (2015c). The climate hazards infrared precipitation with stations—a new environmental record for monitoring extremes. *Scien. Data* 2:66. doi: 10.1038/sdata.2015.66

Funk, C., Senay, G., Asfaw, A., Verdin, J., Rowland, J., Michaelson, J., et al. (2005). Recent drought tendencies in Ethiopia and equatorial-subtropical eastern Africa. *Vulnerability to Food Insecurity: Factor Identification and Characterization Report, NET F, Ed., US Agency for International Development*, 12.

Funk, C., Turner, W., McNally, A., Hoell, A., Harrison, L., Galu, G., et al. (2021). An agro-pastoral phenological water balance framework for monitoring and prediction of growing season water deficits. *Front. Clim.* 10, 1–10. doi: 10.3389/fclim.2021.716568

Funk, C., Verdin, A., Michaelsen, J., Peterson, P., Pedreros, D., and Husak, G. (2015b). A global satellite assisted precipitation climatology. *Earth Syst. Sci. Data Discuss.* 7, 1–13. doi: 10.5194/essdd-8-401-2015

Funk, C. C., and Brown, M. E. (2009). Declining global per capita agricultural production and warming oceans threaten food security. *Food Sec.* 1, 271–289. doi: 10.1007/s12571-009-0026-y

Gao, F., Zhang, Y., Chen, Q., Wang, P., Yang, H., Yao, Y., et al. (2018). Comparison of two long-term and high-resolution satellite precipitation datasets in Xinjiang, China. *Atmosph. Res.* 212, 150–157. doi: 10.1016/j.atmosres.2018.05.016

Gebrechorkos, S. H., Hülsmann, S., and Bernhofer, C. (2019). Long-term trends in rainfall and temperature using high-resolution climate datasets in East Africa. *Sci. Rep.* 9, 1–9. doi: 10.1038/s41598-019-47933-8

Gummadi, S., Dinku, T., Shirsath, P. B., and Kadiyala, D. M. (2021). *Spatial and temporal evaluation of satellite rainfall estimates over Vietnam*.

Harrison, L., Funk, C., and Peterson, P. (2019). Identifying changing precipitation extremes in Sub-Saharan Africa with gauge and satellite products. *Environ. Res. Lett.* 14:085007. doi: 10.1088/1748-9326/ab2cae

Hobbins, M. T., Wood, A., McEvoy, D. J., Huntington, J. L., Morton, C., Anderson, M., et al. (2016). The evaporative demand drought index. Part I: Linking drought evolution to variations in evaporative demand. *J. Hydrometeorol.* 17, 1745–1761. doi: 10.1175/JHM-D-15-0121.1

Hoell, A., and Funk, C. (2013a). Indo-Pacific sea surface temperature influences on failed consecutive rainy seasons over eastern Africa. *Clim.Dynam.* 43, 1645–1660. doi: 10.1007/s00382-013-1991-6

Hoell, A., and Funk, C. (2013b). The ENSO-Related West Pacific sea surface temperature gradient. *J. Clim.* 26, 9545–9562. doi: 10.1175/JCLI-D-12-00344.1

Laudien, R., Schauberger, B., Makowski, D., and Gornott, C. (2020). Robustly forecasting maize yields in Tanzania based on climatic predictors. *Sci. Rep.* 10, 1–12. doi: 10.1038/s41598-020-76315-8

Liebmann, B., Hoerling, M. P., Funk, C., Bladé, I., Dole, R. M., Allured, D., and Eischeid, J. K. (2014). Understanding recent eastern horn of africa rainfall variability and change. *Climate J.* 27, 8630–8645. doi: 10.1175/JCLI-D-13-00714.1

Lyon, B. (2014). Seasonal drought in the greater horn of Africa and its recent increase during the march-may long rains. *J. Clim.* 27, 7953–7975. doi: 10.1175/JCLI-D-13-00459.1

Lyon, B., and DeWitt, D. G. (2012). A recent and abrupt decline in the East African long rains. *Geophys. Res. Lett.* 39:337. doi: 10.1029/2011GL050337

McNally, A., Arsenault, K., Kumar, S., Shukla, S., Peterson, P., Wang, S., et al. (2017). A land data assimilation system for sub-Saharan Africa food and water security applications. *Scien. data.* 4:170012. doi: 10.1038/sdata.2017.12

Paredes Trejo, F. J., Alves Barbosa, H., Peñaloza-Murillo, M. A., Moreno, M. A., and Farias, A. (2016). Intercomparison of improved satellite rainfall estimation with CHIRPS gridded product and rain gauge data over Venezuela. *Atmósfera* 29, 323–342. doi: 10.20937/ATM.2016.29.04.04

Prakash, S. (2019). Performance assessment of CHIRPS, MSWEP, SM2RAIN-CCI, and TMPA precipitation products across India. *J. Hydrol.* 571, 50–59. doi: 10.1016/j.jhydrol.2019.01.036

Retalis, A., Katsanos, D., Tymvios, F., and Michaelides, S. (2018). Validation of the first years of GPM operation over Cyprus. *Rem. Sens.* 10:1520. doi: 10.3390/rs10101520

Rivera, J. A., Marianetti, G., and Hinrichs, S. (2018). Validation of CHIRPS precipitation dataset along the Central Andes of Argentina. *Atmosph. Res.* 213, 437–449. doi: 10.1016/j.atmosres.2018.06.023

Senay, G. B., and Verdin, J. (2003). Characterization of yield reduction in Ethiopia using a GIS-based crop water balance model. *Canad. J. Rem. Sens.* 29, 687–692. doi: 10.5589/m03-039

Shrestha, N. K., Qamer, F. M., Pedreros, D., Murthy, M., Wahid, S. M., and Shrestha, M. (2017). Evaluating the accuracy of Climate Hazard Group (CHG) satellite rainfall estimates for precipitation based drought monitoring in Koshi basin, Nepal. *J. Hydrol. Reg. Stud.* 13, 138–151. doi: 10.1016/j.ejrh.2017.08.004

Shukla, S., Funk, C., and Hoell, A. (2014). Using constructed analogs to improve the skill of March-April-May precipitation forecasts in equatorial East Africa. *Environ. Res. Lett.* 9:094009. doi: 10.1088/1748-9326/9/9/094009

Smirnov, O., Zhang, M., Xiao, T., Orbell, J., Lobben, A., and Gordon, J. (2016). The relative importance of climate change and population growth for exposure to future extreme droughts. *Clim. Change* 138, 41–53. doi: 10.1007/s10584-016-1716-z

Thomas, E., Jordan, E., Linden, K., Mogesse, B., Hailu, T., Jirma, H., et al. (2020). Reducing drought emergencies in the Horn of Africa. *Sci. Total Environ.* 727:138772. doi: 10.1016/j.scitotenv.2020.138772

Thomas, E. A., Needoba, J., Kaberia, D., Butterworth, J., Adams, E. C., Oduor, P., et al. (2019). Quantifying increased groundwater demand from prolonged drought in the East African Rift Valley. *Sci. Total Environ.* 666, 1265–1272. doi: 10.1016/j.scitotenv.2019.02.206

Trenberth, K. E., Dai, A., Rasmussen, R. M., and Parsons, D. B. (2003). The changing character of precipitation. *B Am. Meteorol. Soc.* 84, 1205–1217. doi: 10.1175/BAMS-84-9-1205

Verdin, J., and Klaver, R. (2002). Grid-cell-based crop water accounting for the famine early warning system. *Hydrol. Process.* 16, 1617–1630. doi: 10.1002/hyp.1025

Wainwright, C. M., Marsham, J. H., Keane, R. J., Rowell, D. P., Finney, D. L., Black, E., et al. (2019).'Eastern African Paradox'rainfall decline due to shorter not less intense Long Rains. *npj Clim. Atmosph. Sci.* 2, 1–9. doi: 10.1038/s41612-019-0091-7

Williams, P., and Funk, C. (2011). A westward extension of the warm pool leads to a westward extension of the Walker circulation, drying eastern Africa. *Clim. Dynam.* 37, 2417–2435. doi: 10.1007/s00382-010-0984-y

Yang, W., Seager, R., Cane, M. A., and Lyon, B. (2014). The East African Long Rains in Observations and Models. *J. Clim.* 27, 7185–7202. doi: 10.1175/JCLI-D-13-00447.1

Conflict of Interest: The authors declare that the research was conducted in the absence of any commercial or financial relationships that could be construed as a potential conflict of interest.

Publisher's Note: All claims expressed in this article are solely those of the authors and do not necessarily represent those of their affiliated organizations, or those of the publisher, the editors and the reviewers. Any product that may be evaluated in this article, or claim that may be made by its manufacturer, is not guaranteed or endorsed by the publisher.

frontiers in Climate

ORIGINAL RESEARCH
published: 27 September 2021
doi: 10.3389/fclim.2021.714273

Limitations of Remote Sensing in Assessing Vegetation Damage Due to the 2019–2021 Desert Locust Upsurge

Emily C. Adams[1,2]*, *Helen B. Parache*[1,2], *Emil Cherrington*[1,2], *Walter L. Ellenburg*[1,2], *Vikalp Mishra*[1,2], *Ronan Lucey*[1] and *Catherine Nakalembe*[3]

[1] Earth System Science Center, The University of Alabama in Huntsville, Huntsville, AL, United States, [2] NASA SERVIR Science Coordination Office, Marshall Space Flight Center, Huntsville, AL, United States, [3] Department of Geographical Science, University of Maryland, College Park, MD, United States

The 2019–2020 Desert Locust (DL) upsurge in East Africa threatened food security for millions in the region. This highlighted the need to track and quantify the damaging impacts of the swarming insects on cropland and rangelands. Satellite Earth observations (EO) data have the potential to contribute to DL damage assessments that can inform control measures, aid distribution and recovery efforts. EO can complement traditional ground based surveys (which are currently further limited due to COVID-19), by rapidly and cost effectively capturing the full spatial scale of the DL upsurge. However, EO-based techniques struggled to accurately quantify damage from this DL upsurge due to the sporadic and localized nature of infestations impacting scale, timing, and anomalous vegetation conditions. This study analyzed time series data from MODIS, the harmonized Landsat Sentinel-2 product, and C-band radar data from Sentinel-1 to distinguish DL damage from normal senescence or other confounding factors from January to June 2020. These data were compared to *in situ* locust swarm, band, and non locust observations collected by the Food and Agriculture Organization (FAO) and PlantVillage. The methods presented did not produce results that could confidently differentiate senescence from locust activity, and may represent a limitation of publicly available remotely sensed data to detect DL damage. However, the higher spatial resolution data sets showed promise, and there is potential to explore commercially available satellite products such as Planet Labs for damage assessment protocols.

Keywords: locust, NDVI, vegetation, damage assessment, MODIS, harmonized landsat sentinel

OPEN ACCESS

Edited by:
Colin Kelley,
Columbia University, United States

Reviewed by:
Indu J,
Indian Institute of Technology Bombay, India
Leonardo Porcacchia,
University of Amsterdam, Netherlands

***Correspondence:**
Emily C. Adams
emily.c.adams@nasa.gov

Specialty section:
This article was submitted to Climate Services, a section of the journal Frontiers in Climate

Received: *25 May 2021*
Accepted: *25 August 2021*
Published: *27 September 2021*

Citation:
Adams EC, Parache HB, Cherrington E, Ellenburg WL, Mishra V, Lucey R and Nakalembe C (2021) Limitations of Remote Sensing in Assessing Vegetation Damage Due to the 2019–2021 Desert Locust Upsurge. Front. Clim. 3:714273. doi: 10.3389/fclim.2021.714273

1. INTRODUCTION

Desert locusts (*Schistocerca gregaria*) (DL) are considered one of the most dangerous migratory pests on the planet (Cressman, 2016; Gómez et al., 2018; Shrestha et al., 2021). They typically inhabit the arid regions stretching from West Africa to the Indian subcontinent and exist in a relatively unremarkable solitary phase (Cressman, 2016; Gómez et al., 2020; Shrestha et al., 2021). However, under favorable climatic conditions, DL can phase change into gregarious swarms, breeding, and devoring vegetation at massive scales (Pener, 1991; Sword et al., 2010). DL need wet, sandy soils to lay eggs and fresh green vegetation to sustain themselves (Pener, 1991; Collett et al., 1998).

After hatching, they exist in a hopper phase, when they do not have wings (Pener, 1991). During the gregarious phase, these hoppers form bands of many millions of individuals marching together (Pener, 1991). Upon maturity, the locusts grow wings and swarm and copulate. Once again, the locusts look for the right soil conditions to lay eggs. This life cycle takes ∼2–3 months (Pener, 1991). Utilizing synoptic wind patterns, DL can fly up to 100–150 km per day (Cressman, 2016; Food and of the United, 2020). Thus, when the right precipitation conditions occur and egg laying becomes very successful over a short period of time, swarming occurs (Pener, 1991; Collett et al., 1998; Sword et al., 2010). DL swarms migrate seasonally following well documented migratory routes (Homberg, 2015). These conditions came to fruition in late 2019 following cyclones in the Arabian Sea. Cyclones Mekunu and Luban in 2018 provided enhanced regional rainfall, particularly on the Arabian peninsula, and cyclone Pawan in 2019 created wind patterns enabling the DL to invade East Africa (Salih et al., 2020). An upsurge occurs when a very large increase in locust numbers and multiple outbreaks occur, leading to the production of two or more successive generations of transient-to-gregarious breeding in complementary seasonal breeding areas (Cressman, 2016). Since October 2019, rainfall in East Africa was anomalously high in desert areas, creating favorable conditions for DL activity including breeding and gregarization. **Figure 1** illustrates the 3 month anomalies for the October, November, December 2019 and January, February, March 2020 time periods. These anomalies were calculated using the Climate Hazards Group InfraRed Precipitation with Station Data (CHIRPS) using the deviations from the long term (since 1980) climatology. In fact, due to the conditions outlined above, and the economic instability in Yemen reducing strategic control, the FAO noted in the September 2019 Desert Locust bulletin that the region was under threat for increasing DL activity. DL migratory patterns are also well documented, following the synoptic winds and vegetation green up. During upsurge, a typical 1 km squared swarm can contain 150 million locusts, and consume as much food as 35,000 people each day (Food and of the United, 2020). This can lead to widespread devastation of vegetation and crops over impacted areas, severely effecting local food security.

Control strategies vary widely across the DL impacted areas depending upon the region, growth stage, and resource availability (Djibo et al., 2006; Klein et al., 2021). The FAO, the leading organization in DL control, prediction, and support, operates the Desert Locust Early Warning System, which uses a combination of remotely sensed, modeled, and *in-situ* information to understand DL phase and spread to inform management and control operations (Djibo et al., 2006; Cressman, 2013). The countries along the arid regions in northern Africa and the Arabian Peninsula are frequently impacted by locust infestations. These "front line countries" maintain locust control teams and report sightings and conditions back to the FAO, including the Desert Locust Control Organization for East Africa (DLCO-EA) and the Commission for Controlling the Desert Locust in the Western [Africa] Region (CLCPRO). This information feeds periodic bulletins on regional locust activity and informs control strategies (Cressman, 2013). Remotely sensed information, such as vegetation conditions, soil moisture, and precipitation, provide survey teams with general locations for favorable DL activity. These targets are of limited utility due to their large size, coarse resolution, remoteness, and local instability (Cressman, 2013; Ellenburg et al., 2021). Although control measures, such as localized spraying, burning, or trapping, ideally target sedentary eggs, widespread use of pesticides is also common during the swarming stage. During the most recent outbreak in West Africa, 13 million liters of pesticides were distributed to affected countries at a cost of about 280 million USD (Djibo et al., 2006). Many East African countries, who do not see upsurges often, lack the national capacity and ground presence to implement control measures effectively (Salih et al., 2020).

Satellite EO can complement and augment ground observations and monitoring, providing the potential to consistently monitor surface conditions, particularly over remote and hard to access locations. EO data have been successfully used to identify pest breeding locations (Ellenburg et al., 2021), monitor habitat (Klein et al., 2021), and predict distributions (Klein et al., 2021). As it is impractical to directly map DL from satellite observations due to spatial resolution requirements, typically other parameters are monitored to predict where DL are likely to thrive. For example, soil moisture and wind direction have been used to predict the likely spread of DL swarms for targeted interventions (e.g., Ellenburg et al., 2021). DL populations have also been successfully forecast through mapping emerging vegetation (Latchininsky, 2013).

Many EO-based studies include the use of optical imagery such as Aqua and Terra MODIS and the Landsat series, deriving Normalized Difference Vegetation Index (NDVI) and land cover from these datasets to arrive at DL habitat as described in the review by Klein et al. (2021). Thermal infrared sensors as well as active radar sensors have been used to measure temperature, precipitation, and soil moisture to identify DL habitat (Klein et al., 2021). Limitations of using remote sensing to monitor these proxy variables include low spatial and temporal resolution, as DL have localized impacts and yet travel rapidly over large areas. In addition, many EO-data layers, such as land cover and meteorological variables, that could be useful for DL detection are often out of date and can be time consuming and expensive to generate.

Few studies quantify damage from DL using remote sensing techniques, focusing instead on parameters such as NDVI, precipitation, and wind (Klein et al., 2021). Anomalous behavior of satellite observations such as vegetation conditions can provide significant information on the impact of pest infestations on vegetation (Wójtowicz et al., 2016). There have been instances where remote sensing has been used to assess pest damage or plant stress, but not in context of DL. Studies mapping locust damage such as the above have not focused on *S. gregaria* and the majority have relied on very high spatial resolution (VHR) imagery or hyperspectral data (Chavez, 1994; Genc et al., 2008; Pekel et al., 2011; Cressman, 2013). However, these data are not widely available and are expensive and hence the methods cannot be applied systematically (Klein et al., 2021).

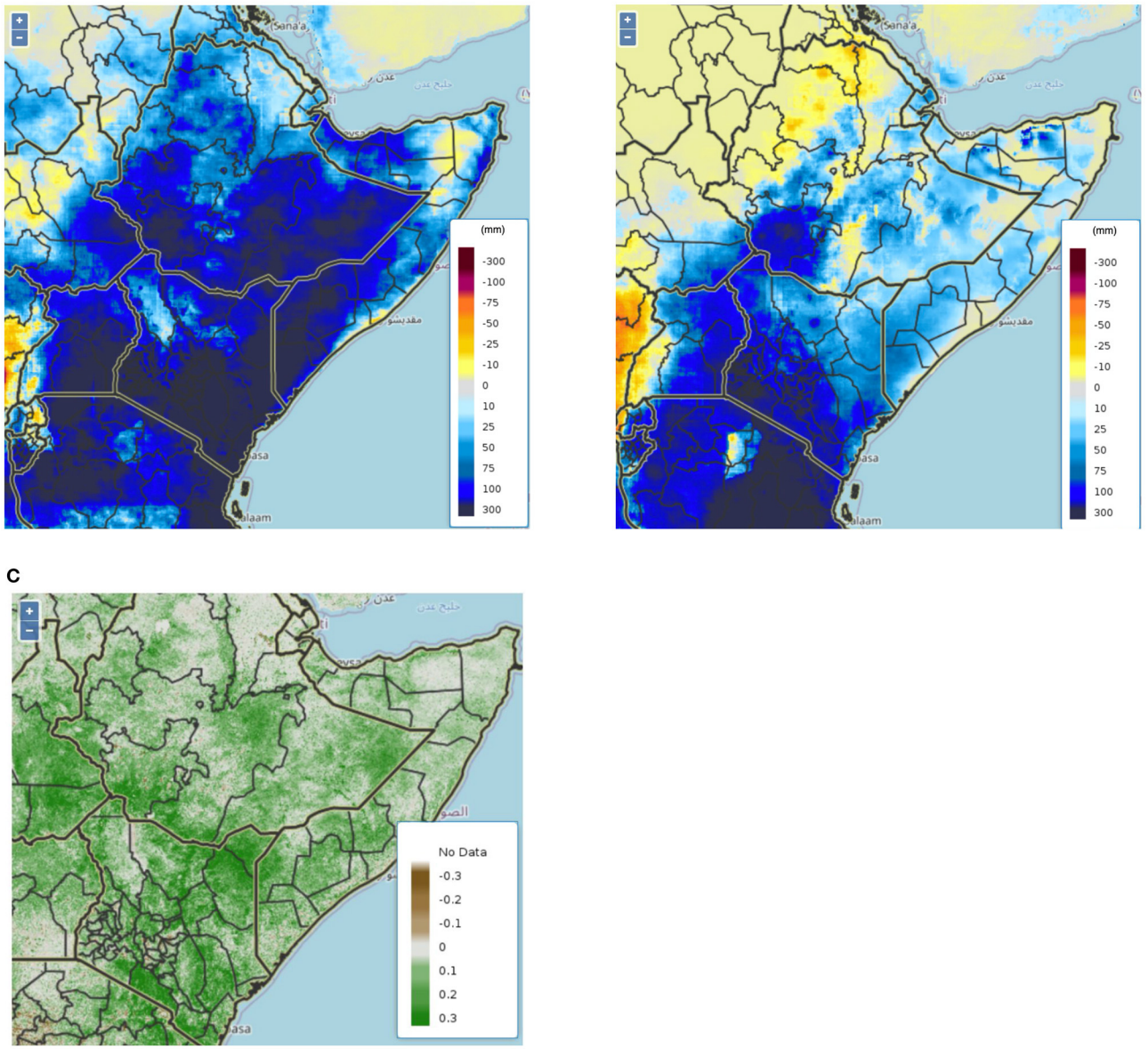

FIGURE 1 | Three month precipitation anomalies derived from the Climate Hazards Group InfraRed Precipitation with Station Data (CHIRPS) for October, November, and December 2019 **(A)**, and January, February, March 2020 **(B)**. The region experienced ∼50–300 mm more precipitation than average 3-monthly periods leading to enhanced greenness throughout the region **(C)** showing MODIS derived NDVI anomalies from the second dekad in January 2020.

Remote sensing of vast areas using multispectral and high spatial resolution (between 10 and 30 m) has become more accessible in recent years, thanks in part to the launch of the Sentinel-2 constellation that complements the Landsat series, as well as increased access to cloud computing resources to process high data volumes, including platforms such as Google Earth Engine (GEE), (Nakalembe et al., 2021). Nonetheless, damage caused by DL can be difficult to quantify with EO-data due to the sporadic and localized nature of infestations, agro-climatology and timing of the event. Yet, this information is valuable, supplementing ground based surveys that inform ground control operations, and aid distribution. In 2020, EO-based assessment were even more critical for capturing the full spatial scale of the DL upsurge limited ground operations due to COVID-19 related travel restrictions. Moreover, the regions in which DL are often active are remote and sparsely populated, limiting accessibility required to quantify impacts. However, these same remote regions often provide valuable resources for pastoral

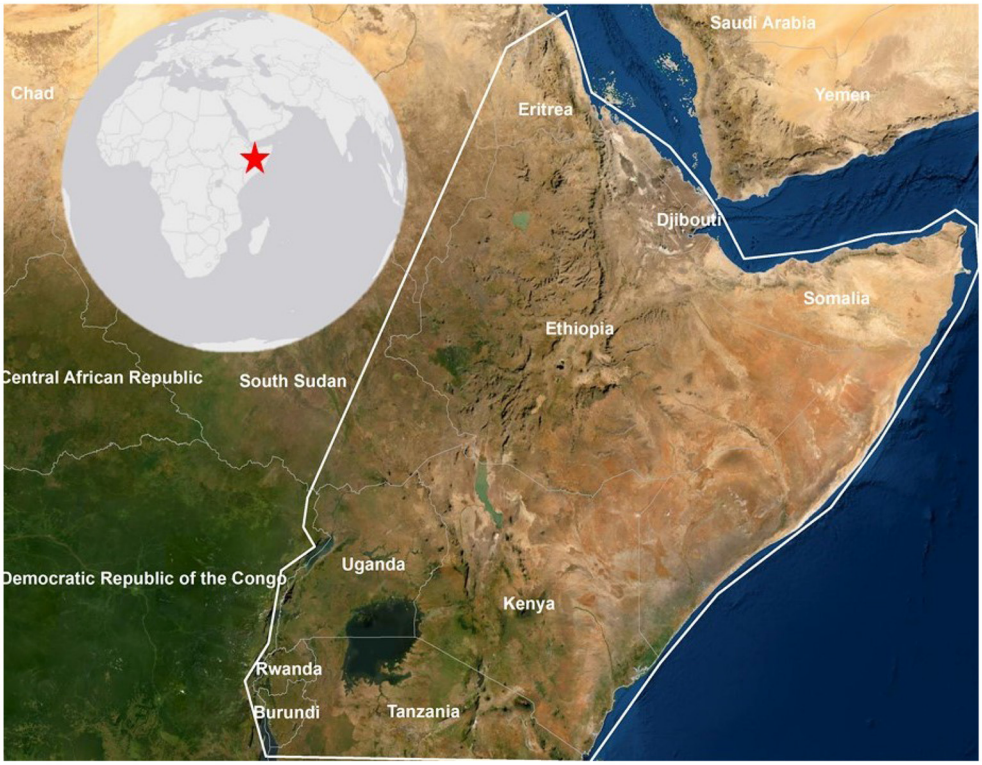

FIGURE 2 | The study area includes Burundi, Djibouti, Eritrea, Ethiopia, Kenya, Rwanda, Somalia, parts of Sudan and South Sudan, Uganda, and Tanzania.

communities, wildlife, and subsistence cropland areas. With increased variability in regional climates and control measures hampered by global geopolitics, regional and national insecurity, DL outbreaks of large magnitude such as the 2019–2020 upsurge in Eastern Africa will likely increase, and the need to develop and improve methods to detect DL damage from remote sensing will become more valuable.

This research presents methodologies that could be used to systematically identify vegetation damage caused by DL. The methods are applied to the 2019–2020 DL upsurge in East Africa described at the worst upsurge in 25 years for Somalia and Ethiopia and worst in 70 years for Kenya (Nakalembe, 2020). Aiming to fill gaps in the research on using EO observations for DL detection, this work focuses on damage detection and acknowledges the need to distinguish DL damage from normal senescence and other confounding factors. The methods described were designed to take into account vegetation cycles, as migratory patterns of DL follow peak vegetation greenness (Pekel et al., 2011; Cressman, 2013; NOA, 2016). This investigation includes a data fusion approach combining higher resolution data and Sentinel 1 Synthetic-aperture radar (SAR) data. Few studies have applied Sentinel 1, VHR, and data fusion to DL damage detection (Klein et al., 2021). Successfully identifying DL damage would enhance the efficiency of distributing aid and measuring the efficacy of control measures.

2. MATERIALS AND METHODS

2.1. Study Area

This study focuses on the Greater Horn of Africa (GHA) region that experienced the 2019–2020 DL upsurge. First reports of DLs in the GHA were received by the FAO in late 2019 (Salih et al., 2020). Djibouti, Eritrea, and Ethiopia began their control efforts as swarms growth increased significantly in Yemen and DL made their way across the Red Sea. Further, the typically "dry" season of January–March saw abnormally high rainfall (**Figure 1**), creating the perfect egg laying conditions across the arid and semi arid regions of the GHA. Soil texture, moisture and temperature are limiting factors for DL breeding and egg incubation, and are also leading indicators for vegetation growth (Batten, 1969; Mukerji and Gage, 1978; Padgham, 1981; Peng et al., 2020; Ellenburg et al., 2021). The incubation period and subsequent life stages of the DL vary widely depending on soil and air temperature. The incubation period ranges between 14 and 22 days and the hopper life stage can last for 35–45 days (NOA, 2016). Therefore, it is expected that egg laying occurred 3–10 weeks prior to hopper observations (Ellenburg et al., 2021) corresponding to vegetation green up. This analysis focused on the period from December 2019 to June 2020 time frame in the GHA (**Figure 2**). This time frame thus includes any areas that would be utilized for rangelands or croplands and would directly impact food security in the region.

TABLE 1 | Remote sensing datasets used in this study.

Satellite	Operating Agency	Spatial Resolution	Temporal Resolution
AQUA/TERRA MODIS	NASA	250 × 250 m	Daily
Landsat 8 OLI	USGS	30 × 30 m	16 days
Sentinel-2 MSI	ESA	10 × 10 m	5 days
Sentinel-1 SAR	ESA	10 × 10 m	12 days

2.2. Data Sets

2.2.1. Remote Sensing Data

A wide variety of remotely sensed datasets were used in this study in order to complement spatial or temporal shortcomings of any particular mission (**Table 1**). Optical data from the Moderate Resolution Imaging Spectroradiometer (MODIS) sensor on board the AQUA and TERRA satellites offer a daily temporal resolution but are limited spatially at 250 m. Whereas the Landsat 8 and Sentinel-2 missions have revisit times of 16 and 5 days, respectively, but have much higher spatial resolutions (30 and 10 m). The relatively low revisit periods of the Landsat and Sentinel satellites often results in data gaps due to cloud cover. Thus, a harmonized Landsat-Sentinel (HLS) product was created in GEE according to the specifications outlined in Claverie et al. (2018). The HLS dataset was used in addition to using MODIS, Landsat 8, and Sentinel-2 separately to compute vegetation condition indices such as the NDVI (Rouse et al., 1974) and Modified Soil Adjusted Vegetation Index (MSAVI) (Qi et al., 1994).

In addition to optical datasets, C-Band synthetic aperture radar (SAR) data from the Sentinel 1 missions were also used. SAR provides information about the texture of the Earth's surface and is not limited by cloud cover. Specifically, Sentinel-1 C-band vertical-vertical (VV) and vertical-horizontal (VH) backscatter are known to be sensitive to changes in vegetation conditions, such as damage caused by hail (Bell et al., 2020) and above ground biomass (AGB) (Pereira et al., 2018). Areas that have been damaged by DL are expected to have lower backscatter power due to a reduction in vegetation cover. As the cross-polarized signal is dominated by vegetation cover, rather than the surface (Woodhouse, 2005), the VH analysis is expected to be more useful for distinguishing potential locust impact.

2.2.2. Ground Data

The FAO maintains a publicly available database of locust reports (FAO, 2020b). These reports are compiled from many sources, but in most cases contain the geographic location of the sighting and the life cycle stage of the locust. The general stages of gregorious DL include egg, hopper bands, and swarm. After the eggs hatch, juvenile DL form large groups of hoppers or hopper bands. At this life stage the DL cannot fly. These observation points, particularly at the swarm and hopper band stages, were used as *in-situ* reference dataset for this study. Non-locust observations, where no DL were observed at that time and place, were acquired from PlantVillage and are available from March 2020. January and February had no non-locust locations with which to compare the swarm and band locations. Observations were not evenly distributed throughout the study period. Bands and none observations increased from December 2019 to June 2020. Swarm observations increased as well, except for a lull in May 2020.

In addition to the ground based data sets available through FAO, the researchers also compiled ancillary information. These ancillary datasets included survey data from the United States Agency for International Development. This supplementary information was used for qualitative comparisons of locust sighting locations.

2.3. Time Series Analysis

Using the HLS and MODIS data, time series at each of the band, swarm, and non-locust observations were analyzed for every available non-cloudy pixel. This analysis utilized vegetation indices such as NDVI and MSAVI to map the presence and health of vegetation. Typically NDVI is used to map vegetation, however MSAVI was developed to account for the impact of soil in areas with low vegetation density (QI1994119) such as is prevalent in GHA. Despite MSAVI's expected advantages in detecting actual vegetation conditions, the analysis showed that both NDVI and MSAVI had very similar temporal dynamics. Thus, only the NDVI results were used in this study for analysis and discussions.

The MODIS NDVI was compared to HLS NDVI over band, swarm, and non-locust observations based on the number of days before and after the observation. The HLS NDVI at the pixel corresponding to the band sighting was averaged with the surrounding eight pixels for all available scenes in the study period. This time series was then smoothed using cubic interpolation (McKinney, 2010) to remove anomalous highs and lows. NDVI before and after the event, i.e., the time of the band/swarm sighting, was divided by NDVI during the event. This is termed relative NDVI. Using relative NDVI normalizes the impact of the natural vegetative cycle and different timings of sighting. Relative NDVI from HLS was then compared with the equivalent MODIS NDVI. Two examples are presented here, located in Ethiopia (**Figure 3**). These sites were selected as representative of the region after a thorough analysis of random sites distributed across the GHA. It was expected that if damage due to DL was detected, the NDVI values would decrease after a band sighting by a larger amount for the higher resolution HLS data set when compared to the lower resolution MODIS data set.

2.4. Monthly Composites Analyses

2.4.1. Harmonized Landsat Sentinel 2 Analysis

Using the HLS data, NDVI and Hue were calculated on a monthly basis to account for regional cloud cover, particularly prevalent during the rainy seasons. The benefits of using NDVI were stated in the previous section. Hue was selected as some studies have found value in using the hue values as a proxy for vegetation condition in the arid and semi arid regions where locusts inhabit (Pekel et al., 2011). Hue, saturation, and value, can be converted from any band, however the red, green, blue, and SWIR bands (bands 4, 3, 2, 7, and 6, respectively) were used for this analysis. This transformation was completed for the HLS data set on a monthly scale. Median NDVI pixel values for each month from December 2019 to June 2020 were calculated. Monthly

FIGURE 3 | Band observation sites in Ethiopia where NDVI derived from HLS was compared with NDVI derived from MODIS.

composites of median NDVI for the time period of 2015 (Sentinel 2 launch) through November 2019 were also created as a baseline reference period. This represented the longest term similar data set for comparison due to the recency of Sentinel 2 data.

2.4.2. Sentinel 1 Analysis

Cloud cover was frequently an issue, therefore, a multitemporal analysis of Sentinel 1 C-band data was conducted, as SAR data is able to penetrate through cloud cover (Woodhouse, 2005). Backscatter power for locust and non-locust locations were compared to see if there were changes indicating the presence of locust damage. First, the median backscatter was selected from a 3-month moving window over the study area for December 2019–June 2020. The resulting six median layers were extracted by known DL locations [band (N = 3,799) and swarm (N = 2,646)], and non-locust locations (N = 13,502) to see if there was a difference in the medians of these groups. Sightings were grouped by the same time periods as the Sentinel 1 imagery. VH and VV backscatter power were extracted by swarm and band sites and non-locust locations and compared. A similar analysis was repeated at a monthly time step to take greater advantage of the temporal resolution of Sentinel 1. A similar analysis was repeated at a monthly time step to take greater advantage of the temporal resolution of Sentinel-1. Single scenes, which would have taken full advantage of the higher temporal resolution of the Sentinel-1 dataset, were not investigated. Evaluating monthly medians also reduced potential impacts from speckle, or natural variation that occurs even over homogeneous surfaces, per Woodhouse (2005). Another reason for using the Sentinel-1 data at a monthly timescale was that it also made the analysis comparable to the one done using the Harmonized Landsat Sentinel-2 (HLS) dataset, which, due to cloud cover, was likewise generated at a monthly timescale. For that reason, use of Sentinel-1 imagery at a monthly timescale was therefore determined to be more appropriate.

3. RESULTS

3.1. MODIS Time Series Analysis

The NDVI values were compared for MODIS and HLS at known band, swarm, and non-locust observation sites as a function of days before and after the observation date (**Figure 4**). Over locust and non-locust sites, the relative HLS NDVI varied more than the relative MODIS NDVI, indicating that the HLS may have recorded greater changes in vegetation than the MODIS. Sixteen days after the observation, the median relative HLS NDVI dropped slightly (<0.1) for band and non-locust sites while the median relative NDVI at swarm sites remained nearly the same. This indicates that the relative HLS NDVI is not immediately detecting notable vegetation change at locust locations.

The case studies of individual band sites, #1321 (**Figure 5B**) and #1700 (**Figure 5A**), illustrated that the average relative NDVI over the average of the pixel corresponding to the band sighting and the surrounding eight pixels from the HLS followed the same trends as the relative NDVI from MODIS, although in general the magnitude of HLS NDVI values were lower. For example, NDVI lows occurred at site #1321 in October, February, and May for both datasets. Similarly, for site #1700, the peaks in November and June appeared in both datasets. Since NDVI from both HLS and MODIS follow the same general trends over the study period, the differences in the NDVI change between the HLS and MODIS during or after a band observation were potentially attributed to vegetation change occurring at a higher spatial resolution, for example DL damage. However, the NDVI trends at site #1321 and site #1700 do not convincingly demonstrate DL damage. At site #1321, the HLS NDVI decreased (<0.05) at the observation date. However, the MODIS NDVI also decreased (∼0.1). This suggests that the vegetation change occurred over an area larger than would be expected than if it were due to DL damage. At site #1700, the HLS NDVI decreased (<0.05) while the MODIS NDVI increased (∼0.05). This lack of a clear pattern in direction and magnitude of NDVI change between HLS and MODIS does not lend itself to identification of DL damage. Ultimately,

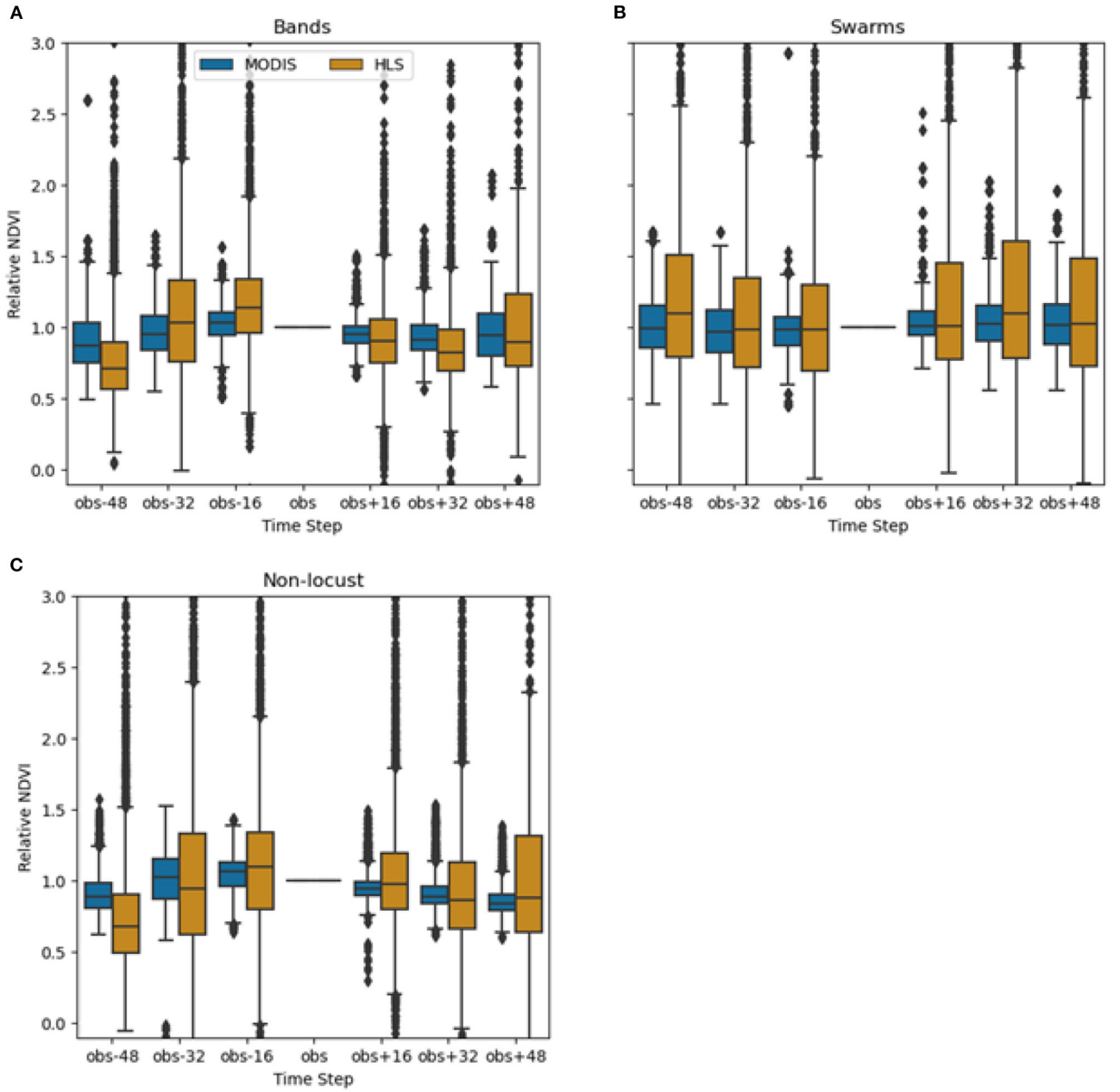

FIGURE 4 | Relative NDVI of MODIS vs. HLS compared over band **(A)**, swarm **(B)**, and non-locust **(C)** sites [$n = 36{,}820$, $n = 24{,}696$, $n = 72{,}863$].

investigating a higher resolution dataset with this method may yield interesting results for DL damage detection.

3.2. Monthly Composites Analyses

3.2.1. Harmonized Landsat Sentinel-2 Analysis

The monthly HLS composite analysis did not show definitive evidence of damage. Band and swarm data sets were compared to non-locust points for the months of March through June 2020 using both NDVI (**Figure 6A**) and Hue calculated with the shortwave infrared band combination 7, 5, 4 (**Figure 6B**). Hue was also calculated using the natural color bands (4, 3, 2) and the shortwave infrared, near infrared, and red channels (6, 5, 4) but the pattern was very similar to the 7, 5, 4 combination and therefore only 7, 5, 4 is presented here.

The NDVI values showed a normal distribution and student pair wise *t*-tests were performed for each month comparing band against non locust and swarm against non locust data points. All comparisons resulted in significant differences between the data sets with *p*-values <0.05. In all months if damage was identified, we would have expected NDVI to be higher at the

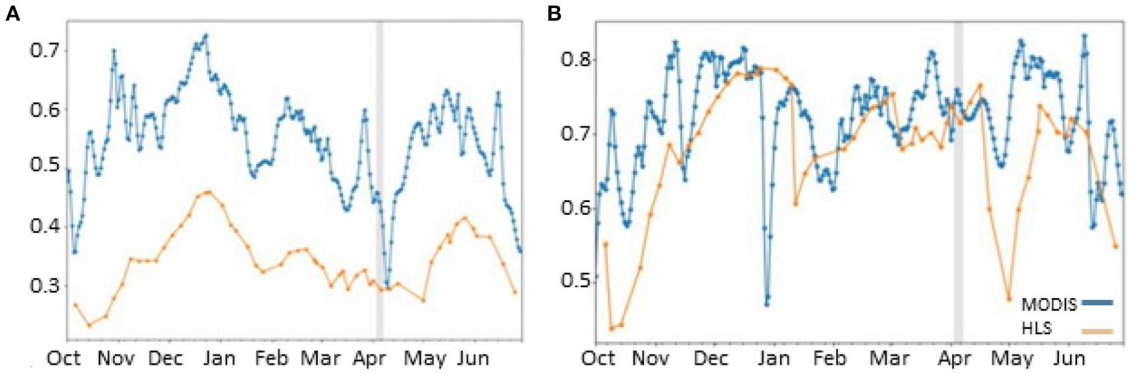

FIGURE 5 | Time series of NDVI from MODIS and averaged HLS at site #1700 **(A)** and site #1321 **(B)**. The vertical grey line indicates the date the band was observed.

none points, however this was not the case. In March and April, NDVI is higher for the bands and swarms compared to the none points. The reverse is true in May, and in June the means are all very close. There was high variability in NDVI within each month, therefore even when an NDVI value was lower it was not conclusively due to locust activity.

The hue transformation showed a similar pattern to NDVI, but reduced the range of values toward 0. This made interpretation more difficult as the means became closer together and the variance remained large across all categories. In this case the use of hue as an index was less useful than NDVI.

3.2.2. Sentinel-1 Analysis

Results of the multitemporal analysis were inconclusive, suggesting that a shorter time frame could reveal more information than the multitemporal, 3-month composites. For the monthly analysis, the VV values for bands, swarm, and none points ranged −26 to 4 db whereas VH ranged from −33 to −4 db (**Figure 7**). Thus, the median backscatter power for VV tends to be higher than VH for all locust and non-locust locations. This trend is expected, as VV and VH respond differently to surface characteristics. More importantly, the differences between the median backscatter power of both swarm and band locations vs. the non-locust locations did not clearly signal vegetation change, including the presence of locust damage.

Taking a closer look at the median backscatter power for VH (**Figure 7**), for March and April, the median backscatter power for non-locust sites was less than the median backscatter power for bands and swarms. For March, the absolute difference between the non-locust the and swarm medians and the absolute difference between the non-locust and band medians were both <0.5 db. For April, the absolute difference between the non-locust and swarm medians was 0.7 db and the absolute difference between the non-locust and band medians was 1.2 db. For May and June, the median backscatter power for non-locust sites was greater than the median backscatter power for bands and swarms. For May, the absolute difference between the non-locust and swarm medians was 1.6 db and the absolute difference between the non-locust and band medians was 2.9 db. For June, the absolute difference between the non-locust and swarm medians was 1.0 db and the absolute difference between the non-locust and band medians was 1.6 db. In addition, the ranges for all location type had a large amount of overlap overall for each month.

Taking a closer look at the median backscatter power for VV (**Figure 7**), for March, May, and June, the median backscatter power for non-locust sites was greater than the median backscatter power for bands and swarms. For March, the absolute difference between the non-locust the and swarm medians and the absolute difference between the non-locust and band medians were both <1.0 db. For April, the median backscatter power for non-locust sites was less than the median backscatter power for bands and swarms. For June, the absolute difference between the non-locust and swarm medians and the absolute difference between the non-locust and band medians were both <2.0 db. For May, the absolute difference between the non-locust and swarm medians was 1.20 db and the absolute difference between the non-locust and band medians was 2.63 db. As with the VH, the ranges for all location types overlapped greatly each month. Thus, there is also no consistent pattern of VV or VH backscatter power that indicates locust damage at this temporal and spatial resolution with this method.

4. DISCUSSION

Several methodologies were tested to attempt to detect DL impact, however, only the HLS monthly composite analysis showed very slight potential evidence of damage and only during March and April. There were several limitations, including spatial and temporal resolution, for each methodology that did not overcome their hypothesized utility. Time series data did not clearly indicate vegetation change. However, these data were very noisy and specific conclusions are uncertain. It is clear that spatial scale could play a role in damage detection of DL.

Leveraging SAR data was also challenging. There is not an extensive catalogue of openly available SAR data to compare current conditions with previous, as Sentinel 1A was launched in 2014 and 1B in 2016. This study chose to also focus on monthly medians which did not take full advantage of the

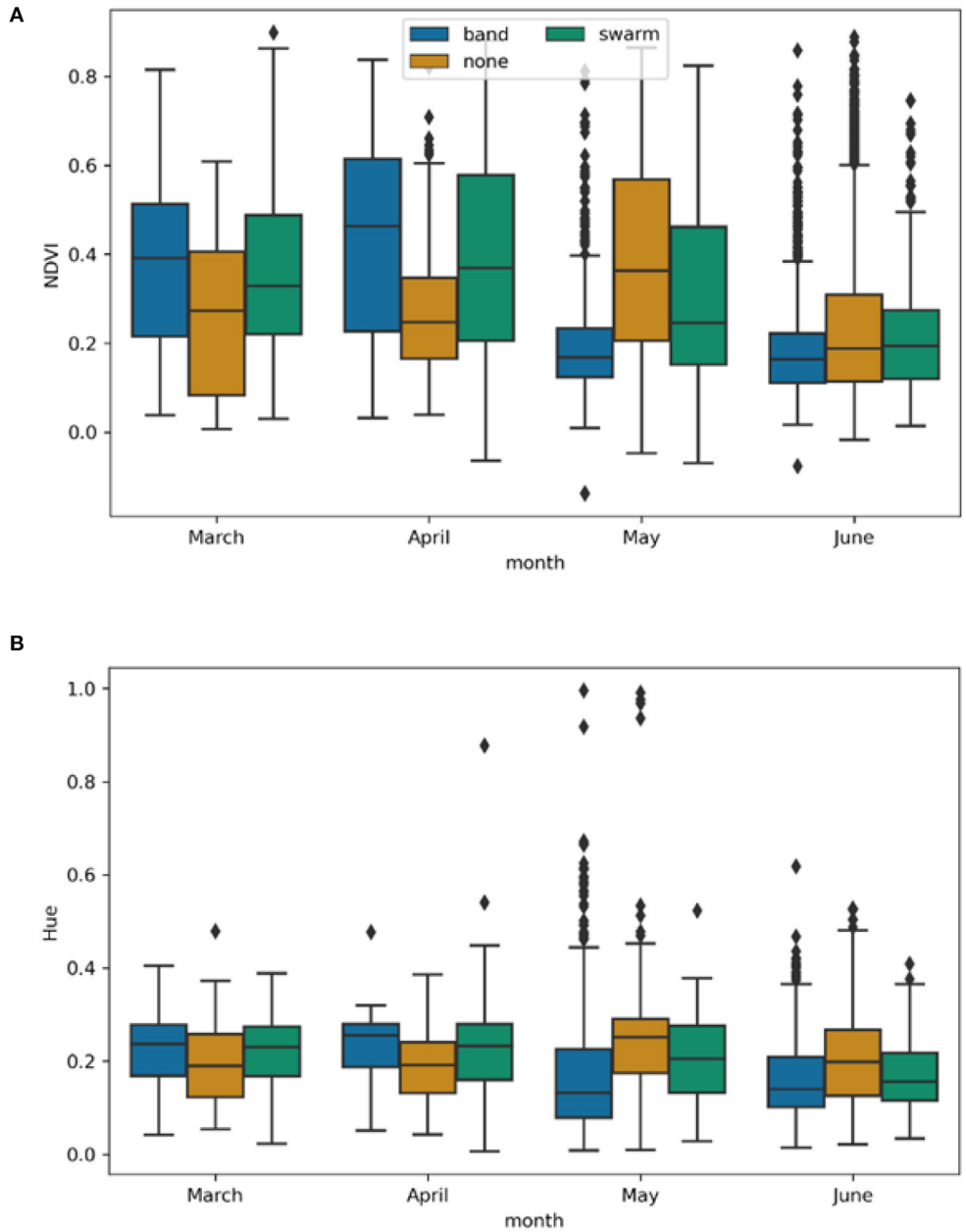

FIGURE 6 | (A) NDVI values at locust swarm, band, and non locust observations for the months of March through June 2020. **(B)** Hue values from the 7, 5, 4 band combination at the locust swarm, band, and no locust observations for the months of March through June 2020. Neither index showed distinct differences between locust activity and non locust activity.

temporal resolution of the Sentinel-1 data set. Future work may want to evaluate every available SAR image for changes in backscatter as opposed to monthly composites. Finally, speckle, or natural backscatter variation that occurs even over homogeneous surfaces (Woodhouse, 2005), may obscure the relatively small areas of locust damage.

There were several confounding factors that made this analysis challenging despite utilizing methods designed to overcome these limitations. Due to the intense rainfall from late 2019 into 2020, the region was exceptionally green. This reduced the utility of comparisons to similar years or anomaly analyses and we did not systematically incorporate these methods for that reason. This enhanced greenness not only made damage assessment challenging, but it also may reduce the successful application of such information for food security assessments. For example, regionally, pasture land had higher than normal vegetation due

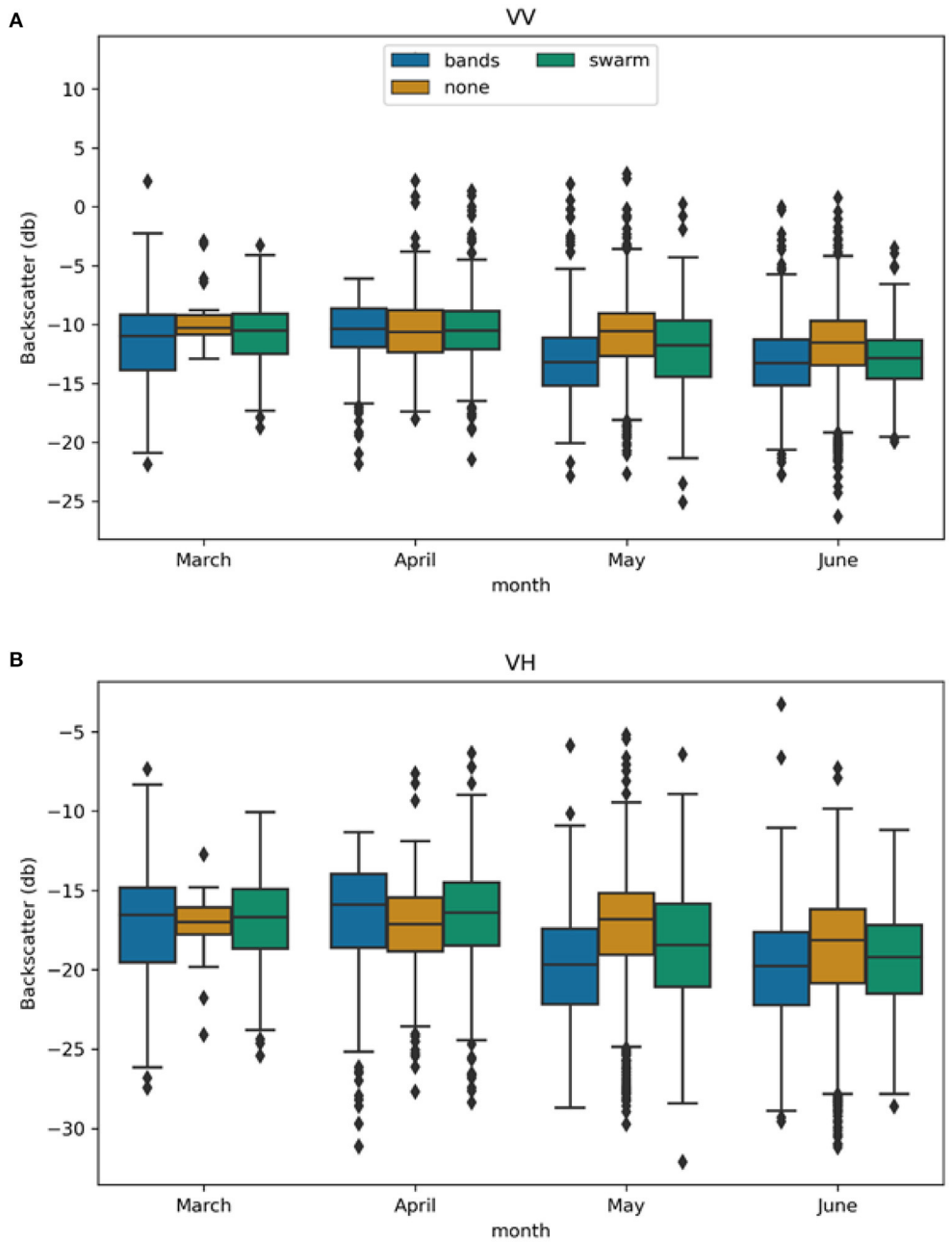

FIGURE 7 | Box plots of monthly VV **(A)** and VH **(B)** median backscatter power from Sentinel 1 C-band at swarm, band, and non-locust locations for March through June 2020.

to the enhanced rainfall, and we could expect that grazing communities had sufficient fodder for their animals and therefore may not have experienced food insecurity despite DL impacts.

Seasonality can also play an important role in impact analysis. Natural senescence grasslands or crop harvesting in agricultural areas will also confound DL damage assessments using remotely sensed data. For this reason, disaggregating the vegetation cover by land use type may prove important in future analyses.

The Food Security and Nutrition Working Group (FSNWG) at the FAO completed several iterations of East African ground based DL impact assessments after harvest (FAO, 2020a, 2021). The first assessment involved interviews from over 10,000 agricultural households across East Africa in June and July of 2020. These interviews were conducted largely after the period included in our remote sensing analysis. They found roughly a third of livestock or cropping households reported losses,

and half of those reporting indicated high losses (FAO, 2020a). These in-person interviews do not align temporally with the remotely sensed information we gathered from this study and were aggregated spatially to protect individual identities. Further, participants were asked to report presence or absence of locusts and did not provide exact dates that could have been correlated to results from this analysis. However, it is important to recognize that farmers are reporting damage while the remotely sensed information does not conclusively detect it.

In general the ground data collected by the FAO proved to be challenging to use as a proxy for damage. While the creation, deployment, and momentum around crowd sourced information is highly commendable in such a short period of time, it became clear through this analysis that a positive or negative locust sighting, and subsequent life stage, was not sufficient to support the identification of locust damage with remotely sensed data. Numerous characteristics associated with these DL populations may also have proven important. For example, size of the swarm, density, or activity of DL could have helped identify which DL points might be expected to show vegetation damage. While this type of information was available for some points, it was not available for the majority. In many cases, DL could have been reported while flying to other locations, so while the data we have show locust observations at a specific latitude and longitude, it is not known if damage would be expected at that location. Further, DL are capable of traveling extensively and quickly over vast distances. Thus, the same swarm may have been reported by several individuals in the same time period, diluting the relevant ground observation data. The successes of the application development and deployment show significant promise for future crowd sourced data, and what has been collected during the course of this upsurge has been incredibly valuable for ground based, real time DL monitoring and other DL applications such as supporting a finer resolution soil moisture product for DL breeding ground forecasting (Ellenburg et al., 2021). We hope this research will be able to inform application updates in order to create data that can be utilized more effectively for this purpose in the future.

Literature and personal testimonies show that Locust damage is sporadic yet highly destructive, similar to that of a tornado; leaving one field totally destroyed while their neighbor is spared (Krall and Herok, 1997; Latchininsky, 2013). The spatial and temporal resolution of the publicly available Earth observation datasets used for this study are unlikely to capture the level of detail associated with that destruction pattern, and may even leave time for vegetation regrowth before a new satellite observation can occur. The higher spatial resolution datasets, like the Sentinel 2 satellites (10 m) have 5 day revisit times during cloudless conditions, which are unlikely in this region. While a 10 m pixel may have a slight decline in greenness due to DL damage, it may not be large enough to convincingly identify decline. Therefore, establishing a decline in vegetation conditions due to DL with data that may not temporally align with cloudless before, during, and after satellite overpasses was challenging. Further, creating cloud free mosaics extends the temporal time scale in order to ensure cloud free pixels. In this region, during this time of year, even monthly scales had cloud contaminated pixels. An additional confounding factor is vegetation recovery. There is limited research on how vegetation damage from DL rebounds and with extended revisit time periods vegetation recovery may dilute a remotely sensed signal. MODIS data, at daily revisit times, and an extensive historical record might prove important, however the spatial scale of 250 × 250 m was too large in this case to assess the sporadic event. The results do show promise as high spatial resolution data sets were evaluated, therefore, there is potential for higher spatial resolution data from the private sector, such as Planet, to support these types of analyses although these data are not publicly available.

It seems as though both the complexities associated with tracking and recording ground observations of DL, and the limitations (spatial and temporal) associated with current publicly available EO capabilities compound to create circumstances that our current understanding of remote sensing cannot overcome. The influence of these confounding factors is challenging and frustrating, particularly in this area where utilizing remote sensing can be an incredibly powerful tool to help overcome data gaps and inform decisions. Nevertheless, as more sophisticated ground data techniques evolve, additional satellite capabilities come on line, and big data techniques become more accessible, there is potential to continue to explore remote sensing for these types of questions. This is particularly important to acknowledge as climate change is currently creating more erratic precipitation patterns in East Africa, which are predicted to become more unpredictable with time (Thornton et al., 2014). It is likely that these erratic precipitation patterns will create more opportunities for DL to survive and thrive in their current range and potentially expand that range to new regions. While this event was a once in 70 year disaster, it is unlikely that another 70 years will pass before seeing a similar event (Salih et al., 2020). Supporting the infrastructure to design and implement ground observations and remote sensing of vegetation conditions for food security are essential to building more resilient communities.

DATA AVAILABILITY STATEMENT

Publicly available datasets from NASA, ESA, and FAO were analyzed in this study as indicated in the Data Sets section. Further inquiries can be directed to the corresponding author.

AUTHOR CONTRIBUTIONS

EA, HB, EC, WL, and VM contributed to the research design and execution of the methods described. EA and HB took the lead on manuscript drafting with support from EC, WL, VM, RL, and CN. RL and CN supported research design and provided valuable inputs into the manuscript. All authors contributed to the article and approved the submitted version.

FUNDING

This research was funded by the joint U.S. Agency for International Development (USAID) and National

Aeronautics and Space Administration (NASA) initiative SERVIR and particularly through the NASA Applied Sciences Capacity Building Program, NASA Cooperative Agreement NNM11AA01A. The Regional hubs, RCMRD, and AGHRYMET provided technical support and in country coordination in the development, implementation. and validation of the methodologies.

ACKNOWLEDGMENTS

The authors would like to acknowledge the following groups and individuals for their support of this research and manuscript: The reviewers whose comments strengthened the manuscript. The editorial team from the Frontiers journal and special collection. The NASA SERVIR Science Coordination Office, particularly Rebekke Muench, Ashutosh Limaye, Eric Anderson, Jason Brent Roberts, Rob Griffin, and Daniel Irwin, the members of the EO-Locust working group, convened by WL and CN, including: FAO, USAID, ICIPE, and WFP members, among many others, members of the SERVIR West Africa, Eastern and Southern Africa and Hindu Kush Himalaya hubs, particularly Paul Bartel, Bako Mamane, Idrisa Maiga, Lilian Ndungu, and Faisal Qamer, and finally Keith Cressman for his Desert Locust wisdom.

REFERENCES

Batten, A. (1969). The senegalese grasshopper Oedaleus senegalensis Krauss. *J. Appl. Ecol*. 6, 27–45. doi: 10.2307/2401299

Bell, J. R., Gebremichael, E., Molthan, A. L., Schultz, L. A., Meyer, F. J., Hain, C. R., et al. (2020). Complementing optical remote sensing with synthetic aperture radar observations of hail damage swaths to agricultural crops in the central United States. *J. Appl. Meteorol. Climatol.* 59, 665–685. doi: 10.1175/JAMC-D-19-0124.1

Chavez, P. S., and MacKinnon, D. J. (1994). Automatic detection of vegetation changes in the southwestern united states using remotely sensed images. *Method Hotogramm. Eng. Remote Sens*. 60, 571–583.

Claverie, M., Ju, J., Masek, J. G., Dungan, J. L., Vermote, E. F., Roger, J.-C., et al. (2018). The harmonized landsat and sentinel-2 surface reflectance data set. *Remote Sens. Environ*. 219, 145–161. doi: 10.1016/j.rse.2018.09.002

Collett, M., Despland, E., Simpson, S. J., and Krakauer, D. C. (1998). Spatial Scales of desert locust gregarization. *Proc. Natl Acad. Sci.* U.S.A. 95, 13052–13055. doi: 10.1073/pnas.95.22.13052

Cressman, K. (2013). Role of remote sensing in desert locust early warning. *J. Appl. Remote Sens*. 7:075098. doi: 10.1117/1.JRS.7.075098

Cressman, K. (2016). "Desert locust," in *Biol. Environ. Hazards, Risks, Disasters*, eds Ramish Sivanpillai and John F. Shroder, MA, Waltham, USA Publisher: Elsevier. 87–105. doi: 10.1016/B978-0-12-394847-2.00006-1

Djibo, H., Faye, F. G., Ghaout, S., Lazar, M., Luzietoso, P. N., and Babah, M. A. O. (2006). *Multilateral Evaluation of the 2003-05 Desert Locust Campaign E Towards a More Effective Response to Desert Locusts and their Impacts on Food Security, Livelihoods and Poverty Multilateral Evaluation of the 2003-05 Desert Locust Campaign*. Food and Agriculture Organization of the United Nations.

Ellenburg, W. L., Mishra, V., Roberts, J. B., Limaye, A. S., Case, J. L., Blankenship, C. B., et al. (2021). Detecting desert locust breeding grounds: a satellite-assisted modeling approach. *Remote Sens*. 13, 1–11. doi: 10.3390/rs13071276

FAO (2020a). *East Africa Regional Desert Locust Impact Monitoring Round 1*. FAO.

FAO (2020b). *Locust Hub*. FAO.

FAO (2020c). *Appeal for Rapid Response and Anticipatory Action in the Greater Horn of Africa*. FAO.

FAO (2021). *East Africa Regional Desert Locust Impact Monitoring Round 2*. FAO.

Genc, H., Genc, L., Turhan, H., Smith, S. E., and Nation, J. L. (2008). Vegetation indices as indicators of damage by the sunn pest (Hemiptera: Scutelleridae) to field grown wheat. *Afr. J. Biotechnol*. 7, 173–180.

Gómez, D., Salvador, P., Sanz, J., Casanova, C., Taratiel, D., and Casanova, J. L. (2018). Machine learning approach to locate desert locust breeding areas based on ESA CCI soil moisture. *J. Appl. Remote Sens*. 12:1. doi: 10.1117/1.JRS.12.036011

Gómez, D., Salvador, P., Sanz, J., and Casanova, J. L. (2020). Modelling desert locust presences using 32-year soil moisture data on a large-scale. *Ecol. Indic*. 117:106655. doi: 10.1016/j.ecolind.2020.106655

Homberg, U. (2015). Sky compass orientation in desert locusts-evidence from field and laboratory studies. *Front. Behav. Neurosci*. 9:346. doi: 10.3389/fnbeh.2015.00346

Klein, I., Oppelt, N., and Kuenzer, C. (2021). Application of remote sensing data for locust research and management-a review. *Insects* 12:233. doi: 10.3390/insects12030233

Krall, S., and Herok, C. (1997). "Economics of desert locust control," in *New Strategies in Locust Control*, eds Stephan Krall, R. Peveling, and B.D. Diallo, Basel, Switzerland:(Springer), 401–413. doi: 10.1007/978-3-0348-9202-5_59

Latchininsky, A. V. (2013). Locusts and remote sensing: A review. *J. Appl. Remote Sens*. 7:075099. doi: 10.1117/1.JRS.7.075099

McKinney, W. (2010). "Data structures for statistical computing in python," in *Proceedings of the 9th Python in Science Conference, Vol. 445*, eds S. van der Walt and J. Millman, TX:Austin, 51–56. doi: 10.25080/Majora-92bf1922-00a

Mukerji, M. K., and Gage, S. H. (1978). A model for estimating hatch and mortality of grasshopper egg populations based on soil moisture and heat1. *Ann. Entomol. Soc. Am*. 71, 183–190. doi: 10.1093/aesa/71.2.183

Nakalembe, C. (2020). Urgent and critical need for sub-Saharan African countries to invest in Earth observation-based agricultural early warning and monitoring systems. *Environ. Res. Lett*. 15, 1–3. doi: 10.1088/1748-9326/abc0bb

Nakalembe, C., Becker-Reshef, I., Bonifacio, R., Hu, G., Humber, M. L., Justice, C. J., et al. (2021). A review of satellite-based global agricultural monitoring systems available for Africa. Glob. *Food Sec*. 29:100543. doi: 10.1016/j.gfs.2021.100543

NOA (2016). *Weather and Desert Locusts*. Technical report, World Meteorological Organization and Food and Agriculture Organization of the United Nations.

Padgham, D. E. (1981). Hatching rhythms in the desert locust, *Schistocerca gregaria. Physiol. Entomol*. 6, 191–198. doi: 10.1111/j.1365-3032.1981.tb00641.x

Pekel, J. F., Vanbogaert, E., Defourny, P., Ceccato, P., Vancutsem, C., and Cressman, K. (2011). Development and application of multi-temporal colorimetric transformation to monitor vegetation in the desert locust habitat. *IEEE J. Select. Top. Appl. Earth Observ. Remote Sens*. 4, 318–326. doi: 10.1109/JSTARS.2010.2052591

Pener, J. M. (1991). Locust phase polymorphism and its endocrine relations. *Adv. Insect Physiol*. 23, 1–79. doi: 10.1016/S0065-2806(08)60091-0

Peng, W., Ma, N. L., Zhang, D., Zhou, Q., Yue, X., Khoo, S. C., et al. (2020). A review of historical and recent locust outbreaks: links to global warming, food security and mitigation strategies. *Environ. Res*. 191:110046. doi: 10.1016/j.envres.2020.110046

Pereira, L. O., Furtado, L. F., Novo, E. M., Santapos;Anna, S. J., Liesenberg, V., and Silva, T. S. (2018). Multifrequency and full-polarimetric SAR assessment for estimating above ground biomass and leaf area index in the amazon várzea wetlands. *Remote Sens*. 10:1355. doi: 10.3390/rs10091355

Qi, J., Chehbouni, A., Huete, A., Kerr, Y., and Sorooshian, S. (1994). A modified soil adjusted vegetation index. *Remote Sens. Environ*. 48, 119–126. doi: 10.1016/0034-4257(94)90134-1

Rouse, J. W., Haas, R. H., Deering, D. W., and Schell, J. A. (1974). Monitoring the vernal advancement and retrogradation (Green wave effect) of natural vegetation. *Final Rep. RSC* 4, 1–371.

Salih, A. A., Baraibar, M., Mwangi, K. K., and Artan, G. (2020). Climate change and locust outbreak in East Africa. *Nat. Clim. Change* 10, 584–585. doi: 10.1038/s41558-020-0835-8

Shrestha, S., Thakur, G., Gautam, J., Acharya, N., Pandey, M., and Shrestha, J. (2021). Desert locust and its management in Nepal: A review. *J. Agric. Nat. Resour*. 4, 1–28. doi: 10.3126/janr.v4i1.33197

Sword, G. A., Lecoq, M., and Simpson, S. J. (2010). Phase polyphenism and preventative locust management. *J. Insect Physiol.* 56, 949–957. doi: 10.1016/j.jinsphys.2010.05.005

Thornton, P. K., Ericksen, P. J., Herrero, M., and Challinor, A. J. (2014). Climate variability and vulnerability to climate change: a review. *Glob. Change Biol*. 20, 3313–3328. doi: 10.1111/gcb.12581

Wójtowicz, M., Wójtowicz, A., and Piekarczyk, J. (2016). Application of remote sensing methods in agriculture. *Commun. Biomet. Crop Sci*. 11, 31–50.

Woodhouse, I. (2005). *Introduction to Microwave Remote Sensing*. CRC Press.

Conflict of Interest: The authors declare that the research was conducted in the absence of any commercial or financial relationships that could be construed as a potential conflict of interest.

frontiers in Climate

CORRECTION
published: 25 November 2021
doi: 10.3389/fclim.2021.809913

Corrigendum: Limitations of Remote Sensing in Assessing Vegetation Damage Due to the 2019–2021 Desert Locust Upsurge

Emily C. Adams[1,2]*, *Helen B. Parache*[1,2], *Emil Cherrington*[1,2], *Walter L. Ellenburg*[1,2], *Vikalp Mishra*[1,2], *Ronan Lucey*[1] and *Catherine Nakalembe*[3]

[1] Earth System Science Center, The University of Alabama in Huntsville, Huntsville, AL, United States, [2] NASA SERVIR Science Coordination Office, Marshall Space Flight Center, Huntsville, AL, United States, [3] Department of Geographical Science, University of Maryland, College Park, MD, United States

OPEN ACCESS

Approved by:
Frontiers Editorial Office,
Frontiers Media SA, Switzerland

***Correspondence:**
Emily C. Adams
emily.c.adams@nasa.gov

Specialty section:
This article was submitted to Climate Services, a section of the journal Frontiers in Climate

Received: 05 November 2021
Accepted: 08 November 2021
Published: 25 November 2021

Citation:
Adams EC, Parache HB, Cherrington E, Ellenburg WL, Mishra V, Lucey R and Nakalembe C (2021) Corrigendum: Limitations of Remote Sensing in Assessing Vegetation Damage Due to the 2019–2021 Desert Locust Upsurge. Front. Clim. 3:809913. doi: 10.3389/fclim.2021.809913

Keywords: locust, NDVI, vegetation, damage assessment, MODIS, harmonized landsat sentinel

A Corrigendum on

Limitations of Remote Sensing in Assessing Vegetation Damage Due to the 2019–2021 Desert Locust Upsurge

by Adams, E. C., Parache, H. B., Cherrington, E., Ellenburg, W. L., Mishra, V., Lucey, R., and Nakalembe, C. (2021). Front. Clim. 3:714273. doi: 10.3389/fclim.2021.714273

An author name was incorrectly spelled as Catherine Nakelembe. The correct spelling is Catherine Nakalembe.

The authors apologize for this error and state that this does not change the scientific conclusions of the article in any way. The original article has been updated.

frontiers in Climate

ORIGINAL RESEARCH
published: 11 November 2021
doi: 10.3389/fclim.2021.715837

Mapping of Winter Wheat Using Sentinel-2 NDVI Data. A Case of Mashonaland Central Province in Zimbabwe

Fadzisayi Mashonganyika[1], *Hillary Mugiyo*[2,3]*, *Ezekia Svotwa*[4†] *and Dumisani Kutywayo*[1]

[1] Department of Research and Specialist Services (Crop Research Division), Harare, Zimbabwe, [2] Agricultural Technical and Extension Services (AGRITEX), Harare, Zimbabwe, [3] Centre for Transformative Agricultural and Food Systems, School of Agricultural, Earth & Environmental Sciences, University of KwaZulu-Natal, Pietermaritzburg, South Africa, [4] Chinhoyi University of Science and Technology, Chinhoyi, Zimbabwe

A robust early warning system can alert to the presence of food crises and related drivers, informing decision makers on food security. To date, decision-makers in Zimbabwe still rely on agriculture extension personnel to generate information on wheat production and monitor the crop. Such traditional methods are subjective, costly and their accuracy depends on the experience of the assessor. This study investigates Sentinel-2 NDVI and time series utility as a wheat-monitoring tool over the wheat-growing areas of Zimbabwe's Bindura, Shamva, and Guruve districts. NDVI was used to classify and map the wheat fields. The classification model's evaluation was done by creating 100 reference pixels across the classified map and constructing a confusion matrix with a resultant kappa coefficient of 0.89. A sensitivity test, receiver operating characteristic (ROC) and area under the curve (AUC) were used to measure the model's efficiency. Fifty GPS points randomly collected from wheat fields in the selected districts were used to identify and compute the area of the fields. The correlation between the area declared by farmers and the calculated area was positive, with an R^2 value of 0.98 and a Root Mean Square Error (RMSE) of 2.23 hectares. The study concluded that NDVI is a good index for estimating the area under wheat. In this regard, NDVI can be used for early warning and early action, especially in monitoring programs like 'Command Agriculture' in Zimbabwe. In current and future studies, the use of high-resolution images from remote sensing is essential. Furthermore, ground truthing is always important to validate results from remote sensing at any spatial scale.

Keywords: food security, grain yield, GIS, remote sensing, Zimbabwe

OPEN ACCESS

Edited by:
Tamuka Magadzire, University of California Santa Barbara, United States

Reviewed by:
Terence Mushore, University of Zimbabwe, Zimbabwe
Uğur Avdan, Eskisehir Technical University, Turkey
Ferdinando Urbano, Joint Research Centre, Italy

***Correspondence:**
Hillary Mugiyo
mugiyoh@gmail.com

[†]*Deceased*

Specialty section:
This article was submitted to Climate Services, a section of the journal Frontiers in Climate

Received: *27 May 2021*
Accepted: *01 October 2021*
Published: *11 November 2021*

Citation:
Mashonganyika F, Mugiyo H, Svotwa E and Kutywayo D (2021) Mapping of Winter Wheat Using Sentinel-2 NDVI Data. A Case of Mashonaland Central Province in Zimbabwe. Front. Clim. 3:715837. doi: 10.3389/fclim.2021.715837

INTRODUCTION

Wheat is one of the cereal grains produced and consumed globally (Igrejas and Branlard, 2020). It is one of the most important crops for national food security and a source of livelihood in developing countries like Zimbabwe (Shiferaw et al., 2013). Wheat is considered the second most important cereal crop in Zimbabwe after maize (Chawarika, 2016). It is grown during the winter season (May–September) under irrigation, and it is the predominant crop grown during winter. The annual wheat consumption for Zimbabwe is above 400 000 metric tons, yet imports of around

80 percent wheat are made each year (Mutambara et al., 2013). This is attributable to several factors such as poor agricultural practices, lack of resources to finance wheat production in winter and, to a certain extent, unfavorable weather conditions. Therefore, the decision-makers must obtain accurate information on the planting area and production of winter wheat to determine how much wheat to import and protect the constrained local farmers who produce 15 to 25% of wheat required in the country.

Traditionally, the country relies on field surveys to monitor wheat production. This method is expensive, time consuming, and sometimes subjective (Wang et al., 2019). It is also not feasible in a large-scale agriculture landscape to facilitate national field crop mapping (Ouzemou et al., 2018). Therefore, cheaper and faster ways of identifying and mapping crop fields have become a necessity. Satellite remote sensing technology has been successfully used to estimate wheat production through vegetation indices (VI) time-series data at large scales (Atkinson et al., 2012; Franch et al., 2019). Crop phenological information can be derived from satellite data, and ground observations can be used for verifications (You et al., 2013). It has been investigated and practiced successfully in retrieving vegetation phenology based on remotely sensed vegetation indices (VI) time-series at broad scales (Atkinson et al., 2012; Zeng et al., 2020). Vegetation index time series are good indicators reflecting the dynamics of vegetation growth and vegetation coverage. This has provided a basis for wheat growth monitoring in this study. Sentinel-2 imagery was used, which provides free and open services and data with a high spatial resolution of 10–60 m (depending on the band). It has a temporal resolution of about 5 days (depending on the latitude) (Escolà et al., 2017a; Isbaex and Margarida Coelho, 2021). Such spatial and temporal resolutions and the availability of images free of charge make Sentinel-2 very appealing for crop monitoring. This includes identifying, mapping and estimating acreage of the field crops for subsequent yield forecasting when using yield statistical records. Therefore, the need to integrate remote sensing in crop monitoring with ground observations cannot be over-emphasized. However, this involves acquiring and using big data to monitor crops in real-time, which needs to be automated for easy management. Cloud based solutions require hardware and software driven by the appropriate applications, packaging and systems, and they require high financial investments.

Vegetation Indices (VIs) are a combination of surface reflectance at two or more different wavelengths and are designed to highlight a specific vegetation property. Vegetation Indices (VIs) obtained from remote sensing-based covers are simple and effective algorithms for quantitative and qualitative evaluations of vegetation cover, vigor, and growth dynamics. They include: normalized difference vegetation index (NDVI), leaf area index (LAI), vegetation condition index (VCI), enhanced vegetation index (EVI) and soil-adjusted vegetation index (SAVI). These vegetation indices have been applied widely in remote sensing using different aerial and satellite platforms. Recent advances involve Unmanned Aerial Vehicles (UAV) (do Amaral et al., 2020), although its application is still new in Zimbabwe. The NDVI, derived from remote-sensing (satellite) data, is commonly used in crop assessments (Stuhlmacher, 2011). NDVI measures the state of plant health based on the plant's reflection of light at specific frequencies (absorbs some waves and reflects others). Therefore, it is instrumental in crop monitoring and evaluation (Suárez et al., 2019).

In Zimbabwe, the estimation of the wheat area is always a challenge because it is the only major cereal winter crop with significant importance to the economy. Unlike other crops such as maize, sorghum, and groundnuts typically grown simultaneously during the rainy season, allowing assessments of multiple crops, monitoring of winter wheat crop is expensive because field assessments are done for a single crop. In addition, the government of Zimbabwe is financing wheat farmers by providing inputs under the 'Command Agriculture' program to improve wheat production (**Supplementary Table 1**). Therefore, cheaper and timely monitoring and evaluation techniques to acquire the planting area of winter wheat are critical for implementing these programs. We can improve the timing of assessment results, reduce cost, address subjectivity, and enhance broad-scale crop monitoring by integrating remote sensing into the current crop assessment programs. However, studies on remote sensing technology in crop monitoring systems are still limited in Zimbabwe. Therefore, the main objective of this study is to investigate the use of remote sensing data in crop monitoring. Sentinel-2 NDVI and time series analysis will be used as monitoring tools to identify, map, and estimate the winter wheat crop area.

METHODS AND MATERIALS

Study Area

The study was carried out in major wheat-growing districts of Mashonaland Central province, namely Bindura, Guruve, and Shamva (**Figure 1**). The province is located between 30.014 ∼ 32.858 degrees East and 15.620 ∼ 17.688 degrees South. The province primarily lies in the agro-ecological region II (Intensive farming), with some small portions falling in regions III (Semi-Intensive farming) and IV (Semi-Extensive farming) (Musemwa and Mushunje, 2012). Rainfall in this region is confined to summer and ranges from moderate (650–800 mm) to moderately high (750–1,000 mm). The soils in this area vary from sandy loams to clays. Similarly, soil fertility varies from place to place. It is suitable for semi-intensive and semi-extensive farming, depending on the prevailing agro-ecological conditions (CIAT; World Bank., 2017). Major crops grown include tobacco, soya beans, citrus, cotton and small grains (including wheat).

Data Collection

Training of Agriculture Extension (AGRITEX) officers was done on Global Positioning System (GPS) technology to capacitate them to collect locational data for the wheat fields in Mashonaland Central districts for the 2019 season. The data was collected using Latitude/Longitude (degrees, minutes, and seconds) coordinate system with the World Geodetic System of 1984 (WGS84) as the reference datum. To cater to the GPS receivers' error margins, the GPS locations were recorded inside the fields about 3 m from the edges of the selected wheat fields.

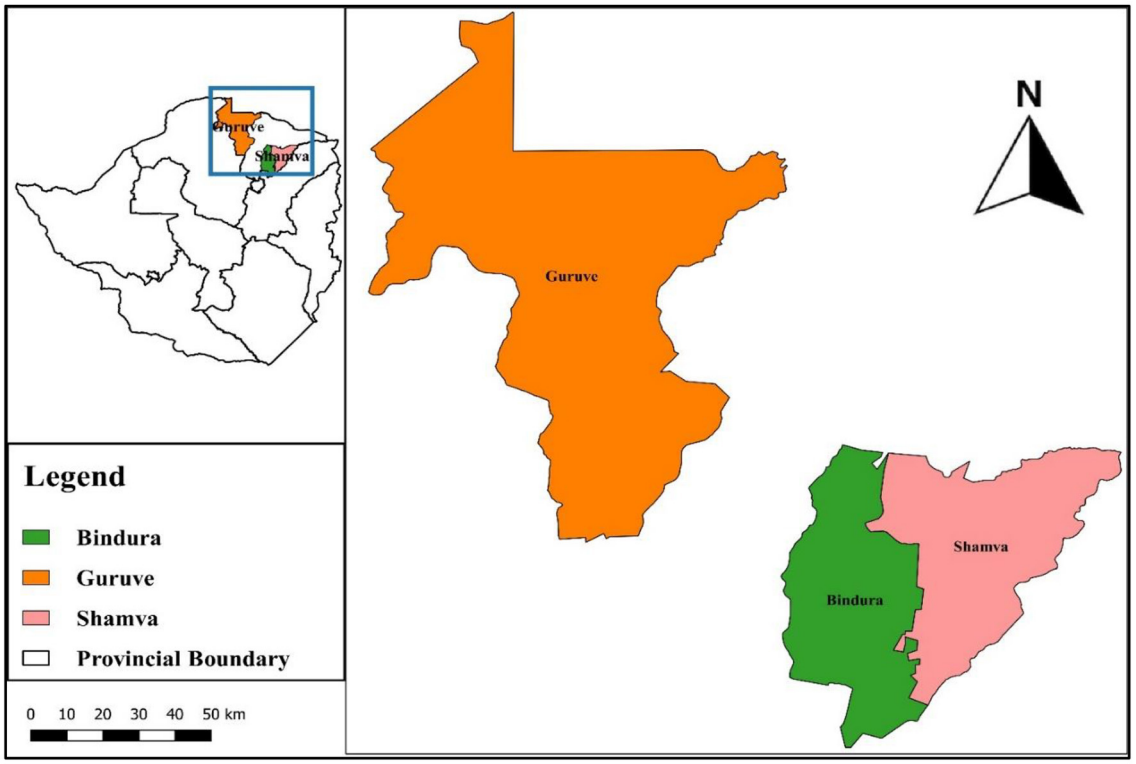

FIGURE 1 | Study area.

These locations and other attributes were captured in a table on a formatted data collection sheet. The data collected included; farm name, farm owner, farm model, an estimated area under wheat, date of planting and date of harvesting. The coordinates were then converted using QGIS software into shapefiles and used for satellite image analysis, i.e., classification of the image, identifying and mapping the fields, and computing area of the fields.

Sample Size

Six districts that grow wheat in Mashonaland Central province were initially targeted, but a few officers collected the data. However, only three sections were visited, namely; Bindura, Guruve, and Shamva districts. A total of 60 GPS locations of wheat fields were randomly collected during the survey. Farmers contracted to the 'Command Agriculture' program was our primary target, although a few commercial farmers who have not joined the program were included. According to statistics, Mashonaland Central had 139 farmers contracted to this program in 2019. Although 60 fields were visited and the relevant data was collected, not all the data collected was usable because of its quality. Some of the coordinates were wrongly captured, thereby falling far away from the actual fields. Some of the data supplied had missing details of critical attributes like the area of the fields. Such data was therefore discarded, and only usable data were considered for the analysis. Our sample size ultimately was 50 wheat fields (**Table 1**).

TABLE 1 | Sites visit in Mashonaland Central province.

District	Captured Sites	Useable sites
Bindura	51	43
Shamva	5	5
Guruve	2	2
Centenary	2	Nil
Total	60	50

Normalized Difference Vegetation Index (NDVI) Data

NDVI data were derived from Sentinel 2 datasets. Sentinel 2 is a component of the Copernicus earth observation program developed by the European Union (EU) to study the earth's surface. It consists of two satellites designed to acquire reflected sunlight in the optical range of the electromagnetic wavelengths. It is susceptible to variations in vegetation and has been extremely useful for monitoring forests and crops (Hill, 2013). The Sentinel-2 images (tiles 36KTG, KUG, KTF and KUF) with zero percent cloud cover were selected and downloaded from the USGS Earth Explorer site: https://earthexplorer.usgs.gov/ for the period 1 May to 30 September 2019. These tiles were joined together by creating a virtual raster in QGIS. Pre-preprocessing, which involved atmospheric correction of the Sentinel-2 images, was

done using the Semi-Automated Classification Plugin. Sentinel-2 contains reflectance data of 13 bands (Escolà et al., 2017a). The temporal resolution of this product is 5 days. The spatial resolution of Sentinel-2 images ranges from 10 to 60 meters. The red (Band 4) and near-infrared (Band 8) spectral bands are of significant importance to this study, with a spatial resolution of 10 meters. Normalized Difference Vegetation Index (NDVI) image was created from the red and near-infrared bands in ArcGIS using the spatial analyst module and the 'raster calculator' tool. The polygon for the study area was used to extract NDVI data for the area of interest for the analysis. The NDVI index is calculated as the ratio between the difference and sum of the reflectance in NIR (B8) and red (B4) regions (Adão et al., 2017).

$$NDVI = ({}_{\mathrm{R}}NIR - {}_{\mathrm{R}}\,RED)/({}_{\mathrm{R}}NIR + {}_{\mathrm{R}}\,RED)$$

The ${}_{\mathrm{R}}$**NIR** represents the reflectance of **NIR** radiation, while ${}_{\mathrm{R}}$**RED** is the reflectance of visible **RED** radiation.

With the formula above, vegetation density at any point of the image is highly correlated to the difference in reflected light's intensity in the red and infrared range divided by the sum of these intensities (Suárez et al., 2019).

Time Series Analysis for Phenology Extraction

We analyzed the NDVI values from May (usually the start of the winter wheat growing season) to September (end of the season). The value tool in QGIS was used to extract pixel data from the NDVI images created for a start to the end of the season. The NDVI values from the random points in the wheat fields were used to construct time series graphs. This is because NDVI time series from satellite data can approximate phenological stages and thus characterize the general vegetation behavior within its spatial footprint (Huang et al., 2019). Therefore, the wheat crop development was studied by looking at its phenological characteristics, including germination, leaf emergence, and up to the start of senescence. This was used as a monitoring tool to confirm the presence or absence during the period under study.

Mapping of Wheat Fields and Calculation of Area Under Wheat

On the NDVI image, wheat fields were an outstanding feature during the period under study. The image was classified into three land-use classes using NDVI thresholds derived from the NDVI raster map, i.e., <0.07 for water bodies, <0.3 for uncultivated land and >0.3 for the cropped area ArcGIS software. Fifty GPS coordinates collected from the fields were used to identify and match with the individual wheat fields to compute the area. The area of each field was calculated using the 'Raster Calculator' tool in ArcGIS. The area computed using this method was compared to the area reported by the farmers (**Supplementary Table 4**). Evaluation of this method of determining the area under wheat was done using a linear regression model. Coefficient of determination (R^2) was used to indicate the consistency and linear correlation between the calculated area and the reference data (area reported by farmers). The closer the R^2 is to 1, the higher the consistency between them. RMSE was also used to assess the model performance.

Validation of the Classification Model

The accurate location of the winter wheat fields is an essential consideration in obtaining accurate results. Therefore, the need to validate the classification process. A point map was created using 100 randomly selected reference points across the NDVI image with 30 points for water (class 1), 40 for uncultivated (class 2), and 30 for cultivated (class 3) land-use classes (**Supplementary Table 2**). The reference points were converted to reference pixels and combined with the NDVI classified map to extract the classified map's pixel values. Data extracted from the combined map was used to compute a confusion matrix (**Supplementary Table 3**). Validation of this model was based on the overall accuracy and the kappa coefficient values from the confusion matrix, the receiver operating characteristic (ROC), and the area under the curve (AUC) analysis. The ROC plot has an x-axis indicating the false-positive error rate, which signifies a wrong prediction by the model. The y-axis shows the actual positive rate, indicating a correct prediction by the model. If the value of AUC is ≤ 0.5, it means a random prediction, while values of AUC higher than 0.5 and closer to 1 indicates a better prediction by the model (Jiménez-Valverde, 2012; Senay and Worner, 2019). The composite operator helps illustrate how well two layers or maps agree on how the categories are clustered spatially.

RESULTS

Time Series Analysis Results for the NDVI on the Wheat Fields

Time-Series Images

NDVI images for the wheat fields understudy for dates ranging from 5 May, 11 June, 1 July, 31 July, 30 August and 29 September 2019 are displayed in **Figure 2**. The NDVI images show a gradual increase in intensity on the wheat fields from May to the end of July, then a gradual decrease after that until there was no significant difference with the nearby environment in September. Therefore, NDVI values assumed an upward trend from early June to the end of July, then a downward trend after that until September (with deeper color standing for higher NDVI values).

Time-Series Graphs

The NDVI time series graphs from the beginning of May to the end of September 2019 are displayed in **Figure 3**. These results agree with results from the time series images. There is an increase in NDVI values from about 0.2 in May, rising to peak values ranging from 0.4 to 0.8 in July before gradually decreasing to around 0.2 again in September.

Classification of the NDVI Image and Mapping of Wheat Fields

Data was collected from selected farms in Bindura, Shamva, and Guruve districts extending from 30.80 to 31.60 E longitude and 16.60 to 17.170 S latitude. From the Sentinel-2 NDVI images, wheat fields were an outstanding observable feature. The image

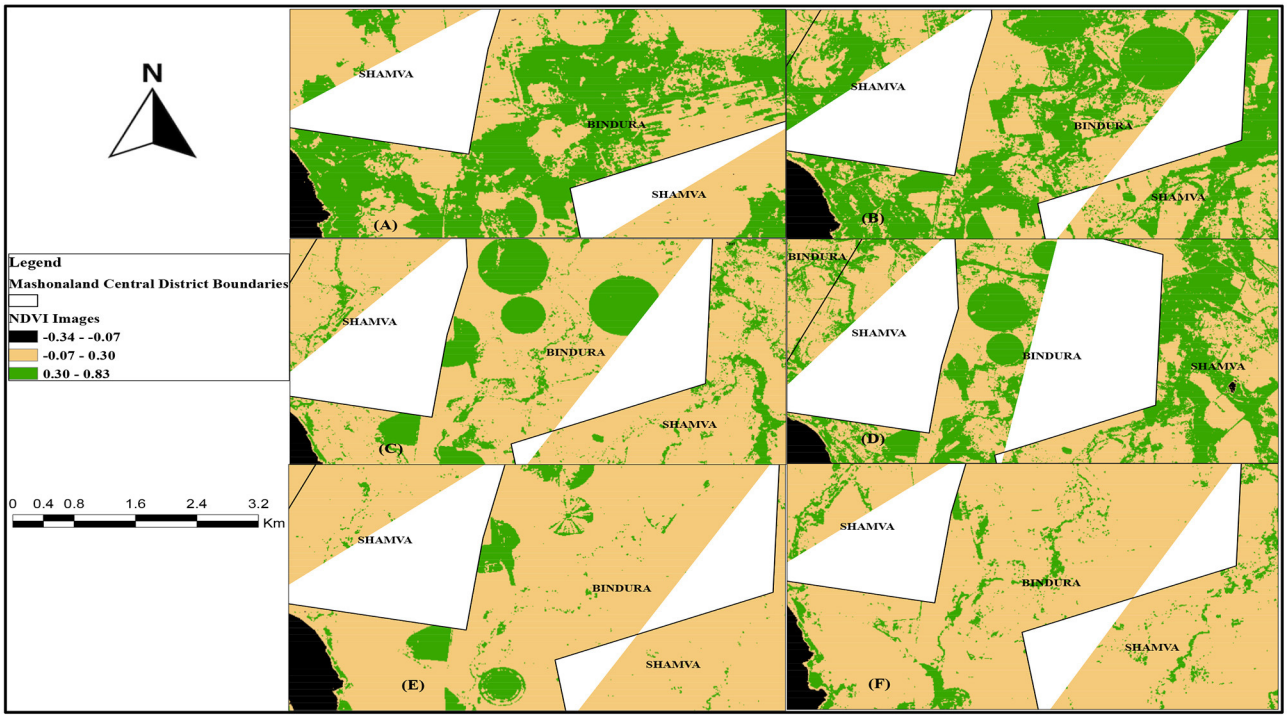

FIGURE 2 | NDVI Time-series images for part of Bindura from May to September 2019. Image Acquisition dates: **(A)** May 2019, **(B)** 11 June 2019, **(C)** 1 July 2019, **(D)** 31 July 2019, **(E)** 30 August 2019, **(F)** 29 Septembers 2019.

acquired on 1 July 2019 was used to classify and map the wheat fields (**Figure 4**). Locational data was used to identify and match the wheat fields with their farm names, farm owners and the area planted (as reported by the farmer).

Computation of Area Under Wheat

Hectarages of wheat fields were computed in ArcGIS to determine the hectarage of wheat planted using satellite imagery. The comparison between the output from these computations with the area reported during the field visits by the farmers was made. The locational, attribute data collected, and area of the wheat fields are displayed in **Supplementary Table 4**. The sizes of the wheat fields ranged from a minimum of 1 hectare to a maximum of 74 hectares.

Validation of the Results for Calculating the Area Under Wheat

The results obtained from calculating the actual hectarages was validated using simple linear regression analysis (**Figure 5**), and an R^2 value of 0.9801 was attained with an RMSE of 2.23 hectares. The regression equation for predicting the area under wheat is;

$$y = 0.992x - 0.3127$$

Validation of the Classification Model

Evaluation of the classification model was done by computing the confusion matrix and through ROC/AUC analysis. The overall accuracy rate was 0.93, and the kappa coefficient was 0.89 (**Supplementary Table 3**). The ROC / AUC analysis results were derived from the logistic regression according to the maximum entropy (MaxEnt) theory (**Figure 6**). The value of AUC for this model is 0.91.

DISCUSSION

Many nations have widely adopted remote sensing data as a crop monitoring tool over the years. However, Zimbabwe seems to be lagging in adopting these new technologies. Relying on field assessments alone has proved to be costly, time-consuming and in some cases subjective. This study investigated the use of remote sensing data in crop monitoring. Sentinel-2 NDVI data and time series analysis were used as monitoring tools to identify, map, and estimate the winter wheat crop area. The NDVI from Sentinel-2 satellite imagery could locate wheat fields and calculate the area under wheat with relatively high precision ($R^2 = 0.98$, RMSE = 2.23). The classification model was evaluated using the confusion matrix with an accuracy of 0.93 and a kappa coefficient of 0.89 (**Supplementary Table 3**). ROC/AUC analysis gave an accuracy of 91 percent (**Figure 6**). These results indicate a better prediction by the model. This implies that detecting wheat fields using Sentinel-2 NDVI as a remote sensing tool agrees with the ground truth. Therefore, NDVI provides a simple, faster and more reliable way of identifying wheat fields to monitor wheat production through the winter season.

The NDVI time series images and graphs obtained in the selected wheat fields generally showed a progression from values of <0.2 at the start of the season to a maximum range of between

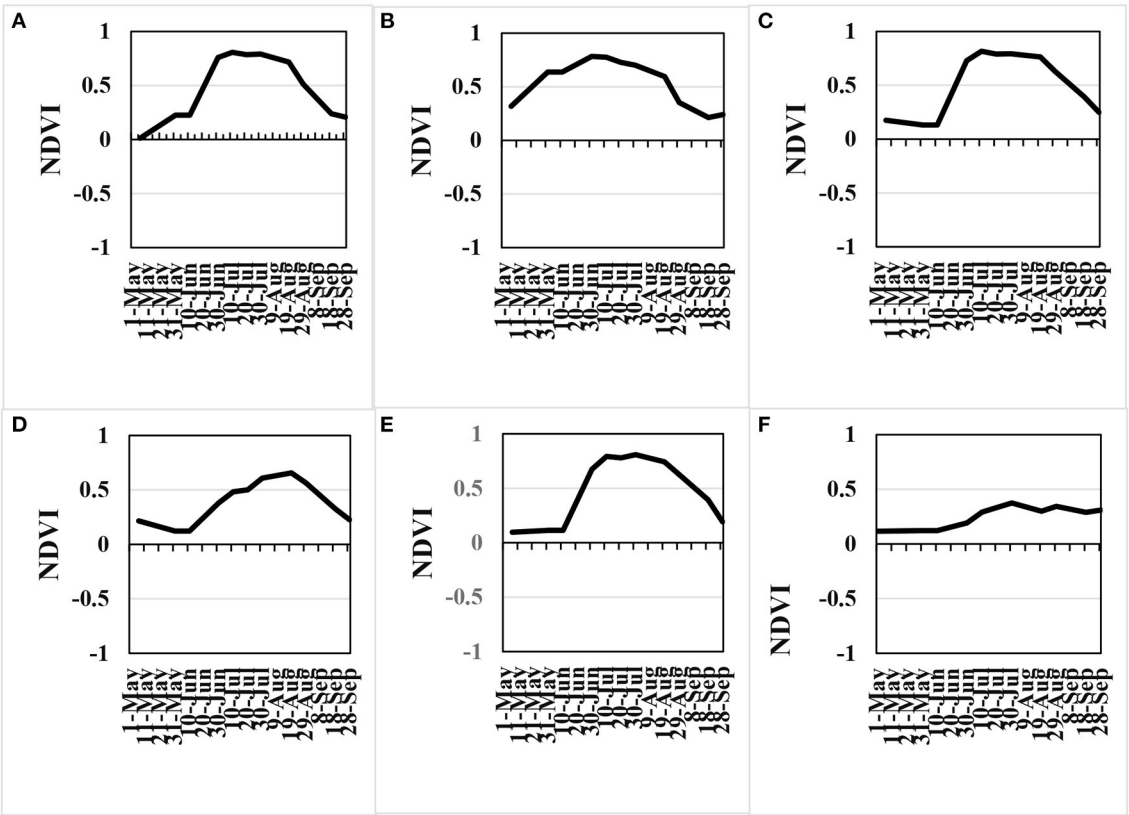

FIGURE 3 | Time series graphs for **(A)** SOS Maizelands, **(B)** Hopedale, **(C)** Vale Farm, **(D)** Northstar, **(E)** Douglyn, **(F)** Kudukloof.

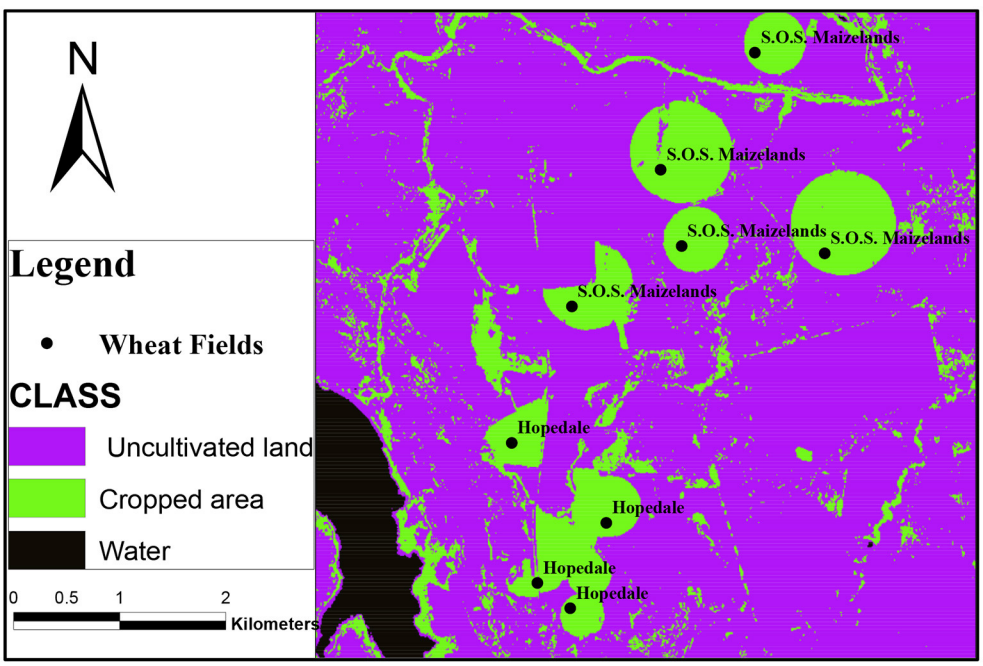

FIGURE 4 | NDVI Classified Map.

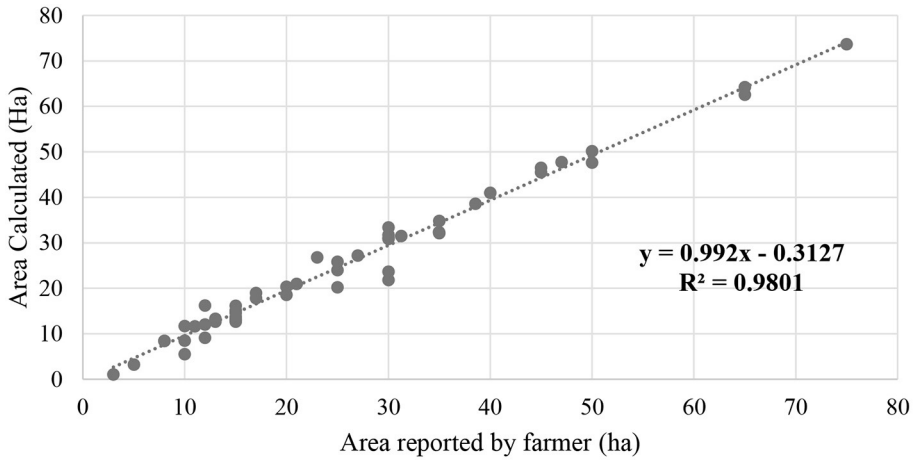

FIGURE 5 | Scatter plot showing the relationship between reported and calculated hectarage for wheat fields in selected farms for Mashonaland Central province.

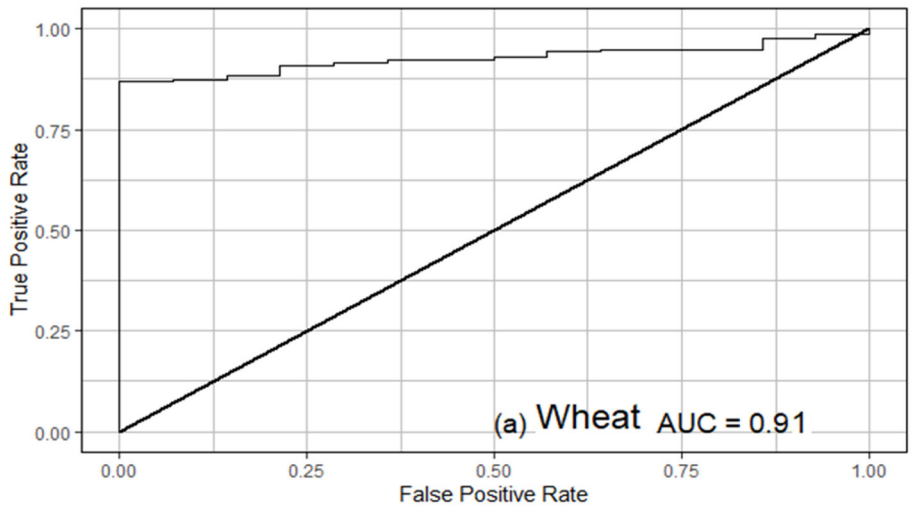

FIGURE 6 | ROC/AUC analysis results.

0.4 and 0.8, then a gradual decrease after that (**Figures 2**, **3**). Similar studies were carried out using EOS/MODIS in Henan Province, China. The results obtained are consistent with the results of this study, where a gradual increase in NDVI values of winter wheat was observed. The signal from NDVI reached peak value at the heading stage, then a gradual decrease toward harvesting (Filippa et al., 2018). This study shows a similar trend, thus confirming that NDVI values can be used for crop growth monitoring. This increase in NDVI is related to increases in the canopy leaf area index (LAI).

In estimating the area under a crop, accurate information on the temporal and spatial resolution of the remote sensing images is essential. In this study, sentinel-2 satellite data was used to provide high-resolution images (10 m), available for free. Sentinel-2 datasets can be used in developing countries like Zimbabwe, where high-resolution images from Light Detection and Ranging (LiDAR) are still expensive. The NDVI from sentinel-2 satellite data is used based on the physics of light reflection and absorption across bands (Suárez et al., 2019). It is known that healthy vegetation reflects light strongly in the near-infrared band and less strongly (absorbs more) in the visible portion of the spectrum (Suárez et al., 2019). The more a plant absorbs visible sunlight (during the growing season), the more photosynthesising and more productive it is (Rafezall et al., 2020).

Conversely, the less sunlight the plant absorbs, the less photosynthesising and the less productive it is. Therefore, a ratio between the light reflected in the near-infrared and light reflected in the visible spectrum will represent areas with wheat. This has formed the basis for using this tool for crop monitoring.

Estimating wheat areas on time will allow decision-makers to take appropriate action toward food security. This is critical in the Zimbabwean context, where the government is funding special agricultural programs to improve crop production and productivity with particular reference to the 'Command agriculture' program. Several challenges are being faced in recovering the total value of these government initiatives because some beneficiaries do not use the inputs for the intended program, thereby derailing the purpose of such initiatives. Due to slackened monitoring and evaluation systems, the government is unable to timely trace whether the farmer or beneficiary has complied or not. Use of NDVI time series can be used to confirm in time whether the beneficiaries of this program have planted wheat within the anticipated period or not. If not, the administrators of the programs can quickly make informed decisions and prevent abuse of resources.

This study shows that hectarages derived from the field images (calculated area) are very close to those reported by farmers (**Supplementary Table 4**). The scatter plot in **Figure 2** shows a positive relationship between the area reported by farmers and the area calculated through the classification model. The simple linear regression analysis obtained a coefficient of determination (R^2 value) of 98%. This means eyeballing and remote sensing determined areas are close to 1. It implies that 98% variation in Y can be explained in X. Therefore, it confirms that NDVI can extract winter wheat fields with high accuracy. Previous studies in China also demonstrated that NDVI could successfully extract winter wheat acreage with an error of 9.66% (Qiao and Cheng, 2009). In recent wheat mapping studies in China's Northern Anhui Counties and Central Anhui Counties, accuracy was obtained between 78 and 95 percent (Zhang et al., 2019). The variation in the accuracy of mapping was mainly due to differences in the size of the wheat fields. Large homogeneous wheat fields were mapped with high precision when compared to areas with smaller fields. In this study, our most minor wheat field was one hectare, but most of the wheat fields were in the range of 10–50 hectares; hence they were mapped with high precision. This study can therefore confirm that NDVI can be used successfully to estimate the area under wheat.

It was also noted during the initial stages of the data analysis process that the error of estimating area under wheat for this study was high, and this was attributed to the existence of many outliers. Most of the discrepancies came from the fact that some farmers contracted to the 'Command Agriculture' program has limited irrigation facilities on their farms but can grow more wheat. These farmers have resorted to increasing their hectarage by out-sourcing land from other farms with idle irrigation facilities to which they are sub-contracted. Many farmers just report the total area intended for wheat growing and get the corresponding inputs without declaring such arrangements. On the other hand, some farm owners who have sub-contracted part of their farms to other farmers only declare their hectarage, which is less than that observed on the satellite images. As a result, the total area under wheat on their farms detected through satellite imagery was much more or less than what is in the official records for 'Command Agriculture' contracts. Efforts were made to contact farmers with such scenarios to clarify these issues, which has greatly reduced the error of the field area calculations. Therefore, the results of this study demonstrate that satellite imagery can more accurately be used to timely estimate the acreage of wheat for each season.

Like most remote sensing studies on identifying and mapping crop fields, this study comes with some limitations. For example, the wheat fields visited were ranging from 1 to 74 hectares. However, we noted that some smaller fields were not included in this study because the field boundaries were not clearly defined on the images, making it difficult to map them. Recent studies in the Netherlands also assessed geospatial parcel parameters on arable land and revealed the same limitation on Sentinel-2 satellites on small agricultural plots (Vajsová et al., 2020). Therefore, higher resolution images like UAV technology may be recommended when mapping smaller agricultural plots. Downloading of images were done manually because of the limited capacity of our computer hardware and software, so we failed to download some of the images and sourced them from other government departments. Therefore, the need for financial investment in these resources should be prioritized. During the present data collection exercise, we have not considered the influence of different farming systems in Mashonaland Central province because the visual selection of occurrence location points may cause substantial bias in sample selection (Araújo and Peterson, 2012; Merow et al., 2013). Again, the three districts and the 50 sites selected in this study may not represent the whole country, Zimbabwe. A systematic random sampling technique is recommended to capture the dynamics of farming systems in the whole of Zimbabwe.

Way Forward

This study demonstrated the potential for remote sensing data to extract wheat fields and compute the area under wheat at the early stages of the wheat growing season, which can be used to predict yield. This has raised the need to roll out the research to a national level to create and deploy a near-real-time early warning system. Therefore, we recommend that more training sites be included across the country to ascertain the applicability of this tool in all scenarios in the wheat growing sector.

While the results of this study remain applicable for use, future research should consider the use of data with a finer resolution to improve the accuracy of crop mapping. This will improve the mapping of smaller agricultural plots and identify specific crops in mixed crop farming, which are now a common phenomenon in the Zimbabwean agricultural systems. The use of unmanned aerial vehicles can be used to capture high-resolution images and to validate satellite-derived data. One such sensor is LiDAR (Light Detection and Ranging) technology, which provides 3D models of croplands (Gago et al., 2015). LiDAR technology can provide accurate maps for farmlands in crop monitoring (Rosell and Sanz, 2012; Lin, 2015). However, the cost-benefit of using LiDAR for smallholder farmer settings needs to be evaluated to determine the feasibility of such investments (Escolà et al., 2017b).

CONCLUSION

Remote sensing technology has a great potential to timely provide national statistics on the area under wheat for the winter season. This study has demonstrated that Sentinel-2 NDVI data is a powerful and valuable tool to identify and map winter wheat fields and can be used at a national scale to calculate wheat acreage. NDVI time series analysis proved to be a tool that can effectively monitor wheat crop growth. A deeper analysis will make these tools relevant in the decision making on food security issues. In order to strengthen monitoring and evaluation of crops in Zimbabwe, integrating the use of GIS and remote sensing technology should be prioritized, especially for the winter wheat crop. Results from remote sensing should be validated with ground-truthed information to increase the confidence of decision-makers in adopting the use of remote sensing in wheat production monitoring in Zimbabwe.

AUTHOR'S NOTE

This study is dedicated to one of the coauthors Dr. Ezekia Svotwa who succumbed to COVID-19 after this article was accepted.

DATA AVAILABILITY STATEMENT

The raw data supporting the conclusions of this article will be made available by the authors, without undue reservation.

AUTHOR CONTRIBUTIONS

All authors listed have made a substantial, direct and intellectual contribution to the work, and approved it for publication.

ACKNOWLEDGMENTS

We acknowledge the services of the SIRDC team led by Dr. K. Murwira for training the AGRITEX officers on GPS technology. We thank SIRDC also for giving us most of the satellite imagery used for this research.

SUPPLEMENTARY MATERIAL

The Supplementary Material for this article can be found online at: https://www.frontiersin.org/articles/10.3389/fclim.2021.715837/full#supplementary-material

REFERENCES

Adão, T., Hruška, J., Pádua, L., Bessa, J., Peres, E., Morais, R., et al. (2017). Hyperspectral imaging: a review on UAV-based sensors, data processing and applications for agriculture and forestry. *Remote Sens*. 9:1110. doi: 10.3390/rs9111110

Araújo, M. B., and Peterson, A. T. (2012). Uses and misuses of bioclimatic envelope modeling. *Ecology* 93, 1527–1539. doi: 10.1890/11-1930.1

Atkinson, P. M., Jeganathan, C., Dash, J., and Atzberger, C. (2012). Inter-comparison of four models for smoothing satellite sensor time-series data to estimate vegetation phenology. *Remote Sens. Environ*. 123, 400–417. doi: 10.1016/j.rse.2012.04.001

Chawarika, A. (2016). An assessment of the critical constraints to wheat production in Zimbabwe. *Bus. Soc. Sci*. 1, 33–48. doi: 10.26831/BSSJ.2016.1.1.33-48

CIAT; World Bank. (2017). *Climate-Smart Agriculture in Zimbabwe*. Washington, DC: CSA Ctry. Profiles Africa Ser. Int. Cent. Trop. Agric. (CIAT), 24.

do Amaral, L. R., Zerbato, C., de Freitas, R. G., Júnior, M. R. B., and da Silva Simões, I. O. P. (2020). UAV applications in Agriculture 4.0. *Rev. Cienc. Agron*. 51. doi: 10.5935/1806-6690.20200091

Escolà, A., Badia, N., Arnó, J., and Martínez-Casasnovas, J. A. (2017a). Using Sentinel-2 images to implement Precision Agriculture techniques in large arable fields: First results of a case study. *Adv. Anim. Biosci*. 8, 377–382. doi: 10.1017/S2040470017000784

Escolà, A., Martínez-Casasnovas, J. A., Rufat, J., Arnó J., Arbonés, A., Sebé, F., et al. (2017b). Mobile terrestrial laser scanner applications in precision fruticulture/horticulture and tools to extract information from canopy point clouds. *Precis. Agric*. 18, 111–132. doi: 10.1007/s11119-016-9474-5

Filippa, G., Cremonese, E., Galvagno, M., Migliavacca, M., Sonnentag, O., Humphreys, E., et al. (2018). NDVI derived from IR-enabled digital cameras: applicability across different plant functional types. *Agric. Forest Meteorol*. 249, 275–285. doi: 10.1016/j.agrformet.2017.11.003

Franch, B., Vermote, E. F., Skakun, S., Roger, J. C., Becker-Reshef, I., et al. (2019). Remote sensing based yield monitoring: application to winter wheat in United States and Ukraine. *Int. J. Appl. Earth Obs. Geoinf*. 76:112–127. doi: 10.1016/j.jag.2018.11.012

Gago, J., Douthe, C., Coopman, R. E., Gallego, P. P., Ribas-Carbo, M., Flexas, J., et al. (2015). UAVs challenge to assess water stress for sustainable agriculture. *Agric. Water Manag*. 153, 9–19. doi: 10.1016/j.agwat.2015.01.020

Hill, M. J. (2013). Vegetation index suites as indicators of vegetation state in grassland and savanna: an analysis with simulated SENTINEL 2 data for a North American transect. *Remote Sens. Environ*. 137, 94–111. doi: 10.1016/j.rse.2013.06.004

Huang, X., Liu, J., Zhu, W., Atzberger, C., and Liu, Q. (2019). The optimal threshold and vegetation index time series for retrieving crop phenology based on a modified dynamic threshold method. *Remote Sens*. 11:2725. doi: 10.3390/rs11232725

Igrejas, G., and Branlard, G. (2020). "The importance of wheat," in *Wheat Quality for Improving Processing and Human Health*. eds G. Igrejas, T. Ikeda, and C. Guzmán (Cham: Springer). doi: 10.1007/978-3-030-34163-3_1

Isbaex, C., and Margarida Coelho, A. (2021). "The potential of sentinel-2 satellite images for land-cover/land-use and forest biomass estimation: a review," in *Forest Biomass - From Trees to Energy*. doi: 10.5772/intechopen.93363

Jiménez-Valverde, A. (2012). Insights into the area under the receiver operating characteristic curve (AUC) as a discrimination measure in species distribution modelling. *Glob. Ecol. Biogeogr*. 21, 498–507. doi: 10.1111/j.1466-8238.2011.00683.x

Lin, Y. (2015). LiDAR: an important tool for next-generation phenotyping technology of high potential for plant phenomics? *Comput. Electron. Agric*. 119, 61–73. doi: 10.1016/j.compag.2015.10.011

Merow, C., Smith, M. J., and Silander, J. A. (2013). A practical guide to MaxEnt for modeling species' distributions: what it does, and why inputs and settings matter. *Ecography* 36, 1058–1069. doi: 10.1111/j.1600-0587.2013.07872.x

Musemwa, L., and Mushunje, A. (2012). Factors affecting yields of field crops and land utilisation amongst land reform beneficiaries of Mashonaland Central Province in Zimbabwe. *J. Dev. Agric. Econ*. 4, 109–118. doi: 10.5897/JDAE12.002

Mutambara, J., Zvinavashe, A. P., and Mwakiwa, E. (2013). A critical review of the wheat industry in Zimbabwe. *Glob. J. Biol. Agric. Heal. Sci*. 2, 23–33.

Ouzemou, J. E., El Harti, A., Lhissou, R., El Moujahid, A., Bouch, N., Ouazzani, R. E., et al. (2018). Crop type mapping from pansharpened Landsat 8 NDVI data: a case of a highly fragmented and intensive agricultural system. *Remote Sens. Appl. Soc. Environ*. 11, 94–103. doi: 10.1016/j.rsase.2018.05.002

Qiao, H. B., and Cheng, D. F. (2009). "Application of EOS/MODIS-NDVI at different time sequences on monitoring winter wheat acreage in Henan

province," in *2009 International Conference on Environmental Science and Information Application Technology, Vol. 2* (Wuhan: IEEE), 113–115. doi: 10.1109/ESIAT.2009.159

Rafezall, C. M., Darwin, N., Ariff, M. F. M., and Majid, Z. (2020). "Detection of palm oil health through multispectral UAV platform," in *IEEE 10th International Conference on System Engineering and Technology (ICSET)* (Shah Alam: IEEE). doi: 10.1109/ICSET51301.2020.9265374

Rosell, J. R., and Sanz, R. (2012). A review of methods and applications of the geometric characterization of tree crops in agricultural activities. *Comput. Electron. Agric*. 81, 124–141. doi: 10.1016/j.compag.2011.09.007

Senay, S. D., and Worner, S. P. (2019). Multi-scenario species distribution modeling. *Insects* 10:65. doi: 10.3390/insects10030065

Shiferaw, B., Smale, M., Braun, H.-J., Duveiller, E., Reynolds, M., Muricho, G. (2013). Crops that feed the world 10. Past successes and future challenges to the role played by wheat in global food security. *Food Security* 5, 291–317. doi: 10.1007/s12571-013-0263-y

Stuhlmacher, M. (2011). Normalized Difference Vegetation Index (NDVI) derived from 2015 National Agriculture Imagery Program (NAIP) data for the central Arizona region. *Environ. Data Initiat*.

Suárez, P. L., Sappa, A. D., Vintimilla, B. X., and Hammoud, R. I. (2019). "Image vegetation index through a cycle generative adversarial network," in *IEEE 2019 IEEE/CVF Conference on Computer Vision and Pattern Recognition Workshops (CVPRW) - Long Beach*, 1014–1021. doi: 10.1109/CVPRW.2019.00133

Vajsová, B., Fasbender, D., Wirnhardt, C., Lemajic, S., and Devos, W. (2020). Assessing spatial limits of Sentinel-2 data on arable crops in the context of checks by monitoring. *Remote Sens*. 12:2195. doi: 10.3390/rs12142195

Wang, Y., Xu, X., Huang, L., Yang, G., Fan, L., Wei, P., et al. (2019). An improved CASA model for estimating winter wheat yield from remote sensing images. *Remote Sens*. 11:1088. doi: 10.3390/rs11091088

You, X., Meng, J., Zhang, M., and Dong, T. (2013). Remote sensing based detection of crop phenology for agricultural zones in China using a new threshold method. *Remote Sens*. 5, 3190–3211. doi: 10.3390/rs5073190

Zeng, L., Wardlow, B. D., Xiang, D., Hu, S., and Li, D. (2020). A review of vegetation phenological metrics extraction using time-series, multispectral satellite data. *Remote Sens. Environ*. 237:111511. doi: 10.1016/j.rse.2019.111511

Zhang, D., Fang, S., She, B., Zhang, H., Jin, N., Xia, H, et al. (2019). Winter wheat mapping based on Sentinel-2 data in heterogeneous planting conditions. *Remote Sens*. 11:2647. doi: 10.3390/rs11222647

Conflict of Interest: The authors declare that the research was conducted in the absence of any commercial or financial relationships that could be construed as a potential conflict of interest.

Publisher's Note: All claims expressed in this article are solely those of the authors and do not necessarily represent those of their affiliated organizations, or those of the publisher, the editors and the reviewers. Any product that may be evaluated in this article, or claim that may be made by its manufacturer, is not guaranteed or endorsed by the publisher.

Advantages of publishing in Frontiers

OPEN ACCESS
Articles are free to read for greatest visibility and readership

FAST PUBLICATION
Around 90 days from submission to decision

HIGH QUALITY PEER-REVIEW
Rigorous, collaborative, and constructive peer-review

TRANSPARENT PEER-REVIEW
Editors and reviewers acknowledged by name on published articles

Frontiers
Avenue du Tribunal-Fédéral 34
1005 Lausanne | Switzerland

Visit us: www.frontiersin.org
Contact us: frontiersin.org/about/contact

REPRODUCIBILITY OF RESEARCH
Support open data and methods to enhance research reproducibility

DIGITAL PUBLISHING
Articles designed for optimal readership across devices

FOLLOW US
@frontiersin

IMPACT METRICS
Advanced article metrics track visibility across digital media

EXTENSIVE PROMOTION
Marketing and promotion of impactful research

LOOP RESEARCH NETWORK
Our network increases your article's readership